THÈSE POUR OBTENIR LE GRADE DE DOCTEUR DE L'INSTITUT AGRO MONTPELLIER ET DE L'UNIVERSITÉ DE MONTPELLIER

En Biochimie et Physicochimie alimentaire

École doctorale GAIA – Biodiversité, Agriculture, Alimentation, Environnement, Terre, Eau
Unité de recherche IATE – Ingénierie des Agropolymères et Technologies Emergentes

Agrégation des arabinogalactane-protéines de la gomme d'Acacia *seyal* déminéralisée en milieu peu hydraté : propriétés structurales, d'hydratation et physicochimiques

Présentée par Amandine ANTOINE-MICHARD
Le 14 novembre 2022

Sous la direction de Christian SANCHEZ
et Michaël NIGEN

Devant le jury composé de

Marie-Hélène FAMELART, chargée de recherche, INRAE	Rapporteure
Sami HALILA, chargé de recherche, CERMAV-CNRS	Rapporteur
Sylvie MARCHESSEAU, professeur des universités, Université de Montpellier	Présidente du jury
Michel GRISEL, professeur des universités, Université du Havre	Examinateur
Isabelle JAOUEN, directrice du pôle R&D, Alland&Robert	Membre invité
Christian SANCHEZ, professeur des universités, Université de Montpellier	Directeur de thèse
Michaël NIGEN, maître de conférences, Université de Montpellier	Co-encadrant de thèse

UNIVERSITÉ DE MONTPELLIER

L'INSTITUT agro Montpellier

Aggregation of Arabinogalactan-Proteins from demineralized Acacia *seyal* gum in low hydration state: structural, hydration and physicochemical properties

Amandine ANTOINE-MICHARD

Ph.D. Thesis

Supervisors: Christian SANCHEZ and Michaël NIGEN

November, 2022

À mes grands-parents,

À Lyana.

« Au plus profond de nous dorment des trésors.
À nous de les découvrir, à nous d'inventer notre vie
pour qu'elle nous rende plus heureux, chaque jour,
et, peut-être, qu'elle participe à rendre ce monde plus beau. »

Cyril Dion

Acknowledgements

Ce travail a été réalisé au sein de l'UMR IATE de Montpellier, sous la direction de Monsieur Christian SANCHEZ, professeur des universités à l'université de Montpellier et la supervision de Monsieur Michaël NIGEN, maître de conférences à l'université de Montpellier. Ce projet de recherche est le fruit d'un partenariat industriel avec l'entreprise Alland & Robert. C'est donc tout naturellement que je commencerai par remercier notre partenaire **Alland & Robert** pour le financement de cette thèse CIFRE et en particulier **Frédéric ALLAND** et **Isabelle JAOUEN** pour avoir mis à ma disposition tous les moyens matériels et financiers nécessaires à la réussite de ce projet.

Merci à mes encadrants **Christian SANCHEZ** et **Michaël NIGEN** de m'avoir fait confiance. Au-delà de la qualité de votre encadrement scientifique qui m'a permis de me former de la meilleure des manières aux métiers de la recherche, merci pour votre investissement, vos conseils, votre patience, votre écoute, votre gentillesse, et votre grande disponibilité.

Je remercie également tous les membres de mon jury : **Sylvie MARCHESSEAU** (Université de Montpellier), **Michel GRISEL** (Université du Havre), **Marie-Hélène FAMELART** (INRAE Rennes), **Sami HALILA** (CERMAV Grenoble) et **Isabelle JAOUEN** (Alland & Robert) d'avoir accepté d'évaluer ces travaux de thèse et d'avoir amené des échanges aussi enrichissants lors de ma soutenance.

Merci aux membres de mon comité de thèse : **Anne BERGERET** (C2MA, Alès), **Carole SAUDEJAUD** (LGC, Toulouse) ainsi que **Jean-Yves DELENNE** (INRAE Montpellier) pour leurs suggestions et remarques intéressantes lors de mes comités.

Je remercie toutes les personnes extérieures à l'UMR IATE avec qui j'ai pu collaborer et acquérir de nouvelles connaissances dans le cadre de ce projet : **Pascale WILLIAMS** et **Thierry DOCO** à l'UMR SPO de Montpellier, **Alicia VALLET** et **Paul SCHANDA** de l'équipe RMN de l'IBS à Grenoble, **Audrey RIC** et **Frédéric VIOLLEAU** de la plateforme TFFFC de l'INP Purpan à Toulouse. J'ai beaucoup appris grâce à vous sur les techniques de caractérisation biochimique des gommes ainsi que l'analyse par AF4 et RMN.

Un grand merci à toutes les personnes de l'équipe I2M, et en particulier à **Céline** pour toute l'aide et les conseils précieux que tu as pu m'apporter au labo. Merci également à **Agathe** et **Margot** qui ont travaillé sur mon projet pendant leurs stages respectifs.

Mille mercis également à tous ceux qui ont partagé ces 4 ans avec moi à Montpellier...

- À tout l'orchestre d'harmonie de Montpellier Jacou et en particulier **Maria, Adrien, Chloé, Jérémy, Thomas, Léa, Valéry, Marion et Géraldine**, merci pour toutes ces jeudis soirs et weekends de répétition, ces concerts ensemble, ces vendredis soirs au QG place Candolle...

- À mes voisins et voisines de bureau **Maude, Maria, Camille, Pauline et Roxane**, merci pour votre bonne humeur, nos discussions qui coupaient un peu avec le rythme fou de la thèse, et surtout ... vos petits gâteaux !

- Aux anciens du labo : **Anaïs, Grégoire, Guilherme** merci de m'avoir accueillie comme il se doit à mes débuts à IATE. **Véro** merci de m'avoir partagé ton expérience sur la gomme et le labo ! **Dani** merci pour ta gentillesse, tes encouragements, les petits verres après le boulot (et mention spéciale pour ton anniversaire à Carnon !). **Naïco**, merci d'avoir toujours été volontaire pour une glace, un daïquiri, merci pour ton sens de l'humour, et tout le reste !

- À tous les membres de la team mie câline : **Alli, Aynura, Benj, Coco, Emma, Estelle, Fanny, Hélo, Marouane, Paulo, Seb, Camille, Chlochlo, Isa, Lulu**. Ces super collègues qui sont vite devenus des amis. Merci pour ces soirées et ces weekends *incroyables* aux quatre coins de la France, toutes ces aventures, tous ces restos et ces gâteaux partagés. Merci d'avoir illuminé mes journées par un sourire, un mot d'encouragement, un câlin réconfortant. Votre bienveillance et votre positivité m'ont permis de tout affronter.

Merci également à mes amis de longue date qui, d'un peu partout en France ou même plus loin ont toujours répondu présents pour m'épauler à distance. Merci à mes amis de Toulouse, pour ces retrouvailles au nouvel an à la Baule ou Paris. **Kevin**, thanks for filling the beginning of this PhD with poetic and joyful moments. **Olivia**, merci de partager quelques-uns de mes voyages, de me redonner confiance, me relever avec patience, et de me rappeler de quoi je suis capable à chaque fois. Ma folle **Mathilde**, merci d'être toujours là après 23 ans, des dizaines de concerts, la prépa et la thèse ! Je nous souhaite encore autant d'années l'une à côté de l'autre. **Charlène**, merci pour tes conseils précieux, ta bienveillance, et ta gentillesse. **Marinette**, merci d'être toujours partante pour un goûter, un squash (avec Gillou !) ou pour me retrouver à

Toulouse, Montpellier en Bretagne ou ailleurs ! **Christy**, merci d'être toujours là, de me rappeler que finalement je ne suis pas si peu sportive, et de m'avoir fait aimer un peu Paris (enfin surtout la boutique de Pierre Hermé) ! Merci d'être dans ma vie.

Enfin, je voudrais remercier du fond du cœur toute ma famille à qui je dois beaucoup : mes **grands-parents**, mes **parents**, ainsi que **Cécé, Erwan** et **Lyana** pour leur soutien et leur amour indéfectibles qui m'ont été si précieux malgré la distance qui nous séparait. Mention spéciale pour m'avoir supportée pendant le confinement, et à ma Cécé pour m'avoir offert le plus beau des cadeaux... Vous m'avez donné la motivation et la force pour me dépasser et tenir jusqu'au bout.

List of figures

List of tables

Abbreviations and symbols

AF4	Asymmetrical flow field-flow fractionation
AGP	Arabinogalactan-protein
A. *senegal*	Acacia *senegal* gum
A. *seyal*	Acacia *seyal* gum
BS	Backscattering intensity
CI	Creaming index
CPMG	Carrel-Purcell-Meiboom-Gill
dn/dC	Refractive index increment
D(4,3)	Volume mean diameter
E'	Interfacial elastic modulus
E"	Interfacial viscous modulus
Ea	Activation energy
EGEO	Ester gum/sweet orange essential oil
FTIR	Fourier transform infrared spectrocopy
G'	Storage modulus
G"	Loss modulus
GA	Acacia gum
HIC	Hydrophobic interaction chromatography
K_s	Bulk modulus
LS	Light scattering
MALLS	Multi-angle light scattering
M_w	Weight-averaged molar mass
N_A	Avogadro's number
NMR	Nuclear magnetic resonance
R_g	Gyration radius
R_h	Hydrodynamic radius
RI	Refractive index
SEC	Size exclusion chromatography
SEM	Scanning electron microscopy
SLS	Static light scattering
T	Trnasmittance intensity
T_2	Spin-spin relaxation time
TD-NMR	Time-domain nuclear magnetic resonance
TSI	Turbiscan scanning index
v_s	Ultrasound velocity
$V°_s$	Partial specific volume
$\beta°_s$	Partial specific adiabatic compressibility coefficient
γ	Interfacial tension
η	Apparent viscosity
π	Surface pressure
ρ	Density
ϕ	Volume fraction
ω	Angular velocity

Table of contents

GENERAL INTRODUCTION

Acacia gum (GA), also called gum arabic, is a natural edible dried gummy exudate collected from Acacia *senegal* and Acacia *seyal* trees (Figure 1). It is defined by the Joint FAO/WHO Expert Committee on food Additives as a "dried exudation obtained from the branches of A. Senegal (L) Willdenow or close species from Acacia (Leguminosae family)" (FAO., 1999). Acacia trees generally exudate in response to an environmental stress such as extreme weather conditions, microbial attack or animal injuries, and may be promoted by the tapping of trees. The Acacia gum production is a defense mechanism of Acacia trees to prevent dehydration, to heal wounds, and prevent insect and mold invasion (Figure 1). GA is mainly produced by Acacia trees located in in arid zones of sub-Saharan Africa (named gum belt region, Figure 2) spreading from Senegal (West) to Ethiopia (East) (Cecil, 2005). The main producer of GA by far is Sudan (66% of total exportations), followed by Chad (13%) and Nigeria (8%). These three countries alone account for 90% of total exportations of crude Acacia gums. Among importing countries, France and India represent 75% of the global crude Acacia gums imports in 2014-2016 (*Commodities at a Glance*, 2018).

Figure 1. Exudation of gum nodules from an Acacia tree after tapping of its trunk.

Figure 2. Acacia gum belt region includes sub-Saharan countries: from Senegal to Ethiopia, the harvest zone covers Mauritania, Mali, Nigeria, Niger, Chad and Sudan. Adapted from ALLAND&ROBERT website.

Among all natural gums, GA is probably one of the first to have been used by humans, since its first reported uses date back to the Stone Age when it served as adhesive in manufacturing of composite tools (Sanchez et al., 2018; Zipkin et al., 2014). In Ancient Egypt, GA was also used as an adhesive to make wrapping for the mummies, and as an ingredient in the preparation of curative recipes (Sanchez et al., 2018). Since then, the scope of applications involving GA significantly increased due to its very interesting structural, biochemical and physicochemical properties. As a food additive, coded E414 in Europe, as well as in non-food applications, GA is used as emulsifier, stabilizer, thickener, humectant, bulking agent, coating agent, or antioxidant (Touré, 2008; Verbeken et al., 2003; Wickens et al., 1995).

In addition to their physicochemical properties, Acacia gums as well as Acacia trees also appear as strategic and relevant assets on environmental, societal and economical aspects for the producing countries. In environmental terms, Acacia tree plantation has become a way to fight desertification and mitigate climate change. Acacia trees contribute to increase soil fertility and other crops yields by fixing nitrogen into the soil (Abdou et al., 2014). They also stabilize the soil thanks to a highly developed rooting system (Djibo et al., 2016; Wickens et al., 1995). Therefore, developing GA production contributes to the "Great Green Wall" project, aiming at promoting sustainable agriculture and forestry, soil improvement and ecosystems enhancement, while improving food safety and ensuring economic and geopolitical stability in the Sahel region, which is particularly vulnerable to climate change (Berrahmouni et al., 2014;

Goffner et al., 2019). Wild and Acacia plantation trees, especially the harvest of Acacia gums also contribute to societal and economical purposes by providing jobs to rural populations, and limiting migratory flows. In producing countries, Acacia gum is important for farmers as it is usually their only source of income. The economic importance of this product for producing countries is related in Figure 3, showing the steady growing of Acacia gum exportations since 1990. Crude GA global exportations have surged over the last 25 years to reach around 120,000 tons in 2016 (Figure 3).

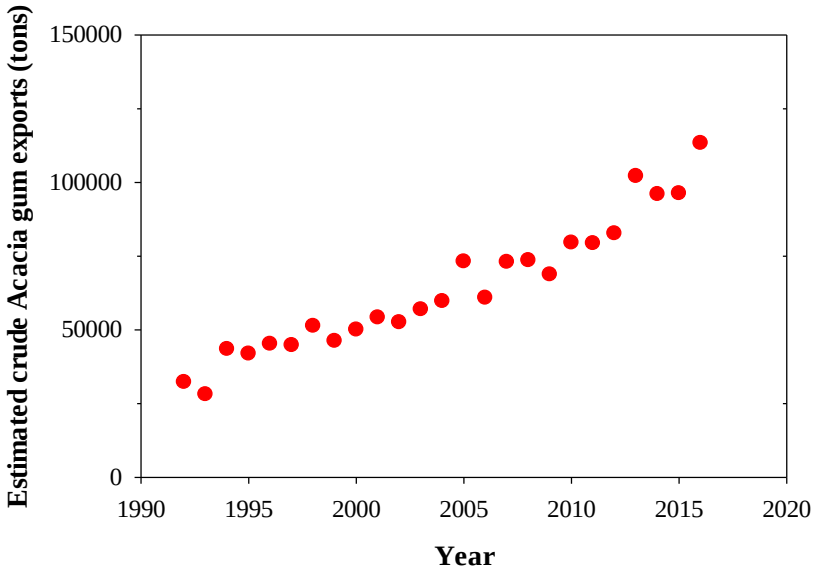

Figure 3. Estimated crude Acacia gum exports, from 1992 to 2016. From (Commodities at a glance, 2018)

This growing demand, confirmed since 2016, combined with an irregular production due to political instability of producing countries and variable climatic conditions (including droughts) gave rise to new challenges for GA industries. The first of them is to ensure a constant GA quality in spite of varying production, harvest, and processing conditions (in particular storage and transport). The second objective is to better understand the links between the composition, the structure and the functionality of Acacia gums. Within this context, a research program, called the DIVA program, was started in 2012 between the JRU (Joint Research Unit) IATE (Agropolymer Engineering and Emerging Technologies) in Montpellier and the French Company ALLAND&ROBERT, the second most important world producer of natural exudates, specialized in Acacia and karaya gums.

To meet these objectives, several projects have been led on various topics in our research group, including the fractionation of Acacia gums by ion exchange and hydrophobic interaction chromatography (Apolinar-Valiente, Williams, et al., 2020) and the characterization of the biochemical composition and structural properties of Acacia gums and their fractions (Apolinar-Valiente et al., 2019; Lopez-Torrez et al., 2015a). In relation to these projects, others investigated and characterized the solution (Mejia Tamayo et al., 2018), interfacial (Aphibanthammakit et al., 2018; Davantès et al., 2019; Renard et al., 2022) and emulsifying properties (Aphibanthammakit et al., 2020) of gums, their colloidal stabilizing properties in red wine (Anaya Castro et al., 2021; Apolinar-Valiente, Salmon, et al., 2020; Nigen et al., 2019) and their aggregation properties (Barbar, 2016; Lopez-Torrez, 2016).

Regarding the question of aggregation, it was observed recently that demineralized Acacia *seyal* gum (*i.e.* arabic acid) was difficult to disperse in water because of its aggregation propensity (Charbonnel, 2017). This aggregation behavior was especially observed when arabic acid powders were stored during several months at ambient temperature. These observations were seen as an opportunity to explore the assembly properties of gums and form the basis of my Ph.D. project. It benefited from a doctoral fellowship CIFRE and was conducted in the I2M (Soft Matter Engineering) team of the JRU IATE. In this project, I aimed to study the influence of storage conditions on the structural, and physicochemical properties of arabinogalactan-proteins (AGPs) from demineralized spray-dried Acacia *seyal* gum. This project provided new knowledge on the assembly properties of demineralized gums during storage and more specifically on the crucial role of AGP-mineral interactions in the structure and stability of Acacia gums.

The following manuscript is divided in seven chapters based on four research articles, one in publication and three in preparation.

The **chapter I** presents an overview of the properties of GA, with a focus on the aggregation properties of its AGPs. The **chapter II** identifies the materials, analytical methods and experimental protocols used or developed in this study.

The **chapter III** focuses on the aggregation kinetics of demineralized A. *seyal* gum powder at different temperatures (25 – 70°C). The structural properties of the aggregates formed all along the kinetics were evaluated. This chapter is based on a research article submitted in International Journal of Biological Macromolecules. The objective of this part was to identify and establish the relationships between the storage conditions of Acacia *seyal* gums and the aggregation of arabinogalactan-proteins (AGPs) from arabic acid. This study enabled us to identify the operating conditions leading to the formation of soluble and insoluble aggregates. In this chapter, the influence of incubation time and temperature of spray-dried gum powders were studied. The biochemical composition (sugar, amino acids and minerals) of the gum powders before and after their dry incubation was characterized. The structural properties of these AGPs were characterized by steric exclusion chromatography (SEC) coupled with quadruple detections (UV, MALLS, Viscometry, RI) and asymmetrical flow field-flow fractionation (AF4) coupled with MALLS and RI. The structural properties of AGPs were also determined by AF4 MALLS in collaboration with Purpan Engineering School in Toulouse, which is equipped with a platform dedicated to this technique. The size and shape of insoluble aggregates formed during incubation were approached by SLS and optical and SEM microscopy.

In **chapter IV**, the hydration properties of AGP aggregates were assessed using FTIR in combination with low-field ^{H}NMR and volumetric methods (sonodensimetry). The partial specific volume and adiabatic compressibility of AGPs – which are two thermodynamic parameters particularly sensitive to hydration – were characterized in a volumetric study. Water dynamics were further assessed by measurement of the proton transverse spin-spin relaxation times (T_2) by Time-Domain Nuclear Magnetic Resonance (TD-NMR). Finally, Fourier transform infrared spectroscopy (FTIR) was used to identify changes in AGP vibration energy during Acacia gum demineralization.

The mechanism of aggregation was studied by characterizing the interactions involved in the aggregation mechanism. The **chapter V** describes the impact of the physicochemical properties of the solvent (ionic strength, pH, presence of a chaotropic agent) on the structural stability of AGP aggregates. The impact of these physicochemical changes on the molar mass and size distributions of AGPs and aggregates was monitored by chromatographic, scattering (SLS, turbidimetry) and microscopic methods. The characterization of chemical groups or bonds involved in this aggregation mechanism was attempted using high-field ^{13}C NMR and IR spectroscopy. NMR characterization was made in collaboration with the NMR research group of the "Institut de Biologie Structurale" (IBS) in Grenoble, specialized in the NMR characterization of proteins.

Chapter VI is devoted to the comparison of the physicochemical properties of aggregates obtained by the dry-state incubation of demineralized Acacia *seyal* gums with those of native A. *seyal* gum. In this section, rheological, interfacial, and emulsifying properties were studied. The objective was to identify the storage conditions leading to an improvement of the physicochemical properties of Acacia gum and/or giving birth to new potential applications. The physicochemical properties of native AGPs (*e.g.* the surface and rheological properties) as well as those of the soluble and insoluble aggregates formed during storage were studied, respectively by the rising drop method (interfacial tension, interfacial dilational rheology) and rheometry (flow curves, viscoelasticity measurements). Emulsifying properties of aggregates were evaluated by the production of emulsions and the optical characterization of their colloidal stability (SLS and turbidimetry).

The **chapter VII** presents the general conclusions and discusses the perspectives of this work.

La gomme d'acacia (GA), aussi appelée gomme arabique est un exsudat gommeux naturel séché et comestible sécrété par les espèces *senegal* et *seyal* des arbres de genre Acacia (Figure 1). Elle est définie par le comité d'experts en additifs alimentaires de la FAO/WHO comme un "exsudat séché obtenu des branches d'Acacia Senegal (L) Willdenow ou d'espèces d'acacia apparentées (de la famille Leguminosae)" (FAO., 1999). Les acacias produisent généralement de la gomme en réponse à un stress environnemental tel que des conditions météorologiques drastiques, une invasion microbienne ou des blessures causées par des animaux, et l'exsudation des acacias est également favorisée par le tapping. La production de gomme d'acacia est considérée comme un mécanisme de défense de l'acacia pour prévenir la déshydratation, guérir les blessures et prévenir l'invasion d'insectes et de moisissures (Figure 4). La GA est principalement produite par des acacias situés dans les zones arides d'Afrique subsaharienne (appelées ceinture de gomme, Figure 5) qui s'étend du Sénégal à l'ouest à l'Éthiopie à l'est (Cecil, 2005). Le principal producteur de GA est de loin le Soudan (66% des exportations totales), suivi du Tchad (13%) et du Nigeria (8%). Ces trois pays représentent à eux seuls 90% des exportations totales de gomme brute. Parmi les pays importateurs, en 2014-2016, la France et l'Inde représentaient 75% des importations mondiales de gommes d'acacia brutes (*Commodities at a Glance*, 2018).

Figure 4. Exsudation de nodules de gomme par un acacia après le tapping de son tronc.

Figure 5. La région de la ceinture de gomme en Afrique subsaharienne : du Sénégal à l'Éthiopie, la zone de récolte inclut la Mauritanie, le Mali, le Nigeria, le Niger, le Tchad et le Soudan. Adapté du site web d'ALLAND&ROBERT.

Parmi toutes les gommes naturelles, la GA est probablement l'une des premières à avoir été utilisée par l'homme puisque ses premières utilisations remontent à l'âge de pierre, où elle servait d'adhésif dans la fabrication d'outils en matériaux composite (Sanchez et al., 2018; Zipkin et al., 2014). Dans l'Égypte ancienne, la GA était également utilisée comme adhésif dans la fabrication des bandelettes pour les momies, et comme ingrédient dans la préparation de recettes curatives (Sanchez et al., 2018). Depuis lors, le champ d'applications de la GA a considérablement augmenté en raison de ses propriétés structurales, biochimiques et physicochimiques particulièrement intéressantes. La GA est utilisée comme émulsifiant, stabilisant, épaississant, humectant, agent d'enrobage ou antioxydant que ce soit en tant qu'additif alimentaire (E414 en Europe) ou dans des applications non alimentaires (Touré, 2008; Verbeken et al., 2003; Wickens et al., 1995).

En plus de leurs propriétés physico-chimiques, les gommes d'acacia ainsi que les acacias apparaissent pour les pays producteurs comme des atouts d'un point de vue environnemental, sociétal et économique. Sur le plan environnemental, la plantation d'acacias est devenue un moyen de lutter contre la désertification et d'atténuer les effets du changement climatique. Les acacias contribuent à augmenter la fertilité des sols et le rendement d'autres cultures en fixant l'azote dans le sol (Abdou et al., 2014). Ils stabilisent également le sol grâce à un système racinaire très développé (Djibo et al., 2016; Wickens et al., 1995). Ainsi, développer la production de GA contribue au projet de la " Grande Muraille Verte " visant à favoriser une agriculture et une sylviculture plus durables par l'amélioration des sols et la valorisation des

écosystèmes, tout en améliorant la sécurité alimentaire et en assurant la stabilité économique et géopolitique de la région du Sahel, particulièrement vulnérable au changement climatique (Berrahmouni et al., 2014; Goffner et al., 2019). Les acacias sauvages ou provenant de plantations, et notamment la récolte de la GA, remplissent également des objectifs sociétaux et économiques en fournissant des emplois aux populations rurales et en limitant les flux migratoires. Dans les pays producteurs, les gommes d'acacia sont importantes pour les agriculteurs car elles constituent souvent leur seule source de revenus. L'importance économique de ce produit est illustrée dans la figure 6 ci-dessous qui montre que les exportations de gomme d'acacia n'ont cessé de croitre depuis 1990. Elles ont été multipliées par 4 au cours des 25 dernières années pour atteindre environ 120 000 tonnes en 2016 (Figure 6).

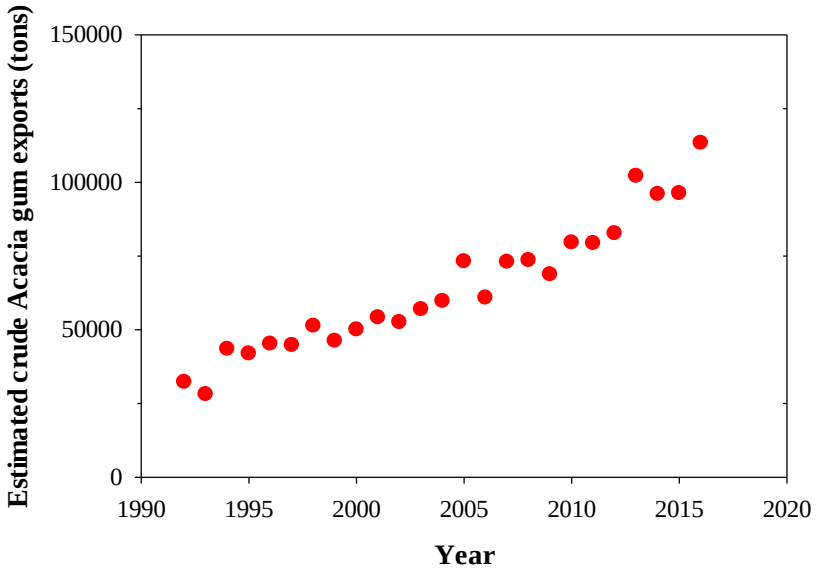

Figure 6. Estimation des exportations de gomme d'acacia brute entre 1992 to 2016. Tiré de (Commodities at a glance, 2018).

Cette demande croissante qui s'est confirmée depuis 2016, ajoutée à une production irrégulière due à l'instabilité politique des pays producteurs ainsi qu'à des conditions climatiques variables (avec notamment des épisodes de sécheresses) a fait émerger de nouveaux défis pour les industriels de la GA. Le premier d'entre eux est d'assurer une qualité de gomme constante malgré des conditions de production, de récolte et de transformation variables (en particulier pendant le stockage et le transport). Le second objectif est de mieux comprendre les liens entre la composition, la structure et la fonctionnalité des gommes d'acacia. Dans ce contexte, un programme de recherche appelé programme DIVA a été initié en 2012 entre l'UMR (Unité Mixte de Recherche) IATE (Ingénierie des Agropolymères et Technologies Emergentes) de

Montpellier et l'entreprise française ALLAND&ROBERT, deuxième producteur mondial d'exsudats naturels, spécialisée dans les gommes d'acacia et la gomme karaya.

Pour répondre à ces objectifs, dans notre groupe de recherche, plusieurs projets ont été menés dans différents domaines avec notamment le fractionnement des gommes d'acacia par chromatographie échangeuse d'ions et chromatographie d'interaction hydrophobe (Apolinar-Valiente, Williams, et al., 2020) et la caractérisation de la composition biochimique et des propriétés structurales des gommes d'acacia et de leurs fractions (Apolinar-Valiente et al., 2019; Lopez-Torrez et al., 2015a). Dans le cadre de ce programme, d'autres projets ont étudié et caractérisé les propriétés des gommes en solution (Mejia Tamayo et al., 2018), aux interfaces (Aphibanthammakit et al., 2018; Davantès et al., 2019; Renard et al., 2022) et émulsifiantes (Aphibanthammakit et al., 2020), leurs propriétés de stabilisation colloïdale dans le vin rouge (Anaya Castro et al., 2021; Apolinar-Valiente, Salmon, et al., 2020; Nigen et al., 2019) ainsi que leurs propriétés d'agrégation (Barbar, 2016; Lopez-Torrez, 2016).

En ce qui concerne l'agrégation, il a été observé récemment qu'il était difficile de disperser la gomme d'acacia *seyal* déminéralisée (acide arabique) dans l'eau en raison de sa tendance à l'agrégation (Charbonnel, 2017). La dispersion a été d'autant plus difficile après le stockage de poudres d'acide arabique à température ambiante pendant plusieurs mois. Ce résultat nous a donné l'occasion d'explorer plus en détail les propriétés d'assemblage des gommes qui sont à la base de mon projet de thèse. Ma thèse a bénéficié d'une bourse de thèse CIFRE et a été menée dans l'équipe I2M (Ingénierie de la Matière Molle) de l'UMR IATE. Dans ce projet, j'ai cherché à étudier l'influence des conditions de stockage sur les propriétés structurales et physico-chimiques des arabinogalactane-protéines (AGP) de gomme d'Acacia *seyal* déminéralisée séchée par atomisation. Ce projet a apporté de nouvelles connaissances sur les propriétés d'assemblage des gommes déminéralisées pendant leur stockage et plus particulièrement sur le rôle crucial des interactions entre AGPs et minéraux sur la structure et la stabilité des gommes d'acacia.

Ce manuscrit est divisé en sept chapitres basés sur quatre articles scientifiques, un en cours de publication et trois en préparation.

Le **chapitre I** donne un aperçu des propriétés de la GA en mettant l'accent sur les propriétés d'agrégation de ses AGPs. Le **chapitre II** identifie le matériel, les méthodes analytiques et les protocoles expérimentaux utilisés ou développés dans cette étude.

Le **chapitre III** se concentre sur la cinétique d'agrégation de la poudre de gomme A. *seyal* déminéralisée à différentes températures (25-70°C). Les propriétés structurales des agrégats formés tout au long de la cinétique ont été évaluées. Ce chapitre est basé sur un article de recherche soumis dans International Journal of Biological Macromolecules. L'objectif de cette partie était d'identifier et d'établir les relations entre les conditions de stockage des gommes d'A. *seyal* et l'agrégation des arabinogalactanes-protéines (AGP) d'acide arabique. Cette étude nous a permis d'identifier les conditions opératoires conduisant à la formation d'agrégats solubles et insolubles. Dans ce chapitre, l'influence du temps et de la température de stockage des poudres de gomme séchées par atomisation a été étudiée. La composition biochimique (en sucres, acides aminés et minéraux) des poudres de gomme avant et après leur incubation à sec a été caractérisée. Les propriétés structurales de ces AGPs ont été caractérisées par chromatographie d'exclusion stérique (SEC) couplée à un quadruple détecteur (UV, MALLS, Viscométrie, RI). Les propriétés structurales des AGPs ont également été déterminées par fractionnement par couplage flux-force (AF4) en collaboration avec l'école d'ingénieurs de Purpan à Toulouse, qui est équipée d'une plateforme dédiée à cette technique. La taille et la forme des agrégats insolubles formés pendant l'incubation ont été étudiées par granulométrie laser, par microscopie optique et microscopie électronique à balayage (MEB).

Dans le **chapitre IV**, les propriétés d'hydratation des agrégats d'AGPs ont été évaluées en utilisant la spectroscopie infrarouge à transformée de Fourier (FTIR) en combinaison avec la ^{1}H RMN bas-champs et des méthodes volumétriques (sonodensimétrie). Le volume spécifique partiel et la compressibilité adiabatique des AGPs - qui sont deux paramètres thermodynamiques particulièrement sensibles à l'hydratation - ont été caractérisés dans une étude volumétrique. Des informations sur la dynamique de l'eau ont également été obtenues en mesurant les temps de relaxation spin-spin transverses des protons (T_2) par RMN bas-champs. Enfin, la FTIR a été utilisée pour identifier les changements d'énergie de vibration des AGPs au cours de la déminéralisation de la gomme d'acacia.

Les interactions impliquées dans le mécanisme d'agrégation ont été caractérisées.

Le **chapitre V** décrit l'impact des propriétés physico-chimiques du solvant (force ionique, pH, présence d'un agent chaotropique) sur la stabilité structurale des agrégats d'AGPs. L'impact de ces changements physico-chimiques sur les distributions de masse molaire et de taille des AGPs et des agrégats a été suivi par des méthodes chromatographiques, de diffusion (granulométrie laser, turbidimétrie) et microscopiques. La RMN du carbone et la spectroscopie infrarouge ont été utilisées pour tenter de caractériser des groupes ou des liaisons chimiques qui pourraient être impliqués dans ce mécanisme d'agrégation. Les analyses RMN ont été faites en collaboration avec le groupe de recherche RMN de l'Institut de Biologie Structurale (IBS) de Grenoble, spécialisé dans la caractérisation RMN des protéines.

Le **chapitre VI** est consacré à la comparaison des propriétés physico-chimiques des agrégats obtenus par l'incubation en voie sèche des gommes d'A. *seyal* déminéralisées avec celles de la gomme A. *seyal* native. Dans cette section, les propriétés rhéologiques, interfaciales et émulsifiantes ont été étudiées. L'objectif était d'identifier les conditions de stockage qui permettaient une amélioration des propriétés physico-chimiques de la gomme d'acacia et/ou donnaient naissance à de nouvelles applications potentielles. Les propriétés physico-chimiques des AGPs natives (propriétés rhéologiques et de surface par exemple) ainsi que celles des agrégats solubles et insolubles formés pendant le stockage ont été étudiées, par rhéométrie (courbes d'écoulement, mesures de viscoélasticité) et par la méthode de la goutte montante (tension interfaciale, rhéologie de dilatation interfaciale). Les propriétés émulsifiantes des agrégats ont quant à elles été évaluées en formulant des émulsions et en caractérisant leur stabilité colloïdale (par granulométrie laser et turbidimétrie).

Le **chapitre VII** présente les conclusions générales et discute des perspectives de ce travail.

References

Abdou, M., Mayaki, Z., Kadri, A., Karimou, J., & Lamso, N. (2014). Effet de l'arbre Acacia senegal sur la fertilité des sols de gommeraies au Niger. *International Journal of Biological and Chemical Sciences*, *7*, 2328–2337. https://doi.org/10.4314/ijbcs.v7i6.13

Anaya Castro, M., Nigen, M., Apolinar-Valiente, R., Iturmendi, N., Williams, P., Doco, T., Moine, V., Massot, A., Jaouen, I., & Sanchez, C. (2021). Stabilisation de la matière colorante d'un vin rouge jeune. *La Revue des Œnologues*, *181*, 47–49.

Aphibanthammakit, C., Barbar, R., Nigen, M., Sanchez, C., & Chalier, P. (2020). Emulsifying properties of Acacia senegal gum: Impact of high molar mass protein-rich AGPs. *Food Chemistry: X*, *6*, 100090. https://doi.org/10.1016/j.fochx.2020.100090

Aphibanthammakit, C., Nigen, M., Gaucel, S., Sanchez, C., & Chalier, P. (2018). Surface properties of Acacia senegal vs Acacia seyal films and impact on specific functionalities. *Food Hydrocolloids*, *82*, 519–533. https://doi.org/10.1016/j.foodhyd.2018.04.032

Apolinar-Valiente, R., Salmon, T., Williams, P., Nigen, M., Sanchez, C., Marchal, R., & Doco, T. (2020). Improvement of the foamability of sparkling base wines by the addition of Acacia gums. *Food Chemistry*, *313*, 126062. https://doi.org/10.1016/j.foodchem.2019.126062

Apolinar-Valiente, R., Williams, P., Nigen, M., Tamayo, V. M., Doco, T., & Sanchez, C. (2019). Recovery, structure and physicochemical properties of an aggregate-rich fraction from Acacia senegal gum. *Food Hydrocolloids*, *89*, 864–873. https://doi.org/10.1016/j.foodhyd.2018.11.054

Apolinar-Valiente, R., Williams, P., Nigen, M., Tamayo, V. M., Doco, T., & Sanchez, C. (2020). Fractionation of Acacia seyal gum by ion exchange chromatography. *Food Hydrocolloids*, *98*, 105283. https://doi.org/10.1016/j.foodhyd.2019.105283

Berrahmouni, N., Tapsoba, F., & Berte, C. J. (2014). The Great Green Wall for the Sahara and the Sahel initiative: Building resilient landscapes in African drylands. In *Genetic considerations in ecosystem restoration using native tree* (pp. 15–18).

Cecil, C. O. (2005). Gum arabic. *Saudi Aramco World*, *56*(2), 36–39.

Davantès, A., Nigen, M., Sanchez, C., D'Orlando, A., & Renard, D. (2019). Adsorption of Hyperbranched Arabinogalactan-Proteins from Plant Exudate at the Solid–Liquid Interface. *Colloids and Interfaces*, *3*, 49. https://doi.org/10.3390/colloids3020049

Djibo, E., Lawali, S., Aichatou, A., Issoufou, H., Abdou, M., Zoubeirou, A., & Mayaki, A. (2016). Local perceptions of climate change and adaptation strategies in the management of Acacia senegal parks in Niger. *Journal of Biodiversity and Environmental Sciences*, *9*(1), 319–328.

FAO. (1999). Gum Arabic. In *Food and nutrition paper* (Vols. 52, addendum 7). https://www.fao.org/3/X3860e/X3860E20.htm#P5107_110391

Goffner, D., Sinare, H., & Gordon, L. J. (2019). The Great Green Wall for the Sahara and the Sahel Initiative as an opportunity to enhance resilience in Sahelian landscapes and livelihoods. *Regional Environmental Change*, *19*(5), 1417–1428. https://doi.org/10.1007/s10113-019-01481-z

Lopez-Torrez, L., Nigen, M., Williams, P., Doco, T., & Sanchez, C. (2015). Acacia senegal vs. Acacia seyal gums – Part 1: Composition and structure of hyperbranched plant exudates. *Food Hydrocolloids*, *51*, 41–53. https://doi.org/10.1016/j.foodhyd.2015.04.019

Mejia Tamayo, V., Nigen, M., Apolinar-Valiente, R., Williams, P., Doco, T., Renard, D., & Sanchez, C. (2018). *Flexibility and*

hydration of amphiphilic hyperbranched Arabinogalactan-protein from plant exudate: A volumetric perspective. https://doi.org/10.3390/colloids2010011

Nigen, M., Valiente, R. A., Iturmendi, N., Williams, P., Doco, T., Moine, V., Massot, A., Jaouen, I., & Sanchez, C. (2019). The colloidal stabilization of young red wine by Acacia senegal gum: The involvement of the protein backbone from the protein-rich arabinogalactan-proteins. *Food Hydrocolloids*, *97*, 105176. https://doi.org/10.1016/j.foodhyd.2019.105176

Renard, D., Davantès, A., D'orlando, A., Cahier, K., Molinari, M., Nigen, M., Chalier, P., & Sanchez, C. (2022). Adsorption of arabinogalactan-proteins from Acacia gums (senegal and seyal) and its molecular fractions onto latex particles. *Food Hydrocolloids*, *125*, 107360. https://doi.org/10.1016/j.foodhyd.2021.107360

Sanchez, C., Nigen, M., Mejia Tamayo, V., Doco, T., Williams, P., Amine, C., & Renard, D. (2018). Acacia gum: History of the future. *Food Hydrocolloids*, *78*, 140–160. https://doi.org/10.1016/j.foodhyd.2017.04.008

Touré, S. (2008). *Gum Arabic*. Market News Service (MNS) (Quaterly edition). International Trading Center. https://ngara.org/pdf/GumArabic_MarketNewsService%20Issue1_08.pdf

Verbeken, D., Dierckx, S., & Dewettinck, K. (2003). Exudate gums: Occurrence, production, and applications. *Applied Microbiology and Biotechnology*, *63*(1), 10–21. https://doi.org/10.1007/s00253-003-1354-z

Wickens, G. E., Seif ElDin, A. G., Sita, G., & Nahal, I. (1995). *Role of Acacia Species in the Rural Economy of Dry Africa and the Near East*. Food & Agriculture Org.

Zipkin, A., Wagner, M., McGrath, K., Brooks, A., & Lucas, P. (2014). An Experimental Study of Hafting Adhesives and the Implications for Compound Tool Technology. *PloS One*, *9*, e112560. https://doi.org/10.1371/journal.pone.0112560

CHAPTER I.

STATE OF THE ART

1. Acacia gums

Hyperbranched macromolecules from Acacia gum are arabinogalactan proteins (AGPs) that belong to the glycoproteins family, together with Proline (Pro)-rich proteins and extensins (Showalter, 2001). These AGPs are ubiquitous in plant kingdom, where they are generally found in leaves, stems, roots, floral parts and seeds (Fincher et al., 1983). Mainly located in cell walls and plasma membranes, they fulfil many functions in plant growth and development including embryogenesis, cell proliferation, Ca^{2+} signaling, cell differentiation, pollen grain development and programmed cell death (Ellis et al., 2010; Showalter, 2001).

1.1. Biochemical composition and structure of AGPs from GA

AGPs are characterized by *(i)* a Hydroxyproline-rich protein backbone (<10 wt%), *(ii)* decorated with polysaccharidic units (> 90 wt%), mainly arabinose and galactose, and *(iii)* the presence of a glycosylphosphatidylinositol (GPI) membrane anchor (Ellis et al., 2010; Showalter, 2001). These AGPs are commonly identified using their ability to bind the β-glucosyl Yariv's reagent (Yariv et al., 1967).

Naturally, GA is a mixed salt of a complex polysaccharide acid (arabic acid). GA is composed of more than 90% of sugars, with a small protein fraction (1 – 3%) and some minor components, which are mainly cationic minerals, including Na, K, Ca and Mg (Debon & Tester, 2001; Idris et al., 1998; Kunkel et al., 1997) and small amounts of polyphenols (Sanchez et al., 2018). The sugar composition, the protein content, as well as the moisture content have been reported to depend on the age and the location of the trees (Idris et al., 1998).

The chemical composition of GA is given in Table I.1. Both gums contain a similar mineral content but A. *senegal* gum contains a higher content in protein (1.5 – 2.6%) than A. *seyal* gum. Both gums are rich in arabinose and galactose, with lower amounts of rhamnose and glucuronic acids. However, the distribution in sugars is somehow different between the two gums with A. *seyal* gum composed of more arabinose (48.5%) than galactose (34.2%), while A. *senegal* being richer in galactose (39 – 42%) than arabinose (24 – 27%). Values of arabinose/galactose ratio around 0.6 for A. *senegal* and 1.3 for A. *seyal* are classically reported (Idris et al., 1998; Islam et al., 1997; Lopez-Torrez et al., 2015a; Nie et al., 2013; Renard et al., 2006). The content in rhamnose and glucuronic acid is also higher for A. *senegal* gums. The carbohydrate structure of GA consists of a core of 1,3-linked β-D-galactopyranosyl units and

the branched structure mainly consists of 1,3-linked β-D-galactopyranosyl units with 1,6-linkages (Defaye & Wong, 1986; Islam et al., 1997; Renard et al., 2012; Street & Anderson, 1983). However, A. *senegal* contain more terminal units and more ramified residues than A. *seyal*, which is composed, in contrast, of long arabinosyl side chains (Lopez-Torrez et al., 2015a; Nie et al., 2013).

Table I.1. Chemical composition of Acacia gums. Adapted from (Aphibanthammakit, 2018; Gashua et al., 2015; Idris et al., 1998; Jurasek et al., 1995; Nie et al., 2013)

	A. *seyal*			A. *senegal*		
Galactose %	37.2	±	3.7	41.8	±	2.6
Arabinose %	47.5	±	4.1	27.1	±	1.7
Rhamnose %	2.4	±	0.9	14.5	±	1.5
Uronic acids %	12.8	±	2.1	16.7	±	1.0
Minerals %	4.0	±	0.1	3.4	±	0.1
Protein %	1.1	±	0.3	2.1	±	0.4
Moisture %	10.7	±	0.0	13.4	±	1.8

The amino acid composition of GA (Table I.2) has been well elucidated (Jurasek et al., 1993, 1995; Lopez-Torrez et al., 2015a) but the amino acid sequence remains unknown. Both gums contain the same amino acids, mainly hydroxyproline, serine, leucine and proline, which account for more than 56% of the total amino acids content. It may be noticed the amount of aspartic and glutamic acids is significantly larger for A. *senegal*, with possible consequences on electrostatic interaction properties.

Table I.2. Amino acid composition of GA in dry basis (mean ± standard deviation). From (Lopez-Torrez et al., 2015)

Amino acid ($mg \cdot g^{-1}$)	A. *seyal*			A. *senegal*		
Alanine	0.22	±	0.01	0.49	±	0.04
Arginine	0.12	±	0.00	0.31	±	0.05
Aspartic acid	0.49	±	0.04	1.24	±	0.04
Glutamic acid	0.28	±	0.00	0.92	±	0.01
Glycine	0.25	±	0.07	0.79	±	0.00
Histidine	0.27	±	0.01	1.37	±	0.01
Hydroxy proline	**2.13**	**±**	**0.19**	**6.26**	**±**	**0.52**
Isoleucine	0.13	±	0.01	0.31	±	0.02
Leucine	**0.60**	**±**	**0.03**	**1.83**	**±**	**0.04**
Lysine	0.12	±	0.01	0.63	±	0.02
Phenylalanine	0.21	±	0.01	0.82	±	0.05
Proline	**0.56**	**±**	**0.00**	**1.61**	**±**	**0.14**
Serine	**0.95**	**±**	**0.03**	**2.50**	**±**	**0.05**
Threonine	0.34	±	0.02	1.42	±	0.02
Tyrosine	0.14	±	0.02	0.31	±	0.04
Valine	0.31	±	0.07	0.71	±	0.00
Total	**7.1**	**±**	**0.16**	**21.5**	**±**	**0.47**

In terms of mineral composition, both gums are rich in cations, mainly calcium, magnesium and potassium, but A. *senegal* gum contains a higher amount of potassium than calcium whereas A. *seyal* gum is way richer in calcium than potassium (Table I.3). Yet, AGPs from GA can tightly bind Ca^{2+} via their glucuronic acid (GlcA) moieties, with a 2:1 GlcA:Ca^{2+} binding stoichiometry and a $K_d \sim 6.5$ µM binding constant at pH 5 (Lamport & Várnai, 2013; Lopez-Hernandez et al., 2020). Lamport suggested that AGPs act as a Ca^{2+} capacitor in order to regulate plant growth and development (Lamport et al., 2014; Lamport & Várnai, 2013).

The differences between the total mineral content found in Table I.1 and Table I.3 might arise from the different mineral quantification methods used, *i.e.* the ash method for the total mineral content and the atomic absorption spectrophotometry (AAS) or atomic emission spectrophotometry (AES) for the determination of the mineral composition.

Table I.3. Mineral composition of GA in dry basis (mean ± standard deviation). From (Buffo et al., 2001; Debon and Tester, 2001; Kunkel et al., 1997; Mhinzi, 2003).

Mineral (%)	A. *seyal*	A. *senegal*
Na	Traces	Traces
Mg	0.11 ± 0.03	0.17 ± 0.03
K	0.25 ± 0.08	0.78 ± 0.07
Ca	0.91 ± 0.17	0.62 ± 0.08
Fe	Traces	Traces
Total	**1.28 ± 0.25**	**1.58 ± 0.12**

In terms of structure, both gums are polydisperse and A. *seyal* has a higher average molar mass (M_w = 8.2·10^5 g·mol^{-1}) than A. *senegal* (M_w = 6.8·10^5 g·mol^{-1}), coupled with a lower intrinsic viscosity indicating a smaller hydrodynamic volume, possibly due to a more packed structure (Al-Assaf et al., 2005a; Gashua et al., 2015; Lopez-Torrez et al., 2015a). More details about the conformation were obtained from studying relationships between the intrinsic viscosity $[\eta]$ (Mark-Houwink-Sakurada (MHS) conformation plots, Figure I.1) or the hydrodynamic radius R_h and the molar mass M_w (Figure I.2). When plotting MHS conformation plots, α power law exponent values ranging from 0 (sphere) to 1.8 (rod) are generally admitted, with intermediate values of 0.5 – 0.8 for flexible or hyperbranched polymers. The MHS plot from A. *seyal* was characterized by one slope with an exponent value of 0.28, whereas A. *senegal* displayed three slopes with exponent values of 0.44, 0.78, and 0.44 (0.55 in average) for AGPs with M_w below 5.4·10^5 g·mol^{-1}, between 5.4·10^5 and 1.3·10^6 g·mol^{-1}, and above 1.3·10^6 g·mol^{-1}, respectively. Thus, these data confirmed the more compact structure of A. *seyal* AGPs. Moreover, the fact that more than one single slope was obtained for A. *senegal* is a peculiar feature of hyperbranched polymers, to which GA belong. Indeed, branching degrees of 78% and 59% were calculated for A. *senegal* and A. *seyal*, respectively (Lopez-Torrez et al., 2015a; Mejia Tamayo et al., 2018).

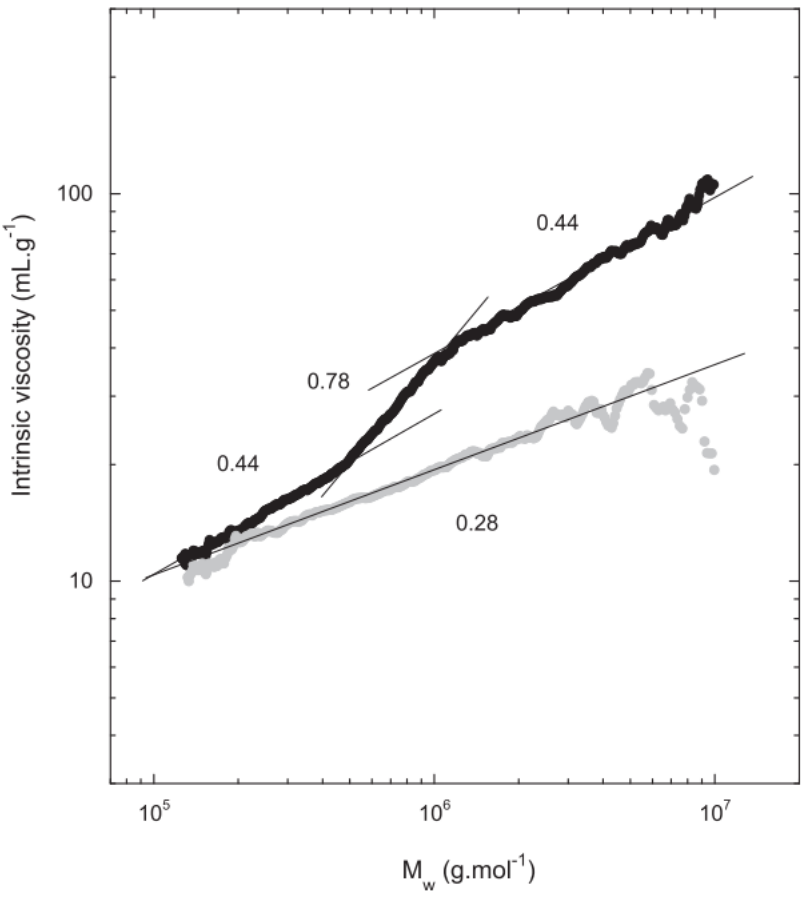

Figure I.1. Mark-Houwink-Sakurada (MHS) plot for A. *senegal* (black) and A. *seyal* (grey) gums prepared in MilliQ water and diluted in 0.1 M $LiNO_3$ ([GA] = 1 $g.L^{-1}$ at pH 5) showing the intrinsic viscosity [η] as a function of molar mass M_w. α values were calculated from the relation $[\eta] = K_\alpha M_w^\alpha$. From (Lopez-Torrez et al., 2015a).

The R_h vs. M_w conformation plots of 202 spray-dried and 100 raw A. *senegal* gums, 28 spray-dried and 6 raw A. *seyal* gums harvested in several countries were also analyzed by Sanchez et al. (Sanchez et al., 2018). For all gum samples, of any gum specie, form or origin, a unique hydrodynamic coefficient ν_h was obtained (Figure I.2), which value ranged from 0.53 to 0.55 for A. *senegal* gums and from 0.43 to 0.44 for A. *seyal* gums. This result confirmed once more the more compact structure of A. *seyal* gum.

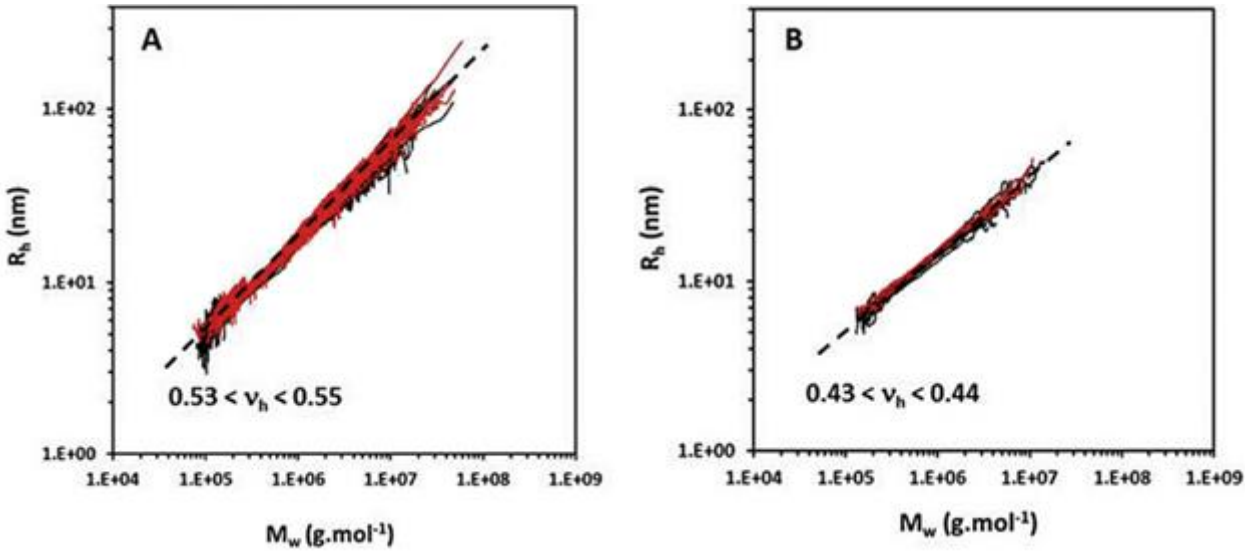

Figure I.2. R_h conformation plots of spray-dried (black) and raw (red) A. *senegal* (A) and A. *seyal* (B) gums. From (Sanchez et al., 2018).

Biopolymers from A. *senegal* can be separated by Hydrophobic Interaction Chromatography (HIC) into three fractions of decreasing polarity, namely HIC-F1, HIC-F2, and HIC-F3 (Randall et al., 1989; Renard et al., 2006). The main features of these fractions are presented in Table I.4.

Table I.4. Biochemical and structural parameters of GA fractions isolated by HIC. From (Renard et al., 2006).

Fraction	% of total GA mass	Molar mass (g·mol^{-1})	Protein content (%)	Charges
HIC-F1	88.3	$2.9 \cdot 10^5$	1.1	223
HIC-F2	10.4	$1.9 \cdot 10^6$	9	1259
HIC-F3	1.3	$2.5 \cdot 10^5 - 2.6 \cdot 10^6$	24.6	1605

HIC-F1, the less charged fraction, represents around 85 – 90% of the total gum, and is characterized by a low peptide content (around 1%) and a low molar mass (M_w) around $3 \cdot 10^5$ g·mol^{-1}. Its structure is more hydrated and less flexible than the two others. HIC-F3 is the minor fraction of GA (1.3% of the total GA). It is also the richest fraction in proteins (24.6%) and the most charged. M_w of the AGPs from HIC-F3 fraction fluctuates from $2.5 \cdot 10^5$ to $2.6 \cdot 10^6$ g·mol^{-1}. HIC-F2 has intermediate structural features, between HIC-F1 and HIC-F3.

Some attempts to describe the complex structure of these fractions have been made (Mahendran et al., 2008; Renard, Lavenant-Gourgeon, et al., 2014; Renard, Lepvrier, et al., 2014; Sanchez et al., 2008).

For HIC-F1, the only existing model described a highly organized open disk-like structure having a diameter of 20 nm and a thickness of less than 2 nm (Sanchez et al., 2008). A salt concentration of 300 mM was sufficiently high to screen charges and thus hinder electrostatic repulsions (Mejia Tamayo, 2018). The patterns obtained at high q-range, where the local structure is probed, suggested an inner dense branched structure.

Two models were first proposed for HIC-F2: the "wattle-blossom" and the "twisted hairy rope" models (Fincher et al., 1983; Qi et al., 1991). In the first model, AGPs from HIC-F2 was described as an assembly of polysaccharide blocks of $2{\cdot}10^5$ g·mol^{-1} attached to a short peptide backbone chain. This model was refined by Mahendran et al. (2008) who suggested GA was made of smaller carbohydrate building blocks of $\sim 4.5{\cdot}10^4$ g·mol^{-1} covalently attached to serine and hydroxyproline residues (Mahendran et al., 2008). The model proposed by Qi et al. (1991) pictured GA as a semi-flexible polypeptide backbone of 150 nm and about 400 amino acids, with small carbohydrate blocks (30 sugar residues) attached along the chain to hydroxyproline residues (Qi et al., 1991). More recently, HIC-F2 was degraded enzymatically by proteases and Renard et al. (2014) proposed a "self-similarity" fractal model. In this model, AGPs from HIC-F2 are seen as triaxial ellipsoids made up of an assembly of two kinds of building blocks, the second building block being a linear repetition of five of the first elementary blocks. The main features of these two blocks are presented in Figure I.3.

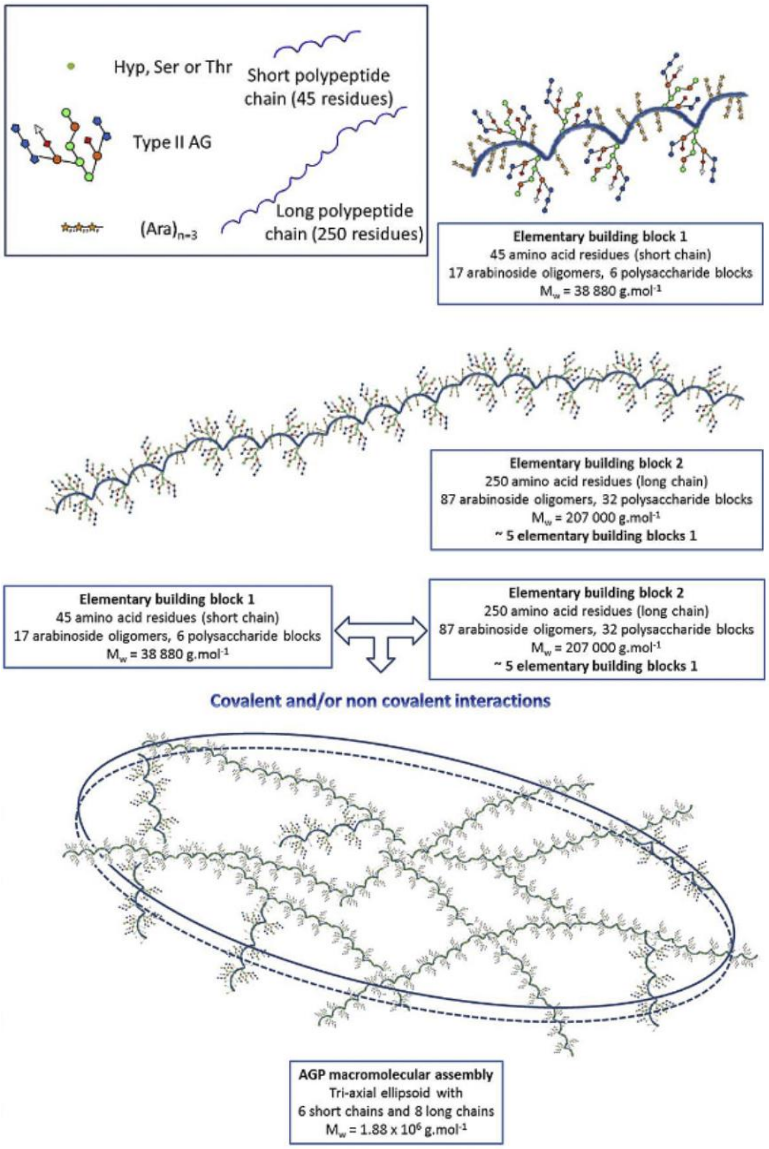

Figure I.3. Self-similarity model proposed for the HIC-F2 fraction. Adapted from (Renard et al., 2014a)

Finally, the HIC-F3 fraction was described as spheroidal ring-like monomers with sizes ranging from 8 to 11 nm surrounded by a thick shell with a width ranging from 2 to 5 nm (Renard, Lepvrier, et al., 2014). Depending on the operating parameters applied to purify this fraction, it was shown to be hard to disperse in water with the formation of aggregates that remained undissolved (Mejia Tamayo et al., 2018; Ray et al., 1995; Renard et al., 2013). Since this hydration behavior is not observed with the other fractions, it was concluded that self-aggregation properties of HIC-F3 fraction was correlated with the hydrophobic nature of these AGPs (Mejia Tamayo et al., 2018; Renard et al., 2006, 2013).

1.2. Physicochemical properties of AGPs from GA

GA is used in food, cosmetic, pharmaceutical or textile industries for its stabilizing, texturing, emulsifying and antioxidant properties. Among all these features, GA is particularly appreciated because it is highly soluble in water, provides low-viscosity dispersions even at concentrations up to 30%, and efficiently stabilizes oil-in-water emulsions. In confectionery products, GA is valued for its thickening properties at high concentration and its ability to retard sugar crystallization (Touré, 2008; Verbeken et al., 2003). In alcoholic beverages, GA improves the foam stability of sparkling wines (Apolinar-Valiente, Salmon, et al., 2020) and beers (Verbeken et al., 2003; Wickens et al., 1995); and stabilizes the coloring matter of young red wines (Nigen et al., 2019). In soft drinks, it is used as emulsifier and mouthfeel improver (Castellani, Guibert, et al., 2010; Erni et al., 2007; Glicksman & Sand, 1973; Verbeken et al., 2003). GA is responsible for the stabilization of aroma compounds, by reducing the surface tension between the two emulsion phases and improving the rigidity of the interface. GA is also used in many non-food applications (see Table I.5). Due to its adhesive properties, it can be found in matchsticks and postage-stamp adhesives (Cossalter, 1991; Harrison, 1940; Sharkey, 1987). In cosmetics, it acts as a natural stabilizer and thickener in lotions or as an adhesive in powders (Touré, 2008; Verbeken et al., 2003). Recently, GA was used in combination with other mineral components to produce functional nanocomposites. GA/hydroxyapatite core-shell nanocomposites were shown to be promising drug delivery vehicles for biomedical applications (Padmanabhan et al., 2018, 2020). Some studies focus on the production of nanocomposites based on GA combined with graphene oxide or iron nanoparticles for the removal of dyes (Silvestri et al., 2019; V. Singh et al., 2018). GA also serves as a corrosion inhibitor of steel in marine environment (Buchweishaija & Mhinzi, 2008), or as a binder for silicon anodes in Li-ion batteries (Ling et al., 2015).

Table I.5. Non-food applications of GA (non-exhaustive list)

Domain	Application	Gum role	Reference
Agriculture	azo dye decontamination	stabilization of iron nanoparticles	(Singh et al., 2018)
	insecticide	encapsulating agent (after complex coacervation with proteins)	(Gao et al., 1984; Omi et al., 1991)
Biomedicine	cancer-targeted optical imaging, sensing and drug delivery	coating agent of magnetic nanoparticles	(Banerjee & Chen, 2008, 2010; Kattumuri et al., 2007; Padmanabhan et al., 2018, 2020; Palma et al., 2015)
	drug delivery	encapsulating agent (after complex coacervation with proteins)	(Aberkane et al., 2012; Ducel et al., 2004; Eratte et al., 2014; Hedayati et al., 2012; Palmieri et al., 1996)
		stabilizer and antioxydant	(Kong et al., 2014)
Cosmetics	face powders, masks	adhesive	(Touré, 2008)
	creams, lotions	smoothing agent	
Materials	sprayed glazes high-tech ceramics	emulsifier	(Cecil, 2005)
Nanotechnologies	carbon nanotubes	dispersing and stabilizing agent	(Amiri et al., 2012; Bandyopadhyaya et al., 2002; Dror et al., 2005; M. T. Kim et al., 2011; Kumar et al., 2008; Najeeb et al., 2010)
	metallic or bioceramic nanoparticles	coating agent	(Batalha et al., 2010; Gils et al., 2010; Kattumuri et al., 2007; Ma et al., 2012; Roque & Wilson, 2008; J. E. Song et al., 2011)
Printing & writing	gum bi-chromate prints	emulsifier, antioxidant	(Cecil, 2005)
	photosensitive plates	coating agent	
	paper	encapsulating and coating agent	
	color pigments in crayons	binder	
	inks and paints	stabilize solid interfaces	(Balantrapu & Goia, 2009; Song et al., 2007; Wang & Zhao, 2009)
Others	laundry detergents	encapsulating agent	(Cecil, 2005)
	moisture-sensitive postage-stamp matchsticks	adhesive	
	green corrosion inhibitor	film-forming agent	(Abu-Dalo et al., 2012; Palumbo et al., 2019)

1.2.1. Hydration properties

Hydration properties of Acacia gums have been rarely studied in the past. As expected from its chemical composition, good hydration properties of GA were observed by DSC and DVS techniques. For A. *senegal*, the total water-holding capacity was reported to be about $3 - 6$ g_{water}/g_{AGP} (G. Phillips et al., 1996), freezing bound water around 2.5 g_{water}/g_{AGP} and non-freezing water around $0.4 - 0.7$ $g_{water}/g_{AGP.}$ (Hatakeyama et al., 2009; Sanchez et al., 2018; Takigami et al., 1995). Studies on the water hydration capacity of GA revealed some subtle differences between the A. *senegal* and A. *seyal* gums, related to their biochemical composition (Lopez-Torrez, 2016). At high a_w values ($a_w = 0.95$), the equilibrium moisture content was higher for A. *senegal* (52%) compared to A. *seyal* (48%) whereas at $a_w < 0.001$, X_m was higher for A. *seyal* (5.5%) compared to A. *senegal* (0.6%). This means that upon hydration, A. *senegal* was able to adsorb more water than A. *seyal*, whereas in dehydrated powders, A. *seyal* was able to retain water more strongly than A. *senegal*. GA hydration can be considered as a three-steps mechanism with *(i)* the formation of a monolayer of water molecules surrounding GA, once polar groups are saturated with water; *(ii)* the bonding of water molecules to this monolayer, creating multilayers and water clusters; and *(iii)* the accumulation of water clusters in the intermolecular voids of GA.

Thus, the good sorption capacity of GA could be attributed to the presence of hydrophilic groups on its carbohydrate moieties (uronic acids and hydroxyl groups of sugars) and possibly hydrophilic amino acids (Serine, Threonine, Aspartic acid and Glutamic acid), which provide many binding sites for water (Hu et al., 2008; G. Phillips et al., 1996). Besides, the higher content of glucuronic acids and rhamnose in A. *senegal* can explain the differences observed between the two gums. Indeed, hexoses are known to have better hydration properties than pentoses, and uronic acids also have good water-holding properties (Eastwood, 1974; Tait et al., 1972). GA hydration properties were also related to its conformation, and in particular to its hyperbranched nature (Mejia Tamayo et al., 2018; G. Phillips et al., 1996). Indeed, this highly branched structure is favorable to the formation of a three-dimensional network of water molecules (step (*iii*)) interacting with AGPs.

1.2.2. Rheological properties

The flow and viscoelastic properties of Acacia gums were also examined. When compared at the same concentration, apparent viscosity of A. *seyal* gum is lower than those of A. *senegal* gum (Lopez-Torrez, 2016). This originates from the smaller hydrodynamic volume and more compact structure of A. *seyal* (Lopez-Torrez et al., 2015a). Both gums exhibit Newtonian-like flow behavior for concentrations up to 15 – 30% (Lopez-Torrez, 2016; Salazar-Montoya et al., 2012). At higher concentrations and for low shear-rates, A. *senegal* gum displays a shear-thinning behavior (Li et al., 2009; Sanchez et al., 2002). This unusual flow behavior was attributed to the formation of micro-aggregates as concentration in GA dispersion increases, that are dissociated under high shear rate (Mothé & Rao, 1999). However, at low concentration, thanks to their good surface properties, GA macromolecules may also form a viscoelastic film at the sample interface (Davantès et al., 2019; Renard et al., 2022; Sanchez et al., 2002), which could also explain this shear thinning-like flow, as observed with BSA (Sharma et al., 2011).

1.2.3. Interfacial properties

The surface properties of GA – including the ability to decrease tension at oil/water interface and film-forming properties (Adamson & Gast, 1997) – are well-known. They have been mainly attributed to the content of high molar mass protein-rich fractions (Randall et al., 1988; Ray et al., 1995). Besides, its low viscosity and high solubility in water makes GA a good candidate to stabilize aroma compounds in beverage emulsions (Dickinson, 2009; McNamee et al., 1998). Indeed, even at high concentrations, the viscosity of GA is not a limiting factor. However, compared to other proteins (for which an emulsifier:oil ratio of 1:10 is generally used), a high concentration of GA and a high ratio GA:oil (typically 1:1) are necessary to efficiently stabilize emulsions.

At a given GA concentration, A. *senegal* is more prone to quickly lower interfacial tension than A. *seyal* (Aphibanthammakit, 2018). This can be related to a higher protein concentration (Dickinson et al., 1988), a higher content of protein-rich high molar mass AGPs (Nishino et al., 2012; Randall et al., 1988), greater accessibility of the protein part (Flindt et al., 2005) and different volumetric properties of the AGPs (Lopez-Torrez et al., 2015a). As a consequence, A. *senegal* is a better emulsifier than A. *seyal* (Flindt et al., 2005; Mansour & Hassan, 2016).

2. Aggregation properties of AGPs from GA

AGPs have the propensity to aggregate both *in vivo* (Baldwin et al., 1993; Kjellbom et al., 1997; Leszczuk, Kalaitzis, et al., 2020) and *in vitro* (Capataz-Tafur et al., 2011; Cheung et al., 1995; Kjellbom et al., 1997).

In vivo, partial aggregation was observed for AGPs from red wine (Belleville et al., 1993) or from apple juice after enzymatic degradation (dearabinosylation) (Brillouet et al., 1996; Churms et al., 1983). Similarly, Baldwin et al. showed the aggregation of AGPs isolated from a carrot cell suspension (*Daucus carota*) into higher-ordered structures composed of smaller ellipsoidal building blocks, with an approximate size of 25 nm x 15 nm (Baldwin et al., 1993) (Figure I.4).

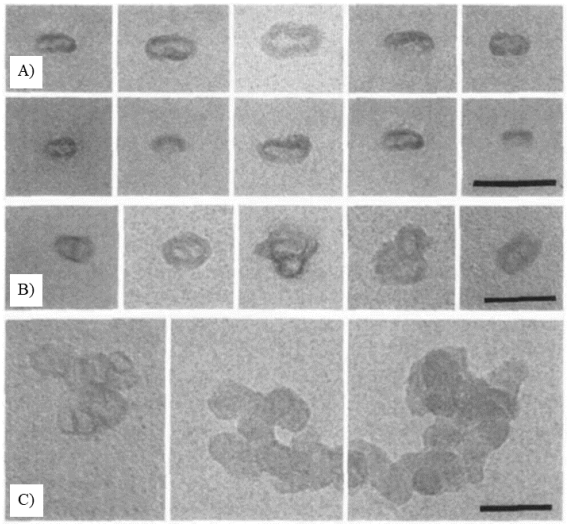

Figure I.4. Rotary-shadowed images of putative monomers (A) and small (B) and large aggregates (C) of AGPs from carrot cells. The scale bar represents 50 nm. From (Baldwin et al., 1993).

SEM images showed *in vitro* polymerization of AGPs from tobacco plants (*Nicotiana tabacum*) into aggregates composed of 10 – 15 transmitting tissue-specific (TTS) monomers, round to elliptical in shape, and of a diameter about 30 nm. This polymerization occurs in a head-to-tail way, in order to adopt structures that are the most energetically favorable (Cheung et al., 1995). Aggregation of AGPs is also a natural mechanism that occurs during the maturation of apple fruits (Leszczuk, Cybulska, et al., 2020).

When deposited on artificial substrates (mica or graphite surfaces), AGPs isolated from *Arabidopsis thaliana* leaves revealed a tendency to form aggregates of different shapes, from clusters to arcs or branched rings. The two latter structures suggest a particular organization

of AGPs in aggregates, with large carbohydrate moieties on the outside and its protein part inside (L. Zhou et al., 2014). Similar results were obtained with AGPs from GA deposited on different supports (mica or glass) and observed by AFM and TEM (Aphibanthammakit et al., 2018; Renard et al., 2013; Sanchez et al., 2008). In sugar beet, AGPs from plasma membranes are organized in two subfamilies with apparent molar mass of 82 and 97kDa. Excision of leaves causes AGPs to cross-link and form aggregates of 120, 170 and 210kDa, suggesting that AGP cross-linking is a protective mechanism in response to wounding. *In vitro*, oxidative cross-linking of these AGPs was also achieved in presence of H_2O_2 (Kjellbom et al., 1997). The presence of AGPs is also fundamental for cell aggregation in cultures of *Beta vulgaris* L. as cell aggregation had been shown to be concomitant with an increase in AGPs content in both cell walls and culture medium (Capataz-Tafur et al., 2011).

These self-association properties are consistent with the adhesive nature of AGPs. For instance, they are involved in the adhesion mechanism observed in charophytes in which they act both in cell to cell and cell to surface adhesion (Palacio-López et al., 2019) in English ivy (*Hedera helix*) whose adventitious roots are able to climb vertical surfaces (Huang et al., 2016), or in GA (Renard et al., 2012).

The aggregation of AGPs from GA is a natural and biological mechanism related to the tree physiology and occurring especially during the maturation of GA (Idris et al., 1998). Ageing of Acacia trees influences the structural properties (gyration radius R_g, hydrodynamic radius R_h, molar mass M_w) of AGPs from harvested GA. For instance, an increase in AGPs molar mass from $3.2{\cdot}10^5$ to $7.9{\cdot}10^5$ g·mol^{-1} was observed when Acacia trees get older, from 5 to 15 years, with a maximum M_w value reached between 10 and 15 years (Idris et al., 1998). The enrichment in high molar mass AGPs was correlated with a higher proportion of aggregates in solution. Other authors observed different hydration properties between the outside shell and the interior of GA nodules, the latter being harder to disperse in water than the former. Material collected from these two parts was dissolved in water and analyzed by electrophoresis. Electrophoretic pattern of the inside exhibited one peak, whereas material from the outside displayed two peaks, revealing the presence of a hydrolysis product. This result was explained by a dehydration of the tears as they age, which causes a weakening of glucosidic linkages and makes them more prone to hydrolyze when dispersed in water (Nelson & Ander, 1972).

These molecular associations affect the molar mass, size and shape of macromolecules, and can consequently deeply affect their physical properties. There are several factors, including solvent, macromolecules physicochemical properties and post-harvested treatments that can modify the way in which the AGPs assemble, and consequently the physicochemical properties of the formed aggregates.

2.1. Aggregation in solution of AGPs from GA

Several kinds of forces can promote an association process of GA, including covalent (Ziegler & Foegeding, 1990), and non-covalent interactions: hydrogen bonding between saccharidic residues (Mahendran et al., 2008; Nelson & Ander, 1972), van der Waals forces, hydrophobic association between polypeptide backbones (Renard et al., 2012), or electrostatic interactions. Thus, controlling macromolecules parameters (concentration, protein content), solvent properties (pH, ionic strength) and temperature is essential to monitor functional properties of the assemblies.

Association properties of GA are known for a long time (Nelson & Ander, 1972; Sloniewsky & Ander, 1971). Sloniewsky & Ander worked on the size and shape of arabate aggregates in solution. They showed that molar mass of arabate salts depended on the way in which samples were prepared: the longer the dissolution time, the higher the intrinsic viscosity and so the molar mass. Intrinsic viscosity of potassium arabate in 20 mM NaCl increased by 3 when increasing the dissolution time from 30min to 12h (Sloniewsky & Ander, 1971). This result was confirmed by Nelson & Ander who studied aggregation of GA by electrophoresis combined with light-scattering. Gum samples dissolved very quickly in water displayed one peak on electrophoretic patterns whereas gum samples that underwent very slow dissolution for three days resulted in two peaks. They suggested hydrolysis of GA may occur under slow dissolution and the formation of loose aggregates through hydrogen bonding in the hydrolysis products may occur (Nelson & Ander, 1972).

The structure of GA was highlighted over a wide concentration range using scattering and microscopic techniques (Dror et al., 2006; Renard et al., 2012; Sanchez et al., 2008; Wang et al., 2008). By static light scattering measurements, Wang et al. showed an increase in the association process as the concentration of GA increased from 0.3 to 5.2 $g \cdot L^{-1}$, indicated by an increase in R_g from 19.1 to 49.5 nm and M_w from 0.53 to $1.35 \cdot 10^6$ $g \cdot mol^{-1}$. In order to better

understand properties of GA, Dror et al. focused on characterizing the microstructure of GA in aqueous solution using scattering methods (SANS, SAXS) (Dror et al., 2006). At concentrations above 0.5%w/w, SAXS patterns of GA solutions showed a well-defined correlation peak in the low-q range. With increasing concentration, they observed a shift of the peak to higher values of q, as well as peak broadening. This finding was characteristic of the presence of aggregates. These authors revealed the existence of an overlap concentration (10 – 30 %w/w), above which the peak becomes significantly broader due to overlapping of polymer aggregates. This result is in accordance with rheological studies that showed a sharp increase in viscosity around the same concentration (Mothé & Rao, 1999; Whistler, 1973), due to intermolecular interactions. The high overlap concentration (30%w/w) is consistent with the hyperbranched structure of GA (Lopez-Torrez et al., 2015a; Sanchez et al., 2018). Upon addition of salt (up to 0.5M NaCl), the correlation peak progressively disappears, revealing the weak polyelectrolyte behavior of GA aggregates – extensively studied in the Ph.D. work of Mejia (Mejia Tamayo, 2018) –, as reported for other polyelectrolytes (Nishida et al., 2002) and charged polymer dendrimers (Nisato et al., 1999). Hence, the less charged character of arabinogalactan may explain the absence of the polyelectrolyte peak on its scattering patterns (Mucalo et al., 2002; Whistler, 1973). The impact of addition of NaCl on rheological properties of GA was also assessed: an increase in NaCl concentration resulted in a decrease in viscosity. It was assumed that addition of an electrolyte could screen intermolecular protein-carboxylate repulsions observed on GA macromolecules. Consequently, AGPs would adopt a more compact structure as concentration of NaCl increases. This also explains that association of AGPs in aqueous solution was inhibited in the presence of electrolyte (Gashua et al., 2015).

In A. *seyal* gum dispersions, AGP aggregate to a lower extent compared to A. *senegal,* and form ellipsoidal structures, with a radius of ~ 60 nm. Studies on chemical composition of these two gums showed that the A. *senegal* gum contains a higher content in protein and glucuronic acid (Lopez-Torrez et al., 2015a; Osman et al., 1993). Atgié et al. also reported the aggregation behavior of GA in solution and at the oil/water interface in emulsions (Atgié et al., 2018, 2019). In solution, they pictured the HIC-F2 fraction as a combination product resulting from polypeptidic associations between HIC-F1 and HIC-F3 and this aggregation behavior was shown to be drastically fostered in concentrated conditions (Atgié et al., 2019). Besides, hexadecane-in-water emulsion formulated with 0.6wt% GA exhibited perfect metastability over

three years which could be explained by the formation of an AGP aggregates network at the oil/water interface (Atgié et al., 2018).

2.2. Aggregation in dry state of AGPs from GA

Although the self-association properties of GA in solution are better documented, aggregation of GA in low-hydrated environment had also been reported, both *in vivo* during the gum exudation and its maturation on the Acacia tree (Capataz-Tafur et al., 2011; Idris et al., 1998; G. O. Phillips, 2009), and *in vitro*, after its harvest, during its processing or storage.

Some studies also evidenced the sensitivity of AGPs to physical treatments such as spray-drying, irradiation and storage conditions that could promote the AGP aggregation in dry state. Some authors reported that the mean molar mass of GA submitted to spray-drying was twice higher as that of a control GA, with the presence of an aggregate peak on the SEC MALLS chromatograms. Therefore, aggregation was promoted by spray-drying, which is a process involving high temperatures, and thus modifies the hydration of the protein part of GA (Al-Assaf et al., 2009). Irradiation of GA induces the formation of C – C covalent bonds between the carbohydrate blocks of AGPs (Al-Assaf et al., 2009). Irradiation of GA powder at 10.6kGy leads to an increase by 3.3 of the molar mass, along with an improvement of the functional properties of the modified gum. The shear-flow behavior of this irradiated GA switched from Newtonian to shear-thinning, and emulsifying properties were enhanced, due to a higher amount of high molar mass AGPs (Al-Assaf, Phillips, Williams, et al., 2007).

A few papers deal with aggregation of GA in dry state. The effect of heating on powdered GA has been studied for a long time (Gabel, 1930; Moorjani & Narwani, 1948). Gabel et al. studied the effect of temperature and heating time on the viscosity of GA mucilage after its dispersion in water. They reported an increase in viscosity with temperature and heating time, and a loss of weight of the samples. Moorjani and Narwani added that above 170°C GA became totally insoluble after its dispersion in water (Moorjani & Narwani, 1948). Both suggested a dehydration of the samples as an explanation for their observations.

The AGP aggregation was reported when GA was stored in the dry state on a wide range of temperatures, from 20°C to 200°C. Table I.6 gathers the conditions (gum specie and form, storage time, temperature and %RH) in which aggregation of AGPs from GA was observed, as

well as the different functional properties evaluated on these aggregates. Patent EP1505078B1 focuses on the effect of relative humidity (from 10 to 90%) during storage of GA powder on the aggregation kinetics. In this patent, an increase in molar mass by 1.5 was observed after incubation of GA powder at 40°C, under 30%RH for 7 days. Under the same time-relative humidity conditions, temperature had a kinetic effect on molar mass (Figure I.5A). After 12h of dry heating at 70%RH, M_w of AGPs from A. *senegal* gum increased by 55% at 60°C and up to 195% at 150°C. Similarly, for given incubation time and temperature (90°C and 150°C), an increase in relative humidity was correlated with a further increase in the molar mass (Figure I.5B). After 12h of dry heating at 90°C, M_w of AGPs from A. *senegal* gum increased by only 15% under low relative humidity storage (10%) while AGP aggregated faster when incubated in a more humid environment, with for instance an increase of M_w by 160% under 90%RH. The aggregation was enhanced during GA storage at 150°C compared to 90°C, at any %RH, but the effect of %RH on M_w increase was more moderated in this range of %RH. An increase of M_w from 165% (at 30 %RH) to 195% (at 70 %RH) and from 60% (at 30 %RH) to 140% (at 70 %RH) were reported when GA was stored at 150°C and 90°C, respectively. Moreover, in extreme conditions, the appearance of the samples was affected with dehydration on the surface observed for gum powder particles stored in dry environment (%RH ≤ 20%) or agglomeration for gums stored in wet environment (%RH ≥ 70%).

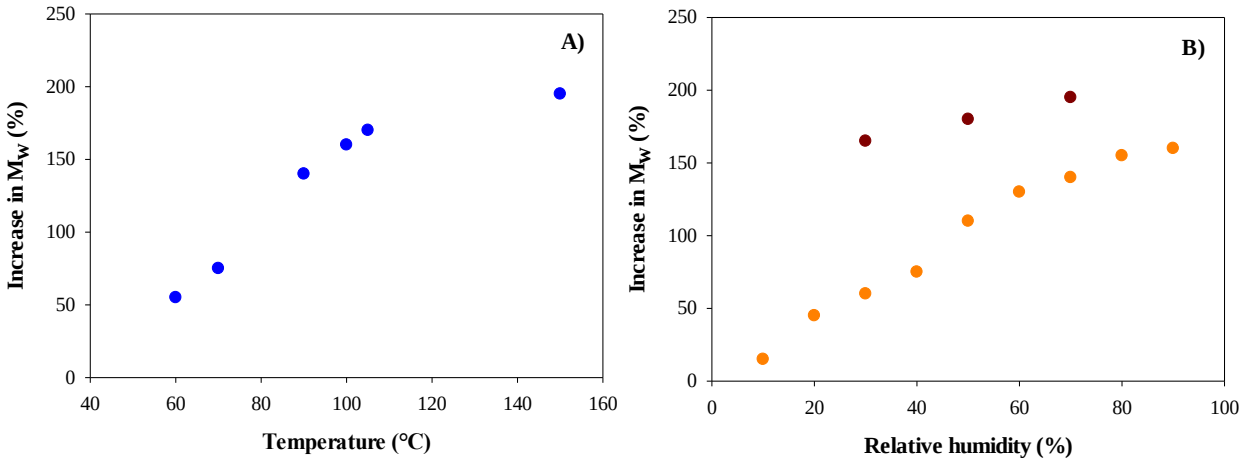

Figure I.5. Influence of A. *senegal* powder dry heating (for 12h) under different temperature and RH conditions on the AGPs molar mass. A) Effect of temperature at 70%RH (●) and B) Effect of %RH at constant temperature of 90°C (●) or 150°C (●). From (Hayashi, 2002).

The heating at 110°C for not less than 15h of several Acacia gum species (*senegal* or *seyal*) in different forms (spherical clusters, cracked gum or spray-dried gum) was also studied (Patent

WO2004089991A1). Authors reported an increase in M_w for all samples after at least 15h of heating at 110°C (Al-Assaf et al., 2004) (Figure I.6).

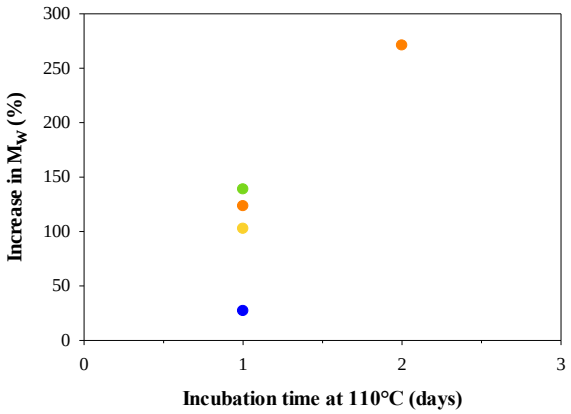

Figure I.6. Influence of dry heating at 110°C on M_w of AGPs from spray-dried A. *seyal* (●), spray-dried A. *senegal* (●), cracked A. *senegal* (●) or spherical clusters of A. *senegal* (●). From (Al-Assaf et al., 2004).

For instance, M_w of a spray-dried A. *seyal* gum heated for 24h at 110°C increased by 27%, from $1.15 \cdot 10^6$ to $1.45 \cdot 10^6$ g·mol^{-1}. In comparison, a spray-dried A. *senegal* heated for 24h at 110°C aggregated to a higher extent, with an increase in M_w by 139%, from $0.60 \cdot 10^6$ to $1.43 \cdot 10^6$ g·mol^{-1}. In cracked A. *senegal* and clusters of A. *senegal*, M_w increased by 123% and 102%, from $0.52 \cdot 10^6$ to $1.15 \cdot 10^6$ and from $0.81 \cdot 10^6$ to $1.63 \cdot 10^6$ g·mol^{-1}, respectively, after 24h of heating at 110°C. These results show a positive correlation between the average particle diameter and the extent of aggregation of AGPs from GA: the smaller the particle size, the higher the surface exchange and the more AGPs aggregate.

Similar results were obtained by Sasaki et al. (2014) after the heating at 125°C for not less than 1h of A. *senegal* gum in different forms (spray-dried gum and pulverizates of different sizes, from 83 µm to 6 mm) (Patent US 8,722,129 B2). They showed that dry heating of A. *senegal* induced a discoloration of GA with storage time, that was found to be the fastest and the most pronounced for GA with the biggest particle sizes (Sasaki et al., 2014). They also measured the influence of the incubation pressure on aggregation properties of AGPs from GA (Sasaki et al., 2014). Experiments were lead at atmospheric pressure (*i.e.* 1 atm) or under reduced pressure (*i.e.* around 0.03 atm). First, modification of samples aspect was reported in almost all experimental conditions tested, showing slight color change (yellowish-white

samples) at reduced pressure or browning and caking at normal pressure. Again, aggregation of GA occurred for all samples after at least 1h of heating at 125°C (Figure I.7): at both pressures, an increase of M_w was observed, even at short incubation times (*e.g.* 11% and 16% increase after 1h of incubation at 125°C under reduced or normal pressure, respectively). At early stages of incubation (≤ 2h), the gap between the two storage conditions was very small, but increased with incubation time. After 8h of incubation at 125°C under reduced or normal pressure, M_w of GA increased by 1.8 and 2.4 respectively.

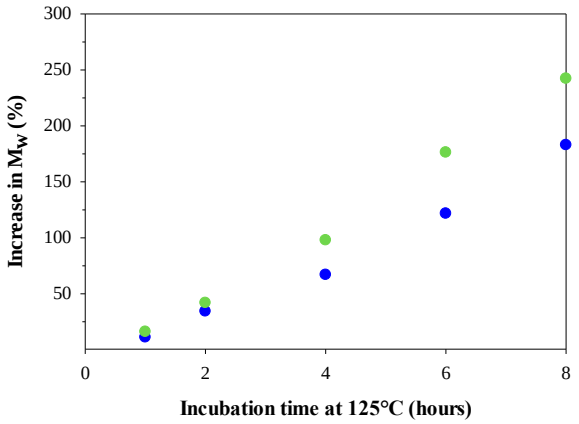

Figure I.7. Influence of dry heating at 125°C under atmospheric (●) or reduced pressure (●) on M_w of AGPs from spray-dried A. *senegal*, From (Sasaki et al., 2014).

Table I.6. Summary of storage conditions inducing the aggregation of AGPs from GA in dry state, and evaluated properties of the formed aggregates.

Reference	Gum specie	Gum particle size	Temperature (°C)	Specific conditions	Incubation time	Aggregates properties
(Al-Assaf et al., 2004)		cracked gum			24 – 48h	
WO 2004/089991 A1	*senegal*	spray-dried			24h	
		clusters	110		24h	Structural and emulsifying properties
		cracked gum			15h	
	seyal	spray-dried			24h	
(Al-Assaf, Phillips, Aoki, et al., 2007b)	*senegal*	kibbled	110		24 – 96h	Structural, hydration, emulsifying and viscoelastic properties
(Aoki, Al-Assaf, et al., 2007)	*senegal*	kibbled	110		24 – 72h	Structural properties and biochemical composition
(Aoki, Katayama, et al., 2007)	*senegal*	kibbled	110		24 – 72h	Emulsifying properties
(Castellani, Guibert, et al., 2010)	*senegal*	kibbled	110			Emulsifying properties
(Castellani, Al-Assaf, et al., 2010)	*senegal*	kibbled	110			Interfacial properties (hexadecane/water)

Table I.6. (continued from the previous page)

(Castellani, Gaillard, et al., 2010)	*senegal*	kibbled	110			Surface properties (air/water)
(Flanagan et al., 2008)	*senegal*	kibbled	110			Encapsulating properties
(Glover et al., 2009)	*senegal*	kibbled	110			Potential effects on health (blood pressure)
(Hayashi, 2002)			20	70%RH	7days	
EP 1 505 078 B1			40	30 – 70%RH	7days	
			50	30 – 70%RH	7days	
			60	30 – 90%RH	7days	
	senegal	raw (exudate)	60 – 100	70%RH	12h	Structural and emulsifying properties
			70	70%RH	7days	
			80	60%RH	7days	
			90	10 – 90%RH	12h	

Table I.6. (continued from the previous page)

(Hayashi, 2002) **EP 1 505 078 B1**	*senegal*	raw (exudate)	105	70%RH	12h	Structural and emulsifying properties
			150	30 – 70%RH	12h	
(Katayama et al., 2008) US20080038436 A1	*senegal*	spray-dried	120		12 – 240h	Hydration properties
(Matsumoto et al., 2006)	*senegal*	kibbled	110			Potential effects on health (renal activity)
(A. O. Phillips & Phillips, 2011)	*senegal*	kibbled	110			Potential effects on health (blood pressure and renal activity)
(Sasaki et al., 2014) US 8,722,129 B2	*senegal*	spray-dried	125	Reduced pressure	1h – 8h	Discoloration, changes in appearance, flavor, structural and emulsification properties
			125		1h – 8h	
			90	Reduced pressure	30min	
		unpulverizates	125		3h – 12h	
		coarse pulverizates	125		3h – 12h	

Table I.6. (continued from the previous page)

		pulverizates	125		3h – 12h
		fine pulverizates	125		3h – 12h
			125	Reduced pressure	1h – 8h
		spray-dried	125	Reduced pressure	1h – 10h
			70 – 110	Reduced pressure	24h
			125	Reduced pressure	4h
			140	Reduced pressure	2h
			180	Reduced pressure	10min
			200	Reduced pressure	10min
(Su et al., 2008)	*senegal*	kibbled	110		Encapsulating properties
(Tipvarakarnkoon et al., 2010)	*senegal*	kibbled	110		Emulsifying properties
(Wang et al., 2008)	*senegal*	kibbled	110		Structural properties

Following this patent, a series of articles aiming to characterize the structural, biochemical (Al-Assaf, Phillips, Aoki, et al., 2007b), and the physical properties (Al-Assaf, Phillips, Aoki, et al., 2007b; Aoki, Al-Assaf, et al., 2007; Castellani, Guibert, et al., 2010) of these matured gums (usually referred as SUPER GUM™ in literature) as well as the chemical groups involved in this process (Cui et al., 2007) was released.

Surprisingly, the biochemical composition (amino acid and sugar content) did not change during the process (Aoki, Al-Assaf, et al., 2007). However, spectroscopic analyses of the samples (IR and NMR) revealed minor changes in GA structure after maturation: a shift in ^{H}NMR from 4.5 to 4.8 ppm and two changes in IR spectra in the region of 600 cm^{-1} (ring breathing vibration C-C-C-O or C-O-C) and 1600 – 1630cm^{-1} (COO^{-} asymmetrical stretching COOH glucuronic acids). The shift at 4.5 ppm was previously attributed to H-1 of β-DGlcA and β-DGalp (side chains of GA). These observations enabled the authors to assign AGP aggregation to dehydration in the carboxyl group of uronic acids (Cui et al., 2007). This maturation process modified the structural properties of GA, with an increase in intrinsic viscosity of GA in 0.2M NaCl from 18.3 to 22.2 $mL{\cdot}g^{-1}$ after maturation, concomitant with higher amount of high M_w AGPs and a more branched structure (Aoki, Al-Assaf, et al., 2007).

As a consequence of the aggregation, the hydration, interfacial and emulsifying properties of GA were modified by this process. Emulsifying properties of this aggregated GA were extensively reported in literature (Table I.6). Oil-in-water emulsions were formulated with GA or matured gums as emulsifier, and a medium-chain triglyceride (octanoic/decanoic acid triglyceride O.D.O™) as oil phase. The change in oil droplet size $D_{4,3}$ between emulsions formulated with native or matured gums was assessed (Figure I.8). All emulsions formulated with matured gums showed better emulsifying ability with a reduction of oil droplet size compared to the control gum, and less destabilization over time (Al-Assaf et al., 2004; Hayashi, 2002; Sasaki et al., 2014).
For instance, $D_{4,3}$ was decreased by 31% in emulsions freshly prepared using GA stored for 12h at 60°C and 70%RH (Hayashi, 2002). In aged emulsions, this effect was even stronger with for instance 82% decrease in $D_{4,3}$ for the same emulsion stored for 7 days at 60°C. The incubation temperature and relative humidity were both positively correlated with the emulsifying capacity of GA. In the temperature range 60 – 150°C, an increase in temperature resulted in a stronger decrease in $D_{4,3}$ between 60°C and 90°C (from 31% to 46%). Incubation at temperatures higher than 90°C did not improve further emulsifying properties as reduction in $D_{4,3}$ reaches a plateau at a value of ~ 46%

between 90°C and 150°C. For gums incubated at 90°C, reduction of the $D_{4,3}$ was more pronounced for higher relative humidity: from 10% at 10%RH to 46% at 60%RH. Between 60%RH and 90%RH, $D_{4,3}$ did not decrease further, reaching a plateau at a value of ~ 47%. However, in the case of dry heating at 150°C, relative humidity showed no effect on emulsifying properties of GA.

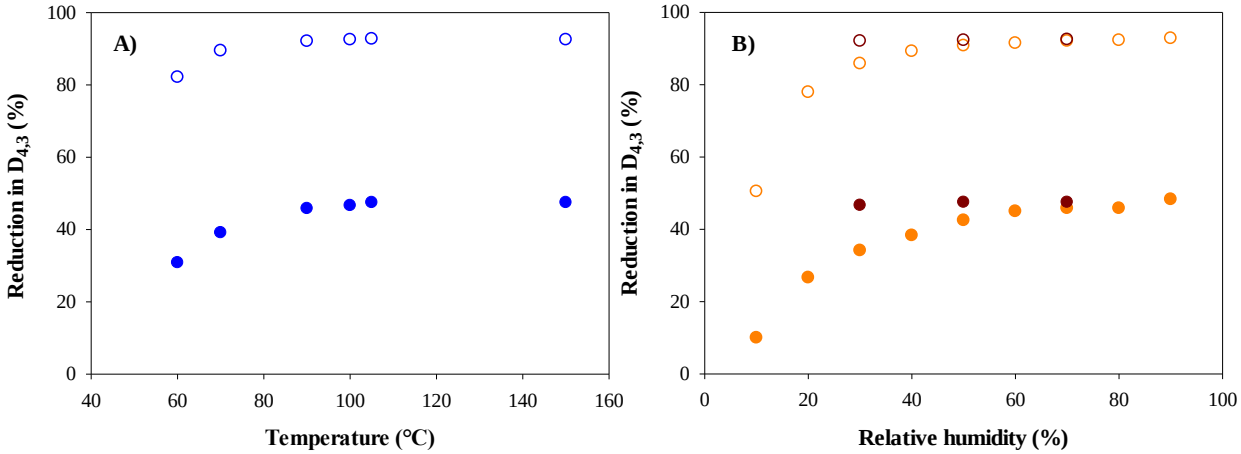

Figure I.8. Influence of A. *senegal* dry heating (for 12h) on emulsifying properties ($D_{4,3}$) of AGPs: reduction in $D_{4,3}$ in fresh emulsions (filled symbols) and emulsions stored for 7 days (open symbols). A) Effect of temperature at 70%RH (●) and B) effect of %RH at constant temperature: 90°C (●) or 150°C (●). From (Hayashi, 2002).

At 110°C, the aggregation of AGPs from cracked GA was also prone to improve the emulsifying properties of GA (Al-Assaf et al., 2010). The authors showed that these aggregated gums improved the colloidal stability of emulsions, with 20% reduction of the initial oil droplet size for aggregated samples compared to the control one and higher homogeneity of the oil droplet size distribution (Castellani, Guibert, et al., 2010). More precisely, emulsions were formulated with various amounts of matured GA (*i.e.* aggregated AGPs) in cracked form (from 6wt% to 16wt%). For all emulsifier concentrations evaluated, a decrease in $D_{4,3}$ was noticed (Figure I.9). At low GA concentration, in fresh emulsions, the differences in emulsifying properties were slightly more pronounced with ~17% decrease in $D_{4,3}$ at $C < 10$wt% and only 7% decrease in $D_{4,3}$ at $C = 16$wt%. However, in aged emulsions, the $D_{4,3}$ gap between native and matured GA was much higher (*e.g.* 70% decrease in $D_{4,3}$ for emulsions formulated at $C_{GA} = 6$wt%), showing a significant improvement in emulsion stability when using matured GA.

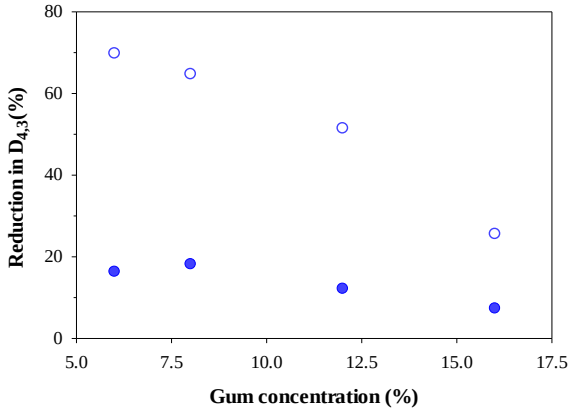

Figure I.9. Influence of 36h of dry heating at 110°C on emulsifying properties of cracked A. *senegal*: reduction in $D_{4,3}$ in fresh emulsions (●) and emulsions stored for 2 days at 60°C (○): effect of gum concentration. From (Al-Assaf et al., 2004).

The change in oil droplet size $D_{4,3}$ between emulsions formulated with native or matured GA in different forms at 125°C was also evaluated (Figure I.10A) (Sasaki et al., 2014). Here again, all emulsions formulated with these matured gums showed better emulsifying ability with a reduction of oil droplet size ($D_{4,3}$) of at least 25% compared to the control gum. It can be seen that the lower the GA particle size are, the more AGPs from GA aggregate and consequently the better the emulsifying properties are. Dry heating of A. *senegal* also induced a dehydration of the samples, from 15% to less than 5% after 12h, which was the fastest for GA in the form of fine pulverizates, and the slowest for unpulverized GA. The emulsion efficiency was therefore higher for matured gums having the smallest water content (Figure I.10B). Moreover, the biggest particle diameter of GA in the forms of beads induced heterogeneity during incubation, with lower moisture content on the particle surface which is favorable to improve emulsifying properties and higher moisture content in the particle core, which is the starting point for the formation of a hydrogel upon incubation. As a consequence of this moisture content gap, extensive incubation ($>$ 3h at 125°C) had a deleterious effect on emulsion stability, with an increase in $D_{4,3}$, which even becomes higher than in emulsion formulated with native GA (Figure I.10A).

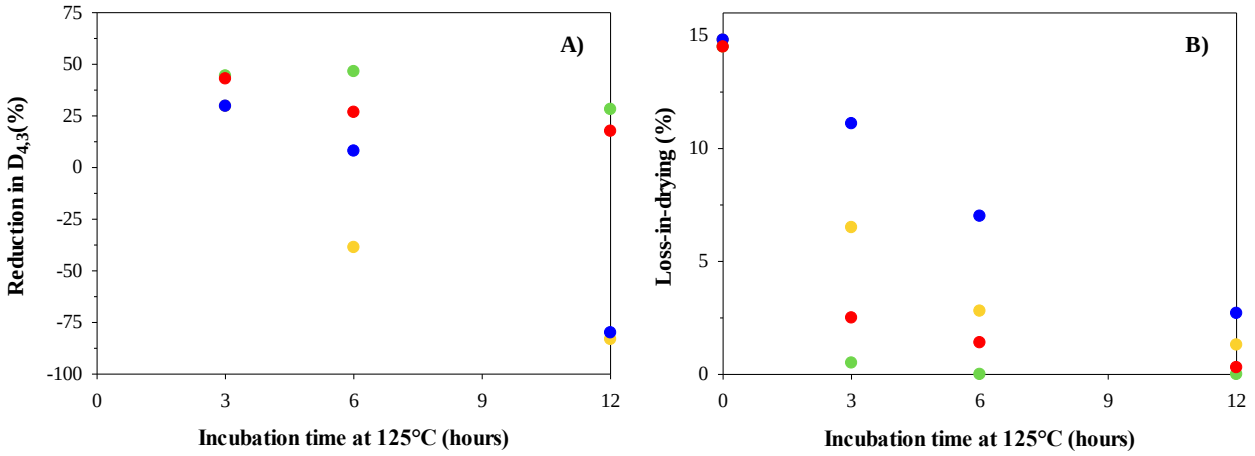

Figure I.10. A) Influence of dry heating at 125°C on emulsifying properties of raw or crude A. *senegal* with particles of different sizes: reduction in $D_{4,3}$ in fresh emulsions. B) Extent of dehydration as a function of incubation time: fine pulverizates d = 83 µm (●), pulverizates d = 1.5 mm (●), coarse pulverizates d = 6 mm (●) or beads d = 30 mm (●) of A. *senegal*. From (Sasaki et al., 2014)

Besides emulsifying properties, hydration properties of GA were also deeply affected after incubation in the dry state, with the formation of a hydrogel composed of poorly soluble AGPs during incubation at 110°C (Al-Assaf, Phillips, Aoki, et al., 2007b). For instance, the hydrogel content represented 23% and 28% of the whole sample after 72h and 96h of heating at 110°C, respectively. The formation of a hydrogel when aggregates reach a certain degree of polymerization and become insoluble was reported elsewhere (Katayama et al., 2008). Mantell also showed the formation of insoluble compounds during the dehydration of arabic acid (Mantell, 1954). In Figure I.11 it can be seen that with incubation time, the hydrogel content increases following a sigmoidal-like curve with a lag phase between 0 and 12h of incubation, followed by a steep increase from 0 to 67% between 12 and 60h, and finally a slowdown for incubation times above 60h, up to reach a value of 92% after 240h of incubation at 120°C. Incubation in the dry state also greatly improved the

water-binding ability of A. *senegal* (Al-Assaf, Phillips, Aoki, et al., 2007b; Katayama et al., 2008). For instance, water-retention ability of GA incubated at 120°C between 36 and 60h was increased by 5. An increased elasticity (increase of G' modulus by 6 after maturation for 24h at 110°C) was also noticed (Al-Assaf, Phillips, Aoki, et al., 2007b).

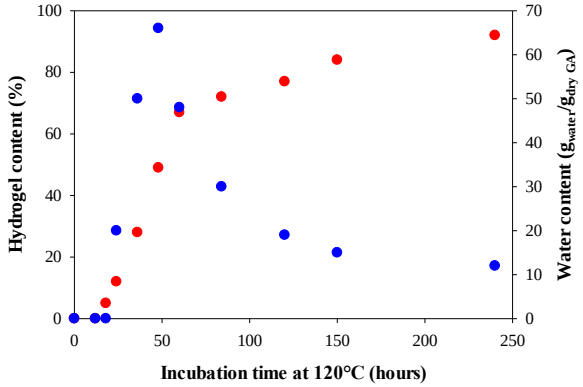

Figure I.11. Influence of dry heating at 120°C on hydration properties of spray-dried A. *senegal*: hydrogel content (●) and water content (●) as a function of incubation time. From (Katayama et al., 2008).

This section summarized the physicochemical parameters such as time, temperature, and relative humidity, which influence the way AGP aggregates form in dry state. The aggregation of AGPs is an interesting way to improve their functional properties. However it can be noticed in this summary that all the studies reported had been conducted with Acacia gums loaded in minerals, in most cases with Acacia *senegal* gum, and at temperatures higher than 70°C, and even often higher than 110°C (Table I.6). Therefore, my Ph.D. project that is focused on the aggregation of AGPs from demineralized Acacia *seyal* gum at temperatures below 70°C is well complementary to these studies.

3. References

Aberkane, L., Jasniewski, J., Gaiani, C., Hussain, R., Scher, J., & Sanchez, C. (2012). Structuration mechanism of β-lactoglobulin – acacia gum assemblies in presence of quercetin. *Food Hydrocolloids*, *29*(1), 9–20. https://doi.org/10.1016/j.foodhyd.2012.01.010

Abu-Dalo, M., Othman, A., & Al-Rawashdeh, N. (2012). Exudate Gum from Acacia Trees as Green Corrosion Inhibitor for Mild Steel in Acidic Media. *International Journal of Electrochemical Science*, *7*.

Adamson, A. W., & Gast, A. P. (1997). *Physical chemistry of surfaces* (6th ed.). Wiley.

Al-Assaf, S., Phillips, G. O., Aoki, H., & Sasaki, Y. (2007). Characterization and properties of Acacia senegal (L.) Willd. var. senegal with enhanced properties (Acacia (sen) SUPER GUM™): Part 1—Controlled maturation of Acacia senegal var. senegal to increase viscoelasticity, produce a hydrogel form and convert a poor into a good emulsifier. *Food Hydrocolloids*, *21*(3), 319–328. https://doi.org/10.1016/j.foodhyd.2006.04.011

Al-Assaf, S., Phillips, G. O., Sasaki, Y., & Katayama, T. (2004). *Modified gum arabic* (Patent No. WO 2004/089991 A1).

Al-Assaf, S., Phillips, G. O., Sasaki, Y., & Katayama, T. (2010). *Modified gum arabic from Acacia senegal* (Patent No. EP1611159B1). (WO-A-02/072862)

Al-Assaf, S., Phillips, G. O., Williams, P. A., & du Plessis, T. A. (2007). Application of ionizing radiations to produce new polysaccharides and proteins with enhanced functionality. *Nuclear Instruments and Methods in Physics Research Section B: Beam Interactions with Materials and Atoms*, *265*(1), 37–43. https://doi.org/10.1016/j.nimb.2007.08.015

Al-Assaf, S., Phillips, G., & Williams, P. (2005). Studies on acacia exudate gums. Part I: The molecular weight of gum exudate. *Food Hydrocolloids*, *19*(4), 647–660. https://doi.org/10.1016/j.foodhyd.2004.09.002

Al-Assaf, S., Sakata, M., McKenna, C., Aoki, H., & Phillips, G. O. (2009). Molecular associations in acacia gums. *Structural Chemistry*, *20*(2), 325. https://doi.org/10.1007/s11224-009-9430-3

Amiri, A., Shanbedi, M., Eshghi, H., Heris, S. Z., & Baniadam, M. (2012). Highly Dispersed Multiwalled Carbon Nanotubes Decorated with Ag Nanoparticles in Water and Experimental Investigation of the Thermophysical Properties. *The Journal of Physical Chemistry C*, *116*(5), 3369–3375. https://doi.org/10.1021/jp210484a

Aoki, H., Al-Assaf, S., Katayama, T., & Phillips, G. O. (2007). Characterization and properties of Acacia senegal (L.) Willd. var. senegal with enhanced properties (Acacia (sen) SUPER GUM™): Part 2—Mechanism of the maturation process. *Food Hydrocolloids*, *21*(3), 329–337. https://doi.org/10.1016/j.foodhyd.2006.04.002

Aoki, H., Katayama, T., Ogasawara, T., Sasaki, Y., Al-Assaf, S., & Phillips, G. O. (2007). Characterization and properties of Acacia senegal (L.) Willd. var. Senegal with enhanced properties (Acacia (sen) SUPER GUM™): Part 5. Factors affecting the emulsification of Acacia senegal and Acacia (sen) SUPER GUM™. *Food Hydrocolloids*, *21*(3), 353–358. https://doi.org/10.1016/j.foodhyd.2006.04.014

Aphibanthammakit, C. (2018). *Interfacial and emulsifying properties of Acacia gums and their fractions* [These de doctorat, Montpellier, SupAgro]. http://www.theses.fr/2018NSAM0029

Aphibanthammakit, C., Barbar, R., Nigen, M., Sanchez, C., & Chalier, P. (2020). Emulsifying properties of Acacia senegal gum: Impact of high molar mass protein-rich AGPs. *Food Chemistry: X*, *6*, 100090. https://doi.org/10.1016/j.fochx.2020.100090

Apolinar-Valiente, R., Salmon, T., Williams, P., Nigen, M., Sanchez, C., Marchal, R., & Doco, T. (2020). Improvement of the foamability of sparkling base wines by the addition of Acacia gums. *Food Chemistry*, *313*, 126062. https://doi.org/10.1016/j.foodchem.2019.126062

Atgié, M., Garrigues, J. C., Chennevière, A., Masbernat, O., & Roger, K. (2019). Gum Arabic in solution: Composition and multi-scale structures. *Food Hydrocolloids*, *91*, 319–330. https://doi.org/10.1016/j.foodhyd.2019.01.033

Atgié, M., Masbernat, O., & Roger, K. (2018). Emulsions Stabilized by Gum Arabic: Composition and Packing within Interfacial Films. *Langmuir*. https://doi.org/10.1021/acs.langmuir.8b02715

Balantrapu, K., & Goia, D. V. (2009). Silver nanoparticles for printable electronics and biological applications. *Journal of Materials Research*, *24*(9), 2828–2836. https://doi.org/10.1557/jmr.2009.0336

Baldwin, T. C., McCann, M. C., & Roberts, K. (1993). *A Novel Hydroxyproline-Deficient Arabinogalactan Protein Secreted by Suspension-Cultured Cells of Daucus carota*. 9.

Bandyopadhyaya, R., Nativ-Roth, E., Regev, O., & Yerushalmi-Rozen, R. (2002). Stabilization of Individual Carbon Nanotubes in Aqueous Solutions. *Nano Letters*, *2*(1), 25–28.

Banerjee, S. S., & Chen, D.-H. (2008). Multifunctional pH-sensitive magnetic nanoparticles for simultaneous imaging, sensing and targeted intracellular anticancer drug delivery. *Nanotechnology*, *19*(50), 505104. https://doi.org/10.1088/0957-4484/19/50/505104

Banerjee, S. S., & Chen, D.-H. (2010). Grafting of 2-Hydroxypropyl-β-Cyclodextrin on Gum Arabic-Modified Iron Oxide Nanoparticles as a Magnetic Carrier for Targeted Delivery of Hydrophobic Anticancer Drug. *International Journal of Applied Ceramic Technology*, *7*(1), 111–118. https://doi.org/10.1111/j.1744-7402.2008.02332.x

Batalha, I. L., Hussain, A., & Roque, A. C. A. (2010). Gum Arabic coated magnetic nanoparticles with affinity ligands specific for antibodies. *Journal of Molecular Recognition*, *23*(5), 462–471. https://doi.org/10.1002/jmr.1013

Belleville, M. P., Williams, P., & Brillouet, J. M. (1993). A linear arabinan from a red wine. *Phytochemistry*, *33*(1), 227–229. https://doi.org/10.1016/0031-9422(93)85429-U

Brillouet, J., Williams, P., Will, F., Müller, G., & Pellerina, P. (1996). Structural characterization of an apple juice arabinogalactan-protein which aggregates following enzymic dearabinosylation. *Carbohydrate Polymers*, *29*(3), 271–275. https://doi.org/10.1016/0144-8617(95)00152-2

Buchweishaija, J., & Mhinzi, G. (2008). Natural Products as a Source of Environmentally Friendly Corrosion Inhibitors: The Case of Gum Exudate from Acacia seyal var. seyal. *Portugaliae Electrochimica Acta*, *26*, 257–265. https://doi.org/10/3912

Buffo, R. A., Reineccius, G. A., & Oehlert, G. W. (2001). Factors affecting the emulsifying and rheological properties of gum acacia in beverage emulsions. *Food Hydrocolloids*, *15*(1), 53–66. https://doi.org/10.1016/S0268-005X(00)00050-3

Capataz-Tafur, J., Trejo-Trapia, G., Rodríguez-Monroy, M., & Sepulveda-Jiménez, G. (2011). Arabinogalactan proteins are involved in cell aggregation of cell

suspension cultures of Beta vulgaris L. *Plant Cell Tiss Organ Cult*, *106*, 169–177. https://doi.org/10.1007/s11240-010-9905-3

Castellani, O., Al-Assaf, S., Axelos, M., Phillips, G., & Anton, M. (2010). Hydrocolloids with emulsifying capacity. Part 2 – Adsorption properties at the n-hexadecane–Water interface. *Food Hydrocolloids*, *24*(2), 121–130. https://doi.org/10.1016/j.foodhyd.2009.07.006

Castellani, O., Gaillard, C., Vié, V., Al-Assaf, S., Axelos, M., Phillips, G. O., & Anton, M. (2010). Hydrocolloids with emulsifying capacity. Part 3 – Adsorption and structural properties at the air–water surface. *Food Hydrocolloids*, *24*(2–3), 131–141. https://doi.org/10.1016/j.foodhyd.2009.07.009

Castellani, O., Guibert, D., Al-Assaf, S., Axelos, M., Phillips, G. O., & Anton, M. (2010). Hydrocolloids with emulsifying capacity. Part 1 – Emulsifying properties and interfacial characteristics of conventional (Acacia senegal (L.) Willd. Var. Senegal) and matured (Acacia (sen) SUPER GUM™) Acacia senegal. *Food Hydrocolloids*, *24*(2–3), 193–199. https://doi.org/10.1016/j.foodhyd.2009.09.005

Cecil, C. O. (2005). Gum arabic. *Saudi Aramco World*, *56*(2), 36–39.

Cheung, A. Y., Wang, H., & Wu, H. (1995). A floral transmitting tissue-specific glycoprotein attracts pollen tubes and stimulates their growth. *Cell*, *82*(3), 383–393. https://doi.org/10.1016/0092-8674(95)90427-1

Churms, S., Merrifield, E., Stephen, A., Walwyn, D., Polson, A., van der Merwe, K., Spies, H., & Costa, N. (1983). An L-arabinan from apple-juice concentrates. *Carbohydrate Research*, *113*(2), 339–344. https://doi.org/10.1016/0008-6215(83)88251-2

Cossalter, C. (1991). Acacia senegal: Gum tree with promise for agroforestry. *Acacia Senegal: Gum Tree with Promise for Agroforestry.*, *No. 91-02*. https://www.cabdirect.org/cabdirect/abstract/19920657801

Cui, S. W., Phillips, G. O., Blackwell, B., & Nikiforuk, J. (2007). Characterisation and properties of Acacia senegal (L.) Willd. var. senegal with enhanced properties (Acacia (sen) SUPERGUM™): Part 4. Spectroscopic characterisation of Acacia senegal var. senegal and Acacia (sen) SUPERGUM™ arabic. *Food Hydrocolloids*, *21*(3), 347–352. https://doi.org/10.1016/j.foodhyd.2006.05.009

Davantès, A., Nigen, M., Sanchez, C., D'Orlando, A., & Renard, D. (2019). Adsorption of Hyperbranched Arabinogalactan-Proteins from Plant Exudate at the Solid–Liquid Interface. *Colloids and Interfaces*, *3*, 49. https://doi.org/10.3390/colloids3020049

Debon, S. J. J., & Tester, R. F. (2001). In vitro binding of calcium, iron and zinc by non-starch polysaccharides. *Food Chemistry*, *73*(4), 401–410. https://doi.org/10.1016/S0308-8146(00)00312-5

Defaye, J., & Wong, E. (1986). Structural studies of gum arabic, the exudate polysaccharide from Acacia senegal. *Carbohydrate Research*, *150*(1), 221–231. https://doi.org/10.1016/0008-6215(86)80018-0

Dickinson, E. (2009). Hydrocolloids as emulsifiers and emulsion stabilizers. *Food Hydrocolloids*, *23*(6), 1473–1482. https://doi.org/10.1016/j.foodhyd.2008.08.005

Dickinson, E., Murray, B. S., Stainsby, G., & Anderson, D. M. W. (1988). Surface activity and emulsifying behaviour of some Acacia gums. *Food Hydrocolloids*, *2*(6), 477–490. https://doi.org/10.1016/S0268-005X(88)80047-X

Dror, Y., Cohen, Y., & Yerushalmi-Rozen, R. (2006). Structure of gum arabic in aqueous solution. *Journal of Polymer Science Part B: Polymer Physics*, *44*(22), 3265–3271. https://doi.org/10.1002/polb.20970

Dror, Y., Pyckhout-Hintzen, W., & Cohen, Y. (2005). Conformation of Polymers Dispersing Single-Walled Carbon Nanotubes in Water: A Small-Angle Neutron Scattering Study. *Macromolecules*, *38*(18), 7828–7836. https://doi.org/10.1021/ma0503615

Ducel, V., Richard, J., Saulnier, P., Popineau, Y., & Boury, F. (2004). Evidence and characterization of complex coacervates containing plant proteins: Application to the microencapsulation of oil droplets. *Colloids and Surfaces A: Physicochemical and Engineering Aspects*, *232*(2), 239–247. https://doi.org/10.1016/j.colsurfa.2003.11.001

Eastwood, M. (1974). Vegetable fibre: Its physical properties. *The Proceedings of the Nutrition Society*, *32*, 137–143. https://doi.org/10.1079/PNS19730031

Ellis, M., Egelund, J., Schultz, C., & Bacic, A. (2010). Arabinogalactan-Proteins: Key Regulators at the Cell Surface? *Plant Physiology*, *153*(2), 403–419. https://doi.org/10.1104/pp.110.156000

Eratte, D., Wang, B., Dowling, K., Barrow, C. J., & Adhikari, B. P. (2014). Complex coacervation with whey protein isolate and gum arabic for the microencapsulation of omega-3 rich tuna oil. *Food & Function*, *5*(11), 2743–2750. https://doi.org/10.1039/C4FO00296B

Erni, P., Windhab, E. J., Gunde, R., Graber, M., Pfister, B., Parker, A., & Fischer, P. (2007). Interfacial rheology of surface-active biopolymers: Acacia senegal gum versus hydrophobically modifed starch. *Biomacromolecules*, *8*(11), 3458–3466. https://doi.org/10.1021/bm700578z

Fincher, G. B., Stone, B. A., & Clarke, A. E. (1983). Arabinogalactan-Proteins: Structure, Biosynthesis, and Function. *Annual Review of Plant Physiology*, *34*(1), 47–70. https://doi.org/10.1146/annurev.pp.34.060183.000403

Flanagan, J., Su, J., O'Brien, C., O'Riordan, B., Singh, H., & Dunne, C. P. (2008). Microencapsulating properties of acacia (sen) SUPER GUM. *Foods and Food Ingredients Journal of Japan*, *213*(3), 256–262.

Flindt, C., Al-Assaf, S., Phillips, G. O., & Williams, P. A. (2005). Studies on acacia exudate gums. Part V. Structural features of Acacia seyal. *Food Hydrocolloids*, *19*(4), 687–701. https://doi.org/10.1016/j.foodhyd.2004.09.006

Gabel, L. F. (1930). The effect of heat on acacia. *Journal of the American Pharmaceutical Association*, *19*(8), 828–830.

Gao, Y.-T., Shen, P.-Y., Wang, B.-H., Lü, S.-D., Huang, G.-C., & Ho, L.-S. (1984). Controlled release effect of insecticide microcapsules and their results in common household insect pest control. *Journal of Microencapsulation*, *1*(4), 307–315. https://doi.org/10.3109/02652048409031543

Gashua, I. B., Williams, P. A., & Baldwin, T. C. (2016). Molecular characteristics, association and interfacial properties of gum Arabic harvested from both Acacia senegal and Acacia seyal. *Food Hydrocolloids*, *61*, 514–522. https://doi.org/10.1016/j.foodhyd.2016.06.005

Gashua, I. B., Williams, P. A., Yadav, M. P., & Baldwin, T. C. (2015). Characterisation and molecular association of Nigerian and Sudanese Acacia gum exudates. *Food Hydrocolloids*, *51*, 405–413. https://doi.org/10.1016/j.foodhyd.2015.05.037

Gils, P. S., Ray, D., & Sahoo, P. K. (2010). Designing of silver nanoparticles in gum arabic based semi-IPN hydrogel. *International Journal of Biological Macromolecules*, *46*(2), 237–244.

https://doi.org/10.1016/j.ijbiomac.2009.12.014

Glicksman, M., & Sand, R. E. (1973). Gum arabic. In *Industrial Gums: Polysaccharides and Their Derivatives* (Academic press, pp. 223–226). Whistler.

Glover, D. A., Ushida, K., Phillips, A. O., & Riley, S. G. (2009). Acacia(sen) SUPERGUMTM (Gum arabic): An evaluation of potential health benefits in human subjects. *Food Hydrocolloids*, *23*(8), 2410–2415.

Harrison, B. G. (1940). The postage stamp. *Journal of the Royal Society of Arts*, *88*(4562), 650–662.

Hatakeyama, T., Uetake, T., Inui, Y., & Hatakeyama, H. (2009). Freezing Bound Water Restrained by Gum Arabic. In *Gums and Stabilisers for the Food Industry 15* (pp. 69–76). https://doi.org/10.1039/9781849730747-00069

Hayashi, H. (2002). *Method of modifying gum arabic* (European Union Patent No. EP1505078B1). https://patents.google.com/patent/EP1505078B1/ja

Hedayati, R., Jahanshahi, M., & Attar, H. (2012). Fabrication and characterization of albumin-acacia nanoparticles based on complex coacervation as potent nanocarrier. *Journal of Chemical Technology & Biotechnology*, *87*(10), 1401–1408. https://doi.org/10.1002/jctb.3758

Hu, X., Kaplan, D., & Cebe, P. (2008). Dynamic protein-water relationships during β-sheet formation. *Macromolecules*, *41*(11), 3939–3948. https://doi.org/10.1021/ma071551d

Huang, Y., Wang, Y., Tan, L., Sun, L., Petrosino, J., Cui, M.-Z., Hao, F., & Zhang, M. (2016). Nanospherical arabinogalactan proteins are a key component of the high-strength adhesive secreted by English ivy. *Proceedings of the National Academy of Sciences*, *113*(23), E3193–E3202. https://doi.org/10.1073/pnas.1600406113

Idris, O. H. M., Williams, P. A., & Phillips, G. O. (1998). Characterisation of gum from Acacia senegal trees of different age and location using multidetection gel permeation chromatography. *Food Hydrocolloids*, *12*(4), 379–388. https://doi.org/10.1016/S0268-005X(98)00058-7

Islam, A. M., Phillips, G. O., Sljivo, A., Snowden, M. J., & Williams, P. A. (1997). A review of recent developments on the regulatory, structural and functional aspects of gum arabic. *Food Hydrocolloids*, *11*(4), 493–505. https://doi.org/10.1016/S0268-005X(97)80048-3

Jurasek, P., Kosik, M., & Phillips, G. O. (1993). The classification of natural gums. Part II. Characterisation of the gum arabic of commerce based on a chemometric study of amino-acid compositions. *Food Hydrocolloids*, *7*(2), 157–174. https://doi.org/10.1016/S0268-005X(09)80167-7

Jurasek, P., Varga, S., & Phillips, G. O. (1995). Classification of natural gums. VII. Relationships between the series Vulgares (Acacia senegal) and Gummiferae (Acacia seyal). *Food Hydrocolloids*, *9*(1), 17–34. https://doi.org/10.1016/S0268-005X(09)80190-2

Katayama, T., Ogasawara, T., Sasaki, Y., Al-Assaf, S., & Phillips, G. (2008). *Composition Containing Hydrogel Component Derived from Gum Arabic* (United States Patent No. US20080038436A1). https://patents.google.com/patent/US20080038436A1/en

Kattumuri, V., Katti, K., Bhaskaran, S., Boote, E. J., Casteel, S. W., Fent, G. M., Robertson, D. J., Chandrasekhar, M., Kannan, R., & Katti, K. V. (2007). Gum Arabic as a Phytochemical Construct for the Stabilization of Gold Nanoparticles: In Vivo Pharmacokinetics and X-ray-

Contrast-Imaging Studies. *Small*, *3*(2), 333–341. https://doi.org/10.1002/smll.200600427

Kim, M. T., Park, H. S., Hui, D., & Rhee, K. Y. (2011). Carbon Nanotube Modification Using Gum Arabic and Its Effect on the Dispersion and Tensile Properties of Carbon Nanotubes/Epoxy Nanocomposites. *Journal of Nanoscience and Nanotechnology*, *11*(8), 7369–7373. https://doi.org/10.1166/jnn.2011.4791

Kjellbom, P., Snogerup, L., Stöhr, C., Reuzeau, C., McCabe, P. F., & Pennell, R. I. (1997). Oxidative cross-linking of plasma membrane arabinogalactan proteins. *The Plant Journal*, *12*(5), 1189–1196. https://doi.org/10.1046/j.1365-313X.1997.12051189.x

Kong, H., Yang, J., Zhang, Y., Fang, Y., Nishinari, K., & Phillips, G. O. (2014). Synthesis and antioxidant properties of gum arabic-stabilized selenium nanoparticles. *International Journal of Biological Macromolecules*, *65*, 155–162. https://doi.org/10.1016/j.ijbiomac.2014.01.011

Kumar, K., Hoshino, K., & Zhang, X. (2008). Handheld subcellular-resolution single-fiber confocal microscope using high-reflectivity two-axis vertical combdrive silicon microscanner. *Biomedical Microdevices*, *10*(5), 653. https://doi.org/10.1007/s10544-008-9176-5

Kunkel, M. E., Seo, A., & Minten, T. A. (1997). Magnesium binding by gum arabic, locust bean gum, and arabinogalactan. *Food Chemistry*, *59*(1), 87–93. https://doi.org/10.1016/S0308-8146(96)00173-2

Lamport, D., & Várnai, P. (2013). Periplasmic arabinogalactan glycoproteins act as a calcium capacitor that regulates plant growth and development. *New Phytologist*, *197*(1), 58–64. https://doi.org/10.1111/nph.12005

Lamport, D., Varnai, P., & Seal, C. (2014). Back to the future with the AGP-Ca2+ flux capacitor. *Annals of Botany*, *114*. https://doi.org/10.1093/aob/mcu161

Leszczuk, A., Kalaitzis, P., Blazakis, K., & Zdunek, A. (2020). The role of arabinogalactan proteins (AGPs) in fruit ripening—A review. *Horticulture Research*, *7*(1), 176. https://doi.org/10.1038/s41438-020-00397-8

Li, X., Fang, Y., Al-Assaf, S., Phillips, G. O., Nishinari, K., & Zhang, H. (2009). Rheological study of gum arabic solutions: Interpretation based on molecular self-association. *Food Hydrocolloids*, *23*(8), 2394–2402. https://doi.org/10.1016/j.foodhyd.2009.06.018

Ling, M., Xu, Y., Zhao, H., Gu, X., Qiu, J., Li, S., Wu, M., Song, X., Yan, C., Liu, G., & Zhang, S. (2015). Dual-functional gum arabic binder for silicon anodes in lithium ion batteries. *Nano Energy*, *12*, 178–185. https://doi.org/10.1016/j.nanoen.2014.12.011

Lopez-Hernandez, F., Tryfona, T., Rizza, A., Yu, X., Harris, M. O. B., Webb, A., Kotake, T., & Dupree, P. (2020). Calcium Binding by Arabinogalactan Polysaccharides Is Important for Normal Plant Development. *The Plant Cell*, *32*(10), 3346–3369. https://doi.org/10.1105/tpc.20.00027

Lopez-Torrez, L. (2016). *Characterisation of Acacia gums and development of heat-induced Acacia gum/potato proteins microparticles*.

Lopez-Torrez, L., Nigen, M., Williams, P., Doco, T., & Sanchez, C. (2015). Acacia senegal vs. Acacia seyal gums – Part 1: Composition and structure of hyperbranched plant exudates. *Food Hydrocolloids*, *51*, 41–53. https://doi.org/10.1016/j.foodhyd.2015.04.019

Ma, R., Levard, C., Marinakos, S. M., Cheng, Y., Liu, J., Michel, F. M., Brown, G. E., & Lowry, G. V. (2012). Size-Controlled Dissolution of Organic-Coated Silver

Nanoparticles. *Environmental Science & Technology*, *46*(2), 752–759. https://doi.org/10.1021/es201686j

Mahendran, T., Williams, P. A., Phillips, G. O., Al-Assaf, S., & Baldwin, T. C. (2008). New Insights into the Structural Characteristics of the Arabinogalactan−Protein (AGP) Fraction of Gum Arabic. *Journal of Agricultural and Food Chemistry*, *56*, 9269–9276.

Mansour, R. M. A., & Hassan, E. A. (2016). Effect of gum concentration and gum protein concentration on emulsifying properties of some Acacia gums. *International Journal of Basic and Applied Chemical Sciences*, *6*(2), 23–35.

Mantell, C. (1954). Technology of Gum Arabic. *Natural Plant Hydrocolloids*, *11*, 20–32. https://doi.org/10.1021/ba-1954-0011.ch005

Matsumoto, N., Riley, S., Fraser, D., Al-Assaf, S., Ishimura, E., Wolever, T., Phillips, G. O., & Phillips, A. O. (2006). Butyrate modulates TGF-β1 generation and function: Potential renal benefit for Acacia(sen) SUPERGUM™ (gum arabic)? *Kidney International*, *69*(2), 257–265. https://doi.org/10.1038/sj.ki.5000028

McNamee, B. J., O'Riordan, E. D., & O'Sullivan, M. (1998). Emulsification and microencapsulation properties of gum arabic. *Journal of Agricultural and Food Chemistry*, *46*(11), 4551–4555. https://doi.org/10.1021/jf9803740

Mejia Tamayo, V. (2018). *Volumetric properties of Arabinogalactan-proteins from Acacia Gum*.

Mejia Tamayo, V., Nigen, M., Apolinar-Valiente, R., Williams, P., Doco, T., Renard, D., & Sanchez, C. (2018). *Flexibility and hydration of amphiphilic hyperbranched Arabinogalactan-protein from plant exudate: A volumetric perspective*. https://doi.org/10.3390/colloids2010011

Mhinzi, G. S. (2003). Intra-species variation of the properties of gum exudates from Acacia Senegal var. Senegal and Acacia seyal var. Fistula from Tanzania. *Bulletin of the Chemical Society of Ethiopia*, *17*(1). https://doi.org/10.4314/bcse.v17i1.61734

Moorjani, M. N., & Narwani, C. S. (1948). Influence of heat on the physico-chemical properties of gum-arabic. *Current Science*, *17*(4), 123–124.

Mothé, C. G., & Rao, M. A. (1999). Rheological behavior of aqueous dispersions of cashew gum and gum arabic: Effect of concentration and blending. *Food Hydrocolloids*, *13*(6), 501–506. https://doi.org/10.1016/S0268-005X(99)00035-1

Mucalo, M. R., Bullen, C. R., Manley-Harris, M., & McIntire, T. (2002). Arabinogalactan from the Western larch tree: A new, purified and highly water-soluble polysaccharide-based protecting agent for maintaining precious metal nanoparticles in colloidal suspension. *Journal of Materials Science*, *37*, 493–504.

Najeeb, C. K., Lee, J.-H., Chang, J., & Kim, J.-H. (2010). The effect of surface modifications of carbon nanotubes on the electrical properties of inkjet-printed SWNT/PEDOT–PSS composite line patterns. *Nanotechnology*, *21*(38), 385302. https://doi.org/10.1088/0957-4484/21/38/385302

Nelson, R. E., & Ander, P. (1972). Heterogeneity of gum arabic and its salts. *Carbohydrate Research*, *25*(1), 81–98. https://doi.org/10.1016/S0008-6215(00)82749-4

Nie, S.-P., Wang, C., Cui, S. W., Wang, Q., Xie, M.-Y., & Phillips, G. O. (2013). The core carbohydrate structure of Acacia seyal var. Seyal (Gum arabic). *Food Hydrocolloids*, *32*(2), 221–227. https://doi.org/10.1016/j.foodhyd.2012.12.027

Nigen, M., Valiente, R. A., Iturmendi, N., Williams, P., Doco, T., Moine, V., Massot, A., Jaouen, I., & Sanchez, C. (2019). The colloidal stabilization of young red wine by Acacia senegal gum: The involvement of

the protein backbone from the protein-rich arabinogalactan-proteins. *Food Hydrocolloids*, *97*, 105176. https://doi.org/10.1016/j.foodhyd.2019.105176

Nisato, G., Ivkov, R., & Amis, E. J. (1999). Structure of Charged Dendrimer Solutions As Seen by Small-Angle Neutron Scattering. *Macromolecules*, *32*(18), 5895–5900. https://doi.org/10.1021/ma990631h

Nishida, K., Kaji, K., Kanaya, T., & Fanjat, N. (2002). Determination of intrinsic viscosity of polyelectrolyte solutions. *Polymer*, *43*(4), 1295–1300. https://doi.org/10.1016/S0032-3861(01)00682-6

Nishino, M., Katayama, T., Sakata, M., Al-Assaf, S., & Phillips, G. O. (2012). Effect of AGP on emulsifying stability of gum Arabic. In *Gum Arabic* (J.F. Kennedy, G.O. Phillips, P.A.Williams, pp. 269–274). RSC Publishing. https://www.researchgate.net/publication/281348374_Effect_of_AGP_on_emulsifying_stability_of_gum_Arabic

Omi, S., Umeki, N., Mohri, H., & Iso, M. (1991). Microencapsulation of pheromone-analogue and measurement of the sustained release. *Journal of Microencapsulation*, *8*(4), 465–478. https://doi.org/10.3109/02652049109021870

Osman, M. E., Williams, P. A., Menzies, A. R., & Phillips, G. O. (1993). Characterization of commercial samples of gum arabic. *Journal Of Agricultural & Food Chemistry*, *41*, 71–77.

Padmanabhan, V., Balakrishnan, S., Kulandaivelu, R., N, S., Lakshmipathy, M., Sagadevan, S., Mohammad, F., Al-Lohedan, H., Paiman, S., & Oh, W. (2020). Nanoformulations of core–shell type hydroxyapatite-coated gum acacia with enhanced bioactivity and controlled drug delivery for biomedical applications. *New Journal of Chemistry*, *44*(17), 7175–7185. https://doi.org/10.1039/D0NJ00668H

Padmanabhan, V., Kulandaivelu, R., & Nellaiappan, S. (2018). New core-shell hydroxyapatite/Gum-Acacia nanocomposites for drug delivery and tissue engineering applications. *Materials Science and Engineering: C*, *92*, 685–693. https://doi.org/10.1016/j.msec.2018.07.018

Palacio-López, K., Tinaz, B., Holzinger, A., & Domozych, D. (2019). Arabinogalactan Proteins and the Extracellular Matrix of Charophytes: A Sticky Business. *Frontiers in Plant Science*, *10*. https://doi.org/10.3389/fpls.2019.00447

Palma, S. I. C. J., Carvalho, A., Silva, J., Martins, P., Marciello, M., Fernandes, A. R., del Puerto Morales, M., & Roque, A. C. A. (2015). Covalent coupling of gum arabic onto superparamagnetic iron oxide nanoparticles for MRI cell labeling: Physicochemical and in vitro characterization. *Contrast Media & Molecular Imaging*, *10*(4), 320–328. https://doi.org/10.1002/cmmi.1635

Palmieri, G. F., Martell, S., Lauri, D., & Wehrle, P. (1996). Gelatin-Acacia Complex Coacervation as a Method for Ketoprofen Microencapsulation. *Drug Development and Industrial Pharmacy*, *22*(9–10), 951–957. https://doi.org/10.3109/03639049609065925

Palumbo, G., Górny, M., & Banaś, J. (2019). Corrosion Inhibition of Pipeline Carbon Steel (N80) in CO2-Saturated Chloride (0.5 M of KCl) Solution Using Gum Arabic as a Possible Environmentally Friendly Corrosion Inhibitor for Shale Gas Industry. *Journal of Materials Engineering and Performance*, *28*. https://doi.org/10.1007/s11665-019-04379-3

Phillips, A. O., & Phillips, G. O. (2011). Biofunctional behaviour and health benefits of a specific gum arabic. *Food Hydrocolloids*, *25*(2), 165–169. https://doi.org/10.1016/j.foodhyd.2010.03.012

Phillips, G. O. (2009). Molecular association and function of arabinogalactan protein complexes from tree exudates. *Structural Chemistry*, *20*(2), 309–315. https://doi.org/10.1007/s11224-009-9422-3

Phillips, G., Takigami, S., & Takigami, M. (1996). *Hydration characteristics of the gum exudate from Acacia senegal*. https://doi.org/10.1016/S0268-005X(96)80048-8

Qi, W., Fong, C., & Lamport, D. T. A. (1991). Gum Arabic Glycoprotein Is a Twisted Hairy Rope: A New Model Based on O-Galactosylhydroxyproline as the Polysaccharide Attachment Site. *PLANT PHYSIOLOGY*, *96*(3), 848–855. https://doi.org/10.1104/pp.96.3.848

Randall, R. C., Phillips, G. O., & Williams, P. A. (1988). The role of the proteinaceous component on the emulsifying properties of gum arabic. *Food Hydrocolloids*, *2*(2), 131–140. https://doi.org/10.1016/S0268-005X(88)80011-0

Randall, R. C., Phillips, G. O., & Williams, P. A. (1989). Fractionation and characterization of gum from Acacia senegal. *Food Hydrocolloids*, *3*(1), 65–75. https://doi.org/10.1016/S0268-005X(89)80034-7

Ray, A., Bird, P., Iacobucci, G., & Clark, B. (1995). Functionality of gum arabic. Fractionation, characterization and evaluation of gum fractions in citrus oil emulsions and model beverages. *Food Hydrocolloids*, *9*(2), 123–131. https://doi.org/10.1016/S0268-005X(09)80274-9

Renard, D., Davantès, A., D'orlando, A., Cahier, K., Molinari, M., Nigen, M., Chalier, P., & Sanchez, C. (2022). Adsorption of arabinogalactan-proteins from Acacia gums (senegal and seyal) and its molecular fractions onto latex particles. *Food Hydrocolloids*, *125*, 107360. https://doi.org/10.1016/j.foodhyd.2021.107360

Renard, D., Garnier, C., Lapp, A., Schmitt, C., & Sanchez, C. (2012). Structure of arabinogalactan-protein from Acacia gum: From porous ellipsoids to supramolecular architectures. *Carbohydrate Polymers*, *90*(1), 322–332. https://doi.org/10.1016/j.carbpol.2012.05.046

Renard, D., Garnier, C., Lapp, A., Schmitt, C., & Sanchez, C. (2013). Corrigendum to "Structure of arabinogalactan-protein from Acacia gum: From porous ellipsoids to supramolecular architectures" [Carbohydr. Polym. 90 (2012) 322-332]. *Carbohydrate Polymers*, *97*(2), 864–867. https://doi.org/10.1016/j.carbpol.2013.05.006

Renard, D., Lavenant-Gourgeon, L., Lapp, A., Nigen, M., & Sanchez, C. (2014). Enzymatic hydrolysis studies of arabinogalactan-protein structure from Acacia gum: The self-similarity hypothesis of assembly from a common building block. *Carbohydrate Polymers*, *112*, 648–661. https://doi.org/10.1016/j.carbpol.2014.06.041

Renard, D., Lavenant-Gourgeon, L., Ralet, M.-C., & Sanchez, C. (2006). Acacia senegal Gum: Continuum of Molecular Species Differing by Their Protein to Sugar Ratio, Molecular Weight, and Charges. *Biomacromolecules*, *7*(9), 2637–2649.

Renard, D., Lepvrier, E., Garnier, C., Roblin, P., Nigen, M., & Sanchez, C. (2014). Structure of glycoproteins from Acacia gum: An assembly of ring-like glycoproteins modules. *Carbohydrate Polymers*, *99*, 736–747. https://doi.org/10.1016/j.carbpol.2013.08.090

Roque, A. C. A., & Wilson, O. C. (2008). Adsorption of gum Arabic on bioceramic nanoparticles. *Materials Science and Engineering: C*, *28*(3), 443–447. https://doi.org/10.1016/j.msec.2007.04.009

Salazar-Montoya, J. A., Jiménez-Avalos, H. A., & Ramos-Ramírez, E. G. (2012). Effects of Gum Arabic Concentration and Soy Proteins on the Flow and Viscoelasticity of their Dispersion. *International Journal of Food Properties*, *15*(4), 891–902. https://doi.org/10.1080/10942912.2010.506099

Sanchez, C., Nigen, M., Mejia Tamayo, V., Doco, T., Williams, P., Amine, C., & Renard, D. (2018). Acacia gum: History of the future. *Food Hydrocolloids*, *78*, 140–160. https://doi.org/10.1016/j.foodhyd.2017.04.008

Sanchez, C., Renard, D., Robert, P., Schmitt, C., & Lefebvre, J. (2002). Structure and rheological properties of acacia gum dispersions. *Food Hydrocolloids*, *16*(3), 257–267. https://doi.org/10.1016/S0268-005X(01)00096-0

Sanchez, C., Schmitt, C., Kolodziejczyk, E., Lapp, A., Gaillard, C., & Renard, D. (2008). The Acacia Gum Arabinogalactan Fraction Is a Thin Oblate Ellipsoid: A New Model Based on Small-Angle Neutron Scattering and Ab Initio Calculation. *Biophysical Journal*, *94*(2), 629–639. https://doi.org/10.1529/biophysj.107.109124

Sasaki, Y., Ogasawara, T., Katayama, T., & Sakata, M. (2014). *Process for producing modified gum arabic* (United States Patent No. US8722129B2). https://patents.google.com/patent/US8722129B2/en

Sharkey, J. B. (1987). Chemistry of postage stamps: Dyes, phosphors, adhesives. *Journal of Chemical Education*, *64*(3), 195. https://doi.org/10.1021/ed064p195

Sharma, V., Jaishankar, A., Wang, Y., & McKinley, G. (2011). Rheology of globular proteins: Apparent yield stress, high shear rate viscosity and interfacial viscoelasticity of bovine serum albumin solutions. *Soft Matter*, *7*(11), 5150–5160. https://doi.org/10.1039/C0SM01312A

Showalter, A. M. (2001). Arabinogalactan-proteins: Structure, expression and function. *Cellular and Molecular Life Sciences*, *58*(10), 1399–1417. https://doi.org/10.1007/PL00000784

Silvestri, D., Mikšíček, J., Wacławek, S., Torres-Mendieta, R., Padil, V., & Černík, M. (2019). Production of electrospun nanofibers based on graphene oxide/gum Arabic. *International Journal of Biological Macromolecules*, *124*, 396–402. https://doi.org/10.1016/j.ijbiomac.2018.11.243

Singh, V., Singh, J., & Srivastava, P. (2018). Synthesis and characterization of Acacia gum–Fe0Np–silica nanocomposite: An efficient Fenton-like catalyst for the degradation of Remazol Brilliant Violet dye. *Applied Nanoscience*, *8*(4), 793–810. https://doi.org/10.1007/s13204-018-0732-x

Sloniewsky, A. R., & Ander, P. (1971). Size and shape of potassium and sodium arabate aggregates in aqueous salt solutions. *Carbohydrate Research*, *18*(1), 103–113. https://doi.org/10.1016/S0008-6215(00)80262-1

Song, J. E., Phenrat, T., Marinakos, S., Xiao, Y., Liu, J., Wiesner, M. R., Tilton, R. D., & Lowry, G. V. (2011). Hydrophobic Interactions Increase Attachment of Gum Arabic- and PVP-Coated Ag Nanoparticles to Hydrophobic Surfaces. *Environmental Science & Technology*, *45*(14), 5988–5995. https://doi.org/10.1021/es200547c

Song, J. K., Choi, H. J., & Chin, I. (2007). Preparation and properties of electrophoretic microcapsules for electronic paper. *Journal of Microencapsulation*, *24*(1), 11–19. https://doi.org/10.1080/02652040601058384

Street, C. A., & Anderson, D. M. W. (1983). Refinement of structures previously proposed for gum arabic and other acacia gum exudates. *Talanta*, *30*(11), 887–893.

https://doi.org/10.1016/0039-9140(83)80206-9

Su, J., Flanagan, J., & Singh, H. (2008). Improving encapsulation efficiency and stability of water-in-oil-in-water emulsions using a modified gum arabic (Acacia (sen) SUPER GUM™). *Food Hydrocolloids*, *22*(1), 112–120. https://doi.org/10.1016/j.foodhyd.2007.03.005

Tait, M. J., Suggett, A., Franks, F., Ablett, S., & Quickenden, P. A. (1972). Hydration of monosaccharides: A study by dielectric and nuclear magnetic relaxation. *Journal of Solution Chemistry*, *1*(2), 131–151. https://doi.org/10.1007/BF01028450

Takigami, S., Takigami, M., & Phillips, G. (1995). *Effect of preparation method on the hydration characteristics of hylan and comparison with another highly cross-linked polysaccharide, gum arabic*. https://doi.org/10.1016/0144-8617(95)98828-5

Tipvarakarnkoon, T., Einhorn-Stoll, U., & Senge, B. (2010). Effect of modified Acacia gum (SUPER GUM™) on the stabilization of coconut o/w emulsions. *Food Hydrocolloids*, *24*(6), 595–601. https://doi.org/10.1016/j.foodhyd.2010.03.002

Touré, S. (2008). *Gum Arabic*. Market News Service (MNS) (Quaterly edition). International Trading Center. https://ngara.org/pdf/GumArabic_MarketNewsService%20Issue1_08.pdf

Verbeken, D., Dierckx, S., & Dewettinck, K. (2003). Exudate gums: Occurrence, production, and applications. *Applied Microbiology and Biotechnology*, *63*(1), 10–21. https://doi.org/10.1007/s00253-003-1354-z

Wang, D. W., & Zhao, X. P. (2009). Microencapsulated electric ink using gelatin/gum arabic. *Journal of Microencapsulation*, *26*(1), 37–45. https://doi.org/10.1080/02652040802127806

Wang, Q., Burchard, W., Cui, S. W., Huang, X., & Phillips, G. O. (2008). Solution Properties of Conventional Gum Arabic and a Matured Gum Arabic (Acacia (sen) SUPER GUM). *Biomacromolecules*, *9*(4), 1163–1169. https://doi.org/10.1021/bm7011696

Whistler, R. (1973). *Industrial Gums: Polysaccharides and Their Derivatives*. Elsevier.

Wickens, G. E., Seif ElDin, A. G., Sita, G., & Nahal, I. (1995). *Role of Acacia Species in the Rural Economy of Dry Africa and the Near East*. Food & Agriculture Org.

Yariv, J., Lis, H., & Katchalski, E. (1967). Precipitation of arabic acid and some seed polysaccharides by glycosylphenylazo dyes. *Biochemical Journal*, *105*(1), 1C-2C. https://doi.org/10.1042/bj1050001C

Zhou, L., Weizbauer, R., Singamaneni, S., Xu, F., Genin, G., & Pickard, B. (2014). Structures formed by a cell membrane-associated arabinogalactan-protein on graphite or mica alone and with Yariv phenylglycosides. *Annals of Botany*. https://doi.org/10.1093/aob/mcu172

Ziegler, G. R., & Foegeding, E. A. (1990). The Gelation Of Proteins. *Advances in Food and Nutrition Research*, *34*, 203–298. https://doi.org/10.1016/S1043-4526(08)60008-X

CHAPTER II.

MATERIALS AND METHODS

1. Materials

A. *seyal* gum (lot OF183377), A. *senegal* gum (lot OF152413) and a mix of sweet orange essential oil and ester gum at a ratio 1:1 (used as oil phase to formulate emulsions) were provided by ALLAND & ROBERT Company—Natural and Organic gums (Port Mort, France). An ionic exchange resin (Purolite® C160MBH, Purolite Ltd, Llantrisant, Wales) was used to remove all the minerals (cations) from A. *seyal* gum. All reagents were purchased from Sigma-Aldrich (St. Louis, MO, USA). Ultrapure deionized water (18.2 MΩ·cm) was used in all experiments.

2. Preparation of gum samples and powder incubation

2.1 Arabic acid powder preparation

A 16 wt% A. *seyal* gum dispersion was prepared in water (pH 4.6) and stirred overnight using a magnetic stirring plate at 250 rpm to allow complete hydration of the gum. Cations were removed from the gum using an ionic exchange resin at a mass ratio gum:resin of 1:1 (Figure II.1). The pH of the dispersion was verified and the demineralization was complete once it reached the value of 2.1. The demineralized A. *seyal* gum was then named as usual arabic acid. Arabic acid dispersion was centrifuged (12,000 rpm, 30 min, 20 °C) with an Avanti J-26S XP (Beckman Coulter) to remove insoluble material ($< 1\%$) before spray-drying (Büchi B-290, Büchi Labortechnik AGt, Switzerland). The outlet and inlet spray drying temperatures were maintained at 70 – 80°C and 190°C, respectively. The flow rate of the feed dispersion was adjusted to 40 mm·min^{-1} by keeping the pump capacity at 30%, and the aspiration was set up at 70 – 75%.

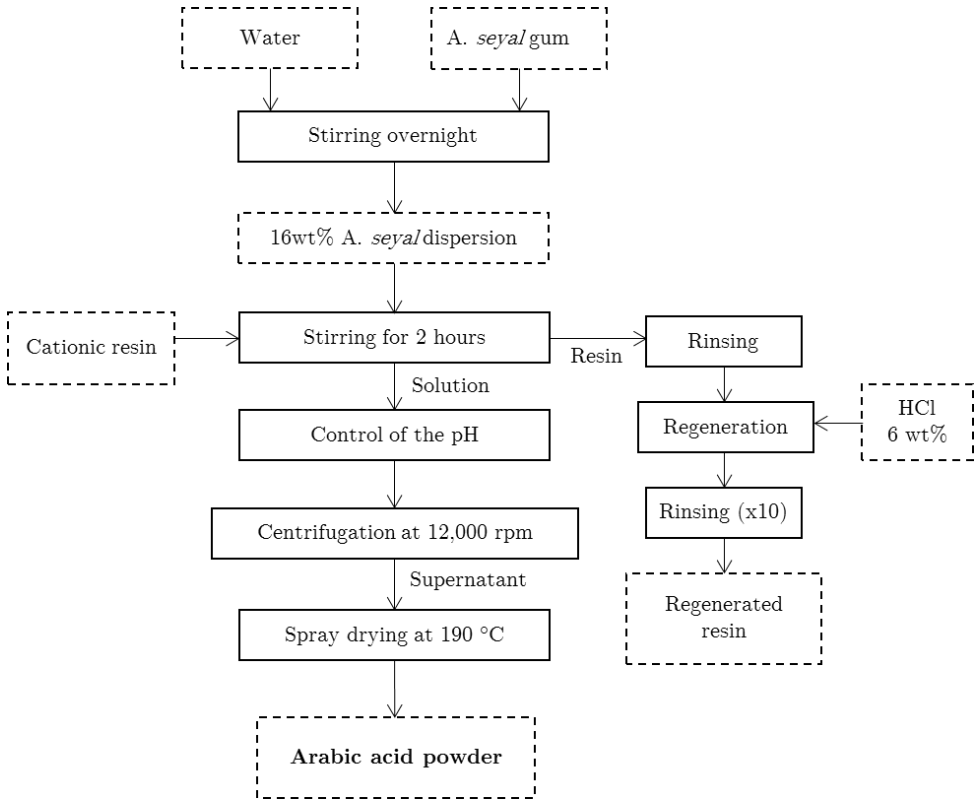

Figure II.1. Flow diagram of the production process of arabic acid powder

2.2 Incubation of arabic acid powder

About 300 mg of arabic acid powder were incubated in closed glass vessels at 25°C, 40°C, 55°C and 70°C in a HPP 260 climate chamber (Memmert, Schwabach, Germany). Samples were regularly collected during incubation kinetics and directly stored at -20°C to stop their aggregaion.

2.3 Preparation of GA dispersions

The GA dispersions at concentrations from 0.5 to 30wt% (db) were prepared in milliQ water using A. *seyal*, A. *senegal*, and incubated arabic acid powders. Dispersions were stirred overnight using an orbital plate at 250 rpm. At 5wt%, the pH of arabic acid dispersions was around 2.4 whereas pH of GA (A. *seyal* and A. *senegal* gums) was around 4.5.

The stability in water of arabic acid aggregates at 1% concentration was studied by varying the physicochemical conditions of dispersion solvent. The objective was to estimate the importance of weak energy interactions (electrostatic and hydrogen bond interaction, van der waals forces) in the formation mechanism of aggregates. The effect of chaotropic agent was investigated using 0, 2, 4 and 8 $mol.L^{-1}$ urea solutions at pH 2.4. The influence of pH between 2.4 and 9.5 was studied upon dispersion of arabic acid powder in water (pH 2.4), 50 $mmol.L^{-1}$ acetate buffer (pH 3.7, 4.4, 5.0), 50 $mmol.L^{-1}$ MES buffer (pH 4.5, 5.5, 6.1, 6.5), 50 $mmol.L^{-1}$ Tris buffer (pH 6.7, 7.5, 7.8, 8.1, 8.6) and 50 $mmol.L^{-1}$ Capso buffer (pH 8.7, 9.5). The potential synergy between pH and ionic strength was also studied using water (zero added ionic strength), and 50 $mmol.L^{-1}$ acetate (pH 4.5), MES (pH 6.5), Tris (pH 7.5, 8.5) and CAPSO (pH 9.5) buffers containing 0.1, 0.5 and 1 $mol.L^{-1}$ NaCl to obtain final ionic strength between about 0 and 1 $mol.L^{-1}$. We also probed the effect of calcium, the main cation interacting with AGPs, dispersing arabic acid powders in water (pH 2.4) containing 0.8, 10 and 50 $mmol.L^{-1}$ $CaCl_2$. All dispersions were stirred overnight using an orbital plate at 250 rpm before experiments were done.

For studying interfacial and emulsifying properties, the pH of arabic acid dispersions was adjusted to the pH of A. *seyal* at the same concentration, using a mixture of $Ca(OH)_2$, $Mg(OH)_2$ and KOH. Salt hydroxide ratio was adapted to mimic the mineral composition of A. *seyal* gum and dispersions were further centrifuged (12,000 rpm, 30 min, 25°C) to remove insoluble material.

3. Methods

3.1Biochemical analyzes

3.1.1 Ash and moisture content

Ash content was determined using the following method. Round-shaped quartz crucibles (A7440632, Fisher Scientific) were first oven dried at 130°C for two hours and cooled in a desiccator for 20 min. 400 mg of sample were placed in each crucible. The samples were then placed at 600°C in a muffle furnace (Nabertherm, Lilienthal, Germany) for 3h (first calcination). The samples were cooled in a desiccator for 20min and 500µL of ultrapure water was added in the crucible in order to disperse ashes. Crucibles were oven dried at 130°C for 10min and placed at 600°C in the muffle furnace for 2h (second calcination). The samples were removed, cooled in a desiccator for 20min and weighed. Moisture content of A. *seyal* gum and arabic acid powders was analyzed as follows: 400 mg of sample were placed in each dry crucible, dried at 130°C for 2h. The samples were then removed, cooled in a desiccator for 20min and weighed.

3.1.2 Protein content and amino acid composition

Nitrogen content was determined by the Kjeldhal method, using a conversion factor of 6.6 to calculate the protein content. Amino acid composition was determined as follows. 10 mg of samples were hydrolyzed by HCl (6N) at 110°C for 24h. The excess of acid was eliminated, samples were solubilized in lithium loading buffer at pH 2.2 and filtered. Amino acid composition of hydrolyzed samples was determined by ionic exchange chromatography (BIOCHROM 30, Cambridge, UK) using lithium citrate (0.2 M, pH 2.2) as eluent. Analysis was done in triplicate and norleucine was used as internal standard.

3.1.3 Sugar composition

Neutral and acidic sugar composition was determined as reported by Lopez-Torrez et al. (Lopez-Torrez et al., 2015a). GA underwent solvolysis with anhydrous MeOH containing 0.5M HCl (80°C, 16h): MeOH brings an O–Me group that can be fixed on the carbocation by nucleophilic substitution. The second step consisted in per-O-trimethylsilylation of the monosaccharides, followed by an extraction with hexane. After separation of the TMS

derivatives, described in (Apolinar-Valiente et al., 2014), sugars were analyzed by GC-MS (GCMS-QP2010SE, Shimadzu, Kyoto, Japan).

3.2 Structural properties

3.2.1 Phase contrast microscopy

Arabic acid dispersions were diluted at 0.5wt% in MilliQ water before microscopic observations. Arabic acid-based aggregates and particles were observed by phase contrast microscopy using an optical microscope (Olympus, France) coupled with x10 and x20 zoom objectives. Pictures were acquired with the CellSens software (Olympus, France).

3.2.2 Scanning electron microscopy (SEM)

SEM observations of Acacia gum powders were performed using a field emission scanning electron microscope (Phenom Pro X, ThermoFisher Scientific, USA) using a backscattered electron detector (acceleration voltage of 10 kV, imaging mode). Before observation, Acacia gum powders were mounted and coated with gold/palladium by ion sputtering.

3.2.3 Transmittance and solubility measurements

The light transmittance at 657 nm of arabic acid dispersions was measured at 25°C using a UV-VIS-NIR spectrophotometer (UltroSpec 2000, Pharmacia Biotech). For solubility measurements, dispersions were centrifuged at 12,000 rpm for 30 min at 20 °C using a Heraeus Fresco 21 microcentrifuge (Thermo Fisher Scientific, Osterode, Germany). After centrifugation, the supernatants were recovered, their volume was measured and their refractive index was determined using an Abbemat Refractometer (Anton Paar, Graz, Austria). The arabic acid AGPs in the supernatants were quantified using a previously determined dn/dC for each dispersion condition (Table II.1) and the pelleted ones were then calculated as following:

$$[\text{AGPs (t)}]_{\text{insoluble}}\,(\%) = 100 \cdot \left(1 - \frac{C'V'}{CV}\right)$$

where C and V are, respectively, the concentration ($g_{GA} \cdot g_{dispersion}^{-1}$) and the volume (mL) of dispersion before centrifugation, and C' and V' are the concentration and the volume of supernatant dispersion after centrifugation.

Table II.1. dn/dC values determined according to pH buffer and ionic strength. The ionic strength was adjusted with NaCl in most of the cases, or with $CaCl_2$ (*).

Buffer	pH buffer	Salt concentration ($mmol \cdot L^{-1}$)	dn/dC ($mL \cdot g^{-1}$)
Acetate	3.5	0	0.1472
	4.5	0	0.1477
		100	0.144
		500	0.1499
		1000	0.1406
	5.5	0	0.1508
MES	5.5	0	0.1464
	6.5	0	0.1469
		100	0.1501
		500	0.147
		1000	0.1428
	7.5	0	0.1514
Tris	7.5	0	0.149
		100	0.1435
		500	0.1473
		1000	0.1413
	8.5	0	0.1514
		100	0.146
		500	0.1488
		1000	0.1432
	9.5	0	0.1532
Capso	10	0	0.148
		100	0.1435
		500	0.154
		1000	0.1425
Water	-	0	0.1492
		0.8*	0.149
		10*	0.1489
		50*	0.1477
		100	0.1446
		500	0.1461
		1000	0.1409

3.2.4 Static Light Scattering (SLS) measurements

The volumetric diameter distribution of arabic acid AGP aggregates in water was determined on the whole sample by static laser light scattering using a Mastersizer 2000 (Malvern Instruments, Orsay, France) equipped with the Scirocco 2000 dry dispersion unit and the Hydro 2000S wet dispersion unit, respectively.

In dry state, a refractive index of 1.338 for aggregated samples was used in the recording parameters. For all samples, three cycles of measurements of 10s were performed at room temperature. In wet state, the concentration was adjusted to reach an obscuration around 5 %. Refractive indices of 1.331 for eluent (water) and 1.338 for aggregated samples were used in the recording parameters. For all samples, five cycles of measurements (10 s delay) were performed at room temperature.

The span and the volumetric aggregate diameter ($D_{4,3}$) were determined. The $D_{4,3}$ was calculated as follow:

$$D_{4,3} = \sum n_i d_i^4 \Big/ \sum n_i d_i^3$$

where n_i is the number of particles of diameter d_i.

3.2.5 SEC MALLS and AF4 MALLS characterization

The distribution and structural properties of AGPs and soluble aggregates from arabic acid were characterized by multi-detector high performance size exclusion chromatography (HPSEC) and asymmetrical flow field-flow fractionation (AF4). These experiments were performed on the supernatants obtained after the centrifugation of the dispersions at 12,000 rpm and 20 °C during 30min using a Heraeus Fresco 21 microcentrifuge (Thermo Fisher Scientific, Osterode, Germany). The supernatants were diluted to obtain final concentration of 1 mg·mL^{-1} and 2 mg·mL^{-1} for SEC MALLS and AF4 MALLS measurements, respectively. 50µL of diluted supernatants were injected.

The HPSEC line was constituted of a Shimadzu HPLC system (Shimadzu, Kyoto, Japan) and the AF4 instrument was a Dual Tech Separation System (Wyatt Technology Europe, Dernbach, Germany). Both systems were connected to a 18 angles Dawn Heleos II (MALLS)

detector (Wyatt Technology, Santa Barbara, CA, USA) equipped with a quasi-elastic light scattering (QELS) detector (Wyatt Technology) in position 14 (SEC MALLS) or 12 (AF4 MALLS), and an OptilabRex differential refractive index detector (Wyatt Technology, Santa Barbara, CA, USA). The HPSEC line was additionally coupled to an online Viscometer (VISCOSTAR II, Wyatt, Santa Barbara, CA, USA), and a UV-VIS detector activated at 280 nm (SPD-20A, Shimadzu). The separation of macromolecules by SEC was performed on an OHPAK SB-G guard pre-column followed by four columns in series (OHPAK SB 803, 804, 805 and 806 HQ, Shodex). The mobile phase or eluent (0.01M acNa, 0.3M NaCl, 0.02 % NaN_3) was filtered through 0.1µm filter (Millipore) and pumped at 1 $mL \cdot min^{-1}$.

The AF4 channel had a trapezoidal shape (length = 17.3cm, initial breadth = 1.1cm, final breadth = 0,27cm) and a thickness of 350 µm. The "accumulation wall" was an ultrafiltration cellulose regenerated membrane (Consenxus, Germany) with a M_w cut-off of 10 $kg.mol^{-1}$ (Wyatt Technology Europe, Dernbach, Germany). A Thermo Ultimate 3000 series isocratic pump with an in-line vacuum degasser and an autosampler delivered the carrier flow and handled sample injection onto the AF4 channel. Between the pump and the channel, mobile phase or eluent were filtrated through an online 0.1 µm filter (VVLP, Millipore, Germany). The injection and the detector flow rates were set up at 0.4 $mL \cdot min^{-1}$ and 1 $mL \cdot min^{-1}$, respectively; and the crossflow (V_x) was varied. A 1 min elution step followed by a 1 min focusing step (V_x = 1 $mL \cdot min^{-1}$) were performed prior to injection of the sample. Samples were injected during the 3 min focus+inject step. After a second 2 min focusing step, an exponentially decaying crossflow profile from 3 $mL \cdot min^{-1}$ to 0.13 $mL \cdot min^{-1}$ in 27 min was used to ensure a better resolution and separation of the polydisperse macromolecules (Kirkland et al., 1992; Leeman et al., 2006). The crossflow was then cut off for a 3 min elution step. After elution, the channel was flushed out without crossflow in order to elute the smallest particles and to rinse the injection loop. More details on elution conditions used for the characterization of AGP aggregates is given in Table II.2.

The data were analyzed using the Zimm's model and an experimentally determined refractive index increment (dn/dc) of 0.145 $mL \cdot g^{-1}$, corresponding to the value of dn/dc measured for A. *seyal* gum and other incubated gums in the eluent. Data processing was operated using the ASTRA software 7.1.2 (Wyatt Technologies, Santa Barbara, CA, USA). The obtained gyration

radius (R_g) was considered only for values above 10nm, which is the sensitivity limit of the MALLS detector.

Table II.2. Elution conditions used for the characterization of AGP aggregates by AF4 MALLS.

Start time (min)	End time (min)	Duration (min)	Mode	Crossflow V_x start ($mL \cdot min^{-1}$)	Crossflow V_x end ($mL \cdot min^{-1}$)	Detector flow V_d ($mL \cdot min^{-1}$)
0	1	1	elution	0	0	1
1	2	1	focus	1	1	1
2	5	3	focus+inject	1	1	1
5	7	2	focus	1	1	1
7	34	27	elution	3	0.13	1
34	37	3	elution	0	0	1
37	42	5	elution+inject	0	0	1

3.2.6 Fourier Transform Infrared (FTIR) spectroscopy

Vibrational properties of chemical bonds in GA, arabic acid and incubated arabic acid powders were analyzed using a mid-infrared spectrometer (Vertex 70v, Brüker, Ettlingen, Germany) in Attenuated Total Reflectance (ATR) mode. FTIR-ATR spectra were recorded at room temperature and under vacuum conditions from 4000 to 800 cm^{-1}, at a spectral resolution of 4 cm^{-1} and averaged over 128 scans. Spectra processing including automatic baseline correction, normalization and smoothing, was carried out using the OPUS software version 8.2.28.

3.2.7 High-field NMR spectroscopy

^{13}C NMR spectra were recorded at 25°C using a Bruker AVANCE III HD spectrometer operating at ^{1}H Larmor frequency of 600 MHz. The spectrometer was equipped with a 3.2 mm magic angle spinning (MAS) probe. ^{13}C NMR spectra were recorded by applying a 90° excitation pulse of 3.82 and 3.9µs at 120W for t_0 and t_7 samples respectively, and a 2s recycle delay for accurate integration of the carbon signals. NMR data processing was performed using Topsin 3.5 software.

3.3 Physiscochemical properties

3.3.1 Hydration properties

Volumetric properties measurements

Thermodynamic (volumetric) properties of gum samples were determined from density and sound velocity measurements operated at 25°C and 3 MHz using a DSA 5000M sonodensimeter (Anton Paar, les Ulis, France). Before measurement, all samples were sonicated 15 min in order to minimize dissolved air. The instrument is equipped with a density cell, a sound velocity cell and an automatic sample changer. The repeatability of the instrument is in theory $1 \cdot 10^{-6}$ g·cm^{-3} for density and 0.1 m·s^{-1} for sound velocity. In reality, the measured parameters, especially the adiabatic compressibility, are extremely sensitive to tiny energetic changes in dispersions, leading to measurement errors with heterogeneously aggregated AGPs to around 10 – 20%. Measurements were at least duplicated.

Time-Domain Nuclear Magnetic Resonance spectroscopy (TD NMR)

Transverse spin-spin proton relaxation times (T_2) were obtained from time-domain nuclear magnetic resonance (TD NMR) measurements performed using a Minispec mq spectrometer (Bruker, France) operating at a frequency of 20 MHz (0.47 Tesla). T_2 were determined using the free induction decay (FID) of the signals for T_2 lower than 200 µs and the Carrel-Purcell-Meiboom-Gill (CPMG) sequence for T_2 higher than 200 µs. The CPMG sequence allows to probe only dynamics of water protons while the FID sequence rather probes the gum protons and the gum-water proton exchanges. An acquisition time of 0.15 ms and 16 scans were used for the FID signal and a recycle delay of 2 s was used for the CPMG signal.

A. *seyal* gum powders were weighted and placed in a climatic chamber at 25°C under controlled relative humidity (RH). Samples were weighted daily until the change of weight in time (dm/dt) was lower than 0.002 %·min^{-1}. Samples were carefully introduced into Bruker NMR tubes and tightly compressed to 10 – 12 mm height to improve homogeneity. The tubes were weighted and sealed with Parafilm® to prevent water evaporation. Measurements were performed at 25°C and duplicated. T_2 relaxation data were normalized to take into account the signal intensity and mass of sample.

Data were fitted using the Sigmaplot software (version 13.0) and a combination of sine and exponential functions according to the relation:

$$y(t) = A_i\, e^{\left(-t/T_{21}\right)^2} \frac{\sin(B*t)}{B*t} + \sum_{i=0}^{n} A_i\, e^{-\frac{t}{T_{2i}}}$$

where A is the amplitude, T_2 is the transverse relaxation time, B is a constant and t is the time.

3.3.2 Rheological measurements

Steady-shear and dynamic viscoelastic properties of GA and arabic acid dispersions at 1 – 30wt% were determined at 25 °C using a stress-controlled MCR 702 TwinDrive rheometer (Anton Paar, les Ulis, France) coupled with a sanded coaxial cylindrical geometry (CC20) with 1 mm gap and an outer radius/inner radius ratio of 1.1. Before experiments, all samples were pre-sheared at 5 – 10 s^{-1} for 3 min. All experiments were done in duplicate.

Steady-shear measurements (flow curves)

For A. *seyal* and arabic acid dispersions, flow curves were recorded for shear rates decreasing from 1000 to 0.1 s^{-1}, whereas for arabic acid AGP aggregates dispersions, the lower shear rate bound was decreased to 10^{-6} s^{-1}.

Dynamic viscoelastic measurements

Dynamic oscillatory rheological properties of GA dispersions (15wt %) at 25 °C were determined by frequency sweep measurements at 1% strain for a frequency range from 1 to 100 rad·s^{-1}. The mechanical behavior of samples was analyzed by measuring the frequency-dependent storage (G') and loss (G'') moduli.

3.3.3 Interfacial properties at an oil/water interface

The interfacial tension and dilatational rheological properties at 25°C of arabic acid samples were determined through the rising droplet shape method using a drop tensiometer (Tracker, IT concept, Longessaigne, France). Limonene and octanol were selected as organic compounds representative of hydrophobic and more polar liquids, respectively. A 500µL syringe was filled with oil, and connected to a curved needle. A drop of liquid was formed at the end of the needle immersed in a 5 mL glass cuvette containing a 5wt% gum dispersion. The droplet volume of limonene and octanol was 10µL and 2.5µL, respectively, due to differences in stability

of the formed droplets. The shape of the drop was monitored by a CCD camera and data were recorded for 24h.

The oil-water interfacial tension γ was calculated using the Young-Laplace equation:

$$\Delta P = \gamma \cdot \left(\frac{1}{R} + \frac{1}{R\prime}\right)$$

where R and R' are the main radii of curvature of droplets and ΔP is the Laplace pressure corresponding to the pressure difference across the interface.

Interfacial viscoelastic parameters were obtained by applying a sinusoidal variation to the droplet volume (and thus compression/expansion cycles) at 10% of amplitude (ΔV/V) and 0.1 Hz of oscillation frequency ω. Measurements consisted of a repetition of 5 oscillation cycles, of 10s each, followed by a 50s blank period. The surface dilatational viscoelasticity (Eq. II.3) and the phase angle were obtained from the sinusoidal change in interfacial tension γ (Eq. II.1) resulting from a small change in the surface area (Eq. II.2):

$$\gamma = \gamma_0 \sin(\omega t + \delta) \qquad \text{(II.1)}$$

$$A = A_0 \sin(\omega t) \qquad \text{(II.2)}$$

$$E = A(\Delta\gamma)/\Delta A \qquad \text{(II.3)}$$

The obtained modulus (E*) is a complex quantity that can be expressed as

$$E^* = E' + iE''$$

where the real part E' is dilatational elasticity and the imaginary part E'' corresponds to the surface dilatational viscosity. All measurements were performed in duplicate.

3.3.4 Emulsifying properties

Preparation of oil-in-water emulsions

Two different liquids were used to formulate oil-in-water emulsions, namely limonene and a mix ester gum/sweet orange essential oil formulated at a ratio 1:1. In the following of this study, this mix was named EGEO. Oil was added to GA dispersion and the system was premixed using rotor/stator homogenizer (Silverson L4RT, Evry, France) equipped with a

square hole high shear screen stator at 7,500 rpm for 5 min at room temperature (25°C). Then, the coarse emulsions were homogenized using a microfluidizer with a F12Y diamond interaction chamber (LM20, Microfluidics Corporation, MA, USA) operating at a pressure of 440 bars. The emulsion was passed through the homogenizer 2 times. In order to control the temperature during the emulsification step, the emulsion was recovered in a container immersed in an ice bath. All emulsions were prepared in triplicate.

Volumetric size distribution of emulsion droplets

The volumetric droplet size distribution of emulsions was determined by laser light scattering using a LS 13 320 XR laser diffraction particle size analyzer equipped with the Universal Liquid Module ULM (Beckman Coulter). The obscuration was set up at ~ 10%. Refractive index of 1.33 for water, 1.47 for limonene and 1.50 for ester gum/essential oil mixture were used. For all emulsions, three cycles of measurements were performed 10 min after the emulsification step. The mean volume diameter ($D_{4,3}$) was calculated as follows :

$$D_{4,3} = \sum n_i d_i^4 \Big/ \sum n_i d_i^3$$

where n_i is the number of droplets of diameter d_i.

Estimation of emulsion stability

The colloidal stability of emulsions was monitored using a Turbiscan Tower (Formulaction, Toulouse, France) that allowed characterizing destabilization phenomena such as creaming, sedimentation, flocculation and coalescence. Fifteen mL emulsion sample were loaded into cylindrical glass cells about 5 min after emulsification and scanned over the whole height. The light backscattering (BS in %) and transmittance (T in %) signals from a pulsed near infrared light source (λ = 880 nm) were recorded at least every 5 min during the first 24h before recording one measurement at days 2, 3, 7, and then once a week during the storage of emulsions at 25°C. Signals were then analyzed using the TowerSoft software version 1.3.1.85.

Based on the evolution of backscattered or transmitted light during storage, the Creaming Index (CI) and the Turbiscan Stability Index (TSI) were calculated. The CI is usually calculated as the serum layer height relative to the total emulsion height (Keowmaneechai &

McClements, 2002). In our emulsions, the serum layer was hard to measure in the bottom of emulsions tubes and an alternative formula was preferred (Fligner et al., 1991) in order to better discriminate among our emulsions:

$$CI\ (\%) = 100 \times \frac{H_c}{H_t}$$

where H_c is the height of the cream layer and H_t is the total height of emulsion.

While CI is a specific stability index, the TSI parameter is an indicator of the global stability of emulsions over time. It is arbitrarily calculated using the equation:

$$TSI(t) = \frac{1}{N_h} \sum_{t_i=1}^{t_{max}} \sum_{z_i=z_{min}}^{z_{max}} |BST(t_i, z_i) - BST(t_{i-1}, z_i)|$$

with t_{max} the time t at which the TSI is calculated, z_{min} and z_{max} the lower and upper selected height limits respectively, $N_h = (z_{max} - z_{min}) / \Delta h$ the number of height positions in the selected zone of the scan and BST the light intensity. BST takes values of the BS signal when $T < 0.2\%$ and values of the T signal otherwise.

.

4. References

Apolinar-Valiente, R., Williams, P., Mazerolles, G., Romero-Cascales, I., Gómez-Plaza, E., López-Roca, J. M., Ros-García, J. M., & Doco, T. (2014). Effect of enzyme additions on the oligosaccharide composition of Monastrell red wines from four different wine-growing origins in Spain. *Food Chemistry*, *156*, 151–159. https://doi.org/10.1016/j.foodchem.2014.01.093

Fligner, K. L., Fligner, M. A., & Mangino, M. E. (1991). Accelerated tests for predicting long-term creaming stability of infant formula emulsion systems. *Food Hydrocolloids*, *5*(3), 269–280. https://doi.org/10.1016/S0268-005X(09)80113-6

Keowmaneechai, E., & McClements, D. J. (2002). Influence of EDTA and citrate on physicochemical properties of whey protein-stabilized oil-in-water emulsions containing CaCl2. *Journal of Agricultural and Food Chemistry*, *50*(24), 7145–7153. https://doi.org/10.1021/jf020489a

Kirkland, J. J., Dilks, C. H., Rementer, S. W., & Yau, W. W. (1992). Asymmetric-channel flow field-flow fractionation with exponential force-field programming. *Journal of Chromatography A*, *593*(1), 339–355. https://doi.org/10.1016/0021-9673(92)80303-C

Leeman, M., Wahlund, K. G., & Wittgren, B. (2006). Programmed cross flow asymmetrical flow field-flow fractionation for the size separation of pullulans and hydroxypropyl cellulose. *Journal of Chromatography A*, *1134*(1), 236–245. https://doi.org/10.1016/j.chroma.2006.08.065

Lopez-Torrez, L., Nigen, M., Williams, P., Doco, T., & Sanchez, C. (2015). Acacia senegal vs. Acacia seyal gums – Part 1: Composition and structure of hyperbranched plant exudates. *Food Hydrocolloids*, *51*, 41–53. https://doi.org/10.1016/j.foodhyd.2015.04.019

CHAPTER III.

AGGREGATION KINETICS OF DEMINERALIZED ACACIA *SEYAL* GUM DURING MATURATION IN LOW HYDRATION STATE

1. Influence of the loaded mineral and pH on the aggregation behavior of AGPs from GA

At temperatures above 40°C, the incubation in dry state of GA loaded with minerals can promote the aggregation of AGPs, phenomenon concomitant with an improvement of their surface properties (Al-Assaf, Phillips, Aoki, et al., 2007a; Aoki, Al-Assaf, et al., 2007; Aoki, Katayama, et al., 2007). The aggregation kinetics of AGPs closely depend on the incubation temperature. Usually, temperatures of at least 60°C and even upper than 100°C are used to promote the AGP aggregation of GA in dry state (Al-Assaf et al., 2004; Hayashi, 2002; Katayama et al., 2008; Sasaki et al., 2014). In our research group, we evidenced that the storage at ambient temperature of demineralized GA (arabic acid, AA) during several months modified the physicochemical properties of AGPs from AA in solution. In particular, the time needed to solubilize AA in water was higher after storage and the apparent viscosity of the dispersion increased. In contrary, the storage of GA loaded with its minerals in the same environmental and time conditions did not change the physicochemical and structural properties of GA, maintaining its integrity. Therefore, it seems that the demineralization of GA confers to AGPs a higher reactivity during their incubation in dry state. In addition to the removal of minerals, the demineralization of GA also induced the acidification of GA dispersion. Indeed, the pH of AA dispersions at 5wt% is more acidic (pH 2.4) than those of GA (pH 4.5) at the same concentration. This difference in pH value might also be responsible of the higher reactivity of AA powder by modifying carboxylic acid groups of AGPs.

Thus, in this section, the influence of *(i)* the presence of minerals and *(ii)* the acidification of AGPs dispersions before the drying step on the dry state aggregation properties of AGPs were further investigated. For this purpose, two control samples were used and compared to demineralized GA (*i.e.* AA):

- The first control sample was GA powder: the sample was prepared by solubilizing GA at 5wt% in milliQ water before to spray-dry it again. This sample was processed twice in order to work with a gum that was submitted to the same number of spray-drying steps as the two other samples.

- The second control sample was acidified GA powder: the sample was prepared by solubilizing GA at 5wt%, before to acidify the dispersion at pH 2.4 with HCl and spray-dry it once again.
- The third sample was arabic acid (AA) powder: the sample was prepared as described in the materials and methods section II.2.1.

The GA, acidified GA and AA powders were incubated at 40°C between 0 and 7 days. After their incubation, the GA, acidified GA and AA powder samples were dispersed in milliQ water and centrifuged at 12,000 rpm to separate some putative AGP aggregates. Then, the amount of AGPs involved in the formation of these aggregates was quantified all along the kinetics. The insoluble material (%) in GA, acidified GA and AA powder samples stored at 40°C as a function of incubation time is given in Figure III.1. Incubated AGPs from the two control samples (GA and acidified GA) were completely soluble in water without the formation of pelleted materials after 7 days of incubation at 40°C. In contrary, some pelleted materials were obtained for arabic acid samples incubated longer than 2 days at 40°C. After 2 days of incubation, the amount of pelleted AGPs increased until reaching a plateau at a maximum value around 80% from 5 days of incubation (Figure III.1). Therefore, these first results evidenced that AGPs from GA and acidified GA did not seem to be sensitive to their dry incubation at 40°C, in contrary to those of AA.

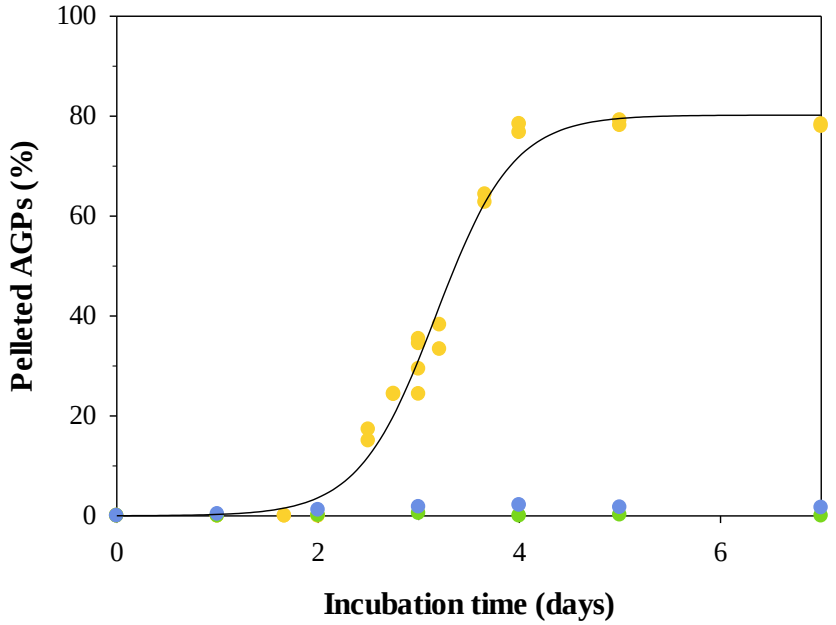

Figure III.1. Percentage of pelleted AGPs in aqueous dispersions of incubated arabic acid (●), GA spray-dried at pH 2.4 (●) and GA (●) as a function of incubation time at 40°C. The continuous line represents the fit obtained with SigmaPlot software.

The AGPs from GA, acidified GA and AA dispersions all along the incubation kinetics were further analyzed using SEC MALLS. As SEC MALLS is susceptible to give information only on the soluble part of the samples, the measurements done on GA and acidified GA (control samples) are representative of the whole sample whereas the measurements done with AA samples reflect the behavior of the whole sample before 2 days of incubation and of AGPs and soluble aggregates above 2 days of incubation. Figure III.2 displays the evolution of the mean molar mass (M_w) of AGPs and soluble aggregates all along the kinetic at 40°C. For GA, the mean M_w was constant with a value around $9.0 \cdot 10^5$ g·mol^{-1} all over the incubation time (7 days). Therefore, the AGPs structural properties from GA were not affected by the dry incubation of GA powder at 40°C. As a comparison, the dry incubation of A. *senegal* gum under 30%RH at 40°C for 7 days induced an increase in molar mass by 1.5 (Hayashi, 2002). The gum specie, A. *senegal* vs. A. *seyal* might explain this difference in reactivity. The mean M_w of the second incubated control sample (acidified GA) slightly but continuously increased with incubation time, from $9.7 \cdot 10^5$ (t_0) to $2.3 \cdot 10^6$ g.mol^{-1} (t_7). Therefore, AGPs from acidified GA slightly aggregated during their dry incubation without the formation of pelleted aggregates as shown by solubility measurements (Figure III.1). With incubated arabic acid samples, the mean M_w greatly increased from $1 \cdot 10^6$ g·mol^{-1} (t_0) to reach a maximum M_w at $6.7 \cdot 10^6$ g·mol^{-1}

after 1.66 days of incubation at 40°C, before dropping to a mean M_w value around $5 \cdot 10^5$ g·mol^{-1} after 7 days of incubation. The M_w behavior was further described and analyzed in the results section of the following paper (Section III.4.3.2). Using the M_w behavior, the calculated rate of aggregation kinetic of acidified GA and AA powders were 2.1 s^{-1} and 29.9 s^{-1}, respectively. By comparing the solubility and M_w trends of the AGPs from the three A. *seyal* powder samples, they can be classified in the following order by considering their reactivity and ability to aggregate: AA >> GA at pH 2.4 > GA. Therefore, it could be concluded that minerals of GA have a protective role for the structural stability of AGPs upon dry incubation. In addition, the pH of GA dispersions before spray-drying also seemed to influence the AGPs reactivity by slightly promoting their aggregation at acidic pH.

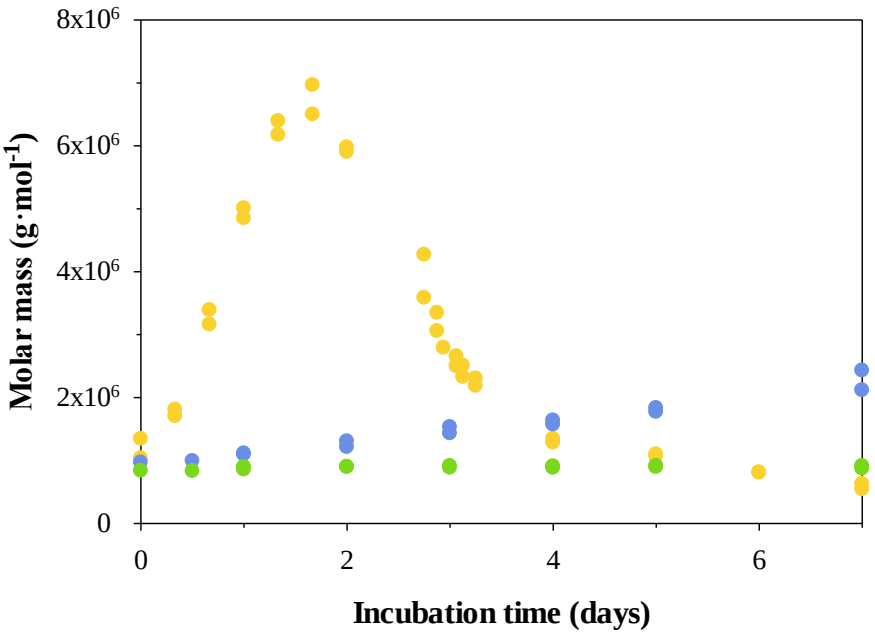

Figure III.2. Calculated mean molar mass determined by SEC MALLS experiments from AGPs and soluble aggregates of arabic acid (●), GA spray-dried at pH 2.4 (●) and GA (●) incubated at 40°C as a function of incubation time.

In the following, the aggregation kinetics of AA AGPs and the structural properties of these aggregates were further investigated.

Maturation of demineralized arabinogalactan-proteins from Acacia *seyal* gum in dry state: Aggregation kinetics and structural properties of aggregates

Amandine Antoine-Michard[a,b], Céline Charbonnel[a], Isabelle Jaouen[b], Christian Sanchez[a] and Michaël Nigen[a,*]

[a] UMR IATE, Univ Montpellier, INRAE, Institut Agro, 34060 Montpellier, France

[b] ALLAND & ROBERT, 75003, Paris, France

* Corresponding author.

E-mail address: michael.nigen@umontpellier.fr

Abbreviations

GA: Acacia gum; AGPs: arabinogalactan-proteins; SEC: size-exclusion chromatography; AF4: asymmetrical flow field-flow fractionation

Abstract

The aggregation in dry state of mineral-loaded arabinogalactan-proteins (AGPs) from Acacia *seyal* gum (GA) generally occur above 70°C. This study focuses on the aggregation sensitivity of AGPs after their demineralization. Arabic acid gum was obtained by demineralization of GA. The dry incubation in mild temperature (25°C to 70°C) of demineralized AGPs induced the formation of aggregates, not observed with GA. AGPs aggregated following a self-assembly mechanism for which temperature only modulated the aggregation rate. The activation energy was around 90 – 100 kJ.mol^{-1} that could correspond to chemical condensation reactions induced by the AGPs surface dehydration. The aggregation kinetics were characterized by the formation of soluble aggregates during the first times of incubation, whose molar mass increased from $1{\cdot}10^6$ g· mol^{-1} to $6.7{\cdot}10^6$ g·mol^{-1} (SEC MALS) or $12{\cdot}10^6$ g·mol^{-1} (AF4 MALS) after 1.66 days of dry heating at 40°C. These soluble aggregates revealed they adopted a similar conformation to that of not aggregated AGPs with a ν_h value around 0.45. Above 1.66 days at 40°C, the soluble aggregates grew up to form microparticles with sizes ranging from 10 to around 200 µm. This study highlighted the protective role of cations from AGPs whose demineralization increased their sensibility to dry heating and their chemical reactivity for aggregation.

Keywords: Acacia gums, Arabinogalactan-proteins, Demineralization, Aggregation, Dry heating, Microparticles.

2. Introduction

Acacia gum (GA) is a natural dried gummy exudate obtained from the branches and trunks of Acacia *seyal* and Acacia *senegal* trees mainly located in the sub-Saharan belt region (Cecil, 2005). GA is composed of arabinogalactan-proteins-type macromolecules (AGPs) belonging to the glycoprotein superfamily (Akiyama et al., 1984). AGPs are ubiquitous in plant kingdom where they fulfill a wide range of biological functions including the plant growth and development (Majewska-Sawka & Nothnagel, 2000; Seifert & Roberts, 2007), cellular

differentiation (M. Gao & Showalter, 2000), cell-cell recognition (Fincher et al., 1983; Majewska-Sawka & Nothnagel, 2000; Showalter, 2001), and mineral carrier (Showalter, 2001). Basically, AGPs are hyperbranched, charged, amphiphilic proteoglycans rich in arabinose and galactose, with a small fraction of proteins, minerals (calcium, magnesium and potassium) and polyphenols (Anderson et al., 1983; Debon & Tester, 2001; Idris et al., 1998; Kunkel et al., 1997; Lopez-Torrez et al., 2015a; Sanchez et al., 2018; Taft & Malm, 1931). They are structured by hyperbranched polysaccharide blocks cross-linked to peptide and polypeptide backbones. GA is a heterogeneous material defined as a continuum of AGPs differing by their biochemical (sugar, amino acids and mineral content and composition, sugar to protein ratio) and structural (molar mass, size and shape) properties (Al-Assaf et al., 2005a, 2005b; Islam et al., 1997; Randall et al., 1989; Renard et al., 2006; Sanchez et al., 2018). These biochemical and structural characteristics are responsible for the numerous physicochemical properties of GA and its various applications in food and non-food areas as stabilizer, emulsifier, surface finishing agent, flavoring agent and thickener (Sanchez et al., 2018; Verbeken et al., 2003). They also underlie the ability of AGPs from GA to self-assemble and aggregate both *in vivo* during the gum exudation and its maturation (Capataz-Tafur et al., 2011; Idris et al., 1998; G. O. Phillips, 2009), and *in vitro* after its harvest during its processing or storage, in solution or dry state (Al-Assaf et al., 2012; Al-Assaf, Phillips, Aoki, et al., 2007b; Aoki, Al-Assaf, et al., 2007; Idris et al., 1998; G. O. Phillips & Williams, 1993; Sanchez et al., 2002). The AGPs aggregation with the formation of high molar mass AGPs is usually associated with the improvement of the physicochemical properties of GA, notably its hydration, interfacial and rheological properties. *In vivo*, AGPs aggregation is evidenced as a natural and biological mechanism related to the tree physiology and occurring especially during the maturation of GA (Idris et al., 1998). Aging of Acacia trees influences the structural properties (gyration radius R_g, hydrodynamic radius R_h, molar mass M_w) of AGPs from harvested GA. For instance, an increase in AGPs molar mass from $3.2 \cdot 10^5$ to $7.9 \cdot 10^5$ g·mol^{-1} was observed when Acacia trees get older, from 5 to 15 years, with a M_w maximum value reached between 10 and 15 years (Idris et al., 1998). The enrichment in high molar mass AGPs was correlated with a higher proportion of aggregates in solution.

Association properties of GA in solution have been highlighted over a large concentration range using size exclusion chromatography (Idris et al., 1998; Ray et al., 1995; Sanchez et al., 2002), scattering and microscopic techniques (Dror et al., 2006; Renard et al., 2012; Wang et al.,

2008). This aggregation behavior is greatly sensitive to the physicochemical conditions of the dispersion as the pH and the ionic strength (Dror et al., 2006; Mejia Tamayo, 2018). The acidification or the increase in ionic strength of the dispersion reduce the aggregation properties of AGPs (Mejia Tamayo, 2018). By static light scattering measurements, Wang et al. showed an increase in R_g from 20 to 50 nm as the concentration of GA increased from 0.04 to 5.21 $g.L^{-1}$ that was attributed to the AGPs aggregation (Q. Wang et al., 2008). The AGPs aggregation was also observed in more concentrated dispersions with the highlight of small-angle scattering methods (SANS, SAXS) and TEM observations (Dror et al., 2006; Gashua et al., 2016).

Less attention had been paid to the aggregation properties of AGPs from GA in dry state. By dry state, we refer to a powder containing about 8% water. Some studies evidenced the sensitivity of AGPs to physical treatments such as spray-drying, irradiation and storage conditions that could promote the AGPs aggregation. Al-Assaf et al. reported an increase of AGPs M_w from 0.72 to $1.67 \cdot 10^6$ $g \cdot mol^{-1}$ during spray-drying (Al-Assaf et al., 2009). The AGPs aggregation was also promoted by the irradiation of GA through the formation of C-C covalent bonds between the carbohydrate blocks of AGPs (Al-Assaf et al., 2009). Heating GA powder at 100°C for two days resulted in an increase of Acacia dispersion viscosity by 3 (Gabel, 1930). Above 170°C, GA powder became totally insoluble in water (Moorjani & Narwani, 1948). AGPs aggregation was also evidenced upon their storage above 40°C and relative humidities from 30 to 100% (Al-Assaf et al., 2004; Hayashi, 2002). The latter authors reported a M_w increase after at least 15h of heating at 110°C. For instance, M_w of a spray-dried A. *seyal* heated for 24h increased from 1.15 to $1.45 \cdot 10^6$ $g \cdot mol^{-1}$. The aggregation of these AGPs improved the emulsifying properties of A. *senegal* gums (Al-Assaf et al., 2010). In particular, aggregated AGPs improved the colloidal stability of emulsions, through obtention of smaller average diameter of oil droplets and reduced droplet size distribution (Castellani, Guibert, et al., 2010). The increase in M_w of aggregated AGPs resulted in changes in hydrodynamic volume (Aoki, Al-Assaf, et al., 2007), an improvement in water-binding properties and an increased elasticity of concentrated dispersions (Al-Assaf, Phillips, Aoki, et al., 2007b).

Any of the reported studies have considered the possible effect of minerals on the aggregation propensity of AGPs in dispersion or dry state. However, we experienced recently some trouble for dispersing GA powder depleted of its minerals (*i.e.* Arabic acid) and stored at ambient temperature. This behavior is not observed with GA loaded with its minerals. These observations suggest that minerals could play a role in the aggregation properties of AGPs and

that demineralization of GA could be used to change its physicochemical properties by the formation of AGPs aggregates under controlled and mild temperature condition.

Here, we studied and characterized the aggregation properties of AGPs from Arabic acid stored in dry state between 25 and 70°C. These conditions notably differ from previous reported studies, where aggregation of AGPs was induced by an important energy input such as heating above 70°C or irradiation at 6 – 50 kGy. The aggregation kinetics were characterized by measuring the solubility of Arabic acid AGPs and the optical stability of colloidal dispersions. The shape and size of insoluble AGPs aggregates were estimated using optical microscopy in combination with SLS, while the structural properties (molar mass, gyration and hydrodynamic radii, and conformation) of soluble AGPs aggregates were investigated by coupled chromatographic techniques (SEC MALLS and AF4 MALLS).

3. Materials and methods

3.1. Materials

All experiments were carried out with A. *seyal* gum (M_w = 0.85·10^6 g·mol^{-1}, [η] = 17 mL·g^{-1}, RH = 7%), provided by Alland & Robert Company–Natural and Organic gums (Port Mort, France) and composed of about 1% of proteins, 1.6% of minerals and more than 90% of sugars. An ionic exchange resin (Purolite® C160MBH, Purolite Ltd, Llantrisant, Wales) was used to remove all the minerals (cations) from A. *seyal* gum. All reagents were purchased from Sigma-Aldrich (St. Louis, MO, USA). Ultrapure deionized water (18.2 MΩ·cm) was used in all experiments.

3.2. Arabic acid powder preparation

A 16 wt% A. *seyal* gum dispersion was prepared in water (pH 4.6) and stirred overnight using a magnetic stirring plate at 250 rpm to allow complete hydration of the gum. Cations from A. *seyal* gum were removed using an ionic exchange resin at a mass ratio gum:resin of 1:1. pH of the dispersion was checked and the demineralization was complete once it reached the value of 2.1. The demineralized A. *seyal* gum was then named Arabic acid in this study. Arabic acid dispersion was centrifuged with an Avanti J-26S XP (Beckman Coulter) to remove insoluble material (12,000 rpm, 30 min, 20 °C) before spray-drying using a benchtop spray-dryer (Büchi

B-290, Büchi Labortechnik AGt, Switzerland). The outlet and inlet spray drying temperatures were maintained at 70 – 80°C and 190°C, respectively. The flow rate of the feed dispersion was adjusted to 40 mm·min^{-1}.

3.3. Chemical analyzes

3.3.1. *Ash and moisture content*

Ash content was determined using the following method. Round-shaped quartz crucibles (A7440632, Fisher Scientific) were first oven dried at 130°C for two hours and cooled in a desiccator for 20 min. 400 mg of sample were placed in each crucible. The samples were then placed at 600°C in a muffle furnace (Nabertherm, Lilienthal, Germany) for three hours (first calcination). The samples were cooled in a desiccator for 20 min and 500µL of ultrapure water was added in the crucible in order to disperse ashes. Crucibles were oven dried at 130°C for 10 minutes and placed at 600°C in the muffle furnace for two hours (second calcination). The samples were removed, cooled in a desiccator for 20 min and weighed. Moisture content of A. *seyal* gum and Arabic acid powders was analyzed as follows: 400 mg of sample were placed in each dry crucible, dried at 130°C for two hours. The samples were then removed, cooled in a desiccator for 20 min and weighed.

3.3.2. *Nitrogen and protein content*

Nitrogen content was determined by the Kjeldahl method, by acidic hydrolysis with sulfuric acid 0.1N and using selenium as catalyst. Samples were neutralized and distilled in a distillation unit BUCHI K-350 using boric acid to recover the nitrogen released. The nitrogen content was determined by titration of the ammonium borate solution with sulfuric acid. The protein content was calculated from the nitrogen content using a conversion factor of 6.6. Experiments were triplicated.

3.3.3. *Amino acid composition*

Amino acid composition was determined after hydrolysis by HCl (6N) at 110°C for 24h. The excess of acid was eliminated and samples were solubilized in lithium loading buffer at pH 2.2 and filtered. Amino acid composition was determined by ionic exchange chromatography

(BIOCHROM 30, Cambridge, UK) using lithium citrate (0.2 M, pH 2.2) as eluent and norleucine as internal standard. Analyzes were triplicated.

3.3.4. *Sugar composition*

GA underwent solvolysis with anhydrous MeOH containing 0.5M HCl (80°C, 16h): MeOH brings an O-Me group that can be fixed on the carbocation by nucleophilic substitution. The second step consisted in per-O-trimethylsilylation of the monosaccharides, followed by an extraction with hexane. After separation of the TMS derivatives, as described in [41], sugars were analyzed by GC-MS (GCMS-QP2010SE, Shimadzu, Kyoto, Japan). Experiments were triplicated.

3.4. Incubation of Arabic acid powder and preparation of Arabic acid dispersions

About 300 mg of spray-dried Arabic acid were incubated in closed glass vessels at 25°C, 40°C, 55°C and 70°C in a HPP 260 climate chamber (Memmert, Schwabach, Germany). Samples were regularly collected during incubation kinetics and directly stored at -20°C to stop their evolution before further analyzes. 5 wt% Arabic acid dispersions were prepared in milliQ water using incubated Arabic acid powder. The dispersions were stirred overnight using an orbital plate at 250 rpm. pH of all dispersions was around 2.4.

3.5. Transmittance and solubility measurements

The light transmittance at 657 nm of Arabic acid dispersions was measured at 25°C using a spectrophotometer (UltroSpec 2000, Pharmacia Biotech). For solubility measurements, dispersions were centrifuged at 12,000 rpm for 30 min at 20 °C using a Heraeus Fresco 21 microcentrifuge (Thermo Fisher Scientific, Osterode, Germany). After centrifugation, the supernatants were recovered, their volume was measured and their refractive index was determined using an Abbemat Refractometer (Anton Paar, Graz, Austria). The Arabic acid AGPs in the supernatants were quantified using a previously determined dn/dc of 0.1492 $mL \cdot g^{-1}$, and the pelleted ones were then calculated as following:

$$[\text{AGPs (t)}]_{\text{insoluble}}\ (\%) = 100 \cdot \left(1 - \frac{C'V'}{CV}\right)$$

where C and V are, respectively, the concentration ($g_{GA} \cdot g_{dispersion}^{-1}$) and the volume (mL) of dispersion before centrifugation, and C' and V' are the concentration and the volume of supernatant dispersion after centrifugation.

3.6. Phase contrast microscopy

Arabic acid dispersions were diluted at 0.5wt% in MilliQ water before microscopic observations. Arabic acid aggregates were observed by phase contrast microscopy using an optical microscope (Olympus, France) coupled with x10 and x20 zoom objectives. Pictures were acquired and analyzed with the CellSens software (Olympus, France).

3.7. Static Light Scattering (SLS) measurements

The volumetric diameter distribution of the AGP aggregates in water was determined on the whole sample by static laser light scattering using a Mastersizer 2000 (Malvern Instruments, Orsay, France) with an obscuration around 5 %. Refractive indices of 1.331 for eluent and 1.338 for aggregated samples were used in the experiment parameters. For all samples, five cycles of measurements (10 s delay) were performed at room temperature. The span and the volumetric aggregate diameter ($D_{4,3}$) were determined. The $D_{4,3}$ was calculated as follow:

$$D_{4,3} = \sum n_i d_i^4 \Big/ \sum n_i d_i^3$$

where n_i is the number of particles of diameter d_i.

3.8. SEC MALLS and AF4 MALLS characterization

The distribution and structural properties of soluble aggregates and AGPs from Arabic acid were characterized by multi-detector high performance size exclusion chromatography (HPSEC) and asymmetrical flow field-flow fractionation (AF4). These experiments were performed on the supernatants obtained after the centrifugation of the dispersions. The supernatants were diluted to obtain final concentrations of 1 $mg \cdot mL^{-1}$ and 2 $mg \cdot mL^{-1}$ for SEC

MALLS and AF4 MALLS measurements, respectively. 50µL of diluted supernatants were injected.

The HPSEC line was constituted of a Shimadzu HPLC system (Shimadzu, Kyoto, Japan) and the AF4 instrument was a Dual Tech Separation System (Wyatt Technology Europe, Dernbach, Germany). Both systems were connected to a 18 angles Dawn Heleos II (MALLS) detector (Wyatt Technology, Santa Barbara, CA, USA) equipped with a QELS (Wyatt Technology) in position 14 (SEC MALLS) or 12 (AF4 MALLS), and an OptilabRex differential refractive index detector (Wyatt Technology, Santa Barbara, CA, USA). The HPSEC line was additionally coupled to an online Viscometer (VISCOSTAR II, Wyatt, Santa Barbara, CA, USA), and a UV-VIS detector activated at 280 nm (SPD-20A, Shimadzu). The separation of macromolecules by SEC was performed on an OHPAK SB-G guard pre-column followed by four columns in series (OHPAK SB 803, 804, 805 and 806 HQ, Shodex). The mobile phase or eluent (0.01M acNa, 0.3M NaCl, 0.02 % NaN_3) was filtered through 0.1 µm filter (Millipore) and pumped at 1 $mL{\cdot}min^{-1}$.

The AF4 channel had a trapezoidal shape (length = 17.3 cm, initial breadth = 1.1 cm, final breadth = 0,27 cm) and a thickness of 350 µm. The "accumulation wall" was an ultrafiltration cellulose regenerated membrane (Consenxus, Germany) with a M_w cut-off of 10 $kg.mol^{-1}$ (Wyatt Technology Europe, Dernbach, Germany). A Thermo Ultimate 3000 series isocratic pump with an in-line vacuum degasser and an autosampler delivered the carrier flow and handled sample injection onto the AF4 channel. Between the pump and the channel, mobile phase or eluent were filtrated through an online 0.1 µm filter (VVLP, Millipore, Germany). The injection and the detector flow rates were set up at 0.4 $mL{\cdot}min^{-1}$ and 1 $mL{\cdot}min^{-1}$, respectively; and the crossflow (V_x) was varied. A 1 min elution step followed by a 1 min focusing step (V_x = 1 $mL{\cdot}min^{-1}$) were performed prior to injection of the sample. Samples were injected during the 3 min focus+inject step. After a second 2 min focusing step, an exponentially decaying crossflow profile from 3 $mL{\cdot}min^{-1}$ to 0.13 $mL{\cdot}min^{-1}$ in 27 min was used to ensure a better resolution and separation of the polydisperse macromolecules (Kirkland et al., 1992; Leeman et al., 2006). The crossflow was then cut off for a 3 min elution step. After elution, the channel was flushed out without crossflow in order to elute the smallest particles and to rinse the injection loop.

The data were analyzed using the Zimm's model and an experimentally determined refractive index increment (dn/dc) of 0.145 $mL \cdot g^{-1}$, corresponding to the value of dn/dc measured for A. *seyal* gum and other incubated gums in the eluent. Data processing was operated using the ASTRA software 7.1.2 (Wyatt Technologies, Santa Barbara, CA, USA), and the gyration radius (R_g) was considered only for values above 10 nm, which is the sensitivity limit of the MALLS detector.

4. Results and discussion

4.1. Biochemical composition and structural properties of Arabic acid

The biochemical composition (moisture, sugar, protein and ash content in dry basis) of A. *seyal* gum and Arabic acid powders is presented in Table III.1. The mineral, sugar and protein contents of A*. seyal* gum are in accordance with values previously reported in literature for other batches. Depending on the tree age and the location of production, the mineral content varies from 1.4 to 4 % (Lopez-Torrez et al., 2015a; Mejia Tamayo et al., 2018; Mhinzi, 2003; Sara et al., 2018), the protein content fluctuates from 0.7 to 1.2% (Al-Assaf et al., 2005b; Lopez-Torrez et al., 2015a) and the sugar content ranges from 90 to 95% (Al-Assaf et al., 2005b; Al-Assaf & Phillips, 2006b; Lopez-Torrez et al., 2015a). After the demineralization process, A. *seyal* gum was completely devoid of its minerals (Table III.1), which confirmed the efficiency of the process. The demineralization process also induced the loss of around 10% of the protein content. The amino acids as well as the sugar compositions of both A. *seyal* and Arabic acid gums were similar before and after removal of minerals (Supplementary data, Table III.3 and III.4).

Table III.1. Biochemical composition of A. *seyal* gum and spray-dried Arabic acid in dry basis (mean ± standard deviation).

Component ($mg \cdot g^{-1}$)	A. *seyal*	Arabic acid
Total dry matter	933.7 ± 2.9	929.2 ± 8.4
Sugars[a]	908.6	920.9
Proteins	9.56 ± 0.07	8.29 ± 0.02
Minerals	15.5 ± 1.4	Traces (< 0.01)

[a] Total content of sugars was calculated by the difference of proteins and minerals from 1000 $mg.g^{-1}$ in dry basis.

The structural properties of AGPs from GA throughout the entire demineralization process were characterized by SEC MALLS. Figure III.3 shows the corresponding relative light scattering (LS) and refractive index (RI) signals of AGPs from initial A. *seyal* gum, after their demineralization (Arabic acid solution) and spray-drying (Arabic acid powder). The LS and RI profiles of AGPs before and after their demineralization were superimposed suggesting that the demineralization step did not modify the elution profiles of AGPs. These two samples showed a superimposition of the molar mass distributions (Figure III.3), identical mean molar mass ($M_w = 0.85 \cdot 10^6$ $g \cdot mol^{-1}$) and mean gyration radius ($R_g = 17.4$ nm) values. These data are in the range of the $1.00 \cdot 10^6$ $g \cdot mol^{-1}$ values previously reported for Arabic acid (Veis & Eggenberger, 1954) and various A. *seyal* gums (Apolinar-Valiente, Williams, et al., 2020; Lopez-Torrez et al., 2015a). In turn, the LS and RI profiles of AGPs from Arabic acid powder shifted to smaller elution volumes (Figure III.3), suggesting spray-drying induced the formation of higher molar mass AGPs. This also suggests that dehydration of AGPs could be partly related to its aggregation. The mean M_w and R_g of these soluble aggregates increased respectively from $0.85 \cdot 10^6$ $g \cdot mol^{-1}$ to $1.02 \cdot 10^6$ $g \cdot mol^{-1}$ and from 17.4 to 21.7 nm. As a consequence, the amount of AGPs with $M_w > 10^6$ $g \cdot mol^{-1}$ also increased from 26 % to 33 %.

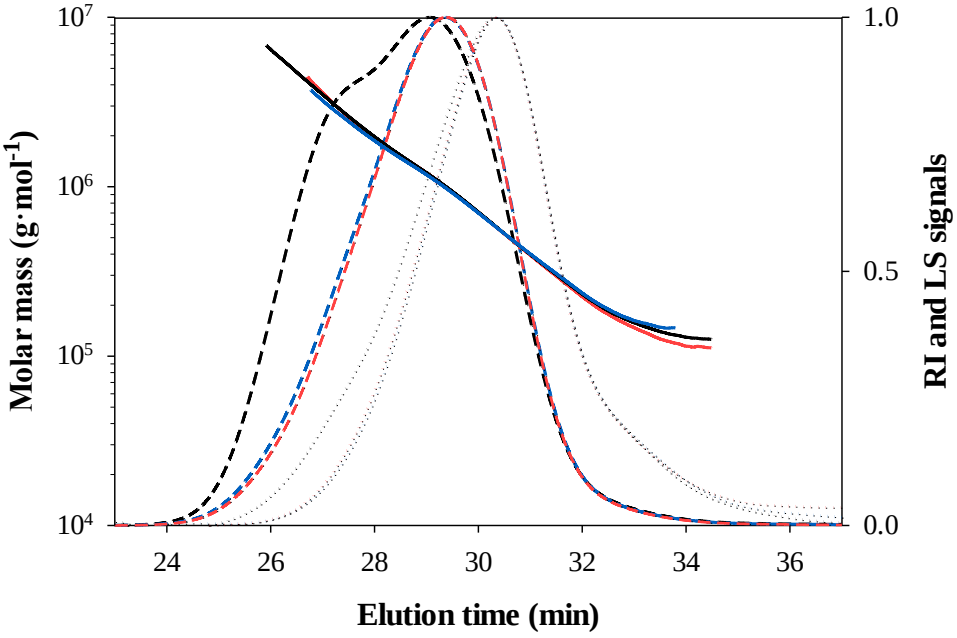

Figure III.3. Light scattering (dotted line) and refractive index (dashed line) signals, represented on relative scale, and molar mass (continuous line) profiles as a function of elution time for A. *seyal* gum (blue), and Arabic acid before (red) and after (black) spray-drying. From SEC MALLS data.

The aggregation of Acacia gum AGPs subjected to heat treatments such as pasteurization and spray-drying has been already reported (Al-Assaf et al., 2005a, 2009). In the present study, the aggregation of AGPs was not observed when non-demineralized A. *seyal* gum was spray-dried (data not shown). Therefore, demineralization improves the thermal sensitivity and reactivity of AGPs.

4.2. Aggregation kinetics of Arabic acid powder

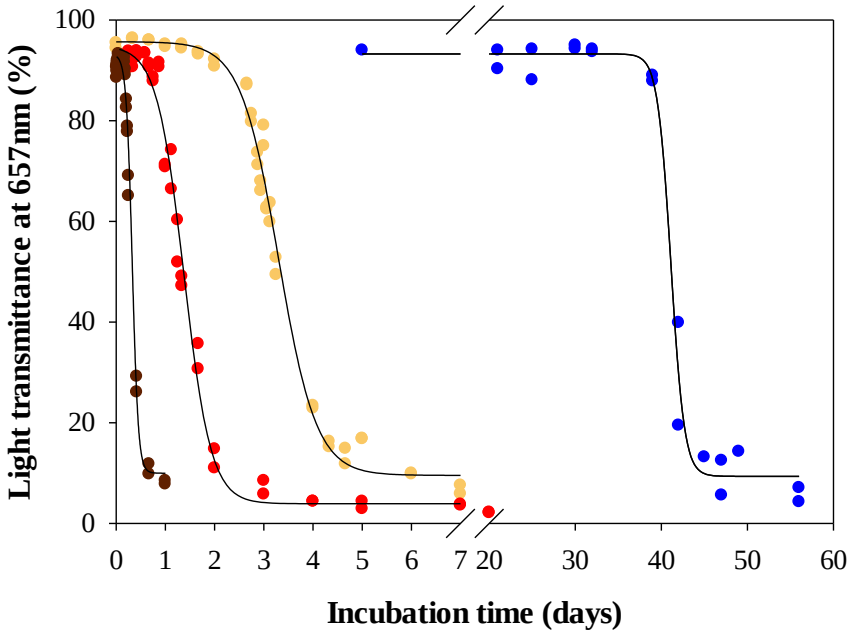

Figure III.4. Light transmittance at 657 nm of Arabic acid dispersions as a function of incubation time for Arabic acid stored at different temperatures: 25°C (●), 40°C (●), 55°C (●), and 70°C (●).

Upon incubation at temperatures ranging from 25°C to 70°C and dispersion in water, Arabic acid dispersions appeared visually more opalescent when the incubation time was longer. (Figure III.4A) Experimentally, the transmittance of Arabic acid dispersions followed a sigmoidal-like curve (Figure III.4B). According to the incubation time, and for all the temperatures studied, a first plateau around 95% transmittance was observed, followed by a steep decrease of the transmittance until a second plateau for transmittance values between 5 to 15%. The time position of the sigmoidal-like curve closely depended on incubation temperature: the most elevated the temperature, the fastest the transmittance decrease. Complementary phase contrast micrographs (Figure III.5) also showed that dispersions prepared with Arabic acid powder stored at 40°C were devoid of aggregates up to 2 days of incubation, while from day 3 large size aggregates were observed. Therefore, the loss in transmittance above day 3 at 40°C is due to the presence of AGPs aggregates and associated light scattering phenomena. Aggregates looked like microparticles characterized by a spherical shape and heterogeneous surface with sizes ranging from 10 to around 200 µm (Figure III.5). Part of these aggregates are surface remnants of not totally dispersed powder particles. The microstructure of these microparticles was similar to those formed in aged micellar casein

powders and milk protein concentrates (Burgain et al., 2016; Mimouni et al., 2010; Nasser et al., 2017).

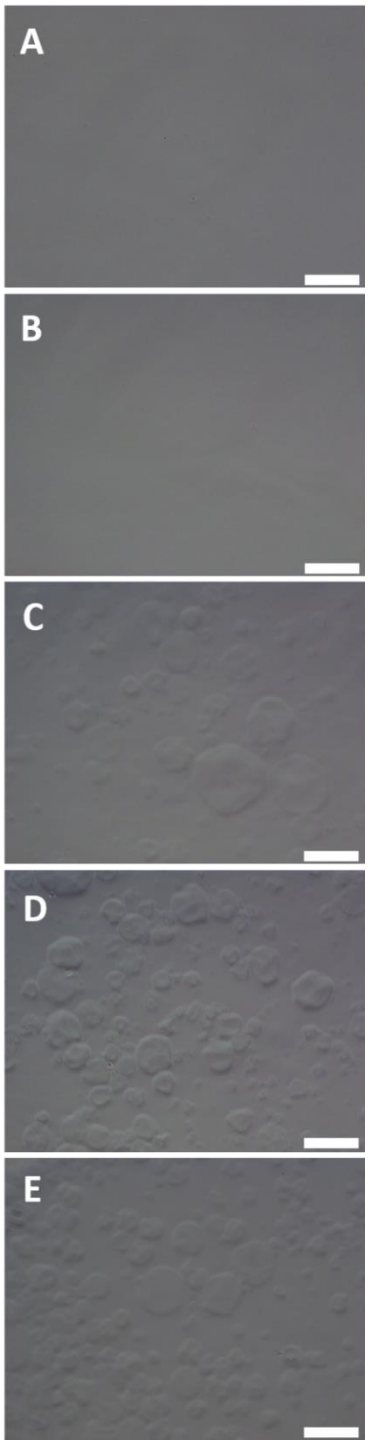

Figure III.5. Phase contrast micrographs of Arabic acid dispersions prepared with powders incubated at 40°C for 0 (A), 2 (B), 3 (C), 4 (D) and 5 days (E). The magnification was x20 and the scale bar indicates 100 µm length.

The amount of AGPs involved in these microparticles all along the kinetics were quantified after centrifugation of the dispersions. The pelleted material (%) in Arabic acid powder stored at 25°C, 40°C, 55°C and 70°C as a function of incubation time is given in Figure III.6. The evolution of the pelleted AGPs, which could be related to insolubility curves, followed the same trend at all temperatures. First, a lag phase was observed during which the AGPs remained highly soluble after being stored 0.13, 0.67, 2 and 18 days at 70°C, 55°C, 40°C and 25°C, respectively. Then, the amount of pelleted AGPs exponentially increased, until reaching a plateau at a maximum value around 80% after 0.38, 1.7, 5 and 40 days at 70°C, 55°C, 40°C and 25°C. The same insolubility behavior was reported with non-demineralized A. *senegal* gum after its dry heating at 110°C (Katayama et al., 2008). Then, as noted above, demineralization of GA improved its sensitivity and reactivity towards AGPs aggregation.

Since the insolubility curves followed the same sigmoidal shape and reached a constant soluble AGPs fraction around 20%, they were normalized using a dimensionless time τ ($\tau = t/t_{plateau}$) with $t_{plateau}$ the time for which the maximum insoluble AGPs value was reached.

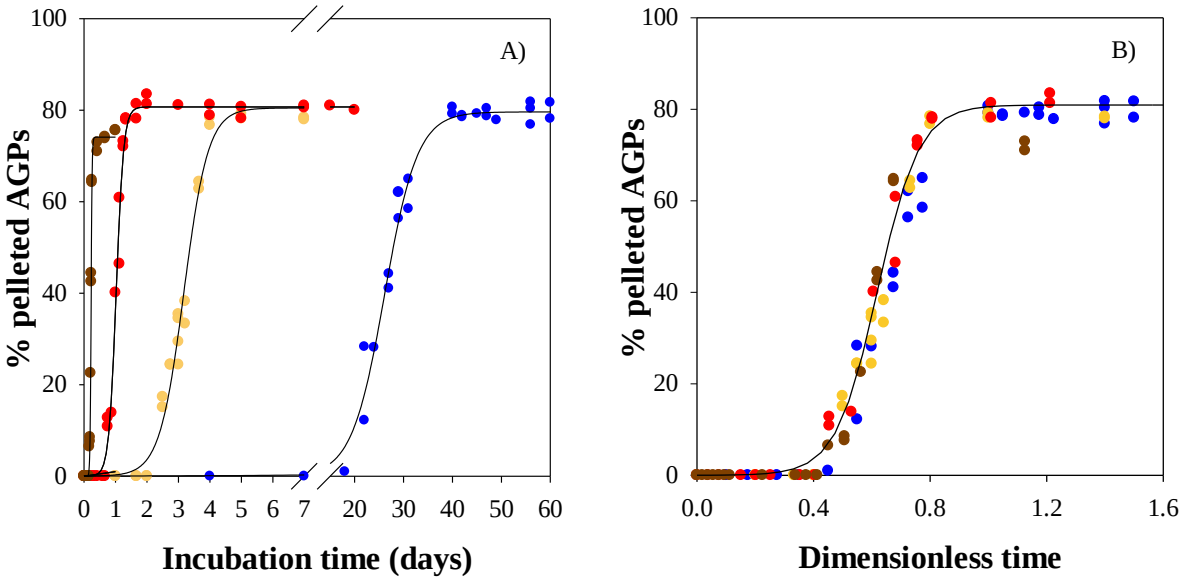

Figure III.6. Percentage of pelleted AGPs in aqueous dispersions as a function of A) Arabic acid powder incubation time and B) the dimensionless time τ at 25°C (●), 40°C (●), 55°C (●) and 70°C (●). The continuous lines represent the fits obtained at each temperature (A) or the fit obtained using all the data available at 4 temperatures (B) with SigmaPlot software.

Thus, all the data overlapped to form a single master curve (Figure III.6B) suggesting a similar temperature-independent aggregation mechanism. Temperature only modulated the aggregation rate. The insolubility curves at 25°C, 40°C, 55°C and 70°C were consequently fitted

using a logistic function depending on incubation time (Figure III.6B) in order to establish a general equation allowing the prediction of the percentage of insoluble aggregates at each time-temperature couple:

$$[\text{AGPs (t)}]_{\text{insoluble}} = \frac{a}{1+e^{-\frac{t-t_{1/2}}{b}}} \qquad \text{(III.1)}$$

The parameter a is the maximal amount of insoluble aggregates at a given temperature, $t_{1/2}$ (*i.e.* half-life time) corresponds to the time for which insoluble AGPs reached half of its maximum value at a given temperature, and 1/b was defined as the logistic growth rate, *i.e.* the initial rate during the exponential increase phase. The half-life time corresponded to 0.22, 1.03, 3.17, and 26.2 days for Arabic acid AGPs stored at 70°C, 55°C, 40°C and 25°C, respectively. Interestingly, $t_{1/2}$ and 1/b parameters determined at 25°C, 40°C, 55°C and 70°C were expressed as a function of temperature using an exponential law (Supplementary data, Figure III.11) which equations were the following:

$$t_{1/2}(T) = 808.8e^{-0.14T} \qquad \text{(III.2)}$$

$$1/b(T) = \frac{1}{106e^{-0.14T}} \qquad \text{(III.3)}$$

The substitution of $t_{1/2}$ and 1/b parameters into equation (III.1) by equations (III.2) and (III.3) and the use of the mean maximal amount of insoluble AGPs aggregates give a general equation that can be used to predict the amount of pelleted AGPs aggregates at each time-temperature couple between 25 and 70°C:

$$[\text{AGPs (t, T)}]_{\text{insoluble}} = \frac{78,7}{1+e^{-\frac{t-808.8e^{-0.14T}}{106e^{-0.14T}}}} \qquad \text{(III.4)}$$

4.3. Structural characterization of AGPs aggregates

This section is devoted to the structural description of AGPs aggregates formed all along the aggregation kinetic. The characterization was done at all the temperatures studied but only the results obtained at 40°C are discussed as identical ones were obtained for the three other temperatures. The microparticles were analyzed by SLS experiments, while the AGPs and soluble aggregates were characterized using SEC and AF4 MALLS experiments on supernatants obtained after centrifuging aggregates aqueous dispersions.

4.3.1. Size distribution of microparticles

As seen with microscopy observations and transmittance measurements, long storage time promotes the aggregation of AGPs with the formation of microparticles allowing SLS measurements. Samples stored between 2 and 4 days at 40 °C displayed a bimodal distribution with a first population showing a mean $D_{4,3}$ around 800 nm, and a second one with a mean $D_{4,3}$ around 50 µm (Figure III.7A). For Arabic acid samples incubated for less than 2 days, the particle size was too low to be correctly analyzed by SLS. As the storage time increased, the volume percentage of the first population decreased until the Arabic acid sample was only characterized by an almost monomodal distribution corresponding to the second population with a mean $D_{4,3}$ around 70 µm for Arabic acid incubated more than 4 days (Figure III.7). In line with this result, the width of the size distribution (span) decreased from around 1.8 at 2.3 days to around 0.8 at day 7. The mean $D_{4,3}$ as well as the polydispersity of microparticles were constant beyond 5 days of storage. These measurements confirmed the size range of microparticles observed by microscopy (Figure III.5). However, the mean size of microparticle is larger than that of the mean powder particle size that was found to be around 15 µm (data not shown). A similar behavior was observed with whey proteins microparticles during dry heating (Schong & Famelart, 2018). It is worth noting that mean $D_{4,3}$ of these powder particles increased from around 15 µm to 80 µm upon rehydration. Thus, it can be suggested that AGPs microparticles observed by microscopy (Figure III.5) were hydrated powder particles. The size ($D_{4,3}$) of these AGPs aggregates obtained for long incubation time was therefore closely related and guided by the properties of the spray-drying nozzle.

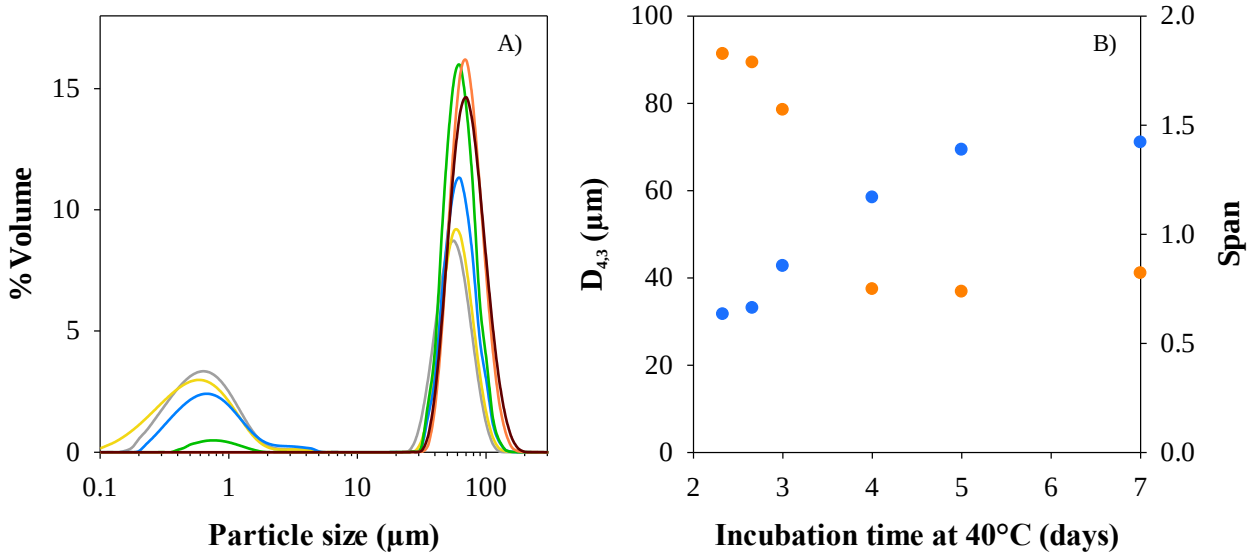

Figure III.7. A) Size distribution of AGPs aggregates after 2.33 days (grey), 2.66 days (yellow), 3 days (blue), 4 days (green), 5 days (orange) and 7 days (brown) of incubation at 40°C. Measurements were done in water using SLS and an obscuration of 5%. B) Evolution of the volume mean diameter ($D_{4,3}$) (●) and the polydispersity (●) of AGPs aggregates according to the incubation time.

4.3.2. Structural properties of soluble aggregated AGPs from Arabic acid

4.3.2.1. Molar mass distribution

The molar mass and structural dimensions (M_w, polydispersity index, R_g, R_h) of AGPs and aggregated AGPs were determined from coupled SEC and AF4 analyzes all along the incubation kinetic at 40°C (Figure III.8). Since insoluble aggregates were removed by centrifugation, only the initial AGPs and soluble aggregates were characterized.

The SEC normalized concentration profiles (plotted from the Refractive Index signal) of Arabic acid before incubation and at storage times from 0.66 to 7 days are shown in Figure III.8A. The initial gum sample consisted in mainly one polydisperse population of AGPs (Elution time: 25 – 36 min). After incubation, even for short storage times, the concentration profiles split in two thinner peaks. The first one, for elution time between 22 and 28 min, is characterized by the presence of high molar mass AGPs whereas the second population, eluted between 28 and 37 min, accounted for the main part of the AGPs and was characterized by smaller molar masses. Beyond 2 days of storage, a shoulder between 32.5 and 36 min whose intensity rose up with incubation time appeared (Figure III.8A). Arbitrarily, the profiles were further analyzed by considering these three populations and plotting their proportion according to the incubation

time (Figure III.8B). From 0 to 2 days, the AGPs proportion in population 3 remained almost constant, while the percentage of population 1 increased by 30% to the detriment of population 2. This resulted in the mean molar mass on the whole peak rising from $1{\cdot}10^6$ g·mol^{-1} (t_0) to reach a maximum at $6.7{\cdot}10^6$ g·mol^{-1} (SEC MALLS) or $24{\cdot}10^6$ g·mol^{-1} (AF4 MALLS) after 1.66 days of storage (Figure III.8C). The molar mass difference between SEC and AF4 MALLS experiments around 1.66 days was explained by the retention of the most aggregated AGPs by the pre-column matrix. This M_w growth confirmed the propensity of AGPs from Arabic acid to aggregate upon heating in dry state and evidenced the formation of soluble aggregates before two days of storage. As reported in the introduction, the dry state aggregation of non-demineralized AGPs from A. *seyal* and *senegal* gums has been previously reported for temperatures of at least 40°C (Hayashi, 2002) and usually higher than 60°C (Al-Assaf et al., 2004; Al-Assaf, Phillips, Aoki, et al., 2007b; Aoki, Al-Assaf, et al., 2007). The dry incubation of these gums during 7 days at 40°C and 1 day at 110°C induced a molar mass increase by 1.2 and 2.2, respectively (Al-Assaf et al., 2004; Aoki, Al-Assaf, et al., 2007; Hayashi, 2002). Using Arabic acid, the rate of aggregation is greatly accelerated as a molar mass increase of around 2 was reached after dry heating at 40°C during 0.35 day. The cross-linking of acidic AGPs was previously reported both *in vivo* and *in vitro* in mild temperature conditions (20 to 25°C) and oxidative environment (Kjellbom et al., 1997).

Beyond 2 days of storage, the percentage of population 1 diminished from 40% to reach a 10% plateau after 5 days. In contrary, the percentage of populations 2 and 3 rose up each by 15% to reach a plateau around 65% and 25% after 5 days, respectively. The evolution of the 3 populations was in accordance with the calculated mean M_w which decreased from $6.7{\cdot}10^6$ g·mol^{-1} (SEC MALLS) or $12{\cdot}10^6$ g·mol^{-1} (AF4 MALLS) at 1.66 days to a mean constant M_w value around $5{\cdot}10^5$ g·mol^{-1} after 5 days. As shown in Figure III.8C, the decrease in the mean M_w was concomitant with the formation of microparticles. The behavior of M_w beyond 2 days of storage could be explained by the growth of soluble AGP aggregates to form the microparticles that were not characterized in these experiments. After 5 days of storage, the mean M_w of soluble AGPs which corresponded to 20% of the initial Arabic acid (Figure III.6A and III.8C) was twice lower than the mean M_w of AGPs from initial Arabic acid. Therefore, this soluble fraction was enriched in low molar masses AGPs as shown in Figure III.8A, with both the shift of the peak maximum to higher elution volume (from 30 to 31 min) and the rise of the proportion of low molar mass AGPs (population 3). This result suggests a higher

reactivity towards the aggregation of demineralized high molar mass AGPs. Between 2.5 and 7 days, some differences in M_w were also observed between SEC and AF4 MALLS experiments with higher mean M_w values for SEC MALLS. It is well known that hyperbranched macromolecules like dendrimers (Percec et al., 1998) and AGPs (Mejia Tamayo et al., 2018; Podzimek et al., 2001) as well as high molar mass macromolecules (aggregates) can be submitted to a retardation to elution during SEC MALLS experiments (Gaborieau & Castignolles, 2011; Podzimek et al., 2001). Therefore, the higher calculated M_w values for SEC MALLS experiments were certainly due to the co-elution of aggregated hyperbranched AGPs with normally eluting smaller hyperbranched AGPs.

The lag phase of the sigmoidal profile describing the aggregation kinetics of Arabic acid AGPs (Figure III.4 and III.6) can be related to the initiation of the AGP aggregation, with the formation of primary soluble AGPs aggregates as shown by the molar masses increase (Figure III.8). For longer incubation times, the primary aggregates were involved in further aggregation and grew up to form microparticles until a solubility plateau was reached (Figure III.4). By considering the natural interaction of cations with AGPs, we can argue that beyond their physiological functions in the plants, the cations of AGPs from GA certainly also have a role in the structural stability of AGPs by controlling and preventing their aggregation. This statement was confirmed with the A. *seyal* gum used in this study as the AGPs from this gum loaded with its cations were stable towards their dry heating at 40°C during at least 7 days, without the variation of the mean molar mass and the formation of insoluble materials (Figure III.12).

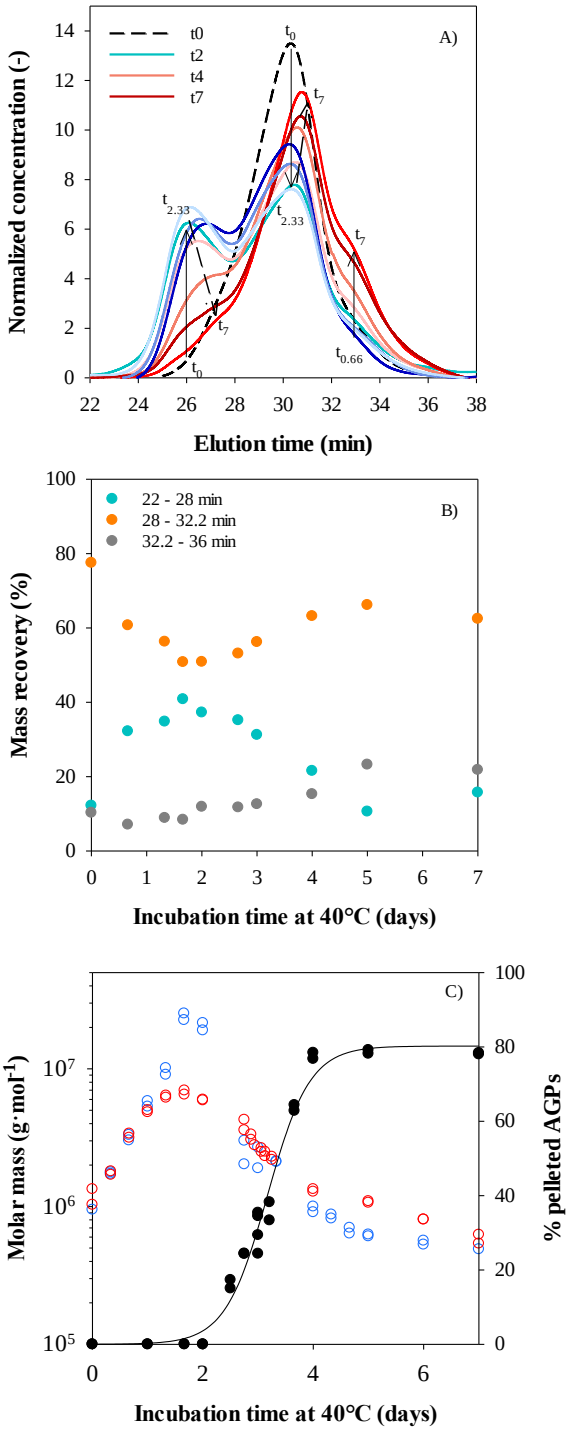

Figure III.8. A) Normalized concentration profile obtained from SEC MALLS experiments and B) Proportion of AGPs and soluble aggregates according to their elution volume from Arabic acid powder incubated between 0 and 7 days at 40°C. Concentration was normalized by the injected concentration. C) Calculated mean molar mass determined by SEC MALLS (○) and AF4 MALLS (○) experiments from AGPs and soluble aggregates and pelleted fraction (•) of Arabic acid incubated between 0 and 7 days at 40°C. The continuous line represents the fit of the data obtained at 40°C with SigmaPlot software.

4.3.2.2. Possible conformation of AGPs and soluble AGPs aggregates

The conformation of AGPs and soluble AGPs aggregates can be roughly approached using the so-called R_g vs. M_w and R_h vs. M_w conformation plots. In general, R_g and R_h are related to M_w by a simple power law relationship according to $R_g = K_g M_w^{\nu_g}$ and $R_h = K_h M_w^{\nu_h}$, where ν_g and ν_h are the static and hydrodynamic coefficients and K_g and K_h are the corresponding constants (Burchard, 1999). The ν_g and ν_h parameters depend both on conformation of the polymer and its affinity for the solvent (polymer-solvent interaction) (Burchard, 1994, 1999). The K_g and K_h parameters also depend on the affinity for the solvent, but they were not further analyzed in the present study. Theoretically, ν_g and ν_h values of 0.33, 0.5 – 0.6 and 1 are expected for homogeneous spheres, random coils and rods, respectively (Burchard, 1994, 1999). The R_g vs. M_w conformation plots of AGPs from Arabic acid samples were only considered for R_g values above 10 nm, which is the sensitivity limit of the MALLS detector. For not incubated Arabic acid, a ν_g value of 0.53 was measured, which is consistent with the average value of 0.5 reported for A. *seyal* gums (Aoki, Al-Assaf, et al., 2007; Lopez-Torrez et al., 2015a). After incubation, ν_g values remained constant taking a mean value of 0.55 ± 0.06 (Table III.2). Thus, the conformation and the solvent affinity of AGPs and aggregated AGPs were similar. This can be explained in part by the weight of high mass AGPs in the R_g measurements and the fact that aggregates were present in Arabic acid powder before incubation. Previously, a slight decrease of ν_g value from 0.5 to 0.4 after maturation of A. *senegal* gum in the dry state at 110°C was explained by changes in the conformation of incubated AGPs which adopted a more compact conformation (Aoki, Al-Assaf, et al., 2007). In this case, strong heat-induced dehydration may contribute to the compaction of formed aggregates.

Table III.2. Calculated ν_h and ν_g exponents from relations $\mathbf{R_g = K_g M_w^{\nu_g}}$ and $\mathbf{R_h = K_h M_w^{\nu_h}}$ for Arabic acid incubated at 40°C.

Incubation time (days)	ν_h	M_w range ($\cdot 10^6$g.mol^{-1})	ν_g	M_w range ($\cdot 10^6$g.mol^{-1})
0	0.45	0.49 – 8.06	0.53	0.50 – 7.02
1	0.48	0.80 – 29.50	0.55	0.66 – 19.50
2	0.49	1.24 – 45.71	0.58	3.47 – 20.66
3	0.44	0.52 – 17.86	0.59	5.95 – 25.06
4	0.46	0.15 – 33.6	0.58	0.66 – 10.05
5	0.43	0.10 – 9.85	0.59	7.77 – 25.70
7	0.45	0.12 – 3.89	0.57	0.38 – 3.77

The analysis of R_h vs. M_w conformation plots concerned all the AGP species (aggregated or not), even those showing R_g values lower than 10 nm. A simple power law described the relationship between R_h and M_w for all samples (Figure III.9). The conformation plot for non-incubated Arabic acid gave a ν_h exponent value of 0.45, in good agreement with values of 0.43-0.44 reported for 28 spray-dried A. *seyal* (Sanchez et al., 2018), and also in line to the hyperbranched nature of AGPs from the latter (Lopez-Torrez et al., 2015a; Mejia Tamayo et al., 2018; Renard et al., 2012). For all the dry heated samples, ν_h values between 0.43 and 0.49 were found. Then no apparent difference in conformation was noticed between AGPs of initial gum, demineralized gum or dry heated demineralized gum (Table III.2). Renard et al. showed that enzymatic hydrolysis of AGPs from A. *senegal* gum by proteases in acidic (pH 4) or neutral (pH7) conditions did not modify the conformation of resulting hydrolyzed AGPs. They concluded that AGPs from GA would probably result from a self-similar assembly of elementary blocks, *via* covalent bonds and/or hydrophobic and H-bonding, with a symmetrical distribution of arabinosides and polysaccharide substituents (Renard, Lavenant-Gourgeon, et al., 2014). Therefore, AGPs from Arabic acid aggregated following a self-similar aggregation mechanism respecting the molecular organization and conformation of the elementary AGPs without disturbing this primitive conformation.

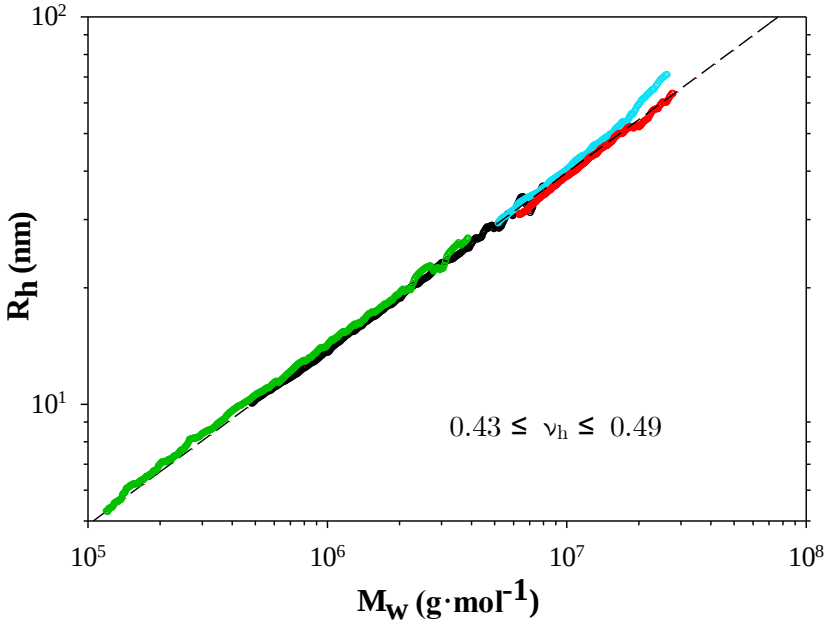

Figure III.9. R_h conformation plots of AGPs and soluble aggregates from Arabic acid powder before (○), and after incubation for 1.66 days (○), 2.66 days (○) and 7days (○) at 40°C. From SEC MALLS data.

4.4 Activation energy of Arabic acid AGPs aggregation mechanism

The activation energy (E_a) of the aggregation reaction involving the Arabic acid AGPs was calculated by considering the soluble aggregates with the SEC MALLS data and the pelleted aggregates with the insolubility curves. Using the insolubility curves obtained at 25, 40, 55 and 70°C (Figure III.6A), the rate constants (k) at each temperature were considered as the inverse of $t_{1/2}$ ($k = \frac{1}{t_{1/2}}$). k values were $3.1 \cdot 10^{-3}$, $6.7 \cdot 10^{-4}$, $1.3 \cdot 10^{-4}$, and $2.5 \cdot 10^{-5}$ min^{-1} at 70°C, 55°C, 40°C and 25°C, respectively. Using the SEC MALLS data, k values were calculated on the whole sample during the first time of the aggregation reaction, before the appearance of the pelleted AGPs aggregates. For the four temperatures, k values were determined by plotting the molar masses (M_w) according to the incubation time (Figure III.10A). From the slopes of these linear relationships, k values were found to be 0.24, 0.12, 0.01 and 0.002 min^{-1} at 70°C, 55°C, 40°C and 25°C, respectively. The rate constants determined from SEC MALLS and insolubility experiments were then plotted on an Arrhenius representation allowing the calculation of E_a (Figure III.10B). E_a calculated from SEC MALLS data and insolubility curves were 98.9 kJ·mol^{-1} and 91.1 kJ·mol^{-1} respectively. Interestingly, E_a values determined considering

two different levels of aggregation (soluble and pelleted aggregates) were relatively close (< 10%), suggesting the involvement of the same energy level all along the aggregation mechanism: from the formation and the growth of soluble aggregates until pelleted aggregates were reached.

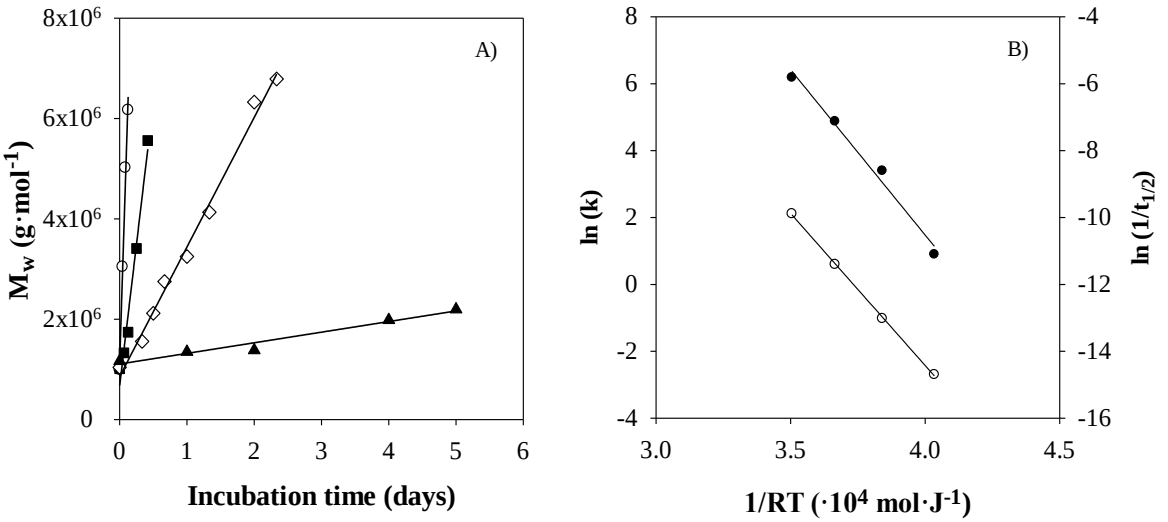

Figure III.10. Determination of activation energy E_a of the aggregation reaction: A) Evolution of molar mass of Arabic acid incubated at 25°C (▲), 40°C (◇), 55°C (■) and 70°C (○) as a function of incubation time. The reaction rates were then determined choosing a 0-order reaction. B) Arrhenius plots from the reaction rates obtained from Figure III.10A) (●) and solubility measurements (○).

These values were in accordance with the involvement of covalent interactions in this aggregation mechanism, even if the establishment of weak physical bonds such as hydrogen and Van der Waals bonds could not be excluded yet. In this study, the storage conditions, notably heating, anhydrous medium and acidic pH are suitable for dehydration reactions. Indeed, protonation of AGPs carboxylic groups is favored by the acidic pH of demineralized AGPs and could lead to chemical condensation reactions such as esterification or etherification, possibly at the surface of AGPs. Dehydration is a prerequisite for these condensation reactions involved in proteins and polysaccharides polymerization, or Maillard reactions (Brovarone et al., 2020; Hodge, 1953; Hulshof & Ponnamperuma, 1976; Runnels et al., 2018). For instance, decreasing locally the hydration level of amyloid peptide molecules in solution led to an enhancement of their aggregation rate (Mukherjee et al., 2009). Under storage in anhydrous conditions (and at T ≥ 25°C), gelatin cross-linking was promoted by dehydration rather than oxidation (Yannas & Tobolsky, 1967). In turn, Kjellbom et al. showed that the cross-linking of acidic AGPs could be promoted in oxidative environment (Kjellbom et al., 1997). They assumed the possible involvement of amino acids (Tyrosine and Lysine) in the intermolecular

linkages between acidic AGPs. In that regard, Squier suggested the selective oxidation of calcium-regulatory proteins could regulate protein aggregation (and subsequent amyloid formation) (Squier, 2001). In this study, the removal of minerals from GA promoted the aggregation of its AGPs during their storage in dry conditions. This highlights the role of minerals and the importance of charges. Interestingly, the Faraday constant, which represents the electric charge carried by one mole of electrons (*i.e.* the energy corresponding to 1eV ≡ 96.485 kJ·mol^{-1}) is also in the range of the calculated E_a.

The dry aggregation of AGPs from loaded mineral A. gums at temperature above 90°C was supposed to occur through Maillard reaction, inducing also the powder yellowing and browning (Al-Assaf, Phillips, Aoki, et al., 2007b; Aoki, Al-Assaf, et al., 2007; Sanchez et al., 2018). This reaction was also identified as the origin of several milk protein aggregation during their dry heating in combination with carbohydrates (Schong & Famelart, 2019b, 2019a). This reaction is especially promoted at high temperature (Martins et al., 2000). The dry incubation of Arabic acid powder during several days, even at 70°C, did not result in the browning of Arabic acid powders. Moreover, the Arabic acid AGPs aggregates were also formed in mild temperature conditions such as 25°C, and even at sub-zero temperature as -20°C during long storage period (several months) of Arabic acid powders, *i.e.* conditions not favorable to the Maillard reaction. Therefore, this reaction cannot be assumed to occur with certainty during the dry aggregation of Arabic acid AGPs, as for A. gums loaded in minerals. Further experiments (FTIR and NMR) will be carried out to better identify the chemical bonds involved in this aggregation mechanism.

5. Conclusions

The demineralization of AGPs from A. *seyal* gum influenced the chemical and colloidal stability of AGPs by promoting their reactivity for their aggregation in dry state and mild temperature conditions (25°C to 70°C). The Arabic acid AGPs aggregated following a similar self-assembly mechanism for which the temperature only modulated the kinetics and rate of the aggregation reaction. The aggregation kinetics were characterized by the formation of soluble aggregates during the first incubation times whose size grew up for longer incubation period to form microparticles with $D_{4,3}$ around 70 µm. The soluble aggregates adopted a similar conformation to that of not aggregated AGPs. The demineralization of A. *seyal* gum appeared as a new way to elaborate various AGPs aggregates from soluble aggregate to microparticles with specific functionalities. In the following of this study, the physicochemical properties of these aggregates as their hydration, interfacial and emulsifying and rheological properties will be further characterized.

6. Acknowledgments

The authors gratefully acknowledge ALLAND & ROBERT Company (Port Mort, France) and the French Ministry of Research and Education (2017/1727) for the financial support (Ph.D. Amandine Antoine-Michard). We also would thank A. Ric and F. Violleau (Plateforme TFFFC, Université de Toulouse, INP-PURPAN, Toulouse, France) for the AF4 MALLS experiments.

7. Supplementary data

Table III.3. Amino acid composition of A. *seyal* and Arabic acid from A. *seyal* in dry basis (mean ± standard deviation).

Amino acid (%)	A. *seyal*	Arabic acid
Alanine	3.2 ± 0.1	2.6 ± 0.2
Arginine	2.2 ± 0.7	1.4 ± 0.0
Aspartic acid	7.8 ± 0.2	6.3 ± 0.0
Cysteic acid	1.9 ± 0.4	2.5 ± 0.3
Cystine	0.0 ± 0.0	1.6 ± 0.1
Glutamic acid	4.5 ± 0.2	3.8 ± 0.0
Glycine	3.4 ± 0.0	3.0 ± 0.2
Histidine	3.8 ± 0.1	4.1 ± 0.1
Hydroxy proline	24.6 ± 1.7	27.1 ± 1.3
Isoleucine	1.9 ± 0.3	1.7 ± 0.1
Leucine	8.3 ± 0.1	8.8 ± 0.3
Lysine	2.5 ± 0.6	1.5 ± 0.1
Phenylalanine	3.1 ± 0.3	2.3 ± 0.0
Proline	6.9 ± 0.2	6.9 ± 0.3
Serine	13.2 ± 0.9	14.2 ± 0.6
Threonine	5.3 ± 0.0	2.1 ± 0.2
Tyrosine	1.3 ± 0.4	1.4 ± 0.1
Valine	5.7 ±0.6	5.4 ± 0.2

Table III.4. Sugar composition of A. *seyal* and Arabic acid from A. *seyal* in dry basis (mean ± standard deviation).

Sugar (%)	A. *seyal*	Arabic acid
Arabinose	42.3 ± 2.9	42.5 ± 2.5
Galactose	33.0 ± 1.3	30.8 ± 2.5
Glucuronic acid	9.9 ± 0.7	10.3 ± 0.2
4-O-Me Glucuronic acid	11.8 ± 1.0	13.1 ± 0.2
Rhamnose	2.9 ± 0.1	3.3 ± 0.0

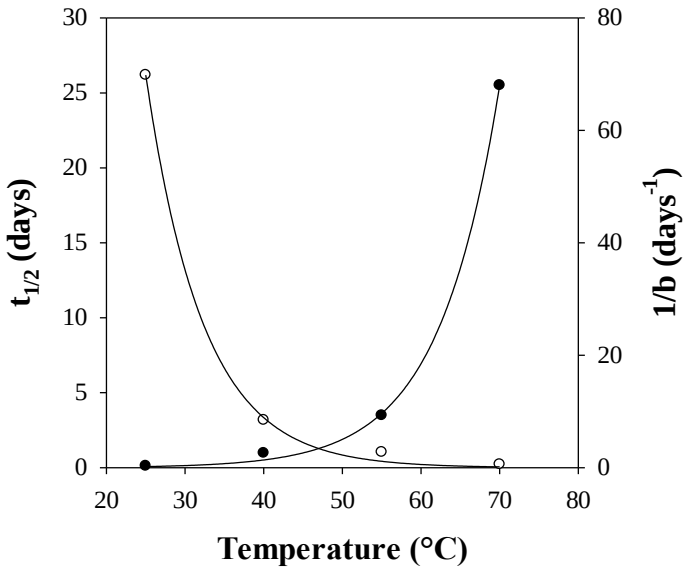

Figure III.11. Influence of temperature on parameters $t_{1/2}$ (○) and 1/b (●).

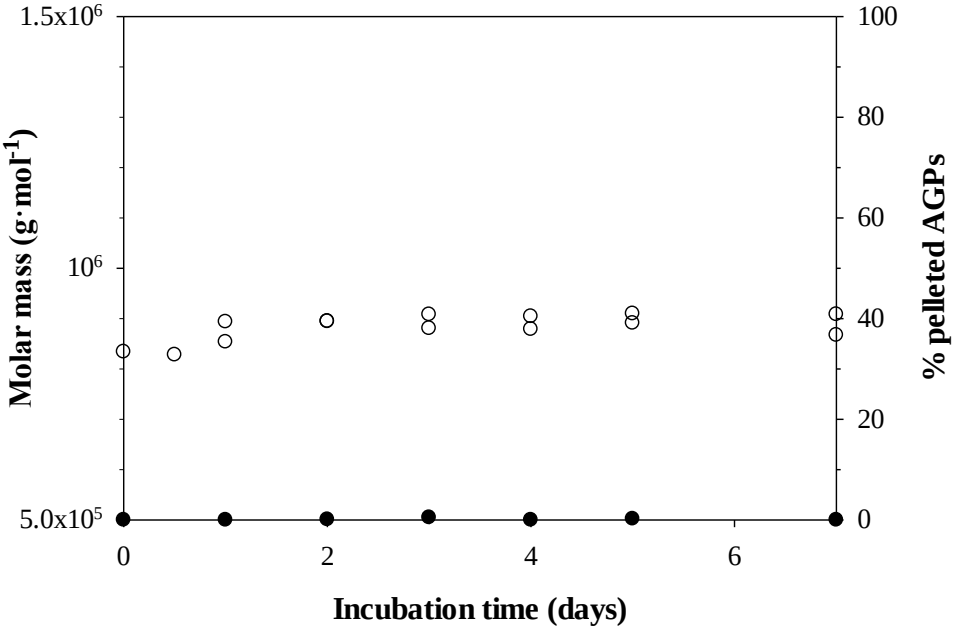

Figure III.12. Calculated mean molar mass (○) determined by SEC MALLS experiments from AGPs, and pelleted fraction (●) of GA incubated between 0 and 7 days at 40°C.

8. Complementary studies

8.1. Swelling properties of arabic acid aggregates

Size distributions of powder particles from GA, arabic acid and incubated arabic acid are displayed in Figure III.13. GA was characterized by a bimodal distribution: the first main peak, with a mean $D_{4,3}$ around 29.6 µm accounted for 99% of the particles, and a few bigger particles with a mean $D_{4,3}$ of 450 – 500 µm were also found (Table III.5). Whatever the incubation time (between 0 and 7 days), the particle size distributions of incubated arabic acid powders were similar: bimodal, with a mean $D_{4,3}$ around 11.5 µm for the first population (99% of the whole particles) and a mean $D_{4,3}$ between 142 and 188 µm for the second population (1% of the whole particles) (Table III.5). No significant change in the size distribution of incubated arabic acid powder was observed in comparison to that of non-incubated arabic acid. This reveals that dry heating of arabic acid powder did not induce any powder particle agglomeration.

The mean powder particles from arabic acid were characterized by a smaller size than that of GA particles (13.9 µm vs. 34.0 µm). The difference in particle size obtained between GA with or without minerals can be related to the spray-drying step. Indeed, the particle size of the

powder depends on the size of the fine droplets which are formed in the spray-drying tower. It is possible to tune the size of powder particles by changing the properties of the atomizing nozzle.

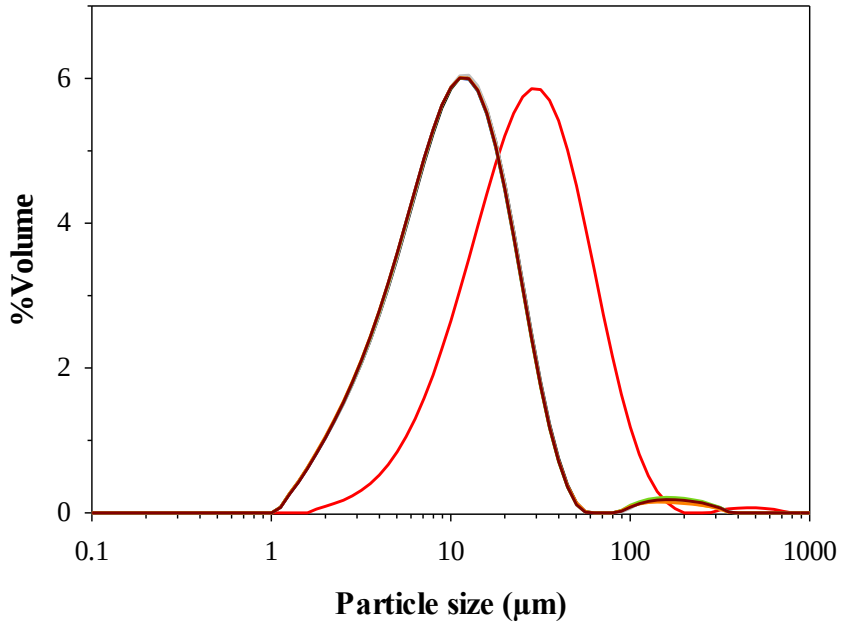

Figure III.13. Size distribution of powder particles of GA (red) and arabic acid incubated at 40°C for 0 day (black), 1 day (grey), 2 days (yellow), 3 days (blue), 4 days (green), 5 days (orange) and 7 days (brown).

Table III.5. Size distributions ($D_{4,3}$) of powder particles from GA, AA and incubated AA determined by SLS.

	Peak 1		Peak 2		Mean
	$D_{4,3}$ (µm)	% particles	$D_{4,3}$ (µm)	% particles	$D_{4,3}$ (µm)
GA	29.6 ± 1.8	99.4 ± 0.6	495.1 ± 84.7	0.6 ± 0.6	34.0 ± 2.8
t_0	13.4 ± 0.8	98.8 ± 0.3	188.5 ± 40.1	1.2 ± 0.3	13.9 ± 0.3
t_1	12.3 ± 0.7	98.5 ± 0.1	164.2 ± 17.6	1.5 ± 0.1	13.8 ± 0.1
t_2	11.2 ± 0.0	98.4 ± 0.0	165.3 ± 11.2	1.6 ± 0.0	14.0 ± 0.0
t_3	11.2 ± 0.0	98.5 ± 0.2	153.1 ± 10.0	1.5 ± 0.2	13.7 ± 0.3
t_4	11.2 ± 0.0	98.2 ± 0.1	158.9 ± 0.0	1.8 ± 0.1	14.3 ± 0.1
t_5	11.2	98.7	141.6	1.3	13.4
t_7	11.2	98.4	158.9	1.6	13.9

In a second time, the particle size distribution of arabic acid powder incubated for 7 days at 40°C was compared to the size distribution of pelleted AGP aggregates from the same powder after its dispersion in MilliQ water (Figure III.14). As previously reported, arabic acid aggregates in dispersion were characterized by a monomodal distribution with a mean $D_{4,3}$ around 70µm (Section III.4.3.1). We suggested that the aggregates observed by optical microscopy would be hydrated powder particles (Figure III.5). However, the mean $D_{4,3}$ of particle powder (~ 14 µm) is way smaller than the $D_{4,3}$ of aggregates in solution (~ 70 µm). This reflects the capacity of particles from incubated arabic acid (from 2.33 days at 40°C) to swell in water. Schong and Famelart (2018) reported similar results during the heating of whey proteins after their heating in solid state (100°C, 36h, pH 9.5), with an increase of the mean $D_{4,3}$ of particles from 19 µm to 59 µm when dispersed in water (Schong & Famelart, 2018). This swelling property would be of interest in industry for uses in dessert creams, wound dressings or diapers.

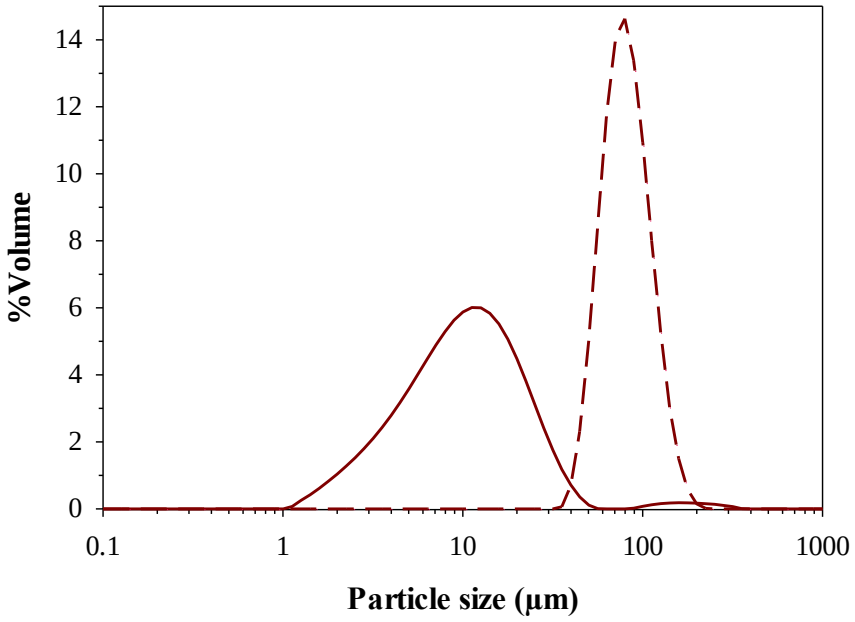

Figure III.14. Size distribution of AGP aggregates (dashed line) and powder particles (continuous line) of arabic acid incubated at 40°C for 7 days.

8.2. Kinetics of formation of soluble AGP aggregates from arabic acid powder

As it was done at 40°C, the structural parameters of AGPs and soluble aggregates were also calculated for samples incubated at 25°C, 55°C and 70°C from SEC MALLS analyzes. At all temperatures studied, molar mass followed the same trend (Figure III.15). First, M_w increased from $1 \cdot 10^6$ g·mol^{-1} (t_0) to reach a maximum at $\sim 6 - 7 \cdot 10^6$ g·mol^{-1} after 28, 1.66, 0.58 and 0.17 days of incubation at 25°C, 40°C, 55°C and 70°C, respectively. As shown in Figure III.6, this time is well in accordance with the duration of the lag phase during which no pelleted material is formed. Whatever the incubation temperatures between 25 and 70°C, this phase corresponded to the formation and the growth of soluble AGP aggregates until a similar AGPs and soluble AGP aggregates distribution characterized by a similar mean M_w was reached. For longer incubation times, molar mass decreased whatever the temperature, until it reached a plateau at a constant value between 4 and $5 \cdot 10^5$ g·mol^{-1} for samples incubated at 40°C, 55°C and 70°C. At 25°C, the aggregation was much slower and the data obtained at this temperature appeared more dispersed. No plateau was reached after 60 days of incubation but it would probably if samples were stored for longer storage times. As previously discussed, the M_w decrease was explained by the growth of the soluble AGP aggregates to form the pelleted ones that were not characterized in these experiments.

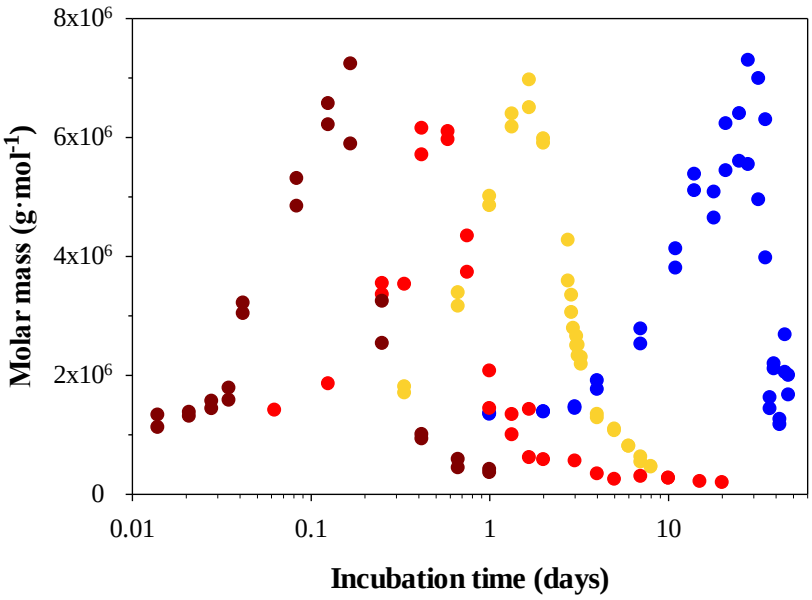

Figure III.15. Calculated mean molar mass determined by SEC MALLS experiments from AGPs and soluble aggregates of arabic acid incubated at 25°C (●), 40°C (●), 55°C (●) and 70°C (●).

Since the evolution of the molar mass of soluble aggregates followed the same shape in the range of temperatures studied, they were normalized using a dimensionless time τ' defined as following:

$$\tau' = {}^{t}/_{t(M_w)_{max}}$$

with $t(M_w)_{max}$ the time for which the molar mass of soluble aggregates and AGPs reaches its maximum.

Using this representation, the molar mass data obtained at 25°C, 40°C, 55°C and 70°C overlapped to form a single curve (Figure III.16). This suggests that the formation of soluble aggregates from arabic acid AGPs followed a similar aggregation mechanism for temperatures ranging from 25 to 70°C and that only the rate of the aggregation reaction was modulated by the temperature. This representation also confirms that a longer storage time is needed to reach the plateau at 25°C, as observed for the other temperatures.

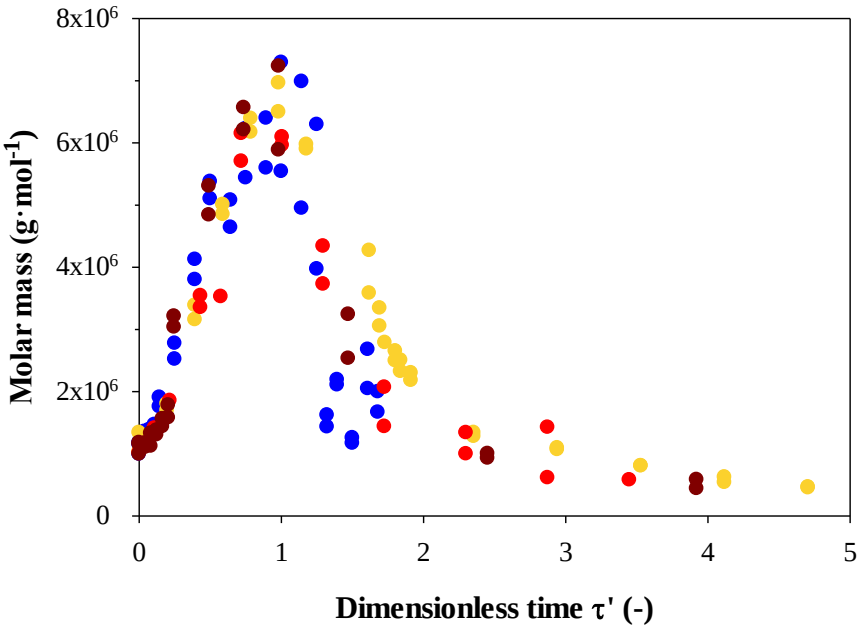

Figure III.16. Calculated mean molar mass determined by SEC MALLS experiments from AGPs and soluble aggregates of arabic acid incubated at 25°C (●), 40°C (●), 55°C (●) and 70°C (●) as a function of the dimensionless time τ'.

From SEC MALLS data, the analysis of R_h vs. M_w conformation plots of incubated arabic acid samples all along the kinetic of aggregation was done at 25°C, 40°C, 55°C and 70°C (Figure III.17). At all temperatures studied, R_h vs. M_w plots followed a linear relationship on a log-log plot scale for all the samples which indicated that R_h could be described by a simple power-law. The conformation plots obtained at 25°C, 40°C, 55°C and 70°C were compared at the same aggregation stages: when soluble aggregates become twice or four times bigger than the native AGPs, when aggregates molar mass reaches its maximum ($t = t(M_w)_{max}$) and when the maximum amount of pelleted aggregates is obtained ($t = t_{plateau}$). At a given level of aggregation, the slope of the conformation plots obtained at the four temperatures was identical, suggesting that the aggregates conformation is not temperature-dependent.

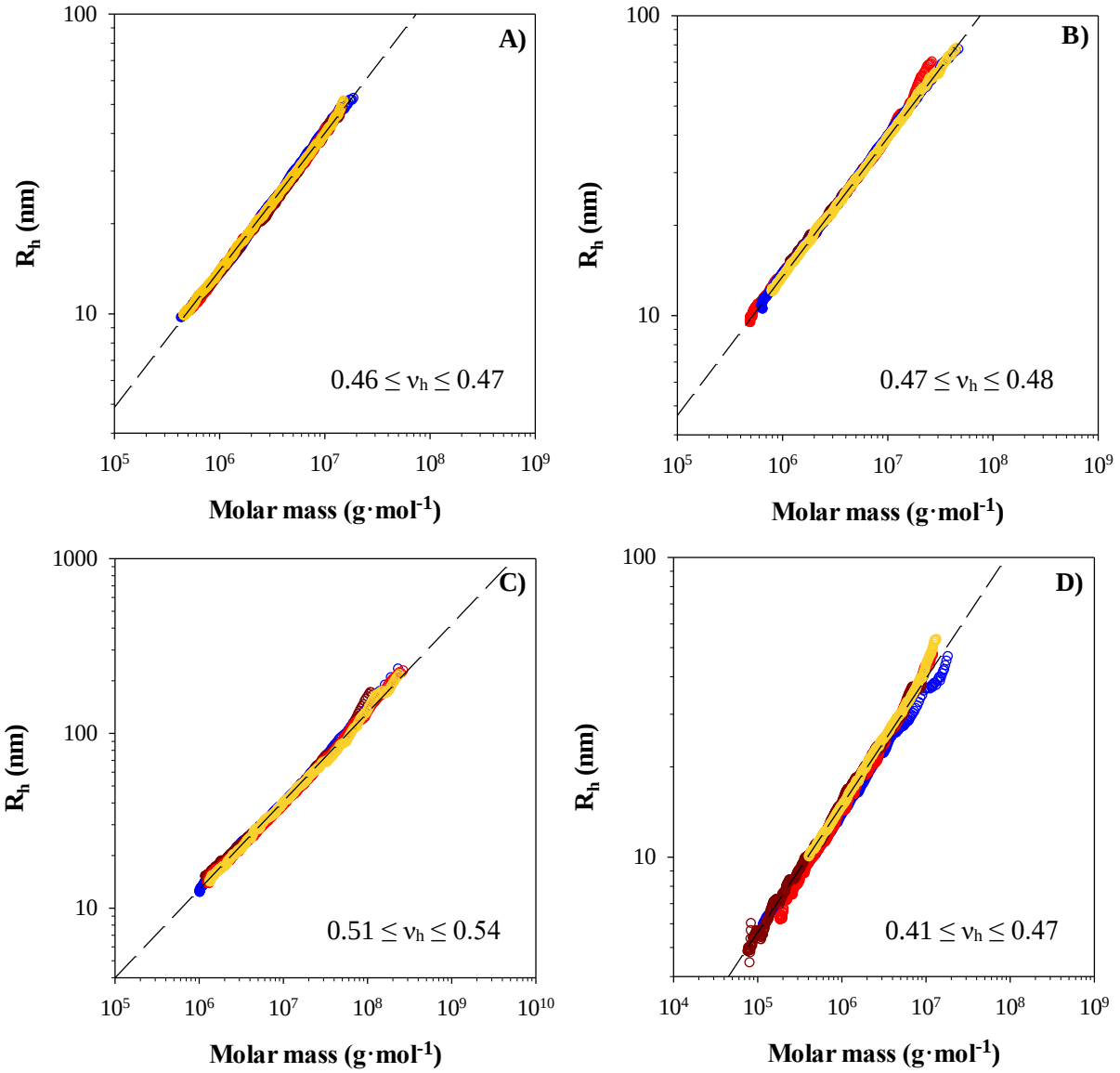

Figure III.17. R_h vs. M_w conformation plots of AGPs and soluble aggregates from arabic acid powder incubated at 25°C (●), 40°C (●), 55°C (●) and 70°C (●) until different aggregation stages are reached: $M_w = 2M_w(t_0)$ (A), $M_w = 4M_w(t_0)$ (B), $M_w = (M_w)_{max}$ (C) and when the maximum amount of pelleted aggregates is obtained (D). From SEC MALLS data.

Considering all the conformation plots obtained for arabic acid incubated at T = 25-70°C, ν_h values were comprised between 0.36 and 0.54 with a mean value of $\nu_h = 0.47 \pm 0.03$ (Figure III.18). This mean ν_h value is in good agreement with values of 0.43 – 0.44 reported for 28 spray-dried A. *seyal* (Sanchez et al., 2018). The low dispersion of the ν_h values between samples reflects that (*i*) at 25°C, 55°C and 70°C the conformation of AGPs from arabic acid and their soluble aggregates was not affected by their storage in dry state, and (*ii*) the incubation temperature does not impact the conformation of soluble aggregates. The

conclusions previously drawn at 40°C (Section III.4.3.2.2) could thus be extended to the whole temperature range: AGPs from arabic acid aggregate following a self-similar mechanism, respecting their molecular organization and conformation.

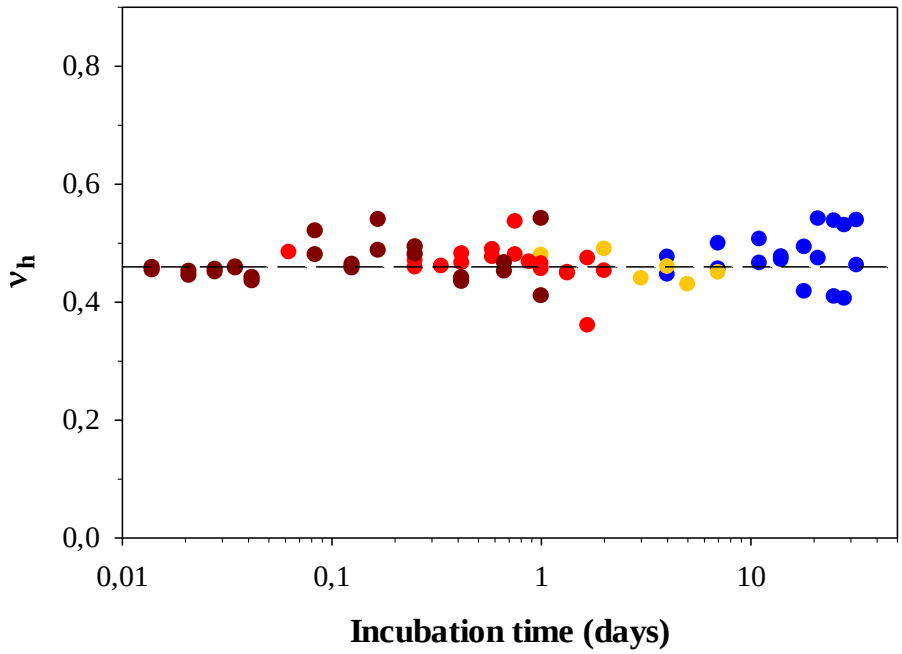

Figure III.18. ν_h exponents from the relation $\mathbf{R_h = K_h M_w^{\nu_h}}$ determined from SEC MALLS data for arabic acid incubated at 25°C (●), 40°C (●), 55°C (●) and 70°C (●) as a function of the incubation time.

8.3. Influence of the drying process on the aggregation behavior of arabic acid AGPs

Spray-drying and freeze-drying are the two main drying processes widely used in food industry for polysaccharides such as GA. In spray-drying, a dispersion is sprayed into a fog of fine droplets through a nozzle inside the spray-drying tower. There, it comes into contact with a current of hot air at 190°C to evaporate the water. When the powder is recovered at the outlet, temperature is still around 70 – 80°C. The high temperatures involved in this process can therefore cause some modifications of the structure (aggregation) of arabic acid AGPs as it undergoes spray-drying. As observed with AA, the spray-drying step induced a slight aggregation of the AGPs (Figure III.3). In order to investigate the influence of the spray-drying step in the reactivity of AA AGPs and the enhancement of their aggregation, the AA dispersion was freeze-dried instead of being spray-dried. Freeze-drying is a gentler process in which the

AA dispersion – frozen at -30°C in advance – underwent slow dehydration at low pressures and through a sublimation step.

8.3.1. Aggregation kinetics of spray-dried and freeze-dried arabic acid

Figure III.19 presents the aggregation kinetics at 40°C of spray-dried and freeze-dried arabic acid powder. Upon dry heating of arabic acid powder, aggregation was observed whatever the drying method used (freeze-drying or spray-drying) to obtain the starting material. Even if it will be necessary to have some complementary data, the insolubility curve of freeze-dried arabic acid incubated at 40°C followed the same trend than for spray-dried arabic acid. Arabic acid remained 100% soluble up to 1.75 days or 2 days, before pelleted material quickly formed, until reaching a plateau after 3 days and 5 days of incubation at a plateau value of ~ 85% and ~ 80% for freeze-dried and spray-dried arabic acid, respectively. Formation of pelleted material for freeze-dried arabic acid seemed to be a little faster than with spray-dried arabic acid.

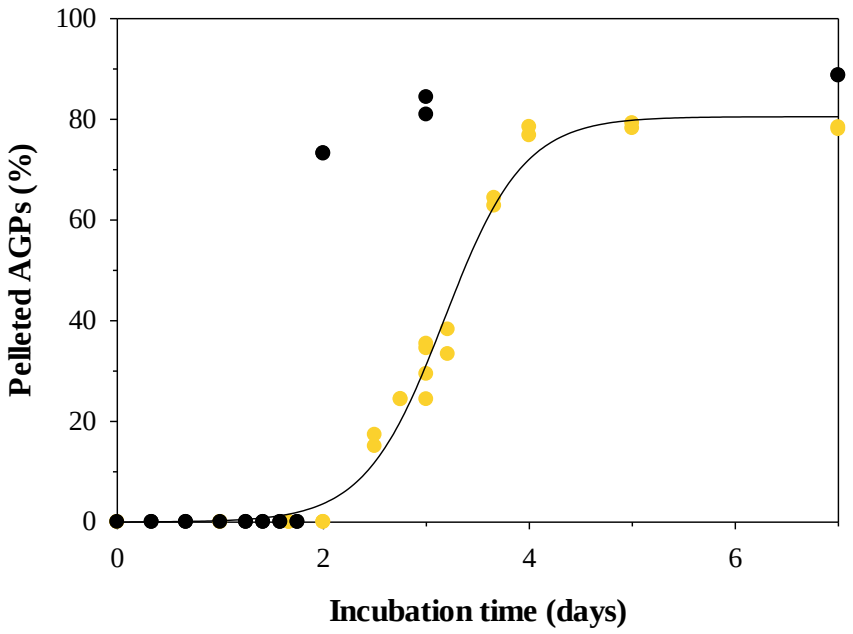

Figure III.19. Percentage of pelleted AGPs in aqueous dispersions as a function of incubation time of spray-dried (●) or freeze-dried (●) arabic acid powder. The continuous line represent the fit obtained with SigmaPlot software.

The impact of the method of drying on the structural properties of milk protein aggregates was also studied (Schong, 2017). After 36h of drying at 100°C, unexpectedly, lyophilized powder appeared more brownish than the spray-dried powder, reflecting a higher reactivity of proteins from the former. They suggested that the freeze-drying process might denature proteins in

another way than spray-drying, and makes them more prone to form pelleted protein aggregates. In our opinion, the amount of protein in AA is too low (< 1%) to be at the origin of the difference in aggregation kinetics observed.

It had been shown also that the more humid the GA powder, the faster the aggregation kinetics of AGPs (Hayashi, 2002). Molar mass of A. *senegal* gum increased from $2.0 \cdot 10^5$ to $2.3 \cdot 10^5$ g·mol^{-1} during heating at 90°C under 10%RH for 12h, whereas M_w increased up to $5.2 \cdot 10^5$ g·mol^{-1} when %RH was set up to 90%RH. In this study, before incubation, the moisture content in lyophilized arabic acid powder (8.4%) was slightly higher than the moisture content in the spray-dried powder (6.5%). Thus, the moisture content of the powders could be one of the reasons to explain their difference in reactivity. It would be interesting to further investigate the influence of powder humidity on the AA AGPs reactivity and aggregation kinetics.

The structure of the pelleted aggregates from freeze-dried and spray-dried arabic acid powder incubated at 40°C for 3 days was characterized by phase contrast microscopy (Figure III.20). Dispersions of arabic acid incubated for less than 2 days were devoid of aggregates, regardless the drying method used to obtain arabic acid. For longer storage times, aggregates obtained with the freeze-dried powder appear as sheets, with very heterogeneous sizes, unlike aggregates obtained with the spray-dried arabic acid, which were characterized by a spherical shape and a heterogeneous surface. SEM micrograph of spray-dried arabic acid powder incubated at 40°C for 3 days are shown in Figure III.20C. The process of spray-drying is responsible for the spherical shape of the particles as they are obtained from the drying of fine droplets. In the case of freeze-drying, the dry product is recovered in the form of a cake that has to be mashed using mortar and pestle to obtain a powder. Thus, these images are in line with the assumption formulated in Section III.5 that "aggregates" observed in dispersions by microscopy are in fact hydrated but poorly dispersed powder particles. As a result, they have a macroscopic organization similar to that of the powder from which they come from, as it was already reported in the case of milk proteins (Schong, 2017).

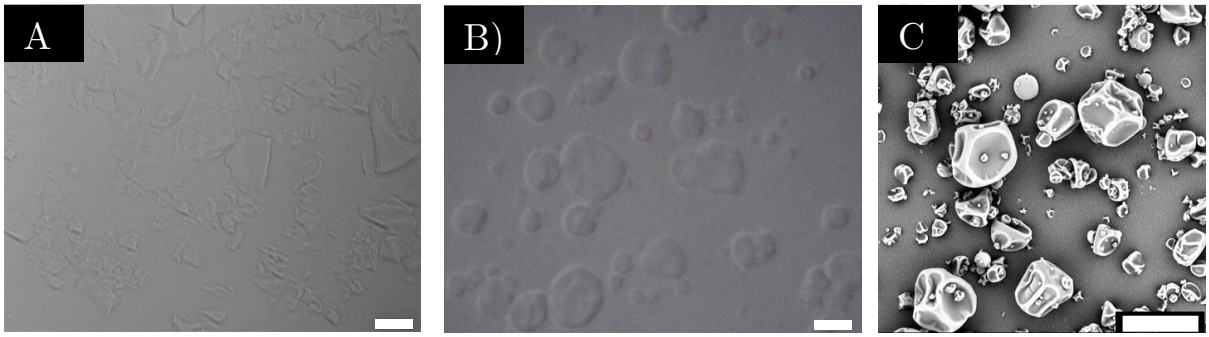

Figure III.20. Influence of the drying method of arabic acid on the shape of insoluble microparticles: phase contrast micrograph of arabic acid dispersions prepared with A) freeze-dried arabic acid or B) spray-dried arabic acid powder incubated at 40°C for 3 days. The magnification was x20 and the scale bar indicates 50 µm length. C) SEM picture of spray-dried arabic acid powder incubated at 40°C for 3 days. The magnification was x2000 and the scale bar indicates 30 µm length.

8.3.2 Structural properties of AGPs from spray-dried and freeze-dried arabic acid

The structural properties of AGP aggregates from the two powders were characterized at the molecular scale by SEC MALLS, all along the storage kinetics (Figure III.21 and III.22). The calculation of the mean molar masses of AGPs from freeze-dried arabic acid incubated at 40°C confirmed the self-aggregation of AGPs into soluble aggregates, with an increase in M_w from $1{\cdot}10^6$ g·mol^{-1} to $5.5{\cdot}10^6$ g·mol^{-1} after 1.25 days of incubation (Figure III.21). With spray-dried arabic acid this maximum was reached a few hours later (t = 1.66 days). From the evolution of M_w, the calculated kinetic constants were 46.4 s^{-1} vs. 57.6 s^{-1} for spray-dried and freeze-dried powder, respectively. This would confirm that the freeze-drying process provides a higher heat sensitivity to AGPs from arabic acid than spray-drying, as observed with other proteins, that aggregated faster during storage after being freeze-dried compared to spray-dried proteins (Fiedler et al., 2021; Schong, 2017).

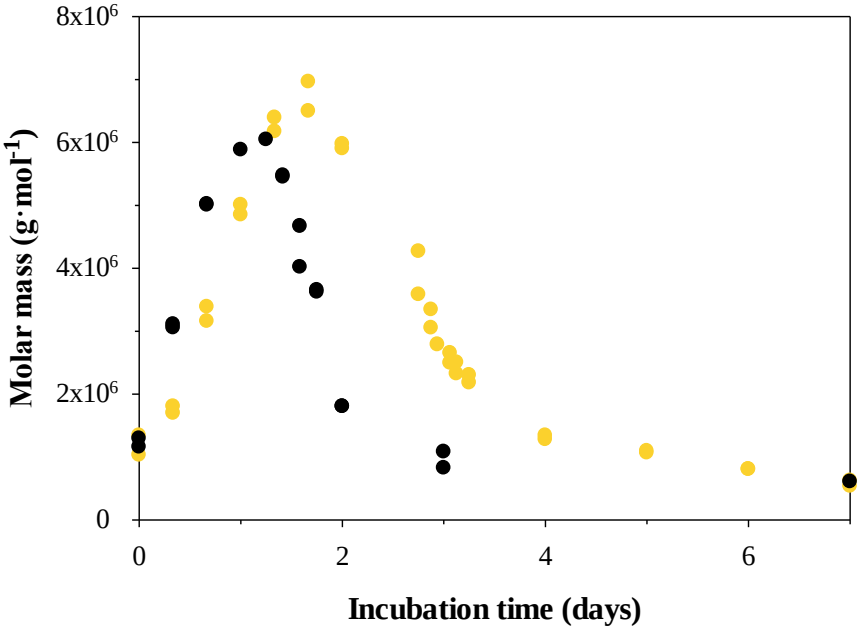

Figure III.21. Influence of the drying method of arabic acid dispersion, spray-drying (●) or freeze-drying (●) on the calculated mean molar mass of AGPs and soluble aggregates of arabic acid powder. From SEC MALLS measurements.

The structural properties of the AGPs and soluble aggregates from incubated arabic acid samples were further characterized using the R_h vs. M_w conformation plots (Figure III.22). On a log-log scale, R_h was linearly related to M_w for both non-incubated arabic acid powders, with a slope of 0.45 (Figure III.22A). Throughout incubation, for a given aggregation stage, the R_h vs. M_w conformation plots of the two samples superimpose in a wide range of M_w, suggesting the conformation of their soluble aggregates was the same (Figure III.22B and Figure III.22C). Like spray-dried arabic acid (see Section III.4.3.2.2), as incubation goes on, the conformation of AGPs and soluble aggregates from the freeze-dried arabic acid was not modified, with a mean value of $\nu_h = 0.48 \pm 0.03$ (data not shown).

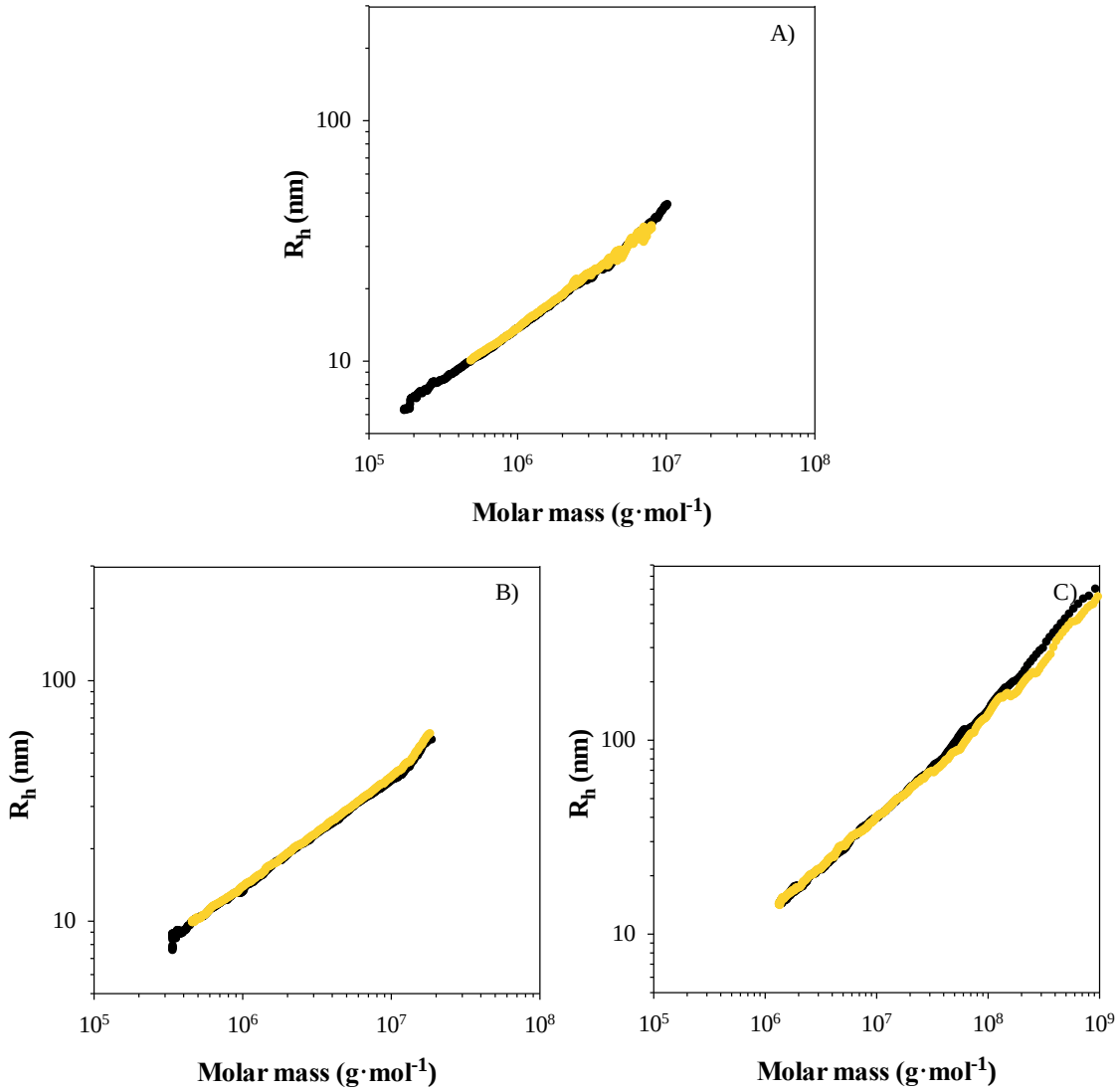

Figure III.22. Influence of the drying method of arabic acid dispersion, spray-drying (●) or freeze-drying (●) on the R_h vs. M_w conformation plots of AGPs and soluble aggregates from arabic acid powder at different aggregation stages: A) before incubation, B) when $M_w = 2M_w(t_0)$ and C) when $M_w = M_{w\,max}$. From SEC MALLS measurements.

Therefore, at the scale of soluble aggregates, it seems that the structural organization is identical, similar to those of the native AGPs. The aggregation mechanism is the same regardless the drying process, but the powder organization at the macroscopic scale seems to influence the final structure of the pelleted aggregates.

9. Highlights

In this chapter, we reported the aggregation behavior of AGPs from Acacia gums during their storage in the dry state. The influence of incubation parameters (*i.e.* time and temperature) and gum properties (*i.e.* mineral content, pH, and method of drying) on the aggregation kinetics of GA and the properties of aggregates formed during storage were evaluated. A special focus was set on the incubation of demineralized Acacia *seyal* gum (arabic acid) at 40°C. The main results obtained are described below:

Aggregation kinetics of AGPs from arabic acid at 40°C:

- AGPs from arabic acid aggregated during their storage in the dry state.
- Molar mass of AGPs increased by 7 during the two first days of storage.
- Soluble aggregates adopted the same conformation than native AGPs from arabic acid, suggesting these aggregates could be seen as a self-similar assembly of elementary units, AGPs.
- For incubation times longer than 2 days, pelleted aggregates formed, the amount of which increased following a sigmoidal curve before reaching a plateau at a plateau value of 80%.
- Incubation induced changes in the hydration properties of arabic acid powder, especially swelling as showed by the increase in $D_{4,3}$ of the powder particles from 14 µm to 70 µm when dispersed in water.

Impact of the incubation temperature:

- From 25°C to 70°C, temperature had only a kinetic effect on aggregation.
- At all temperatures studied, the evolution of M_w of AGPs and soluble aggregates with incubation time was the same and a single master curve was obtained after normalization.
- The formation of pelleted material during incubation also followed a similar mechanism whatever the incubation temperature, showing that temperature only influenced the aggregation kinetics.
- When compared at different temperatures, for a given aggregation stage, the conformation of aggregates did not vary: AGPs from arabic acid aggregated

following a self-similar mechanism, respecting their molecular organization and conformation

- An activation energy of ~ 90 – 100 kJ·mol^{-1} was calculated for the aggregation reaction. This value, combined with the environmental conditions (*i.e.* the dry state and the acidic pH) might be in favor of chemical condensation reactions such as esterification.

Impact of gum properties:

- When incubated in dry state at 40°C, arabic acid aggregated faster than acidified GA and unmodified GA. Minerals from GA have a protective role for the structural stability of AGPs upon dry incubation. The pH of GA in solution before spray-drying also influences the reactivity of GA, promoting their aggregation at pH 2.4. Thus, it seems that the electronic charge on GA is a crucial parameter for its aggregation in dry state.
- Aggregation kinetics of AGPs from freeze-dried were slightly faster compared to spray-dried powder. Aggregates observed in dispersions by microscopy are hydrated but poorly dispersed powder particles having a macroscopic organization similar to that of the powder from which they come from, *i.e.* a spheroidal shape or more irregular shape of sheets for AGPs from incubated spray-dried or freeze-dried arabic acid. The drying method and so the powder organization at the macroscopic scale did not influence the conformation of soluble aggregates formed during incubation.

10. References

Akiyama, Y., Eda, S., & Katō, K. (1984). Gum Arabic is a Kind of Arabinogalactan–Protein. *Agricultural and Biological Chemistry*, *48*(1), 235–237. https://doi.org/10.1080/00021369.1984.10866126

Al-Assaf, S., Andres-Brull, M., Cirre, J., & Phillips, G. O. (2012). Structural changes following industrial processing of Acacia gums. In J. F. Kennedy, G. O. Phillips, & P. A. Williams (Eds.), *Gum Arabic* (RCS Publishing, pp. 153–168). Kennedy J.F., Phillips G.O., Williams P.A. https://doi.org/10.1039/9781849733106-00153

Al-Assaf, S., & Phillips, G. O. (2006). Characterisation of AGPs in Acacia gums. *Foods and Food Ingredients Journal of Japan*, *211*(3), 189–197.

Al-Assaf, S., Phillips, G. O., Aoki, H., & Sasaki, Y. (2007). Characterization and properties of Acacia senegal (L.) Willd. var. senegal with enhanced properties (Acacia (sen) SUPER GUM^{TM}): Part 1—Controlled maturation of Acacia senegal var. senegal to increase viscoelasticity, produce a hydrogel form and convert a poor into a good emulsifier. *Food Hydrocolloids*, *21*(3), 319–328. https://doi.org/10.1016/j.foodhyd.2006.04.011

Al-Assaf, S., Phillips, G. O., Sasaki, Y., & Katayama, T. (2004). *Modified gum arabic* (Patent No. WO 2004/089991 A1).

Al-Assaf, S., Phillips, G. O., Sasaki, Y., & Katayama, T. (2010). *Modified gum arabic from Acacia senegal* (Patent No. EP1611159). https://www.freepatentsonline.com/EP1611159B1.html

Al-Assaf, S., Phillips, G. O., Williams, P. A., & du Plessis, T. A. (2007). Application of ionizing radiations to produce new polysaccharides and proteins with enhanced functionality. *Nuclear Instruments and Methods in Physics Research Section B: Beam Interactions with Materials and Atoms*, *265*(1), 37–43. https://doi.org/10.1016/j.nimb.2007.08.015

Al-Assaf, S., Phillips, G., & Williams, P. (2005a). Studies on acacia exudate gums. Part I: The molecular weight of gum exudate. *Food Hydrocolloids*, *19*(4), 647–660. https://doi.org/10.1016/j.foodhyd.2004.09.002

Al-Assaf, S., Phillips, G., & Williams, P. (2005b). Studies on Acacia exudate gums: Part II. Molecular weight comparison of the Vulgares and Gummiferae series of Acacia gums. *Food Hydrocolloids*, *19*(4), 661–667. https://doi.org/10.1016/j.foodhyd.2004.09.003

Al-Assaf, S., Sakata, M., McKenna, C., Aoki, H., & Phillips, G. O. (2009). Molecular associations in acacia gums. *Structural Chemistry*, *20*(2), 325. https://doi.org/10.1007/s11224-009-9430-3

Anderson, D. M. W., Bridgeman, M. M. E., Farquhar, J. G. K., & McNab, C. G. A. (1983). The chemical characterization of the test article used in toxological studies of gum arabic (Acacia Senegal (L.) Willd). *International Tree Crops Journal*, *2*(3–4), 245–254. https://doi.org/10.1080/01435698.1983.9752758

Anderson, D. M. W., Dea, I. C. M., Karamalla, K. A., & Smith, J. F. (1968). Studies on uronic acid materials: Part XXIV. An analytical study of different forms of the gum from Acacia senegal willd. *Carbohydrate Research*, *6*, 97–103.

https://doi.org/10.1016/S0008-6215(00)80062-2

Anema, S. G., Pinder, D. N., Hunter, R. J., & Hemar, Y. (2006). Effects of storage temperature on the solubility of milk protein concentrate (MPC85). *Food Hydrocolloids*, *20*(2), 386–393. https://doi.org/10.1016/j.foodhyd.2005.03.015

Aoki, H., Al-Assaf, S., Katayama, T., & Phillips, G. O. (2007). Characterization and properties of Acacia senegal (L.) Willd. var. senegal with enhanced properties (Acacia (sen) SUPER GUM™): Part 2—Mechanism of the maturation process. *Food Hydrocolloids*, *21*(3), 329–337. https://doi.org/10.1016/j.foodhyd.2006.04.002

Aoki, H., Katayama, T., Ogasawara, T., Sasaki, Y., Al-Assaf, S., & Phillips, G. O. (2007). Characterization and properties of Acacia senegal (L.) Willd. var. Senegal with enhanced properties (Acacia (sen) SUPER GUM™): Part 5. Factors affecting the emulsification of Acacia senegal and Acacia (sen) SUPER GUM™. *Food Hydrocolloids*, *21*(3), 353–358. https://doi.org/10.1016/j.foodhyd.2006.04.014

Apolinar-Valiente, R., Williams, P., Nigen, M., Tamayo, V. M., Doco, T., & Sanchez, C. (2020). Fractionation of Acacia seyal gum by ion exchange chromatography. *Food Hydrocolloids*, *98*, 105283. https://doi.org/10.1016/j.foodhyd.2019.105283

Burchard, W. (1994). Light Scattering Techniques. In S. B. Ross-Murphy (Ed.), *Physical Techniques for the Study of Food Biopolymers* (pp. 151–213). Springer US. https://doi.org/10.1007/978-1-4615-2101-3_4

Burchard, W. (1999). Solution Properties of Branched Macromolecules. In J. Roovers (Ed.), *Branched Polymers II* (Vol. 143, pp. 113–194). Springer Berlin Heidelberg. https://doi.org/10.1007/3-540-49780-3_3

Burgain, J., Scher, J., Petit, J., Francius, G., & Gaiani, C. (2016). Links between particle surface hardening and rehydration impairment during micellar casein powder storage. *Food Hydrocolloids*, *61*, 277–285. https://doi.org/10.1016/j.foodhyd.2016.05.021

Capataz-Tafur, J., Trejo-Trapia, G., Rodríguez-Monroy, M., & Sepulveda-Jiménez, G. (2011). Arabinogalactan proteins are involved in cell aggregation of cell suspension cultures of Beta vulgaris L. *Plant Cell Tiss Organ Cult*, *106*, 169–177. https://doi.org/10.1007/s11240-010-9905-3

Castellani, O., Guibert, D., Al-Assaf, S., Axelos, M., Phillips, G. O., & Anton, M. (2010). Hydrocolloids with emulsifying capacity. Part 1 – Emulsifying properties and interfacial characteristics of conventional (Acacia senegal (L.) Willd. Var. Senegal) and matured (Acacia (sen) SUPER GUM™) Acacia senegal. *Food Hydrocolloids*, *24*(2–3), 193–199. https://doi.org/10.1016/j.foodhyd.2009.09.005

Cecil, C. O. (2005). Gum arabic. *Saudi Aramco World*, *56*(2), 36–39.

Chen, N., Zhao, M., Chassenieux, C., & Nicolai, T. (2017). The effect of adding NaCl on thermal aggregation and gelation of soy protein isolate. *Food Hydrocolloids*, *70*, 88–95. https://doi.org/10.1016/j.foodhyd.2017.03.024

Debon, S. J. J., & Tester, R. F. (2001). In vitro binding of calcium, iron and zinc by non-starch polysaccharides. *Food Chemistry*, *73*(4), 401–410. https://doi.org/10.1016/S0308-8146(00)00312-5

Devnani, B., Ong, L., Kentish, S., & Gras, S. (2020). Heat induced denaturation, aggregation and gelation of almond proteins in skim and full fat almond milk. *Food Chemistry*, *325*, 126901. https://doi.org/10.1016/j.foodchem.2020.126901

Dror, Y., Cohen, Y., & Yerushalmi-Rozen, R. (2006). Structure of gum arabic in aqueous solution. *Journal of Polymer Science Part B: Polymer Physics*, *44*(22), 3265–3271. https://doi.org/10.1002/polb.20970

Fiedler, D., Hartl, S., Gerlza, T., Trojacher, C., Kungl, A., Khinast, J., & Roblegg, E. (2021). Comparing freeze drying and spray drying of interleukins using model protein CXCL8 and its variants. *European Journal of Pharmaceutics and Biopharmaceutics*, *168*, 152–165. https://doi.org/10.1016/j.ejpb.2021.08.006

Fincher, G. B., Stone, B. A., & Clarke, A. E. (1983). Arabinogalactan-Proteins: Structure, Biosynthesis, and Function. *Annual Review of Plant Physiology*, *34*(1), 47–70. https://doi.org/10.1146/annurev.pp.34.060183.000403

Gabel, L. F. (1930). The effect of heat on acacia. *Journal of the American Pharmaceutical Association*, *19*(8), 828–830. https://doi.org/10.1002/jps.3080190807

Gaborieau, M., & Castignolles, P. (2011). Size-exclusion chromatography (SEC) of branched polymers and polysaccharides. *Analytical and Bioanalytical Chemistry*, *399*(4), 1413–1423. https://doi.org/10.1007/s00216-010-4221-7

Gao, M., & Showalter, A. M. (2000). Immunolocalization of LeAGP-1, a modular arabinogalactan-protein, reveals its developmentally regulated expression in tomato. *Planta*, *210*, 865–874.

Gashua, I. B., Williams, P. A., & Baldwin, T. C. (2016). Molecular characteristics, association and interfacial properties of gum Arabic harvested from both Acacia senegal and Acacia seyal. *Food Hydrocolloids*, *61*, 514–522. https://doi.org/10.1016/j.foodhyd.2016.06.005

Gashua, I. B., Williams, P. A., Yadav, M. P., & Baldwin, T. C. (2015). Characterisation and molecular association of Nigerian and Sudanese Acacia gum exudates. *Food Hydrocolloids*, *51*, 405–413. https://doi.org/10.1016/j.foodhyd.2015.05.037

Hayashi, H. (2002). *Method of modifying gum arabic* (European Union Patent No. EP1505078B1). https://patents.google.com/patent/EP1505078B1/ja

Idris, O. H. M., Williams, P. A., & Phillips, G. O. (1998). Characterisation of gum from Acacia senegal trees of different age and location using multidetection gel permeation chromatography. *Food Hydrocolloids*, *12*(4), 379–388. https://doi.org/10.1016/S0268-005X(98)00058-7

Islam, A. M., Phillips, G. O., Sljivo, A., Snowden, M. J., & Williams, P. A. (1997). A review of recent developments on the regulatory, structural and functional aspects of gum arabic. *Food Hydrocolloids*, *11*(4), 493–505. https://doi.org/10.1016/S0268-005X(97)80048-3

Katayama, T., Ogasawara, T., Sasaki, Y., Al-Assaf, S., & Phillips, G. (2008). *Composition Containing Hydrogel Component Derived from Gum Arabic* (United States Patent No. US20080038436A1). https://patents.google.com/patent/US20080038436A1/en

Kirkland, J. J., Dilks, C. H., Rementer, S. W., & Yau, W. W. (1992).

Asymmetric-channel flow field-flow fractionation with exponential force-field programming. *Journal of Chromatography A*, *593*(1), 339–355. https://doi.org/10.1016/0021-9673(92)80303-C

Kunkel, M. E., Seo, A., & Minten, T. A. (1997). Magnesium binding by gum arabic, locust bean gum, and arabinogalactan. *Food Chemistry*, *59*(1), 87–93. https://doi.org/10.1016/S0308-8146(96)00173-2

Larrañeta, E., Henry, M., Irwin, N., Trotter, J., Perminova, A., & Donnelly, R. (2018). Synthesis and characterization of hyaluronic acid hydrogels crosslinked using a solvent-free process for potential biomedical applications. *Carbohydrate Polymers*, *181*, 1194–1205. https://doi.org/10.1016/j.carbpol.2017.12.015

Leeman, M., Wahlund, K. G., & Wittgren, B. (2006). Programmed cross flow asymmetrical flow field-flow fractionation for the size separation of pullulans and hydroxypropyl cellulose. *Journal of Chromatography A*, *1134*(1), 236–245. https://doi.org/10.1016/j.chroma.2006.08.065

Lim, H. S., BeMiller, J. N., & Lim, S.-T. (2003). Effect of Dry Heating with Ionic Gums at Controlled pH on Starch Paste Viscosity. *Cereal Chemistry*, *80*(2), 198–202. https://doi.org/10.1094/CCHEM.2003.80.2.198

Lopez-Torrez, L., Nigen, M., Williams, P., Doco, T., & Sanchez, C. (2015). Acacia senegal vs. Acacia seyal gums – Part 1: Composition and structure of hyperbranched plant exudates. *Food Hydrocolloids*, *51*, 41–53. https://doi.org/10.1016/j.foodhyd.2015.04.019

Mahendran, T., Williams, P. A., Phillips, G. O., Al-Assaf, S., & Baldwin, T. C. (2008). New Insights into the Structural Characteristics of the Arabinogalactan−Protein (AGP) Fraction of Gum Arabic. *Journal of Agricultural and Food Chemistry*, *56*, 9269–9276.

Mahmoudi, N., Gaillard, C., Boué, F., Axelos, M. A. V., & Riaublanc, A. (2010). Self-similar assemblies of globular whey proteins at the air–water interface: Effect of the structure. *Journal of Colloid and Interface Science*, *345*(1), 54–63. https://doi.org/10.1016/j.jcis.2010.01.036

Majewska-Sawka, A., & Nothnagel, E. A. (2000). The multiple roles of arabinogalactan proteins in plant development. *Plant Physiology*, *122*(1), 3–10. https://doi.org/10.1104/pp.122.1.3

Martins, S., Jongen, W., & van Boekel, M. (2000). A review of Maillard reaction in food and implications to kinetic modelling. *Trends in Food Science & Technology*, *11*(9), 364–373. https://doi.org/10.1016/S0924-2244(01)00022-X

Mejia Tamayo, V. (2018). *Volumetric properties of Arabinogalactan-proteins from Acacia Gum*. Montpellier SupAgro.

Mejia Tamayo, V., Nigen, M., Apolinar-Valiente, R., Williams, P., Doco, T., Renard, D., & Sanchez, C. (2018). *Flexibility and hydration of amphiphilic hyperbranched Arabinogalactan-protein from plant exudate: A volumetric perspective*. https://doi.org/10.3390/colloids2010011

Mhinzi, G. S. (2003). Intra-species variation of the properties of gum exudates from Acacia Senegal var. Senegal and Acacia seyal var. Fistula from Tanzania. *Bulletin of the Chemical Society of*

Ethiopia, *17*(1). https://doi.org/10.4314/bcse.v17i1.61734

Mimouni, A., Deeth, H. C., Whittaker, A. K., Gidley, M. J., & Bhandari, B. R. (2010). Investigation of the microstructure of milk protein concentrate powders during rehydration: Alterations during storage. *Journal of Dairy Science*, *93*(2), 463–472. https://doi.org/10.3168/jds.2009-2369

Moorjani, M. N., & Narwani, C. S. (1948). Influence of heat on the physico-chemical properties of gum-arabic. *Current Science*, *17*(4), 123–124.

Nasser, S., R., R., De-Sa-Peixoto, P., Ronse, G., Nuns, N., Pourpoint, F., Burgain, J., Gaiani, C., Hédoux, A., & Delaplace, G. (2017). Microstructure evolution of micellar casein powder upon ageing: Consequences on rehydration dynamics. *Journal of Food Engineering*, *206*, 57–66. https://doi.org/10.1016/j.jfoodeng.2017.03.004

Nicolai, T. (2019). Gelation of food protein-protein mixtures. *Advances in Colloid and Interface Science*, *270*, 147–164. https://doi.org/10.1016/j.cis.2019.06.006

Pantze, A., Karlsson, O., & Westermark, U. (2008). Esterification of carboxylic acids on cellulosic material: Solid state reactions. *Holzforschung*, *62*(2), 136–141.

Percec, V., Ahn, C.-H., Cho, W.-D., Jamieson, A. M., Kim, J., Leman, T., Schmidt, M., Gerle, M., Möller, M., Prokhorova, S. A., Sheiko, S. S., Cheng, S. Z. D., Zhang, A., Ungar, G., & Yeardley, D. J. P. (1998). Visualizable Cylindrical Macromolecules with Controlled Stiffness from Backbones Containing Libraries of Self-Assembling Dendritic Side Groups. *Journal of the American Chemical Society*, *120*(34), 8619–8631. https://doi.org/10.1021/ja981211v

Phillips, G. O. (2009). Molecular association and function of arabinogalactan protein complexes from tree exudates. *Structural Chemistry*, *20*(2), 309–315. https://doi.org/10.1007/s11224-009-9422-3

Phillips, G. O., & Williams, P. A. (1993). The specification of the gum Arabic of commerce. In *Food hydrocolloids: Structures, Properties, and Functions* (pp. 45–63). Springer Science + Business Media. 10.1007/978-1-4615-2486-1_4

Podzimek, S., Vlcek, T., & Johann, C. (2001). Characterization of branched polymers by size exclusion chromatography coupled with multiangle light scattering detector. I. Size exclusion chromatography elution behavior of branched polymers. *Journal of Applied Polymer Science*, *81*(7), 1588–1594. https://doi.org/10.1002/app.1589

Randall, R. C., Phillips, G. O., & Williams, P. A. (1989). Fractionation and characterization of gum from Acacia senegal. *Food Hydrocolloids*, *3*(1), 65–75. https://doi.org/10.1016/S0268-005X(89)80034-7

Ray, A., Bird, P., Iacobucci, G., & Clark, B. (1995). Functionality of gum arabic. Fractionation, characterization and evaluation of gum fractions in citrus oil emulsions and model beverages. *Food Hydrocolloids*, *9*(2), 123–131. https://doi.org/10.1016/S0268-005X(09)80274-9

Renard, D., Garnier, C., Lapp, A., Schmitt, C., & Sanchez, C. (2012). Structure of arabinogalactan-protein from Acacia gum: From porous ellipsoids to supramolecular architectures. *Carbohydrate Polymers*, *90*(1), 322–332. https://doi.org/10.1016/j.carbpol.2012.05.046

Renard, D., Lavenant-Gourgeon, L., Lapp, A., Nigen, M., & Sanchez, C. (2014). Enzymatic hydrolysis studies of arabinogalactan-protein structure from Acacia gum: The self-similarity hypothesis of assembly from a common building block. *Carbohydrate Polymers*, *112*, 648–661. https://doi.org/10.1016/j.carbpol.2014.06.041

Renard, D., Lavenant-Gourgeon, L., Ralet, M.-C., & Sanchez, C. (2006). Acacia senegal Gum: Continuum of Molecular Species Differing by Their Protein to Sugar Ratio, Molecular Weight, and Charges. *Biomacromolecules*, *7*(9), 2637–2649. https://doi.org/10.1021/bm060145j

Sanchez, C., Nigen, M., Mejia Tamayo, V., Doco, T., Williams, P., Amine, C., & Renard, D. (2018). Acacia gum: History of the future. *Food Hydrocolloids*, *78*, 140–160. https://doi.org/10.1016/j.foodhyd.2017.04.008

Sanchez, C., Renard, D., Robert, P., Schmitt, C., & Lefebvre, J. (2002). Structure and rheological properties of acacia gum dispersions. *Food Hydrocolloids*, *16*(3), 257–267. https://doi.org/10.1016/S0268-005X(01)00096-0

Sara, S. A., Ali, A. R., Hassan, I. A., Tarig, E. M., & Hassan, A. M. (2018). Towards Acacia seyal protocol in Sudan: Preliminary study pertinent to colour identification and physiochemical properties. *Bioactive Carbohydrates and Dietary Fibre*, *15*, 37–40. https://doi.org/10.1016/j.bcdf.2018.02.002

Sasaki, Y., Ogasawara, T., Katayama, T., & Sakata, M. (2014). *Process for producing modified gum arabic* (United States Patent No. US8722129B2). https://patents.google.com/patent/US8722129B2/en

Schong, E. (2017). *Assemblages microniques de protéines sériques produits par étuvage à pH 9,5: Mécanisme de formation et propriétés physico-chimiques et fonctionnelles* [Agrocampus Ouest]. http://theses.fr/2017NSARB302

Schong, E., & Famelart, M. (2018). Dry heating of whey proteins leads to formation of microspheres with useful functional properties. *Food Research International*, *113*, 210–220. https://doi.org/10.1016/j.foodres.2018.07.004

Schong, E., & Famelart, M.-H. (2019a). Influence of casein on the formation of whey protein microparticles obtained by dry heating at an alkaline pH. *Food Research International*, *122*, 96–104. https://doi.org/10.1016/j.foodres.2019.04.001

Schong, E., & Famelart, M.-H. (2019b). Influence of lactose on the formation of whey protein microparticles obtained by dry heating at alkaline pH. *Food Hydrocolloids*, *87*, 477–486. https://doi.org/10.1016/j.foodhyd.2018.08.018

Seifert, G. J., & Roberts, K. (2007). The Biology of Arabinogalactan Proteins. *Annual Review of Plant Biology*, *58*(1), 137–161. https://doi.org/10.1146/annurev.arplant.58.032806.103801

Showalter, A. M. (2001). Arabinogalactan-proteins: Structure, expression and function. *Cellular and Molecular Life Sciences*, *58*(10), 1399–1417. https://doi.org/10.1007/PL00000784

Taft, R., & Malm, L. E. (1931). Some physico-chemical properties of gum Arabic-water systems and their interpretation. *Journal of Physical Chemistry*, *35*(3), 874–892. https://doi.org/10.1021/j150321a015

Veis, A., & Eggenberger, D. N. (1954). Light Scattering in Solutions of a Linear Polyelectrolyte. *Journal of the*

American Chemical Society, *76*(6), 1560–1563. https://doi.org/10.1021/ja01635a026

Verbeken, D., Dierckx, S., & Dewettinck, K. (2003). Exudate gums: Occurrence, production, and applications. *Applied Microbiology and Biotechnology*, *63*(1), 10–21. https://doi.org/10.1007/s00253-003-1354-z

Wang, Q., Burchard, W., Cui, S. W., Huang, X., & Phillips, G. O. (2008). Solution Properties of Conventional Gum Arabic and a Matured Gum Arabic (Acacia (sen) SUPER GUM). *Biomacromolecules*, *9*(4), 1163–1169. https://doi.org/10.1021/bm7011696

CHAPTER IV.

HYDRATION PROPERTIES OF AGP AGGREGATES OBTAINED FROM DEMINERALIZED ACACIA *SEYAL* GUM

Probing hydration of arabinogalactan-protein aggregates: a volumetric and spectroscopic study

Amandine Antoine-Michard[a,b], Michaël Nigen[a,*], Céline Charbonnel[a], Isabelle Jaouen[b], and Christian Sanchez[a]

[a] UMR IATE, Univ Montpellier, INRAE, Institut Agro, 34060 Montpellier, France

[b] ALLAND & ROBERT, 75003, Paris, France

* Corresponding author.

E-mail address: michael.nigen@umontpellier.fr

Abstract

Acacia gum (GA) is defined as a continuum of weakly charged, amphiphilic, hyperbranched arabinogalactan-proteins (AGP). In the food industry, GA is appreciated for its good interfacial properties that are governed by AGP-AGP and AGP-water interactions. However, due to its hydrophilic nature, GA gum hydration properties have been rarely studied in the past. The storage in dry state of demineralized GA had led to dehydration-induced AGP aggregation. This study characterized the hydration properties of AGPs from GA and demineralized GA at different aggregation stages. The aim was to correlate water dynamics with the structure of AGP aggregates formed during storage by a combination of volumetric and spectroscopic methods. For the first time, we determined the intrinsic volumetric properties of AGP aggregates. These aggregates were characterized by their density ρ = 1426 $kg \cdot m^{-3}$, their ultrasound velocity v_s = 1664 $m \cdot s^{-1}$ and their intrinsic adiabatic compressibility $\beta_s^\circ = 2.58 \cdot 10^{-10}$ Pa^{-1} which are three thermodynamic parameters. These values were close to the volumetric properties of globular proteins. The most aggregated samples were more sensitive to the concentration and appeared more porous. Their formation was related to enhanced hydrophobic water dynamics. In turn, enhanced hydrophilic water dynamics were needed to form smaller soluble aggregates. These results were supported by FTIR spectroscopy.

Keywords: Acacia *seyal* gum, Arabinogalactan-proteins, Aggregation, Hydration, Water dynamics

1. Introduction

Hydration water is involved in many biological processes, including protein folding, enzyme activity, macromolecular recognition, and drug binding (Baron et al., 2010; Camino et al., 2021; Chalikian, Sarvazyan, Plum, et al., 1994; Grossutti & Dutcher, 2016; Henzler-Wildman et al., 2007; Kay, 2005; Rau & Parsegian, 1990).

In addition, the importance of biopolymer-water interactions and changes in interfacial water dynamics on the aggregation propensity of biopolymers was pointed out (Costantino et al.,

1994; D. Liu et al., 2011; Y. Liu, 2005; Van der Plancken et al., 2007). In particular, it has been shown the formation of protein (Apicella et al., 2012; Crick et al., 2006; Punihaole et al., 2017; Wen et al., 2017) and polysaccharide (Herrera-Gómez et al., 2002; Viet et al., 2007) aggregates depend on the polarity of the used solvent and the thermodynamic state of interacting water (Camino et al., 2021; Chakraborty et al., 2021). In proteins, increased mobility of interfacial water near apolar protein atoms seems to be a critical step leading to the formation of highly ordered structures (Camino et al., 2021; Fichou et al., 2015; Mukherjee et al., 2007; Pavlova et al., 2016; Reddy et al., 2009, 2010; Thirumalai et al., 2012).

Hydration water refers to water molecules constituting the so-called hydration layers surrounding a solute. It is supposed two hydration layers are mainly constituted around solutes, but the number of layers may be higher depending on the strength of solute-water interactions. In the first hydration layer, where water molecule dynamics are the most perturbed by the presence of the solute, water molecules closely interact (essentially through electrostatic interactions) with the solute whereas in the second hydration layer, they are less tightly interacting but their physicochemical properties would be still disturbed by the presence of the solute. In contrast, bulk water molecules do not interact with macromolecules or in a manner that does not affect their physicochemical properties (Chalikian, 2001; Lee et al., 2005; Shiraga et al., 2015). Understanding how water molecules interact with biopolymers and the consequences of these interactions on the stability of macromolecules in water is of fundamental importance to better apprehend their structural and physicochemical properties. The use of spectroscopic methods such as NMR relaxometry or FTIR in combination with volumetric (density and ultrasound) measurements had appeared as an appropriate tool to study both the structure and the dynamics of water (protons) in the hydration shells. All three methods being dynamic in nature, they allow to probe electrostatic, spin, and volume (energetic) fluctuations, respectively.

Acacia gum or gum arabic (GA) is known to be easily dispersible in water, providing low-viscosity dispersions even at concentrations up to 30% that may efficiently stabilize oil-in-water emulsions (Sanchez et al., 2018; Touré, 2008). All these properties are governed by the structure of its constitutive molecules, the arabinogalactan proteins (AGPs), and more specifically by the interactions between AGPs and water. AGPs from GA have a particularly high affinity for water which had been attributed to the hydrophilic character of GA and its hyperbranched

nature (Hatakeyama et al., 2009; G. Phillips et al., 1996). Both the carbohydrate chains (*via* uronic acid moieties and hydroxyl groups) and the hydrophilic amino acids from GA can interact with water (Renard et al., 2006). However, when heated in dry state above 110°C, then upon dehydration, GA becomes more viscous (Gabel, 1930), and eventually insoluble upon heating, with the formation of a hydrogel (Al-Assaf, Phillips, Aoki, et al., 2007b; Moorjani & Narwani, 1948; Sasaki et al., 2014). These changes had been attributed to the formation of aggregates, following a dehydration mechanism during heating. The aggregation of AGPs from GA in the dry state enhanced GA rheological and emulsifying properties, and was patented (Al-Assaf et al., 2004; Hayashi, 2002; Katayama et al., 2008; Sasaki et al., 2014). Recently, our group showed an improved reactivity of AGPs from demineralized GA during their maturation as compared to native GA, with the formation of aggregates even at mild temperatures ($\leq$ 25°C) (Antoine-Michard et al., 2022, in publication). We demonstrated the essential role of mineral cations (electronic charge) for the stability of AGPs upon storage and suggested that condensation reactions were consistent with our environment conditions (acidic pH, anhydrous medium, heating).

Here, we report the water dynamics of hyperbranched AGPs from demineralized Acacia *seyal* gum as a function of their aggregation state. The partial specific volume and adiabatic compressibility of AGPs – which are two thermodynamic parameters particularly sensitive to hydration – were characterized in a volumetric study. Water dynamics were further assessed by measurement of the proton transverse spin-spin relaxation times (T_2) by Time-Domain Nuclear Magnetic Resonance (TD-NMR). Finally, Fourier transform infrared spectroscopy (FTIR) was used to identify changes in AGP vibration energy during Acacia gum demineralization. Our results highlight a link between the thermodynamic state of AGP aggregates and enhanced water dynamics, in line with the emerging entropy-controlled dehydration-induced aggregation of proteins (Camino et al., 2021; Fichou et al., 2015; Kinoshita, 2009). Fundamentally, this is also the energetic cause of the aggregation mechanism of AGPs, due at the deepest fundamental level to the prohibitive cost of creating a cavity in water to accommodate such large AGP solutes (Graziano, 2006).

2. Materials and methods

2.1. Materials

All experiments were carried out with A. *seyal* gum (lot OF183377), provided by Alland & Robert Company—Natural and Organic gums (Port Mort, France). An ionic exchange resin (Purolite® C160MBH, Purolite Ltd, Llantrisant, Wales) was used to remove all the minerals (cations) from A. *seyal* gum. All reagents were purchased from Sigma-Aldrich (St. Louis, MO, USA). Ultrapure deionized water (18.2 MΩ·cm) was used in all experiments.

2.2. Preparation of arabic acid powder

A 16 wt% A. *seyal* gum dispersion was prepared in water (pH 4.6) and stirred overnight using a magnetic stirring plate at 250 rpm to allow complete hydration of the gum. Cations from A. *seyal* gum were removed using an ionic exchange resin at a mass ratio gum:resin of 1:1. The pH of the dispersion was verified and the demineralization was complete once it reached the value of 2.1. The demineralized A. *seyal* gum was named as usual arabic acid. Arabic acid dispersion was centrifuged (12,000 rpm, 30 min, 20 °C) with an Avanti J-26S XP (Beckman Coulter) to remove insoluble material ($< 1\%$) before spray-drying (Büchi B-290, Büchi Labortechnik AGt, Switzerland).

2.3. Incubation of arabic acid powder and preparation of dispersions

About 300 mg of arabic acid powder were incubated for a given time in closed glass vessels at 40°C in a HPP 260 climate chamber (Memmert, Schwabach, Germany). Samples were regularly collected during incubation kinetics and directly stored at -20°C to stop their structural aggregation. Dispersions were prepared in milliQ water using 0.1 – 6 wt% incubated arabic acid powder. The dispersions were stirred overnight using an orbital plate at 250 rpm. In water, pH of dispersions was around 2.4.

2.4. Volumetric properties measurements

2.4.1. Density and ultrasound velocity measurements

Thermodynamic (volumetric) properties of gum samples were determined from density and ultrasound velocity measurements operated at 25°C and 3 MHz using a DSA 5000M sonodensimeter (Anton Paar, les Ulis, France). Before measurement, all samples were sonicated 15min in order to minimize dissolved air. The instrument is equipped with a density cell, an ultrasound velocity cell and an automatic sample changer. The repeatability of the instrument is in theory $1 \cdot 10^{-6}$ g·cm^{-3} for density and 0.1 m·s^{-1} for ultrasound velocity. In reality, the measured parameters, especially the adiabatic compressibility, are extremely sensitive to tiny energetic changes in dispersions, leading to measurement errors with heterogeneously aggregated AGPs to around 10 – 20%. Measurements were at least duplicated.

2.4.2. Partial specific volume of AGPs

The partial specific volume (V°_s) is a fundamental thermodynamic parameter of a solute, defined as the change on total volume of a system induced by the addition of an infinitesimal amount of solute at constant pressure and temperature, provided that the amount of the solvent is kept constant (Durchschlag, 1986; Høiland, 1986; Kupke, 1973). The V_s° can be calculated using the slope method, since the density difference between the density of solute and solution is important (eq. IV.1). This approximation can be made provided that the solute concentration is low enough to neglect intermolecular solute-solute interactions (Høiland, 1986).

$$V_s^0 = \frac{1}{\rho_0}\left(1 - \frac{\rho - \rho_0}{C}\right) \qquad \text{(IV.1)}$$

where ρ_0 and ρ are the mass density of the solvent and dispersion, respectively, and C is the mass concentration of the solute.

According to the Scaled Particle Theory (Chalikian et al., 1996; Graziano, 2006; Reiss, 1965), the partial specific volume can be expressed as the sum of three contributions: *(i)* an intrinsic contribution (V_M) which considers the volume of the solute which is not accessible to the solvent and the volume of voids inside the solute due to imperfect packing of atoms; *(ii)* the volume of voids around the solute (called thermal volume V_T) and *(iii)* the interaction volume V_I, which considers the effect of interactions between the solvent and surface charged and polar groups of the solute (Bánó & Marek, 2006; Chalikian et al., 1996; Chalikian & Filfil, 2003; Kharakoz, 1989). In particular, the volume of water molecules is assumed to be reduced in the

first hydration shells due to these interactions, contributing negatively to $V°_s$. From this description, $V°_s$ is expressed as:

$$V_s^0 = V_M + V_T + V_l$$

In the following, the description of the specific partial volume of hydrated AGPs, *i.e.* $V°_{s\ AGP–H2O}$, is done considering the thermal volume as comprised in the interaction volume term:

$$V_{s\,AGP-H_2O}^0 = V_{s\,AGP}^0 + V_{s\,l}^0 \qquad \text{(IV.2)}$$

with $V_{s\,AGP}^0$ the intrinsic specific partial volume of AGPs and $V_{s\,l}^0$ the negative contribution due to the interactions between AGPs and water.

2.4.3. Intrinsic volumetric properties of AGPs (density, ultrasound velocity, adiabatic compressibility)

The contribution of the interactions between AGPs and water can be also basically considered by expressing the density of hydrated AGPs $\rho_{AGP–H2O}$ into the sum of two contributions, the one from the AGP itself (ρ_{AGP}) and the other from interfacial water (ρ_l):

$$\rho_{AGP-H_2O} = \rho_{AGP} + \rho_l \qquad \text{(IV.3)}$$

The density of AGPs dispersions can be expressed using the mass conservation law as a function of the density of the bulk and interfacial water ρ_0 and ρ_l, the AGPs intrinsic density ρ_{AGP} and their respective volume fractions Φ_0, Φ_l and Φ_{AGP}, as:

$$\rho_{dispersion} = \Phi_0\rho_0 + \Phi_l\rho_l + \Phi_{AGP}\rho_{AGP} \qquad \text{(IV.4)}$$

and ρ_{AGP} can be calculated as:

$$\rho_{AGP} = \frac{\rho_{dispersion} - \Phi_0\rho_0 - \Phi_l\rho_l}{\Phi_{AGP}} \qquad \text{(IV.5)}$$

The ultrasound velocity of acoustic waves in dispersion was first correlated to the ultrasound velocity in water v_{s0} and in AGPs $v_{s\ AGP}$ in the same manner than density:

$$v_{s\,AGP} = \frac{v_{s\,dispersion} - \Phi_0 v_{s0} - \Phi_l v_{sl}}{\Phi_{AGP}} \quad \text{(IV.6)}$$

Please note the ultrasound velocity is a thermodynamic parameter since it is calculated from the Newton-Laplace equation (see below), that contains only the density and the adiabatic compressibility, two thermodynamic parameters. Also, an alternative additivity model was used based on the Urick equation (Pfeiffer & Heremans, 2005; Urick, 1947). Indeed, the additivity of adiabatic compressibility β gives:

$$\beta_s = \Phi_0\beta_0 + \Phi_l\beta_l + \Phi_{AGP}\beta_{AGP} \quad \text{(IV.7)}$$

Considering the Newton-Laplace equation $\beta = \frac{1}{v_s^2 \rho}$ is valid for dispersions, eq(IV.7) becomes:

$$\frac{1}{v_s^2 \rho} = \frac{\Phi_0}{v_{s0}^2 \rho_0} + \frac{\Phi_l}{v_{sl}^2 \rho_{AGP}} + \frac{\Phi_{AGP}}{v_{sAGP}^2 \rho_{AGP}} \quad \text{(IV.8)}$$

and finally $v_{s\,AGP}$ can be expressed as:

$$v_{sAGP} = \sqrt{\frac{\Phi_{AGP}}{\rho_{AGP}\left(\frac{1}{v_{s\,dispersion}^2 \rho_{dispersion}} - \frac{\Phi_0}{v_{s0}^2 \rho_0} - \frac{\Phi_l}{v_{sl}^2 \rho_l}\right)}} \quad \text{(IV.9)}$$

As detailed below, the two additivity models give similar intrinsic ultrasound velocity value for AGPs (~ 1700 $m.s^{-1}$). This is the first ever estimated intrinsic ultrasound velocity value for AGPs, *i.e.* the propagation of an AGP matter wave.

2.5. Time-Domain Nuclear Magnetic Resonance spectroscopy (TD NMR)

Transverse spin-spin proton relaxation times (T_2) were obtained from time-domain nuclear magnetic resonance (TD NMR) measurements performed using a Minispec mq spectrometer (Bruker, France) operating at a frequency of 20MHz (0.47 Tesla). T_2 were determined using the free induction decay (FID) of the signals for T_2 lower than 200 µs and the Carrel-Purcell-Meiboom-Gill (CPMG) sequence for T_2 higher than 200 µs. The CPMG sequence allows to probe only dynamics of water protons while the FID sequence rather probes the gum protons and the gum-water proton exchanges. An acquisition time of 0.15 ms and 16 scans were used for the FID signal and a recycle delay of 2 seconds was used for the CPMG signal.

A. *seyal* gum powders were weighted and placed in a climatic chamber at 25°C under controlled relative humidity (RH). Samples were weighted daily until the change of weight in time (dm/dt) was lower than 0.002 %·min^{-1}. Samples were carefully introduced into Bruker NMR tubes and tightly compressed to 10 – 12 mm height to improve homogeneity. The tubes were weighted and sealed with Parafilm® to prevent water evaporation. Measurements were performed at 25°C and duplicated. T_2 relaxation data were normalized to take into account the signal intensity and mass of sample.

Data were fitted using the Sigmaplot software (version 13.0) and a combination of sine and exponential functions according to the relation:

$$y(t) = A_1 e^{\left(-t/T_{21}\right)^2} \frac{\sin(B*t)}{B*t} + \sum_{i=2}^{n} A_i e^{-\frac{t}{T_{2i}}} \qquad \text{(IV.10)}$$

where A is the amplitude, T_2 is the transverse relaxation time, B is a constant and t is the time.

2.6. Fourier Transform Infrared (FTIR) spectroscopy

Vibrational energy of AGPs in GA powders were analyzed using a mid-infrared spectrometer (Vertex 70v, Brüker, Ettlingen, Germany) in Attenuated Total Reflectance (ATR) mode. FTIR-ATR spectra were recorded at room temperature and under vacuum conditions, from 4000 to 800 cm^{-1}, at a spectral resolution of 4 cm^{-1} and averaged over 128 scans. About 10 recordings *per powder* with 10 different samples were averaged to integrate the inherent polydispersity of aggregated gums. Spectra processing including automatic baseline correction, normalization and smoothing, was carried out using the OPUS software version 8.2.28.

3. Results and discussion

3.1. Volumetric properties of hydrated AGPs

Volumetric properties of hydrated AGPs were determined combining density and ultrasound velocity measurements. From the density and the ultrasound velocity, the adiabatic compressibility of AGP-based dispersions was calculated. We present these three parameters in two subsections because they merit a separate discussion.

3.1.1 Intrinsic density of "dry" and hydrated AGPs

In literature, it had been proposed that interactions between water and proteins induce a global water molecule volume contraction of 10 – 15% for charged groups and 5 – 10% for polar groups (Chalikian, 2001). Similar results were obtained with sucrose which caused a water molecule volume contraction of 9% (Gharsallaoui et al., 2008). A. *seyal* is composed of 20% of charged groups, namely glucuronic acid and 4-O-Me-glucuronic acid units (Antoine-Michard et al., 2022, in publication). In this study, we assumed that 10% of the interfacial water is highly perturbed by the presence of AGPs. We also considered that the interfacial water has a density around 1100 kg·m^{-3} (*i.e.* 10% larger than bulk water). This value is in the range of the estimated or numerically calculated density for water in the first hydration shell of biopolymers (in the range 1000 – 2000 kg·m^{-3} from 0–3 Å from the surface) (Bull & Breese, 1968; Chalikian, Sarvazyan, & Breslauer, 1994; Davies et al., 1982; Svergun et al., 1998; Voloshin et al., 2011). However, it is important to realize a hydration density equal to, for instance, 2000 kg·m^{-3}, corresponds to a decrease of the water molecule volume at the AGP-water interface by 50% (from 30 to 15 Å^3), which appears huge. This would need a pressure at the interface of thousand bars (Cho et al., 2002; Russo et al., 2017). Thus, interfacial water density values in the range 1000 – 1500 kg·m^{-3} appear more reasonable which is consistent with the value of ρ_h = 1100 kg·m^{-3} chosen.

The intrinsic density of "dry" AGPs refers to the mass of AGP atoms in the AGP molecular volume. Since the density is a specific weight, its inverse is a specific volume, *i.e.* the volume of the mass. Thus, the intrinsic specific volume *is* the *effective* molecular volume. The intrinsic ρ_{AGP} parameter was constant with the gum concentration (Φ_{AGP}) from 0 to 2 days of arabic acid powder incubation, with a ρ_{AGP} value of 1400 kg·m^{-3} (Figure IV.1A). However, ρ_{AGP} was strongly dependent on Φ_{AGP} at longer incubation times, showing AGP aggregates obtained before 2 days of incubation were qualitatively different from those obtained after 5 or 7 days. Since, by definition, ρ_{AGP} is an intrinsic property, it should not depend on the amount of AGPs in solution (Φ_{AGP}). The 20% smaller density value observed at Φ_{AGP} = 0.001 for AGP aggregates above 4 days powder incubation suggest these aggregates were more porous (*i.e.* with a higher void fraction). Similarly, Mimina et al. showed that isothermal compressibility of dispersed particles increases when the concentration decreases (Minina et al., 2018).

A closer look on data reveals smaller ρ_{AGP} are rather observed below 0.01, *i.e.* in a typical concentration range where polyelectrolyte-related effects are observed with charged polymers in water, as we have also shown with GA (Mejia Tamayo, 2018). It is well accepted that the presence of charged sugars (*e.g.* glucuronic acids) and amino acid residues combined with the flexibility of the polymer chain confers to AGPs a polyelectrolyte nature (Mejia Tamayo, 2018; Renard et al., 2006). At low concentration, the charge density of these groups is increased in line with a reduction of the screening effect, which increases the electrostatic repulsion on AGPs. These repulsions lead to an increase of the hydrodynamic volume and in turn, a decrease of *effective density.* One could wonder if these lower density values in very diluted conditions come solely from a charge effect or from a combined effect of surface charges and porosity.

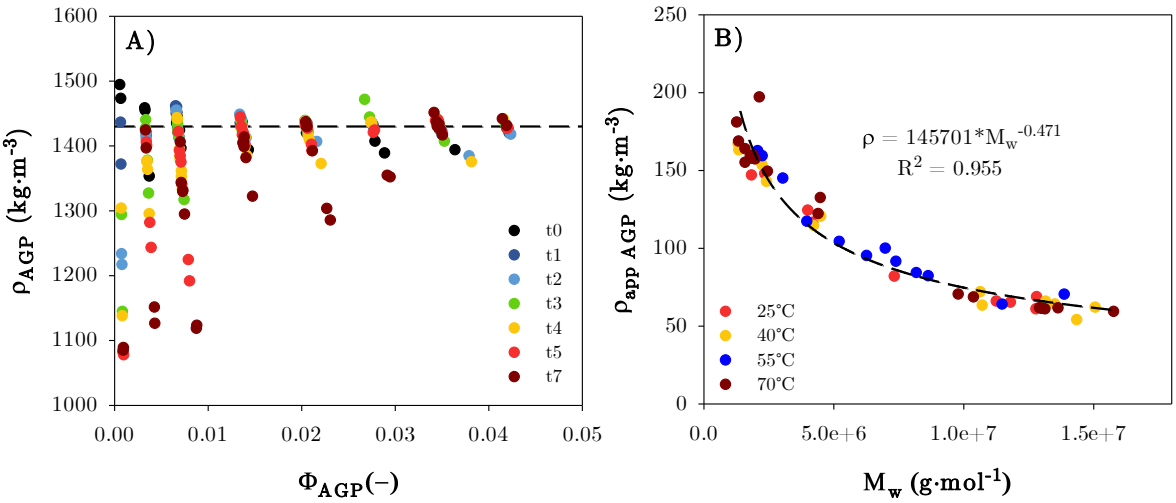

Figure IV.1. Relationship between A) the intrinsic density of AGPs determined by density and ultrasound velocity measurements (in water), and AGP volume fraction. B) AGPs apparent density determined from SEC MALLS data for soluble aggregates as a function of their molar mass. SEC MALLS measurements were done in eluent (0.01M acNa, 0.3M NaCl, 0.02 % NaN_3). AGPs volume was calculated from the hydrodynamic radius and AGPs were assumed spherical.

Soluble AGP aggregates obtained at different temperatures (25 – 70°C) were previously characterized by SEC MALLS measurements (Antoine-Michard et al., 2022, in publication). From the determination of the hydrodynamic radius R_h it was possible to estimate a sphere-equivalent apparent density of AGP aggregates. The apparent density decreased from 170 to 60 kg·m^{-3} when M_w increased from $1.0{\cdot}10^6$ to $1.5{\cdot}10^7$ g·mol^{-1}, which highlights an increase of porosity with the size of aggregates (Figure IV.1B). These results were obtained for low-concentrated samples (C = 0.1wt %) prepared in acetate buffer supplemented with 0.3 mol·L^{-1} NaCl. Since in these conditions the charges are almost screened by the addition of salt, we can reasonably assume that at low concentration, aggregates from t_5 and t_7 are more

porous and display polyelectrolyte behavior. Density of a wide range of rigid aggregates had been shown to decrease when increasing the aggregate size (Fischer et al., 2004; Zangmeister et al., 2014). In fact, the same behavior has been already observed for GA (Alftrén et al., 2012) and may be seen in proteins that display higher intrinsic density at smaller M_w (C. Sanchez, personal communication).

This increase in porosity would imply that there are more volume fluctuations and that consequently, the most dehydrated aggregates would have faster dynamics. Renard et al. showed that the AGP fraction of GA was constituted of an inner porous network of interlaced chains from carbohydrate moieties (Renard et al., 2013). Mejia-Tamayo et al. estimated the void volume in the three fractions of GA obtained by hydrophobic interaction chromatography and showed that it increased with molar mass and hydrophobicity, from ~ 20% to ~ 40%. These authors suggested the increase in void fraction could arise from a combined effect of the increase in relative protein concentration and a more heterogeneous chain packing of sugar blocks and protein domains (Mejia Tamayo et al., 2018). An increase in void fraction would be consistent with the structure of partially insolubilized arabic acid powder particles in solution as observed previously (Antoine-Michard et al., 2022, in publication). After ageing, an increase in porosity of rehydrated milk protein powders was also described (Mimouni et al., 2010; Nasser et al., 2017). However, in the case of casein micelles, these pores were in the range of ~ 100 nm. Aggregation of amyloids into pore-like protofibrils is also a common feature of neurodegenerative diseases (Lashuel & Lansbury, 2006). Thus, these porous aggregates are able to entrap large amounts of confined water inside their voids. In contrast to bulk water, these water molecules exhibit particularly restrained dynamics due to confinement (Arya & Mukhopadhyay, 2014; Camino et al., 2021). Since aggregates are formed first by enhanced water dynamics and protein-protein attractive interactions, the higher void volume fraction of aggregates may be seen as an entropic compensation to the enthalpic AGP-AGP contribution.

To get rid of this peculiar polyelectrolyte effect at low concentration and to be able to compare our results with those of the literature obtained in more concentrated environment, the density values were averaged for $\Phi_{AGP} > 0.035$. Given that the density of hydrated AGP $\rho_{AGP–H2O}$ is inversely proportional to the partial specific volume, the averaged densities of "dry" and hydrated AGP were plotted as a function of incubation time (Figure IV.2). Densities were barely dependent on incubation time, adopting average values of $\rho_{AGP} = 1426 \pm 6$ kg·m^{-3} and $\rho_{AGP–H2O} = 1647 \pm 7$ kg·m^{-3}. These values agree well with $\rho_{AGP} = 1464$ kg·m^{-3} obtained for

another batch of A. *seyal* (Mejia Tamayo et al., 2018). The $\rho_{AGP-H2O}$ parameter is also in the range of 1560 – 1800 kg·m^{-3} calculated from the specific partial volume for A. *seyal* gum (Elsheikh et al., 2015; Mejia Tamayo et al., 2018). Classically, $\rho_{protein-H2O} \sim 1300 - 1400$ kg·m^{-3} (Achterhold & Parak, 2003; Andersson & Hovmöller, 1998; Chalikian et al., 1996; Gekko & Hasegawa, 1986; Pfeiffer et al., 2008; Pfeiffer & Heremans, 2002; Shrestha et al., 2022; Speziale et al., 2003) and $\rho_{polysccharide-H2O} \sim 1600 - 1800$ kg·m^{-3} (Moates et al., 1998; Pfeiffer et al., 2008; Sugiyama et al., 1991) (Table IV.1). Thus, the density of hydrated AGPs from GA is close to those of polysaccharides. This is consistent with the fact that water preferentially interacts with hydroxyl groups from the carbohydrate chains (mainly on the uronic acids) (Hatakeyama et al., 2009; Phillips et al., 1996).

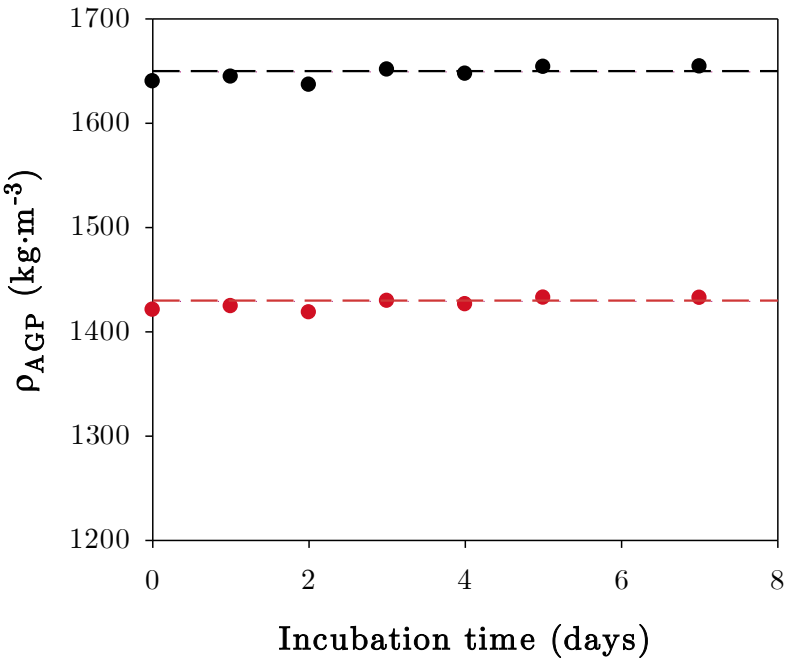

Figure IV.2. Evolution of AGPs intrinsic density ρ_{AGP} (●) and density of hydrated AGPs $\rho_{AGP-H2O}$ (●) from arabic acid incubated at 40°C, averaged between $\Phi_{AGP} = 0.035$ and $\Phi_{AGP} = 0.042$.

Table IV.1. Intrinsic density of dry and hydrated biopolymers obtained from literature. Intrinsic densities determined for "dry" biopolymers were identified by an asterisk *.

System	Intrinsic density	Reference
BSA	1361	(Gekko & Hasegawa, 1986)
α-casein	1366	(Gekko & Hasegawa, 1986)
Hemoglobin	1342	(Chalikian et al., 1996; Gekko & Hasegawa, 1986)
Insulin	1333-1348	(Gekko & Hasegawa, 1986; Pfeiffer et al., 2008)
Lactalbumin	1381-1397	(Chalikian et al., 1996; Pfeiffer et al., 2008)
α-LG	1359	(Gekko & Hasegawa, 1986)
β-LG	1332	(Gekko & Hasegawa, 1986)
Lysozyme*	1210-1270	(Speziale et al., 2003)
Lysozyme	1381-1412	(Chalikian et al., 1996; Gekko & Hasegawa, 1986; Pfeiffer et al., 2008)
Myoglobin	1300-1339	(Chalikian et al., 1996; Gekko & Hasegawa, 1986)
Ovalbumin	1340-1357	(Chalikian et al., 1996; Gekko & Hasegawa, 1986)
Pepsin	1346-1364	(Chalikian et al., 1996; Gekko & Hasegawa, 1986)
Protein crystals*	1220	(Andersson & Hovmöller, 1998)
Trypsin	1342-1391	(Chalikian et al., 1996; Gekko & Hasegawa, 1986)
Trypsinogen	1350-1393	(Chalikian et al., 1996; Gekko & Hasegawa, 1986)
α glycoprotein	1435	(Perkins, 1986)
α macroglobulin	1368	(Perkins, 1986)
IgM GAL	1381	(Perkins, 1986)
C3 of complement	1357	(Perkins, 1986)
IgG3 human	1370	(Perkins, 1986)
Collagen	1434	(Shapiro et al., 2001)
Gelatin	1451	(Gekko & Hasegawa, 1986)
A. *seyal* gum*	1464-1485	(Elsheikh et al., 2015; Mejia Tamayo, 2018)
A. *seyal* gum	1560-1800	(Elsheikh et al., 2015; Mejia Tamayo et al., 2018)
Carrageenans	1984-2375	(Gekko et al., 1985)
Cellulose*	1582-1599	(Sugiyama et al., 1991)
Cellulose	1420-1460	(Sun, 2005)
Glucose	1610	(Pfeiffer et al., 2008)
Raffinose	1754	(Pfeiffer et al., 2008)
Starch*	1472-1485	(Adebayo et al., 2008; Van der Voort Maarschalk et al., 1997)
Starch (amylopectin)	1538-1553	(Moates et al., 1998)
Sucrose*	1550	(Gharsallaoui et al., 2008)
Sucrose	1592	(Pfeiffer et al., 2008)

3.1.2. Intrinsic ultrasound velocity of "dry" AGPs

First, it is important to have in mind that the method used in this study gave access to a low-frequency propagation mode of acoustic waves (named first sound) in the 1000 – 2000 s^{-1} range, whereas a second ultrasound velocity in the range of 3000 $m{\cdot}s^{-1}$ can be measured at high frequency by inelastic scattering methods (Liu, 2005; Russo et al., 2012).

As observed with the intrinsic density parameter, the ultrasound velocity of the AGP aggregates exhibited high dispersion at volume fraction below 0.01 (Figure IV.3A). For all samples, the ultrasound velocity increased with AGP volume fraction. This increase was the most pronounced for t_5 and t_7, whose $v_{s\ AGP}$ increased from ~ 1270 to ~ 1630 $m{\cdot}s^{-1}$ between $\Phi = 0.0001$ and $\Phi = 0.04$. This reflects again a higher sensitivity of volumetric properties of these aggregates to the volume fraction. For $\Phi > 0.02$, $v_{s\ AGP}$ reached almost constant values at around 1600 $m{\cdot}s^{-1}$. These ultrasound velocity values were then averaged between $\Phi = 0.035$ and 0.042, plotted as a function of incubation time and compared to averaged $v_{s\ AGP}$ determined from the Urick equation (eq.IV.9) (Figure IV.3B). Both models gave values in the same order of magnitude with $v_{s\ AGP}$ ~1620 $m{\cdot}s^{-1}$ with our basic approach and about 1710 $m.s^{-1}$ with the Urick equation. This parameter is then the intrinsic sound velocity of dry AGPs and has to be considered as an intrinsic thermodynamic property. The velocity of acoustic waves in AGP aggregates dispersions slightly increased with incubation time (1.6%), which could illustrate an increase in stiffness or in density with dehydration.

Our results are in the range of v_s values reported for proteins by various methods (Table IV.2). The evolution of $v_{s\ AGP}$ observed is in good agreement with the work of Shresta et al. which estimated faster ultrasound velocity in hydrated green fluorescent protein samples compared to dry samples, showing an increase of the global protein rigidity with hydration (Shrestha et al., 2022).

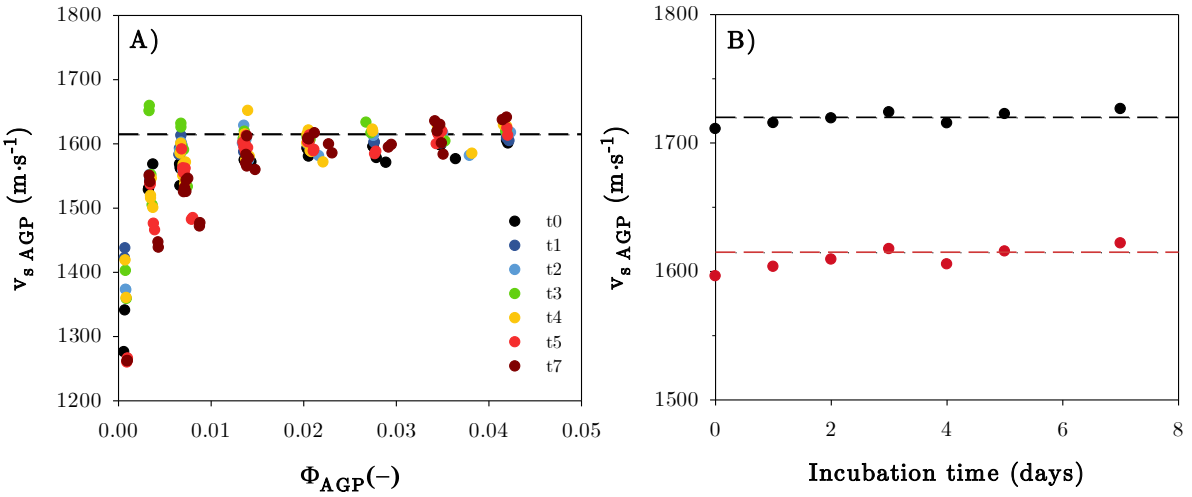

Figure IV.3. A) Evolution of the intrinsic ultrasound velocity of AGPs from arabic acid incubated at 40°C estimated from eq.(IV.6) as a function of AGP volume fraction. B) These ultrasound velocity values were then averaged between Φ_{AGP} = 0.035 and 0.042, plotted as a function of incubation time (●) and compared to $v_{s\ AGP}$ calculated from eq.(IV.9) and averaged over the same volume fraction range (●).

Table IV.2. Intrinsic ultrasound velocity of dry and hydrated biopolymers obtained from literature. Intrinsic ultrasound velocities determined for "dry" biopolymers were identified by an asterisk *.

System	$v_{s\ intrinsic}$ (m·s^{-1})	Method	References
collagen*	1600	laser ablation	(Lazare et al., 2005)
green fluorescent protein*	1194	inelastic neutron scattering	(Shrestha et al., 2022)
green fluorescent protein	1269	inelastic neutron scattering	(Shrestha et al., 2022)
lysozyme*	1817	pulse-echo method	(Tachibana et al., 2000)
lysozyme*	1958	ultrasound velocimetry	(Pfeiffer & Heremans, 2002)
amorphous myoglobin	1605	Mössbauer spectroscopy	(Achterhold & Parak, 2003)
PMMA*	1600	laser ablation	(Lazare et al., 2005)
protein active site mimic*	1011	IXS/vibrational spectroscopy	(Leu et al., 2011)
Satellite Tobacco Mosaic Virus*	1920	Brillouin spectroscopy	(Stephanidis et al., 2007)

3.1.3. Partial specific compressibility and adiabatic bulk elastic moduli of "dry" and hydrated AGPs

The partial specific coefficient of adiabatic compressibility β_s° was calculated as (Gekko & Hasegawa, 1986; Gekko & Noguchi, 1971, 1974; Høiland, 1986):

$$\beta_s^0 = \frac{\beta_0}{C}\left(\frac{\beta_s}{\beta_0} - \Phi_0\right)$$

with $\Phi_0 = \frac{\rho - C}{\rho_0}$.

The sign of the partial specific adiabatic compressibility coefficient informs about the relative contribution of the interactions between water and AGPs ($\beta_s^\circ < 0$), and the intrinsic contribution of volume fluctuations in AGPs ($\beta_s^\circ > 0$) (Buckin et al., 1989; Chalikian et al., 1996; Gekko & Hasegawa, 1986). β_s° of AGP aggregates was plotted as a function of the partial specific volume V°_s (Figure IV.4A). Such a plot was proposed recently to be a polarity-flexibility scale, allowing to distinguish biopolymers based on their charge density and internal fluctuations of cavities (Mejia-Tamayo et al., 2018). AGP aggregates covered a wide range of (β_s°, V°_s) parameters from $V^\circ_s = 0.600$ cm^3·g^{-1} and $\beta_s^\circ = -4.7 \cdot 10^{11}$ Pa^{-1} to $V^\circ_s = 0.842$ cm^3·g^{-1} and $\beta_s^\circ = +24.9 \cdot 10^{11}$ Pa^{-1}. From these results, aggregates were divided into two categories: in small and soluble aggregates, β_s° was negative and the hydration contribution was predominant while volumetric properties of the biggest aggregates were governed by the volume fluctuations, with positive β_s° values.

These AGP aggregates volumetric parameters were compared with those determined in literature for globular and unfolded proteins (Chalikian et al., 1996; Gekko & Hasegawa, 1986; Gekko & Yamagami, 1991), linear and branched polysaccharides (Gekko et al., 1985; Gekko & Noguchi, 1971; Nomura et al., 1982; Suzuki & Uedaira, 1970), Acacia gums (A. *senegal* and A. *seyal*) and their fractions, and arabic acid (Mejia Tamayo, 2018) (Figure IV.4B). For all biopolymer families, including AGP aggregates, β_s° increases in a roughly linear fashion with V°_s. In this β_s° vs. V°_s plot, the polar and rigid charged polysaccharides present low values of V°_s ($V^\circ_s < 0.56$ cm^3·g^{-1}) and negative β_s° whereas the most flexible and least polar proteins show higher values of V°_s ($V^\circ_s > 0.7$ cm^3·g^{-1}) and positive β_s° values. Arabic acid AGP aggregates are more hydrophobic than native A. gums but their β_s° display a similar dependency to their specific volume (Figure IV.4C). They exhibit a large domain of polarity/flexibility: the

most polar aggregates seem to have characteristics close to neutral dextrans whereas other aggregates would be even more flexible and less polar than globular proteins.

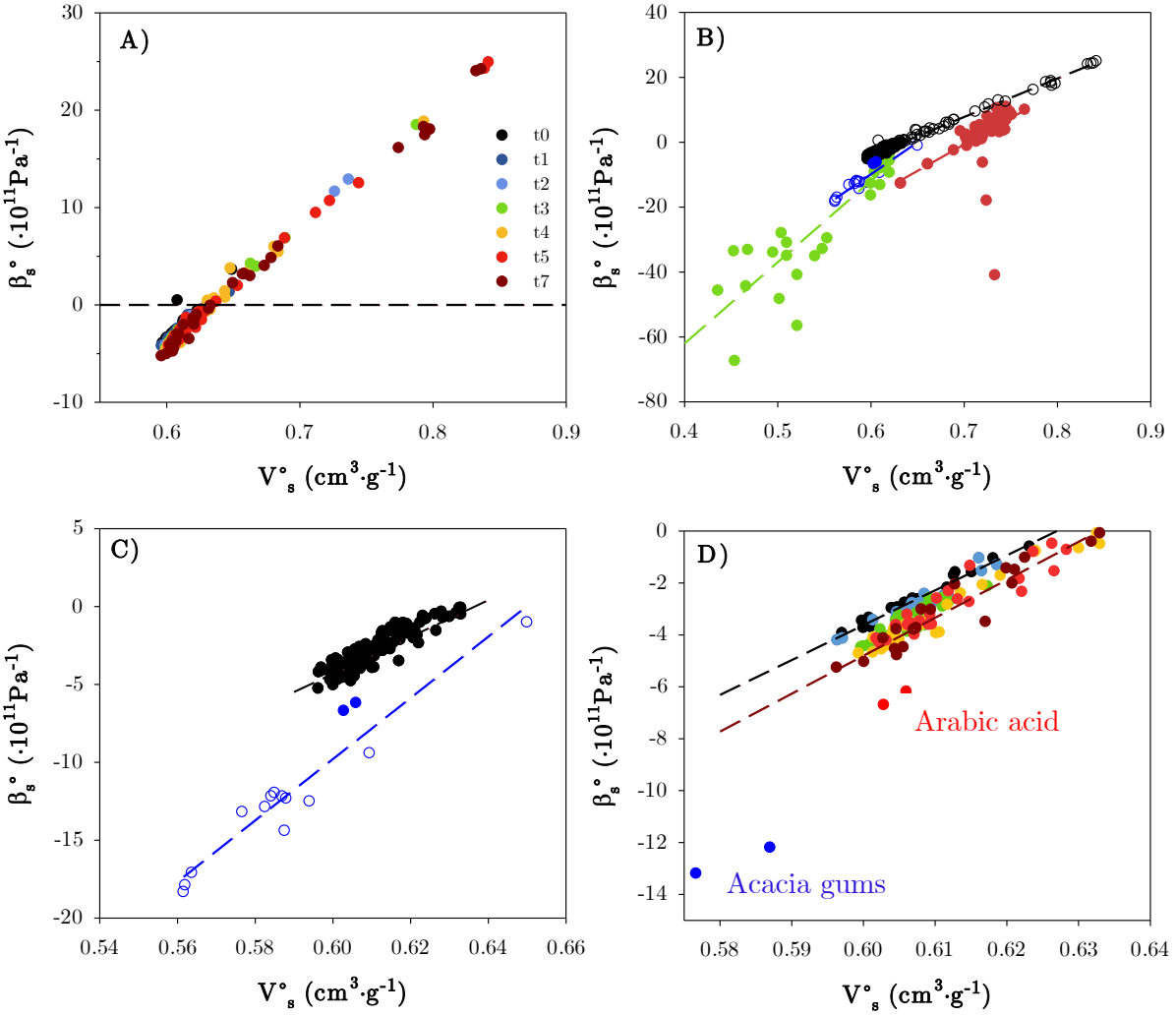

Figure IV.4. Relationship at 25°C between the partial specific volume V°_s and the coefficient of partial specific adiabatic compressibility β_s° for A) AGP aggregates. Two kinds of aggregates were obtained according to the sign of β_s°. B) Volumetric parameters obtained for these aggregates (with $\beta_s^\circ < 0$ (●), or $\beta_s^\circ > 0$ (○)) were then compared to A. gums (A. *senegal* and A. *seyal*), fractions obtained from A. *senegal* gum by HIC or IEC (○) and arabic acid (●), linear and branched polysaccharides (●) and globular proteins (●). C) Particular focus on the comparison between mineralized Acacia gums and arabic acid AGP-based aggregates. D) This relationship was further examined according to the aggregation stage for $\beta_s^\circ < 0$. AGP aggregates density and ultrasound velocity were measured in water.

The β_s° vs. V°_s plot was then examined more in details according to the aggregation stage of AGPs, for aggregates exhibiting negative β_s° values in order to focus on interactions between AGPs and water (Figure IV.4D). Aggregates were also compared with Acacia gums and arabic acids studied in the Ph.D. project of Mejia-Tamayo (Mejia Tamayo, 2018). Acacia gums and their respective arabic acids showed different volumetric properties, with higher V°_s and much

less negative β_s° for arabic acid. This highlights a decrease in the strength of interactions between water and AGP aggregates resulting in enhanced volume fluctuations with demineralization. In comparison, t_0 and the most aggregated AGPs displayed only minor differences showing that the main changes in terms of AGPs hydration properties occurred during the demineralization step. Equations describing β_s° according to V_s° were determined for all samples and showed that all aggregates ranged between two straight lines: $\beta_s^\circ = 134.4\ V_s^\circ - 84.3$ describing t_0 volumetric properties and $\beta_s^\circ = 146.3\ V_s^\circ - 92.6$ related to the biggest aggregates t_7. With storage, β_s° of aggregates decreased showing an increase of hydration and of the rigidity of this kind of aggregates. However, t_5 and t_7 samples were also characterized by more dehydrated aggregates (Figure IV.4A).

Finally, the adiabatic bulk modulus $K_{s\ AGP}$, which is the reciprocal of the adiabatic compressibility coefficient, was estimated from ρ_{AGP} and $v_{s\ AGP}$:

$$K_{s\,AGP} = -\frac{1}{V}\left(\frac{\partial P}{\partial V}\right)_s = \frac{1}{\beta_{s\,AGP}} = \rho_{AGP} v_{s\,AGP}^2 \qquad \text{(IV.11)}$$

By its definition, this bulk elastic modulus K_s expresses a resistance to volume fluctuations. We may also appreciate that equation IV.11 is an energy-mass equation, in fact exactly the same than the Einstein's equation $E = mc^2$. The bulk modulus is then a probe of the total cohesive interaction energy. The AGP bulk modulus measured in solution was not dependent on the aggregation state, adopting constant values of 2.3 ± 0.0 GPa, very close to the bulk modulus of water, *i.e.* 2.2 GPa. The intrinsic bulk modulus $K_{s\ AGP}$ was estimated from ρ_{AGP} and $v_{s\ AGP}$ calculated from volume fractions and averaged for $\Phi > 0.035$. $K_{s\ AGP}$ fluctuates between 3.3 GPa and 3.8 GPa which means that the intrinsic stiffness of AGPs is around 2 times higher than those of water (Figure IV.5).

These values are in good agreement with values reported for proteins (Baarda et al., 2018; Bailey et al., 2010; Meersman et al., 2011; Speziale et al., 2003; Vaughan & Randall, 1980) and polysaccharides (Grossutti & Dutcher, 2016; Kulasinski et al., 2014), in the range 3 – 12 GPa, and mainly confirm biopolymers without water are condensed solid matters.

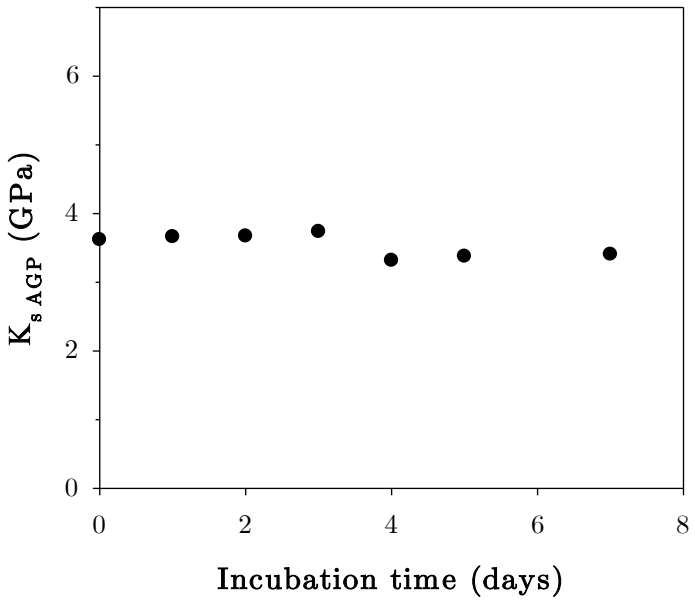

Figure IV.5. Evolution of intrinsic bulk modulus of AGPs K_s with incubation time. K_s was estimated using ρ_{AGP} plotted in Figure IV.2 and $v_{s\,AGP}$ calculated from eq.(IV.6) and plotted in Figure IV.3B. As a comparison, the bulk modulus of water is 2.3 GPa.

This volumetric characterization of the partial specific volume and adiabatic compressibility of AGPs highlighted a particular sensitivity of aggregates to hydration. The most aggregated samples exhibited a peculiar behavior at low concentration which revealed their sensitivity to the charge density. At these concentrations ($\Phi < 0.01$), insoluble microparticles appeared more porous. These aggregates were more dehydrated and flexible and their volumetric properties were mainly regulated by the presence of voids in their structure. On the contrary, volumetric properties of less aggregated samples were greatly influenced by AGPs-water interactions. Table IV.3 gives a characterization of the intrinsic volumetric properties of AGP aggregates for the first time. The intrinsic adiabatic compressibility and the bulk adiabatic modulus calculated in this study were very close to those estimated for proteins from the work of Chalikian (Chalikian et al., 1999; Chalikian, Sarvazyan, Plum, et al., 1994). AGPs are hyperbranched protein-polysaccharide complexes composed of more than 90% of sugar groups. However, this study showed that the hydration behavior of AGP aggregates is closer to those of globular proteins.

Table IV.3. Intrinsic volumetric properties of AGP aggregates determined from density and ultrasound velocity measurements. These aggregates were obtained by the storage in dry state of arabic acid at 40°C. Values were averaged over the whole range of incubation time and compared to volumetric properties of proteins determined in the work of Chalikian* (Chalikian et al., 1999; Chalikian, Sarvazyan, Plum, et al., 1994).

	Average value (independent on concentration)
Dry intrinsic AGP density ($kg \cdot m^{-3}$)	1426
Hydrated intrinsic AGP density ($kg \cdot m^{-3}$)	1647
Average intrinsic sound velocity ($m \cdot s^{-1}$)	1664
Average intrinsic adiabatic compressibility (Pa^{-1})	$2.6 \cdot 10^{-10}$
Estimated intrinsic compressibility proteins* (Pa^{-1})	$1 - 2.5 \cdot 10^{-10}$
Maximum value adiabatic compressibility coefficient (Pa^{-1})	$+ 2.4 \cdot 10^{-10}$
Average intrinsic bulk adiabatic modulus (GPa)	3.5
Estimated bulk adiabatic modulus proteins* (GPa)	4

3.2 Spectroscopic characterization of AGP aggregates

3.2.1 Time Domain Nuclear Magnetic Resonance spectroscopy (TD-NMR)

TD-NMR allows estimating proton nuclear spin polarization relaxation phenomena. This spin polarization is produced in response to the application of a homogeneous static magnetic field. Interactions between nuclear spins are at the origin of spin-spin relaxation – which corresponds to a return to an equilibrium state –, characterized by T_2, the transverse relaxation time (Belton, 2011). T_2 is a purely entropic parameter. It reflects a change in the absolute value of entropy and is associated both to the Gibbs free energy of cavity creation in water and enthalpic-entropic compensation (Allnér et al., 2015; Graziano, 2006 ; Palmer, 2001). Generally, T_2 values can be attributed to *(i)* diffusive motions of water protons from the "bulk" to the AGPs, *(ii)* fast chemical exchange between water protons and the exchangeable protons of AGPs (from –OH, –COOH, or –NH groups), and *(iii)* perturbed diffusive motions of water protons through pores (Belotti et al., 2009; Brosio et al., 2008). Our experiments aimed to check the actual view on the topic of protein aggregation, as described in the introduction of the chapter, *i.e.* a correlation seems to exist between the thermodynamic state of biopolymers and the thermodynamic state of water.

Figure IV.6 displays the distributions of proton transverse relaxation time (T_2) in A. *seyal* before and after the demineralization process. For the two gums, multi-exponential relaxation behavior was found, as generally observed with Acacia gum and biopolymers in general (Belton et al., 1988; Brosio et al., 2008; Hills et al., 1993). The T_2 distributions for A. *seyal* presents two main peaks at 0.01 and 0.8 ms whereas three relaxation events occur for arabic acid, with T_2 at 0.01, 0.25 and 0.6 ms. These values may be compared to T_2 of pure (bulk) water (2.5 – 4.0 s) (Barros et al., 2006; Chiarotti & Giulotto, 1954; Jaeger et al., 2010), and simply indicate water dynamics is strongly perturbed by the presence of gums.

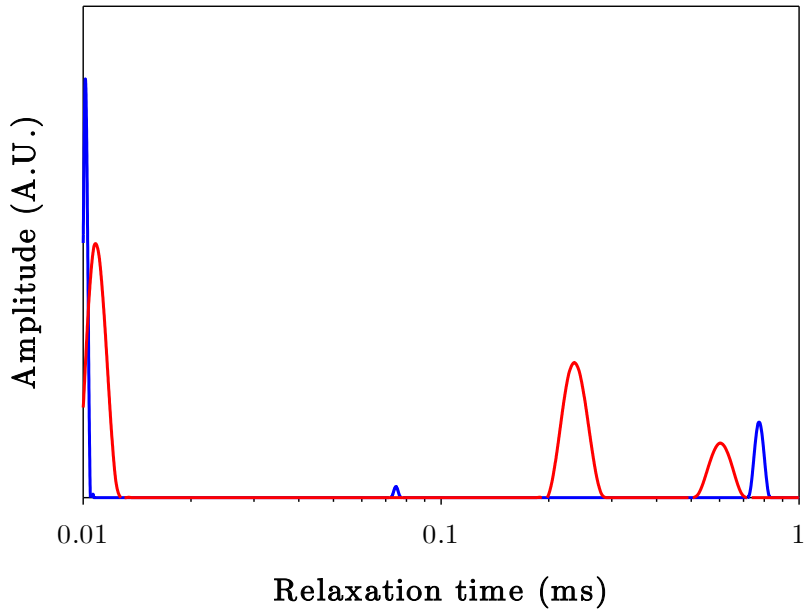

Figure IV.6. Distribution at 25°C of proton T_2 relaxation time in A. *seyal* (blue) and A. *seyal*-based arabic acid (red) powders detemined by FID-CPMG sequence.

A relaxation at ~ 0.010 ms is classically attributed to protein protons, belonging either to the backbone or to amino acid side chains (Maragakis et al., 2008; Shaw et al., 2010; Yoshioka et al., 1996). The relaxation found between 0.1 and 1 ms rather involves the contribution of strongly interacting water (Andrada et al., 2018; Hilton et al., 1977). In the following, strongly interacting water will be referred as hydrophilic water. One can also notice a broadening of the peaks in T_2 distribution of arabic acid compared to those of A. *seyal*, which evidences a richer water dynamic. In addition, the smaller T_2 for the more dynamic water in arabic acid (larger T_{22}) suggests a stronger perturbation of part of interfacial water, either due to enhanced water-aggregate interactions (Coleman et al., 1992; Comez et al., 2016) or/and water confinement in

nano and micropores (Hua et al., 2007, 2008; Mittal et al., 2008). Then a first conclusion is that demineralization of GA, which induced a modification of the pH and the charge of the gum, dramatically modified the dynamics of interfacial hydration water.

In order to focus on water dynamics, transverse relaxation times of arabic acid based aggregates were determined using the CPMG sequence (for $T_2 > 200$ µs). The CPMG sequence allows to extract two proton relaxation times, T_{21} and T_{22} (Figure IV.7A). At t_0, T_{21} and T_{22} were, respectively, 0.852 and 6.949 ms (Figure IV.7A). However, the more dynamic water amounted to an amplitude of only 0.014 as compared to a peak amplitude of 6.025 for the more perturbed one. Then hydrophilic water largely dominates water dynamics, in line with the mainly polar chemical composition of gums (Supplementary Table IV.4). In the following, we suppose T_{22} is the entropic signature of hydrophobic water, in coherence with the low signal amplitude and the larger relaxation time. With incubation time, T_{21} increased to 1.149 ms while T_{21} dropped to about 2 ms. Then the less dynamic hydrophilic water becomes more dynamic with arabic acid storage while the more dynamic one becomes less dynamic. Here, the term "less dynamic" refers to water with lower relaxation time. In both cases, the number of relaxing protons was enhanced during storage, however the relative increase in proton concentration was larger for the water becoming less dynamic (T_{22}) (Figure IV.7B). This can be better appreciated plotting the A_{22}/A_{21} amplitude ratio as a function of incubation time (Figure IV.8A).

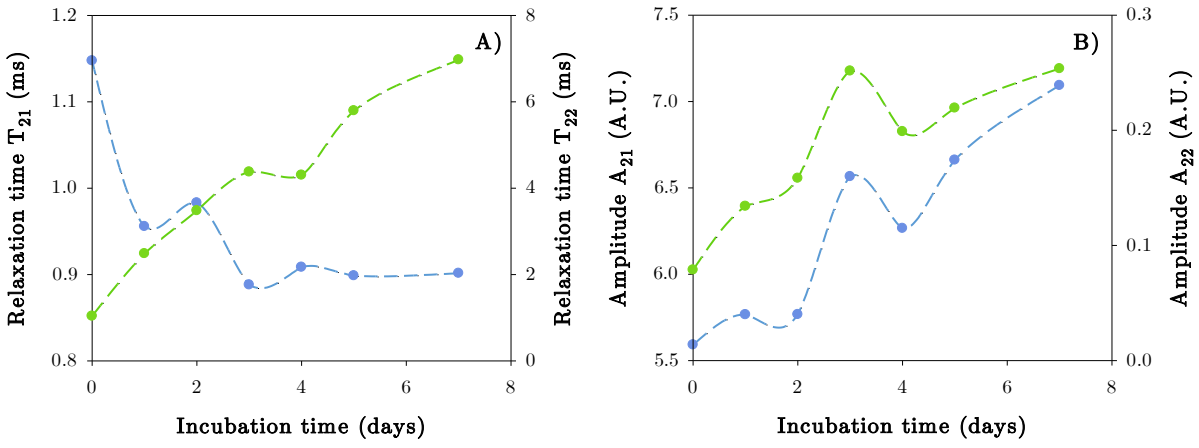

Figure IV.7. Effect of AGPs incubation time on the transverse relaxation time T_2 (A) and the peak area (B) of signals obtained by CPMG. Two proton fractions were obtained at relaxation times around $T_{21} = 1$ ms (●) and $T_{22} = 2 - 7$ ms (●).

The relative weight of the two proton population relaxation during the incubation time of arabic acid powders was estimated normalizing each relaxation signal amplitude $A_{2i}(t_j)$ by the total sum of amplitudes for each incubation time t_j : $\Sigma A_{2i}(t_j)$. This allows to calculate a kind of relative "proton volume fraction". Very interesting features regarding the relative implication of hydrophilic and hydrophobic water dynamic during the powder storage is evidenced (Figure IV.8B). In particular, we may argue enhanced hydrophilic water dynamics dominate the aggregation mechanism until 2 days of storage. In other terms, enhanced entropy of hydrophilic water provides the energy needed for (soluble) aggregates to occur during the two first days at 40°C. The contribution of hydrophilic water dynamics then regularly increased during storage until 20% total increase at 7 days. However, the contribution of the minor hydrophobic water increases four times from two to 3 days of storage, demonstrating a major change in the aggregation mechanism or in the nature of produced aggregates. Since we know from SEC MALLS and solubility measurements (see Chapter III) that insoluble microparticles appear above 2 days of storage at 40°C, we may relate the enhanced water entropy of hydrophobic water and the appearance of insoluble microparticles, as suggested recently for aggregated proteins (Camino et al., 2021; Chong & Ham, 2015; Pavlova et al., 2016). Above 3 – 4 days storage, insoluble microparticles dominate and we then expect a dominant contribution of hydrophobic water dynamic in determining the aggregation process. This is actually the case, as can be seen in Figure IV.8B., where the contribution of water dynamic was the double than the contribution of hydrophilic one. The respective weight of the normalized two kinds of water dynamics (T_{22}/T_{21}) clearly demonstrates enhanced hydrophilic water dynamics are needed to form soluble aggregates, while enhanced hydrophobic water dynamics are needed to form insoluble ones (Figure IV.8B).

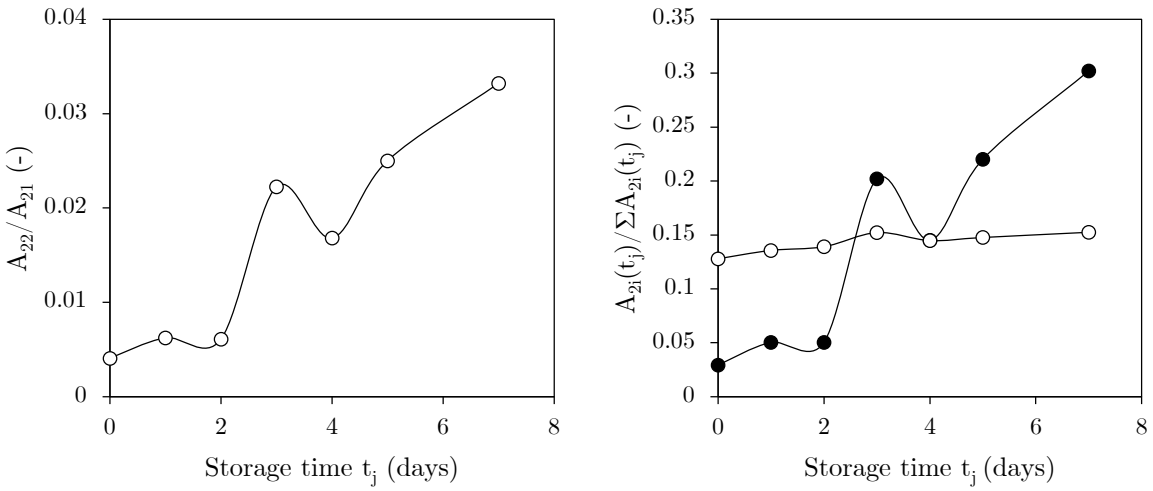

Figure IV.8. Evolution of A) the amplitude ratio of the two proton populations obtained by CPMG (A_{22}/A_{21}) as a function of incubation time and B) the relative "proton volume fraction" for population 1 (○) and 2 (●) estimated by normalizing the relaxation signal amplitude $A_{2i}(t_j)$ by the total sum of amplitudes for each incubation time t_j : $\Sigma A_{2i}(t_j)$.

3.2.2 Fourier Transform Infrared spectroscopy (FTIR)

Fourier Transform Infrared spectroscopy probes vibrations of molecule bonds and provides information on both the structure of biopolymers and their hydration state. The FTIR spectra of A. *seyal* is similar to spectra obtained elsewhere for other A. *seyal* gums (Daoub et al., 2018; Lopez-Torrez et al., 2015a; Shi et al., 2017) (Figure IV.9). Demineralization of A. *seyal* gum induced some major changes in the spectral regions 1500 – 1800 cm^{-1} and 2400 – 3800 cm^{-1}. Since the aim of this section is to study the hydration properties of AGP aggregates, a particular interest focused on the band at 3000 – 3650 cm^{-1} which is characteristic of the stretching vibration of –OH, including the contribution of water. In this region, the absorbance was higher for arabic acid compared to A. *seyal*, with a local maximum observed at ν(–OH) = 3365 and 3356 cm^{-1}, respectively. This blueshift indicates arabic acid-water hydrogen bond interactions were weaker than in the starting gum, in line with volumetric results,

inducing a shortening and stiffening of covalent O–H bonds (Huang et al., 2015; Sun, 2018; Sun et al., 2013).

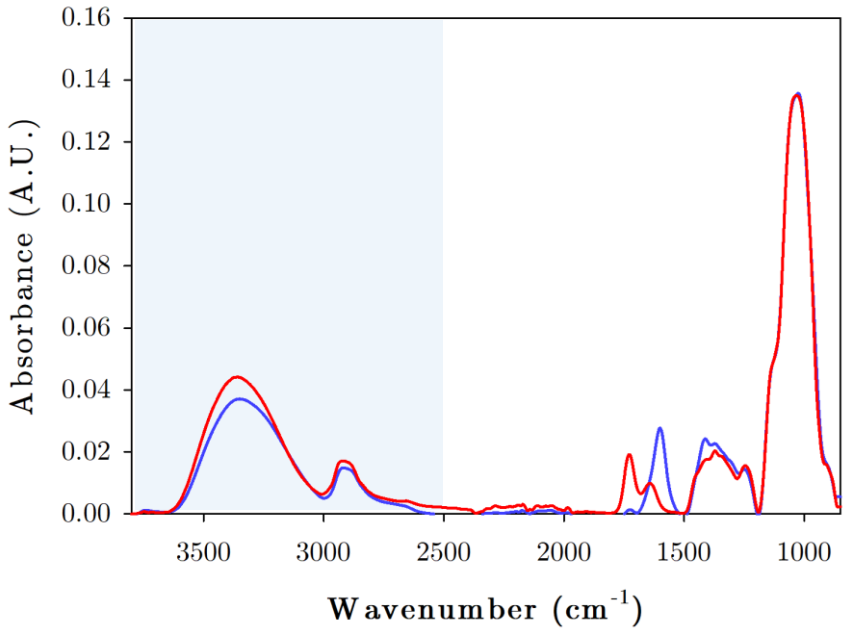

Figure IV.9. Fourier transform infrared (FTIR) spectra of A. *seyal* (blue) and arabic acid from A. *seyal* (red) gums from 850 to 3800 cm^{-1}. The light blue area highlights the wavenumber domain of interest that will be examined in this section.

The spectral subtraction of A. *seyal* from arabic acid (t_0) and aggregated arabic acid ($t_1 - t_7$) in the region between 2400 and 3800 cm^{-1} highlights the differences between A. *seyal* before and after demineralization and aggregation. This allows to better probe the dynamics of water, which are faster compared to the biopolymer ones, due to the very small size of water molecules (Graziano, 2006). This spectral subtraction revealed major changes for wavenumbers ~ 2900 cm^{-1} and ~ 3600 cm^{-1} (Figure V.10A). The region around 2900 cm^{-1} has been associated to stretching vibrations of aliphatic C–H bonds from GA (Daoub et al., 2018; Pal et al., 2019; B. Singh et al., 2017; Tiwari & Singh, 2008) whereas the band at 3600 cm^{-1} can be ascribed to O–H stretching vibrations either from A. *seyal* (Daoub et al., 2018; Shi et al., 2017) or from free water (Olsson & Salmén, 2004; Pavelec et al., 2019; Pogorelov et al., 2017; Vasylieva et al., 2018), *i.e.* water without hydrogen bond interactions (vapor phase).

It can be observed from the differential FTIR spectra that a decrease in the band intensity at 2900 cm^{-1} is accompanied by an increase in the band intensity at 3600 cm^{-1} (Figure V.10A). By plotting the subtracted FTIR intensity of these two bands as a function of the incubation time,

it clearly appears that they display symmetric patterns (Figure V.10B). This very interesting result suggests a correlation between interfacial water and C–H bonds from sugars and/or amino acids, and that hydration/dehydration of AGP-based aggregates is a non-linear phenomenon with incubation time. Schmidt et al. showed a shift to higher frequencies of the band at 2970 cm^{-1} when increasing hydration (Schmidt et al., 2006). This blueshift was attributed to hydrophobic interactions between methyl groups and surrounding water molecules.

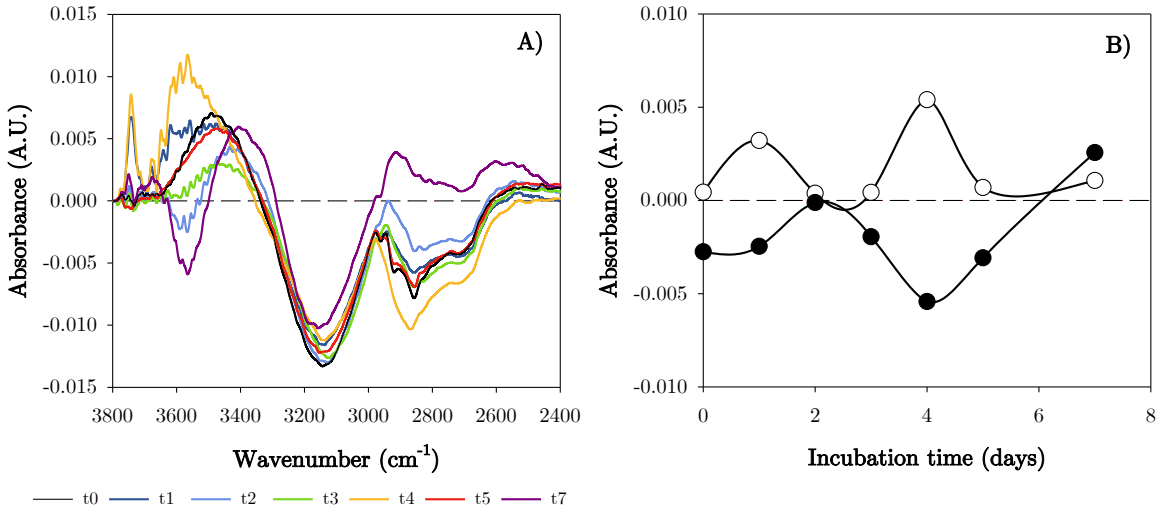

Figure IV.10. A) Differential FTIR spectra obtained by subtraction of A. *seyal* from arabic acid and aggregated arabic acid samples in the 2400 – 3800 cm^{-1} spectral region. B) Intensity of the differential subtracted signals at corresponding to O–H stretching (○) from hydrophobic hydration water and C–H stretching (●). Spline curves are guides to the eye.

Depending on the environment of water molecules, five or six stretching O–H vibration bands are classically displayed by FTIR or Raman spectroscopy. They can be classified from strongly interacting water (*i.e.* slow water) at around 3050 – 3250 cm^{-1} to free water (*i.e.* very dynamic water) at 3630 – 3670 cm^{-1} with intermediate vibration bands around 3250, 3400, 3510, 3550 cm^{-1} (Carey & Korenowski, 1998; Pavelec et al., 2019; Ratajska-Gadomska & Gadomski, 2005; Vasylieva et al., 2018), depending on the amount of water. Between 3000 and 3200 cm^{-1} the decrease in absorbance of all samples compared to GA may indicate that demineralization induced the loss of a part of hydration water. The frequencies of –OH stretching vibrations in this region decrease with the number and the strength of hydrogen bonds water molecules can establish with their neighbors (Dokter et al., 2006; Vasylieva et al., 2018). Thus, the pattern observed in Figure IV.10B could indicate these C–H bonds interact more with free (vapor) water than with liquid water.

4. Conclusions

This work aimed to characterize the influence of demineralization and entropy-controlled dehydration-induced aggregation on the thermodynamic properties of AGPs from A. *seyal* gum and aggregates formed during the storage in dry state of demineralized A. *seyal*. According to the incubation time, two kinds of aggregates were formed. Volumetric properties of the least aggregated samples were governed by AGP–water interactions. The formation of these soluble aggregates was driven by hydrophilic water dynamics. In turn the most aggregated sampled were more porous and sensitive to concentration. At low concentration, due to the polyelectrolyte effect, they were dehydrated, less rigid, and more hydrophobic. As for globular proteins, intrinsic volume fluctuations dominated their volumetric behavior. At high concentration, AGPs volume fluctuations were smoothed by interactions with water and AGPs rigidity increased. The removal of minerals from A. *seyal* caused the major changes observed by FTIR, with a blueshift of the OH stretching vibration band of 9 cm^{-1}. This blueshift was attributed to a shortening and stiffening of covalent O–H bonds and confirmed that surface charges greatly influenced hydration properties.

5. Acknowledgments

The authors gratefully acknowledge ALLAND & ROBERT Company (Port Mort, France) and the French Ministry of Research and Education (2017/1727) for the financial support (Ph.D. Amandine Antoine-Michard).

6. Supplementary data

Table IV.4. Sugar composition of arabic acid and AGP aggregates from arabic acid (t_5) in dry basis.

	t_0	t_5	
		soluble aggregates	microparticles
Arabinose	42.5	38.3	34.9
Galactose	30.8	33.3	37.8
Rhamnose	3.3	3.2	2.8
Glucuronic acid	10.3	11.7	11.7
4-O-Me glucuronic acid	13.1	13.5	12.7

7. Highlights

In this chapter, we studied the hydration properties of AGP aggregates from demineralized A. *seyal* gum obtained by their storage in the dry state. This characterization was carried out using a combination of volumetric (density and ultrasound velocity measurements) and spectroscopic (Time-Domain NMR and FTIR) techniques. Electrostatic, spin, and volume (energetic) fluctuations were probed. In particular, we demonstrated a correlation between AGPs hydration and their aggregation state. The main results obtained are described below:

- The most dramatic changes in AGP hydration properties occurred during the demineralization of A. *seyal*. Density and ultrasound velocity measurements show that demineralization causes a decrease of AGPs polarity. TD-NMR and FTIR confirmed that interfacial water is stronger perturbed by arabic acid, with a weakening of the hydrogen bond interactions.
- The volumetric properties of soluble AGP aggregates and semi-diluted insoluble microparticles ($\phi_{AGP} > 0.02$) dispersions are governed by AGP–water interactions.
- The most aggregated sampled exhibit particular thermodynamic behavior at low concentration where they are dehydrated, less rigid, and more hydrophobic. At these concentrations, in a similar manner than for globular proteins, their volumetric properties are dominated by intrinsic volume fluctuations.
- TD-NMR also showed a correlation between water dynamics and AGP aggregation state: it seems that enhanced hydrophilic water dynamics are needed to form soluble aggregates, while enhanced hydrophobic water dynamics are needed to form insoluble ones.
- Very dynamic water O–H and C–H bonds from sugar and/or amino acids are correlated in a symmetric but non-linear fashion which might indicate that dehydration-induced aggregation of AGPs is a non-linear phenomenon.

8. References

Achterhold, K., & Parak, F. G. (2003). Protein dynamics : Determination of anisotropic vibrations at the haem iron of myoglobin. *Journal of Physics: Condensed Matter*, *15*(18), S1683-S1692. https://doi.org/10.1088/0953-8984/15/18/302

Adebayo, S. A., Brown-Myrie, E., & Itiola, O. A. (2008). Comparative disintegrant activities of breadfruit starch and official corn starch. *Powder Technology*, *181*(2), 98-103. https://doi.org/10.1016/j.powtec.2006.12.013

Al-Assaf, S., Phillips, G. O., Aoki, H., & Sasaki, Y. (2007). Characterization and properties of Acacia senegal (L.) Willd. var. senegal with enhanced properties (Acacia (sen) SUPER GUM^{TM}) : Part 1—Controlled maturation of Acacia senegal var. senegal to increase viscoelasticity, produce a hydrogel form and convert a poor into a good emulsifier. *Food Hydrocolloids*, *21*(3), 319-328. https://doi.org/10.1016/j.foodhyd.2006.04.011

Al-Assaf, S., Phillips, G. O., Sasaki, Y., & Katayama, T. (2004). *Modified gum arabic* (Patent N^{o} WO 2004/089991 A1).

Allnér, O., Foloppe, N., & Nilsson, L. (2015). Motions and Entropies in Proteins as Seen in NMR Relaxation Experiments and Molecular Dynamics Simulations. *The Journal of Physical Chemistry B*, *119*(3), 1114-1128. https://doi.org/10.1021/jp506609g

Andersson, K. M., & Hovmöller, S. (1998). The average atomic volume and density of proteins. *Zeitschrift fur Kristallographie*, *213*, 369-373. https://doi.org/10.1524/zkri.1998.213.7-8.369

Andrada, H. E., Franzoni, M. B., Carreras, A. C., & Chávez, F. V. (2018). Dynamics and spatial distribution of water in Nafion 117 membrane investigated by NMR spin-spin relaxation. *International Journal of Hydrogen Energy*, *43*(18), 8936-8943. https://doi.org/10.1016/j.ijhydene.2018.03.124

Antoine-Michard, A., Charbonnel, C., Jaouen, I., Sanchez, C., & Nigen, M. (2022). Maturation of demineralized arabinogalactan-proteins from Acacia seyal gum in dry state : Aggregation kinetics and structural properties of aggregates. *International Journal of Biological Macromolecules*.

Apicella, A., Natalello, A., Frana, A. M., Baserga, A., Casari, C. S., Bottani, C. E., Doglia, S. M., Tortora, P., & Regonesi, M. E. (2012). Temperature profoundly affects ataxin-3 fibrillogenesis. *Biochimie*, *94*(4), 1026-1031. https://doi.org/10.1016/j.biochi.2012.01.002

Arya, S., & Mukhopadhyay, S. (2014). Ordered Water within the Collapsed Globules of an Amyloidogenic Intrinsically Disordered Protein. *The Journal of Physical Chemistry B*, *118*(31), 9191-9198. https://doi.org/10.1021/jp504076a

Baarda, R. A., Marianchuk, T. L., Toney, M. D., & Cox, D. L. (2018). In silico stress–strain measurements on self-assembled protein lattices. *Soft Matter*, *14*(40), 8095-8104. https://doi.org/10.1039/C8SM00412A

Bailey, S. T., Twa, M. D., Gump, J. C., Venkiteshwar, M., Bullimore, M. A., &

Sooryakumar, R. (2010). Light-scattering study of the normal human eye lens : Elastic properties and age dependence. *IEEE Transactions on Bio-Medical Engineering*, *57*(12), 2910-2917. https://doi.org/10.1109/TBME.2010.2052393

Bánó, M., & Marek, J. (2006). How thick is the layer of thermal volume surrounding the protein? *Biophysical Chemistry*, *120*(1), 44-54. https://doi.org/10.1016/j.bpc.2005.09.024

Baron, R., Setny, P., & McCammon, J. A. (2010). Water in Cavity−Ligand Recognition. *Journal of the American Chemical Society*. https://doi.org/10.1021/ja1050082

Barros, C. N., Arêas, E. P. G., Figueiredo, E. N., & Arêas, J. A. G. (2006). Low-resolution 1H spin-spin relaxation of n-decane/water emulsions stabilized by beta-casein. *Colloids and Surfaces. B, Biointerfaces*, *48*(2), 119-127. https://doi.org/10.1016/j.colsurfb.2006.01.016

Belotti, M., Martinelli, A., Gianferri, R., & Brosio, E. (2009). A proton NMR relaxation study of water dynamics in bovine serum albumin nanoparticles. *Physical Chemistry Chemical Physics*, *12*(2), 516-522. https://doi.org/10.1039/B911433E

Belton, P. (2011). Spectroscopic Approaches to the Understanding of Water in Food. *Food Reviews International.*, *27*(2), 170-191. https://doi.org/10.1080/87559129.2010.535234

Belton, P. S., Hills, B. P., & Raimbaud, E. R. (1988). The effects of morphology and exchange on proton N.M.R. relaxation in agarose gels. *Molecular Physics*, *63*(5), 825-842. https://doi.org/10.1080/00268978800100591

Brosio, E., Belotti, M., & Gianferri, R. (2008). Diffusive and Chemical Exchange Model : Practical Hits to Investigate Water Dynamics in Foods. In *Food Science And Technology : New Research* (L. V. Greco and M. N. Bruno, p. 323-340). Nova Science Publishers. https://vdoc.pub/documents/food-science-and-technology-new-research-3342bcmd5370

Buckin, V., Kankiya, B. I., Sarvazyan, A., & Uedaira, H. (1989). Acoustical investigation of poly(dA)·poly(dT), poly[d(A-T]·poly[d(A-T)], poly(A)·poly(U) and DNA hydration in dilute aqueous solutions. *Nucleic acids research*, *17*, 4189-4203. https://doi.org/10.1093/nar/17.11.4189

Bull, H. B., & Breese, K. (1968). Protein hydration : I. Binding sites. *Archives of Biochemistry and Biophysics*, *128*(2), 488-496. https://doi.org/10.1016/0003-9861(68)90055-6

Camino, J. D., Gracia, P., & Cremades, N. (2021). The role of water in the primary nucleation of protein amyloid aggregation. *Biophysical Chemistry*, *269*, 106520. https://doi.org/10.1016/j.bpc.2020.106520

Carey, D. M., & Korenowski, G. M. (1998). Measurement of the Raman spectrum of liquid water. *The Journal of Chemical Physics*, *108*(7), 2669-2675. https://doi.org/10.1063/1.475659

Chakraborty, I., Kar, R. K., Sarkar, D., Kumar, S., Maiti, N. C., Mandal, A. K., & Bhunia, A. (2021). Solvent Relaxation NMR : A Tool for Real-Time Monitoring Water Dynamics in Protein Aggregation Landscape. *ACS Chemical Neuroscience*, *12*(15), 2903-2916. https://doi.org/10.1021/acschemneuro.1c00262

Chalikian, T. V. (2001). Structural Thermodynamics of Hydration. *The Journal of Physical Chemistry B*,

105(50), 12566-12578. https://doi.org/10.1021/jp0115244

Chalikian, T. V., & Filfil, R. (2003). How large are the volume changes accompanying protein transitions and binding? *Biophysical Chemistry*, *104*(2), 489-499. https://doi.org/10.1016/S0301-4622(03)00037-1

Chalikian, T. V., Sarvazyan, A. P., & Breslauer, K. J. (1994). Hydration and partial compressibility of biological compounds. *Biophysical Chemistry*, *51*(2-3), 89-107. https://doi.org/10.1016/0301-4622(94)85007-0

Chalikian, T. V., Sarvazyan, A. P., Plum, G. E., & Breslauer, K. J. (1994). Influence of base composition, base sequence, and duplex structure on DNA hydration : Apparent molar volumes and apparent molar adiabatic compressibilities of synthetic and natural DNA duplexes at 25 degrees C. *Biochemistry*, *33*(9), 2394-2401. https://doi.org/10.1021/bi00175a007

Chalikian, T. V., Totrov, M., Abagyan, R., & Breslauer, K. J. (1996). The Hydration of Globular Proteins as Derived from Volume and Compressibility Measurements : Cross Correlating Thermodynamic and Structural Data. *Journal of Molecular Biology*, *260*(4), 588-603. https://doi.org/10.1006/jmbi.1996.0423

Chalikian, T. V., Völker, J., Plum, G. E., & Breslauer, K. J. (1999). A more unified picture for the thermodynamics of nucleic acid duplex melting : A characterization by calorimetric and volumetric techniques. *Proceedings of the National Academy of Sciences of the United States of America*, *96*(14), 7853-7858. https://doi.org/10.1073/pnas.96.14.7853

Chiarotti, G., & Giulotto, L. (1954). Proton Relaxation in Water. *Physical Review*, *93*(6), 1241-1241. https://doi.org/10.1103/PhysRev.93.1241

Cho, C., Urquidi, J., Singh, S., Park, S., & Robinson, G. (2002). Pressure Effect on the Density of Water†. *Journal of Physical Chemistry A - J PHYS CHEM A*, *106*. https://doi.org/10.1021/jp0136260

Chong, S.-H., & Ham, S. (2015). Distinct Role of Hydration Water in Protein Misfolding and Aggregation Revealed by Fluctuating Thermodynamics Analysis. *Accounts of Chemical Research*, *48*(4), 956-965. https://doi.org/10.1021/acs.accounts.5b00032

Coleman, A. W., Nicolis, I., Keller, N., & Dalbiez, J. P. (1992). Aggregation of cyclodextrins : An explanation of the abnormal solubility ofβ-cyclodextrin. *Journal of Inclusion Phenomena and Molecular Recognition in Chemistry*, *13*(2), 139-143. https://doi.org/10.1007/BF01053637

Comez, L., Paolantoni, M., Sassi, P., Corezzi, S., Morresi, A., & Fioretto, D. (2016). Molecular properties of aqueous solutions : A focus on the collective dynamics of hydration water. *Soft Matter*, *12*(25), 5501-5514. https://doi.org/10.1039/C5SM03119B

Costantino, H. R., Langer, R., & Klibanov, A. M. (1994). Moisture-induced aggregation of lyophilized insulin. *Pharmaceutical Research*, *11*(1), 21-29. https://doi.org/10.1023/a:1018981208076

Crick, S., Jayaraman, M., Frieden, C., Wetzel, R., & Pappu, R. (2006). Fluorescence correlation spectroscopy shows that monomeric polyglutamine molecules form collapsed structures in aqueous solutions. *Proceedings of the National Academy of Sciences of the United States of America*, *103*, 16764-16769. https://doi.org/10.1073/pnas.0608175103

Daoub, R. M. A., Elmubarak, A. H., Misran, M., Hassan, E. A., & Osman, M. E. (2018). Characterization and functional properties of some natural Acacia gums. *Journal of the Saudi Society of Agricultural Sciences*, *17*(3), 241-249. https://doi.org/10.1016/j.jssas.2016.05.002

Davies, A., Gormally, J., Wyn-Jones, E., Wedlock, D. J., & Phillips, G. O. (1982). A study of hydration of sodium hyaluronate from compressibility and high precision densitometric measurements. *International Journal of Biological Macromolecules*, *4*(7), 436-438. https://doi.org/10.1016/0141-8130(82)90091-5

Dokter, A. M., Woutersen, S., & Bakker, H. J. (2006). Inhomogeneous dynamics in confined water nanodroplets. *Proceedings of the National Academy of Sciences*, *103*(42), 15355-15358. https://doi.org/10.1073/pnas.0603239103

Durchschlag, H. (1986). Specific Volumes of Biological Macromolecules and Some Other Molecules of Biological Interest. In H.-J. Hinz (Éd.), *Thermodynamic Data for Biochemistry and Biotechnology* (p. 45-128). Springer. https://doi.org/10.1007/978-3-642-71114-5_3

Elsheikh, M. A., Al-Assaf, S., Osman, M. E., Hassan, E. A., & Phillips, Glyn. O. (2015). Thermodynamic Properties of Gum Arabic and AcaiaPolyacantha Gum Solutions. *International Journal of Multidisciplinary and Current Research*, *3*, 598-606.

Fichou, Y., Schirò, G., Gallat, F.-X., Laguri, C., Moulin, M., Combet, J., Zamponi, M., Härtlein, M., Picart, C., Mossou, E., Lortat-Jacob, H., Colletier, J.-P., Tobias, D. J., & Weik, M. (2015). Hydration water mobility is enhanced around tau amyloid fibers. *Proceedings of the National Academy of Sciences*, *112*(20), 6365-6370. https://doi.org/10.1073/pnas.1422824112

Fischer, H., Polikarpov, I., & Craievich, A. F. (2004). Average protein density is a molecular-weight-dependent function. *Protein Science*, *13*(10), 2825-2828. https://doi.org/10.1110/ps.04688204

Gabel, L. F. (1930). The effect of heat on acacia. *Journal of the american pharmaceutical association*, *19*(8), 828-830. https://doi.org/10.1002/jps.3080190807

Gekko, K., & Hasegawa, Y. (1986). Compressibility-structure relationship of globular proteins. *Biochemistry*, *25*(21), 6563-6571. https://doi.org/10.1021/bi00369a034

Gekko, K., Mugishima, H., & Koga, S. (1985). Compressibility, densimetric and calorimetric studies of hydration of carrageenans in the random form. *International Journal of Biological Macromolecules*, *7*(1), 57-63. https://doi.org/10.1016/0141-8130(85)90068-6

Gekko, K., & Noguchi, H. (1971). Physicochemical studies of oligodextran. I. Molecular weight dependence of intrinsic viscosity, partial specific compressibility and hydrated water. *Biopolymers*, *10*(9), 1513-1524. https://doi.org/10.1002/bip.360100907

Gekko, K., & Noguchi, H. (1974). Hydration Behavior of Ionic Dextran Derivatives. *Macromolecules*, *7*(2), 224-229. https://doi.org/10.1021/ma60038a014

Gekko, K., & Yamagami, K. (1991). Flexibility of food proteins as revealed by compressibility. *Journal of Agricultural and Food Chemistry*, *39*(1), 57-62. https://doi.org/10.1021/jf00001a010

Gharsallaoui, A., Rogé, B., Génotelle, J., & Mathlouthi, M. (2008). Relationships between hydration number, water activity and density of aqueous sugar solutions. *Food Chemistry*, *106*(4),

1443-1453. https://doi.org/10.1016/j.foodchem.2007.02.047

Graziano, G. (2006). Scaled particle theory study of the length scale dependence of cavity thermodynamics in different liquids. *The Journal of Physical Chemistry. B*, *110*(23), 11421-11426. https://doi.org/10.1021/jp0571269

Grossutti, M., & Dutcher, J. R. (2016). Correlation Between Chain Architecture and Hydration Water Structure in Polysaccharides. *Biomacromolecules*, *17*(3), 1198-1204. https://doi.org/10.1021/acs.biomac.6b00026

Hatakeyama, T., Uetake, T., Inui, Y., & Hatakeyama, H. (2009). Freezing Bound Water Restrained by Gum Arabic. In *Gums and Stabilisers for the Food Industry 15* (p. 69-76). https://doi.org/10.1039/9781849730747-00069

Hayashi, H. (2002). *Method of modifying gum arabic* (European Union Patent Nº EP1505078B1). https://patents.google.com/patent/EP1505078B1/ja

Henzler-Wildman, K. A., Lei, M., Thai, V., Kerns, S. J., Karplus, M., & Kern, D. (2007). A hierarchy of timescales in protein dynamics is linked to enzyme catalysis. *Nature*, *450*(7171), 913-916. https://doi.org/10.1038/nature06407

Herrera-Gómez, A., Canónico-Franco, M., Ramos, G., & Pless, R. C. (2002). Aggregation in cooked maize starch. *Carbohydrate Polymers*, *50*(4), 387-392. https://doi.org/10.1016/S0144-8617(02)00054-1

Hills, B. P., Belton, P. S., & Quantin, V. M. (1993). Water proton relaxation in heterogeneous systems. *Molecular Physics*, *78*(4), 893-908. https://doi.org/10.1080/00268979300100601

Hilton, B. D., Hsi, E., & Bryant, R. G. (1977). 1H nuclear magnetic resonance relaxation of water on lysozyme powders. *Journal of the American Chemical Society*, *99*(26), 8483-8490. https://doi.org/10.1021/ja00468a017

Høiland, H. (1986). Partial Molar Volumes of Biochemical Model Compounds in Aqueous Solution. *Thermodynamic Data for Biochemistry and Biotechnology*, 17-44. https://doi.org/10.1007/978-3-642-71114-5_2

Hua, L., Huang, X., Liu, P., Zhou, R., & Berne, B. J. (2007). Nanoscale Dewetting Transition in Protein Complex Folding. *The journal of physical chemistry. B*, *111*(30), 9069-9077. https://doi.org/10.1021/jp0704923

Hua, L., Zangi, R., & Berne, B. (2008). Hydrophobic Interactions and Dewetting between Plates with Hydrophobic and Hydrophilic Domains. *The Journal of Physical Chemistry C*, *113*. https://doi.org/10.1021/jp8088758

Huang, Y., Zhang, X., Ma, Z., Zhou, Y., Zheng, W., Zhou, J., & Sun, C. Q. (2015). Hydrogen-bond relaxation dynamics : Resolving mysteries of water ice. *Coordination Chemistry Reviews*, *285*, 109-165. https://doi.org/10.1016/j.ccr.2014.10.003

Jaeger, F., Shchegolikhina, A., As, H., & Schaumann, G. (2010). *Proton NMR Relaxometry as a Useful Tool to Evaluate Swelling Processes in Peat Soils*. https://doi.org/10.2174/1874769801003010027

Katayama, T., Ogasawara, T., Sasaki, Y., Al-Assaf, S., & Phillips, G. (2008). *Composition Containing Hydrogel Component Derived from Gum Arabic* (United States Patent Nº US20080038436A1). https://patents.google.com/patent/US20080038436A1/en

Kay, L. E. (2005). NMR studies of protein structure and dynamics. *Journal of Magnetic Resonance*, *173*(2), 193-207. https://doi.org/10.1016/j.jmr.2004.11.021

Kharakoz, D. P. (1989). Volumetric properties of proteins and their analogs in diluted water solutions. 1. Partial volumes of amino acids at 15-55 degrees C. *Biophysical Chemistry*, *34*(2), 115-125. https://doi.org/10.1016/0301-4622(89)80049-3

Kinoshita, M. (2009). Importance of Translational Entropy of Water in Biological Self-Assembly Processes like Protein Folding. *International Journal of Molecular Sciences*, *10*(3), 1064-1080. https://doi.org/10.3390/ijms10031064

Kulasinski, K., Keten, S., Churakov, S. V., Guyer, R., Carmeliet, J., & Derome, D. (2014). Molecular Mechanism of Moisture-Induced Transition in Amorphous Cellulose. *ACS Macro Letters*, *3*(10), 1037-1040. https://doi.org/10.1021/mz500528m

Kupke, D. W. (1973). Density and volume change measurements. In S. J. Leach, *Physical Principles and Techniques of Protein Chemistry* (Academic Press, p. 3-75). Academic Press.

Lashuel, H. A., & Lansbury, P. T. (2006). Are amyloid diseases caused by protein aggregates that mimic bacterial pore-forming toxins? *Quarterly Reviews of Biophysics*, *39*(2), 167-201. https://doi.org/10.1017/S0033583506004422

Lazare, S., Tokarev, V., Sionkowska, A., & Wiśniewski, M. (2005). Surface foaming of collagen, chitosan and other biopolymer films by KrF excimer laser ablation in the photomechanical regime. *Applied Physics A*, *81*(3), 465-470. https://doi.org/10.1007/s00339-005-3260-y

Lee, S. L., Debenedetti, P. G., & Errington, J. R. (2005). A computational study of hydration, solution structure, and dynamics in dilute carbohydrate solutions. *The Journal of Chemical Physics*, *122*(20), 204511. https://doi.org/10.1063/1.1917745

Leu, B. M., Sage, J. T., Silvernail, N. J., Scheidt, W. R., Alatas, A., Alp, E. E., & Sturhahn, W. (2011). Bulk Modulus of a Protein Active-Site Mimic. *The Journal of Physical Chemistry B*, *115*(15), 4469-4473. https://doi.org/10.1021/jp112007z

Liu, D., Zhou, P., Liu, X., & Labuza, T. P. (2011). Moisture-Induced Aggregation of Alpha-Lactalbumin : Effects of Temperature, Cations, and pH. *Journal of Food Science*, *76*(6), C817-C823. https://doi.org/10.1111/j.1750-3841.2011.02277.x

Liu, Y. (2005). *Studies of structure and dynamics of biological macro-molecular assemblies by low angle neutron diffraction and inelastic X-ray scattering* [Massachusetts Institute of Technology]. https://dspace.mit.edu/handle/1721.1/34438

Lopez-Torrez, L., Nigen, M., Williams, P., Doco, T., & Sanchez, C. (2015). Acacia senegal vs. Acacia seyal gums – Part 1 : Composition and structure of hyperbranched plant exudates. *Food Hydrocolloids*, *51*, 41-53. https://doi.org/10.1016/j.foodhyd.2015.04.019

Maragakis, P., Lindorff-Larsen, K., Eastwood, M. P., Dror, R. O., Klepeis, J. L., Arkin, I. T., Jensen, M. Ø., Xu, H., Trbovic, N., Friesner, R. A., Palmer, A. G., & Shaw, D. E. (2008). Microsecond Molecular Dynamics Simulation Shows Effect of Slow Loop Dynamics on Backbone Amide Order Parameters of Proteins. *The Journal of Physical Chemistry B*, *112*(19), 6155-6158. https://doi.org/10.1021/jp077018h

Meersman, F., Cabrera, R. Q., McMillan, P. F., & Dmitriev, V. (2011). Structural and

Mechanical Properties of TTR105-115 Amyloid Fibrils from Compression Experiments. *Biophysical Journal*, *100*(1), 193-197. https://doi.org/10.1016/j.bpj.2010.11.052

Mejia Tamayo, V. (2018). *Volumetric properties of Arabinogalactan-proteins from Acacia Gum*. Montpellier SupAgro.

Mejia Tamayo, V., Nigen, M., Apolinar-Valiente, R., Williams, P., Doco, T., Renard, D., & Sanchez, C. (2018). *Flexibility and hydration of amphiphilic hyperbranched Arabinogalactan-protein from plant exudate : A volumetric perspective*. https://doi.org/10.3390/colloids2010011

Mimouni, A., Deeth, H. C., Whittaker, A. K., Gidley, M. J., & Bhandari, B. R. (2010). Investigation of the microstructure of milk protein concentrate powders during rehydration : Alterations during storage. *Journal of Dairy Science*, *93*(2), 463-472. https://doi.org/10.3168/jds.2009-2369

Minina, E. S., Pyanzina, E. S., Novak, E. V., & Kantorovich, S. S. (2018). Compressibility of ferrofluids : Towards a better understanding of structural properties. *The European Physical Journal. E, Soft Matter*, *41*(5), 67. https://doi.org/10.1140/epje/i2018-11678-7

Mittal, J., Truskett, T. M., Errington, J. R., & Hummer, G. (2008). Layering and Position-Dependent Diffusive Dynamics of Confined Fluids. *Physical Review Letters*, *100*(14), 145901. https://doi.org/10.1103/PhysRevLett.100.145901

Moates, G. K., Parker, R., & Ring, S. G. (1998). Preferential solvent interactions and the dissolution of the B-type crystalline polymorph of starch in aqueous solutions. *Carbohydrate Research*, *313*(3), 225-234. https://doi.org/10.1016/S0008-6215(98)00282-1

Moorjani, M. N., & Narwani, C. S. (1948). Influence of heat on the physico-chemical properties of gum-arabic. *Current science*, *17*(4), 123-124.

Mukherjee, S., Chowdhury, P., DeGrado, W. F., & Gai, F. (2007). Site-Specific Hydration Status of an Amphipathic Peptide in AOT Reverse Micelles. *Langmuir*, *23*(22), 11174-11179. https://doi.org/10.1021/la701686g

Nasser, S., R., R., De-Sa-Peixoto, P., Ronse, G., Nuns, N., Pourpoint, F., Burgain, J., Gaiani, C., Hédoux, A., & Delaplace, G. (2017). Microstructure evolution of micellar casein powder upon ageing : Consequences on rehydration dynamics. *Journal of Food Engineering*, *206*, 57-66. https://doi.org/10.1016/j.jfoodeng.2017.03.004

Nomura, H., Onoda, M., & Miyahara, Y. (1982). Preferential Solvation of Dextran in Water–Ethanol Mixtures. *Polymer Journal*, *14*(4), 249-253. https://doi.org/10.1295/polymj.14.249

Olsson, A.-M., & Salmén, L. (2004). The association of water to cellulose and hemicellulose in paper examined by FTIR spectroscopy. *Carbohydrate Research*, *339*(4), 813-818. https://doi.org/10.1016/j.carres.2004.01.005

Pal, K., Roy, S., Parida, P., Dutta, A., Bardhan, S., Das, S., Jana, K., & Karmakar, P. (2019). Folic acid conjugated curcumin loaded biopolymeric gum acacia microsphere for triple negative breast cancer therapy in invitro and invivo model. *Materials Science and Engineering: C*, *95*, 204-216. https://doi.org/10.1016/j.msec.2018.10.071

Palmer, A. G. (2001). Nmr probes of molecular dynamics : Overview and comparison with other techniques. *Annual Review*

of Biophysics and Biomolecular Structure, *30*, 129-155. https://doi.org/10.1146/annurev.biophys.30.1.129

Pavelec, J., DiGuiseppi, D., Zavlavsky, B. Y., Uversky, V. N., & Schweitzer-Stenner, R. (2019). Perturbation of water structure by water-polymer interactions probed by FTIR and polarized Raman spectroscopy. *Journal of Molecular Liquids*, *275*, 463-473. https://doi.org/10.1016/j.molliq.2018.11.023

Pavlova, A., Cheng, C.-Y., Kinnebrew, M., Lew, J., Dahlquist, F. W., & Han, S. (2016). Protein structural and surface water rearrangement constitute major events in the earliest aggregation stages of tau. *Proceedings of the National Academy of Sciences*, *113*(2), E127-E136. https://doi.org/10.1073/pnas.1504415113

Perkins, S. J. (1986). Protein volumes and hydration effects. *European Journal of Biochemistry*, *157*(1), 169-180. https://doi.org/10.1111/j.1432-1033.1986.tb09653.x

Pfeiffer, H., & Heremans, K. (2002). Apparent sound velocity of lysozyme in aqueous solutions. *Chemical Physics Letters*, *361*(3), 226-230. https://doi.org/10.1016/S0009-2614(02)00809-6

Pfeiffer, H., & Heremans, K. (2005). The Sound Velocity in Ideal Liquid Mixtures from Thermal Volume Fluctuations. *ChemPhysChem*, *6*(4), 697-705. https://doi.org/10.1002/cphc.200400534

Pfeiffer, H., Heremans, K., & Wevers, M. (2008). The influence of correlated protein–water volume fluctuations on the apparent compressibility of proteins determined by ultrasonic velocimetry. *Biochimica et Biophysica Acta (BBA) - Proteins and Proteomics*, *1784*(11), 1546-1551. https://doi.org/10.1016/j.bbapap.2008.08.002

Phillips, G., Takigami, S., & Takigami, M. (1996). *Hydration characteristics of the gum exudate from Acacia senegal*. https://doi.org/10.1016/S0268-005X(96)80048-8

Pogorelov, V., Doroshenko, I., Pitsevich, G., Balevicius, V., Sablinskas, V., Krivenko, B., & Pettersson, L. G. M. (2017). From clusters to condensed phase – FT IR studies of water. *Journal of Molecular Liquids*, *235*, 7-10. https://doi.org/10.1016/j.molliq.2016.12.037

Punihaole, D., Jakubek, R. S., Workman, R. J., Marbella, L. E., Campbell, P., Madura, J. D., & Asher, S. A. (2017). Monomeric Polyglutamine Structures That Evolve into Fibrils. *Journal of Physical Chemistry B*, *121*(24), 5953-5967. https://doi.org/10.1021/acs.jpcb.7b04060

Ratajska-Gadomska, B., & Gadomski, W. (2005). Water structure in nanopores of agarose gel by Raman spectroscopy. *The Journal of chemical physics*, *121*, 12583-12588. https://doi.org/10.1063/1.1826051

Rau, D. C., & Parsegian, V. A. (1990). Direct Measurement of Forces Between Linear Polysaccharides Xanthan and Schizophyllan. *Science*, *249*, 1278-1281. https://doi.org/10.1126/science.2144663

Reddy, G., Straub, J. E., & Thirumalai, D. (2009). Dynamics of locking of peptides onto growing amyloid fibrils. *Proceedings of the National Academy of Sciences of the United States of America*, *106*(29), 11948-11953. https://doi.org/10.1073/pnas.0902473106

Reddy, G., Straub, J. E., & Thirumalai, D. (2010). Dry amyloid fibril assembly in a yeast prion peptide is mediated by long-lived structures containing water wires.

Proceedings of the National Academy of Sciences of the United States of America, *107*(50), 21459-21464. https://doi.org/10.1073/pnas.1008616107

Reiss, H. (1965). Scaled Particle Methods in the Statistical Thermodynamics of Fluids. In *Advances in Chemical Physics* (p. 1-84). John Wiley & Sons, Ltd. https://doi.org/10.1002/9780470143551.ch1

Renard, D., Garnier, C., Lapp, A., Schmitt, C., & Sanchez, C. (2013). Corrigendum to « Structure of arabinogalactan-protein from Acacia gum : From porous ellipsoids to supramolecular architectures » [Carbohydr. Polym. 90 (2012) 322-332]. *Carbohydrate Polymers*, *97*(2), 864-867. https://doi.org/10.1016/j.carbpol.2013.05.006

Renard, D., Lavenant-Gourgeon, L., Ralet, M.-C., & Sanchez, C. (2006). Acacia senegal Gum : Continuum of Molecular Species Differing by Their Protein to Sugar Ratio, Molecular Weight, and Charges. *Biomacromolecules*, *7*(9), 2637-2649. https://doi.org/10.1021/bm060145j

Russo, D., Laloni, A., Filabozzi, A., & Heyden, M. (2017). Pressure effects on collective density fluctuations in water and protein solutions. *Proceedings of the National Academy of Sciences*, *114*(43), 11410-11415. https://doi.org/10.1073/pnas.1705279114

Russo, D., Orecchini, A., Francesco, A., Formisano, F., Laloni, A., Petrillo, C., & Sacchetti, F. (2012). Brillouin Neutron Spectroscopy as a Probe to Investigate Collective Density Fluctuations in Biomolecules Hydration Water. *Journal of Spectroscopy*, *27*. https://doi.org/10.1155/2012/671265

Sanchez, C., Nigen, M., Mejia Tamayo, V., Doco, T., Williams, P., Amine, C., & Renard, D. (2018). Acacia gum : History of the future. *Food Hydrocolloids*, *78*, 140-160. https://doi.org/10.1016/j.foodhyd.2017.04.008

Sasaki, Y., Ogasawara, T., Katayama, T., & Sakata, M. (2014). *Process for producing modified gum arabic* (United States Patent N° US8722129B2). https://patents.google.com/patent/US8722129B2/en

Schmidt, P., Dybal, J., & Trchová, M. (2006). Investigations of the hydrophobic and hydrophilic interactions in polymer–water systems by ATR FTIR and Raman spectroscopy. *Vibrational Spectroscopy*, *42*(2), 278-283. https://doi.org/10.1016/j.vibspec.2006.05.005

Shapiro, E. M., Borthakur, A., Kaufman, J. H., Leigh, J. S., & Reddy, R. (2001). Water distribution patterns inside bovine articular cartilage as visualized by1H magnetic resonance imaging. *Osteoarthritis and Cartilage*, *9*(6), 533-538. https://doi.org/10.1053/joca.2001.0428

Shaw, D. E., Maragakis, P., Lindorff-Larsen, K., Piana, S., Dror, R. O., Eastwood, M. P., Bank, J. A., Jumper, J. M., Salmon, J. K., Shan, Y., & Wriggers, W. (2010). Atomic-Level Characterization of the Structural Dynamics of Proteins. *Science*, *330*(6002), 341-346. https://doi.org/10.1126/science.1187409

Shi, Y., Li, C., Zhang, L., Huang, T., Ma, D., Tu, Z., Wang, H., Xie, H., Zhang, N., & Ouyang, B. (2017). Characterization and emulsifying properties of octenyl succinate anhydride modified Acacia seyal gum (gum arabic). *Food Hydrocolloids*, *65*, 10-16. https://doi.org/10.1016/j.foodhyd.2016.10.043

Shiraga, K., Suzuki, T., Kondo, N., De Baerdemaeker, J., & Ogawa, Y. (2015). Quantitative characterization of hydration state and destructuring effect

of monosaccharides and disaccharides on water hydrogen bond network. *Carbohydrate Research*, *406*, 46-54. https://doi.org/10.1016/j.carres.2015.01.002

Shrestha, U. R., Mamontov, E., O'Neill, H. M., Zhang, Q., Kolesnikov, A. I., & Chu, X. (2022). Experimental mapping of short-wavelength phonons in proteins. *The Innovation*, *3*(1), 100199. https://doi.org/10.1016/j.xinn.2021.100199

Singh, B., Sharma, S., & Dhiman, A. (2017). Acacia gum polysaccharide based hydrogel wound dressings : Synthesis, characterization, drug delivery and biomedical properties. *Carbohydrate Polymers*, *165*, 294-303. https://doi.org/10.1016/j.carbpol.2017.02.039

Speziale, S., Jiang, F., Caylor, C. L., Kriminski, S., Zha, C.-S., Thorne, R. E., & Duffy, T. S. (2003). Sound Velocity and Elasticity of Tetragonal Lysozyme Crystals by Brillouin Spectroscopy. *Biophysical Journal*, *85*(5), 3202-3213. https://doi.org/10.1016/S0006-3495(03)74738-9

Stephanidis, B., Adichtchev, S., Gouet, P., McPherson, A., & Mermet, A. (2007). Elastic Properties of Viruses. *Biophysical Journal*, *93*(4), 1354-1359. https://doi.org/10.1529/biophysj.107.109033

Sugiyama, J., Vuong, R., & Chanzy, H. (1991). Electron diffraction study on the two crystalline phases occurring in native cellulose from an algal cell wall. *Macromolecules*, 4168-4175.

Sun, C. C. (2005). True density of microcrystalline cellulose. *Journal of Pharmaceutical Sciences*, *94*(10), 2132-2134. https://doi.org/10.1002/jps.20459

Sun, C. Q. (2018). Supersolidity of undercoordinated and hydrating water. *Physical Chemistry Chemical Physics*, *20*(48), 30104-30119. https://doi.org/10.1039/C8CP06115G

Sun, C. Q., Zhang, X., Zhou, J., Huang, Y., Zhou, Y., & Zheng, W. (2013). Density, Elasticity, and Stability Anomalies of Water Molecules with Fewer than Four Neighbors. *The Journal of Physical Chemistry Letters*, *4*(15), 2565. https://doi.org/10.1021/jz401029z

Suzuki, Y., & Uedaira, H. (1970). Hydration of Potassium Hyaluronate. *Bulletin of the Chemical Society of Japan*, *43*(6), 1892-1894. https://doi.org/10.1246/bcsj.43.1892

Svergun, D. I., Richard, S., Koch, M. H. J., Sayers, Z., Kuprin, S., & Zaccai, G. (1998). Protein hydration in solution : Experimental observation by x-ray and neutron scattering. *Proceedings of the National Academy of Sciences*, *95*(5), 2267-2272. https://doi.org/10.1073/pnas.95.5.2267

Tachibana, M., Kojima, K., Ikuyama, R., Kobayashi, Y., & Ataka, M. (2000). Sound velocity and dynamic elastic constants of lysozyme single crystals. *Chemical Physics Letters*, *332*(3), 259-264. https://doi.org/10.1016/S0009-2614(00)01267-7

Thirumalai, D., Reddy, G., & Straub, J. E. (2012). Role of water in protein aggregation and amyloid polymorphism. *Accounts of Chemical Research*, *45*(1), 83-92. https://doi.org/10.1021/ar2000869

Tiwari, A., & Singh, V. (2008). Microwave-induced synthesis of electrical conducting gum acacia-graft-polyaniline. *Carbohydrate Polymers*, *74*(3), 427-434. https://doi.org/10.1016/j.carbpol.2008.03.015

Touré, S. (2008). *Gum Arabic*. Market News Service (MNS) (Quaterly edition). International Trading Center.

https://ngara.org/pdf/GumArabic_MarketNewsService%20Issue1_08.pdf

Urick, R. J. (1947). A Sound Velocity Method for Determining the Compressibility of Finely Divided Substances. *Journal of Applied Physics*, *18*(11), 983-987. https://doi.org/10.1063/1.1697584

Van der Plancken, I., Van Loey, A., & Hendrickx, M. (2007). Effect of moisture content during dry-heating on selected physicochemical and functional properties of dried egg white. *Journal of Agricultural and Food Chemistry*, *55*(1), 127-135. https://doi.org/10.1021/jf062370y

Van der Voort Maarschalk, K., Vromans, H., Groenendijk, W., Bolhuis, G. K., & Lerk, C. F. (1997). Effect of water on deformation and bonding of pregelatinized starch compacts. *European Journal of Pharmaceutics and Biopharmaceutics*, *44*(3), 253-260. https://doi.org/10.1016/S0939-6411(97)00128-8

Vasylieva, A., Doroshenko, I., Vaskivskyi, Ye., Chernolevska, Ye., & Pogorelov, V. (2018). FTIR study of condensed water structure. *Journal of Molecular Structure*, *1167*, 232-238. https://doi.org/10.1016/j.molstruc.2018.05.002

Vaughan, J. M., & Randall, J. T. (1980). Brillouin scattering, density and elastic properties of the lens and cornea of the eye. *Nature*, *284*(5755), 489-491. https://doi.org/10.1038/284489a0

Viet, D., Beck-Candanedo, S., & Gray, D. G. (2007). Dispersion of cellulose nanocrystals in polar organic solvents. *Cellulose*, *14*(2), 109-113. https://doi.org/10.1007/s10570-006-9093-9

Voloshin, V. P., Medvedev, N. N., Andrews, M. N., Burri, R. R., Winter, R., & Geiger, A. (2011). Volumetric properties of hydrated peptides : Voronoi-Delaunay analysis of molecular simulation runs. *The Journal of Physical Chemistry. B*, *115*(48), 14217-14228. https://doi.org/10.1021/jp2050788

Wen, J., Scoles, D. R., & Facelli, J. C. (2017). Molecular dynamics analysis of the aggregation propensity of polyglutamine segments. *PLOS ONE*, *12*(5), e0178333. https://doi.org/10.1371/journal.pone.0178333

Yoshioka, S., Aso, Y., & Kojima, S. (1996). Determination of Molecular Mobility of Lyophilized Bovine Serum Albumin and γ-Globulin by Solid-State 1H NMR and Relation to Aggregation-Susceptibility. *Pharmaceutical Research*, *13*(6), 926-930. https://doi.org/10.1023/A:1016069532204

Zangmeister, C. D., Radney, J. G., Dockery, L. T., Young, J. T., Ma, X., You, R., & Zachariah, M. R. (2014). Packing density of rigid aggregates is independent of scale. *Proceedings of the National Academy of Sciences of the United States of America*, *111*(25), 9037-9041. https://doi.org/10.1073/pnas.1403768111

CHAPTER V.

STABILITY AND REVERSIBILITY OF ARABIC ACID AGP AGGREGATES IN DILUTE SOLVENT CONDITIONS

Stability of arabinogalactan-protein aggregates from arabic acid (*seyal* species) depending on the solvent characteristics

Amandine Antoine-Michard[a,b], Michaël Nigen[a,*], Céline Charbonnel[a], Isabelle Jaouen[b], and Christian Sanchez[a]

[a] UMR IATE, Univ Montpellier, INRAE, Institut Agro, 34060 Montpellier, France

[b] ALLAND & ROBERT, 75003, Paris, France

* Corresponding author.

E-mail address: michael.nigen@umontpellier.fr

Abbreviations.

GA: Acacia gum; AGPs: arabinogalactan-proteins; SEC: size-exclusion chromatography

Keywords: Acacia *seyal* gum, Arabinogalactan-proteins, Arabic acid, Aggregation, Stability.

1. Introduction

Acacia gum (GA) is a natural exudate composed of arabinogalactan-proteins (AGPs) macromolecules (~ 95%), associated with minor components such as minerals (mainly Ca, Na and K), tannins and traces of lipids and enzymes (Sanchez et al., 2018). Among GA cations, AGPs particularly interact with calcium *via* their glucuronic acid moieties (Lamport & Várnai, 2013). AGPs contain other ionizable chemical groups in its protein fraction (amine and imidazole) which makes GA sensitive to the pH and ionic strength (Grein-Iankovski et al., 2018; Mejia Tamayo, 2018). GA has the propensity to aggregate *in vivo*, during its exudation by the Acacia tree and during its maturation (Capataz-Tafur et al., 2011; Idris et al., 1998; Phillips, 2009).

Aggregation of AGPs was studied *in vitro*, when the gum is dispersed in aqueous solvents or during its storage in the dry state (Al-Assaf et al., 2007, 2012; Aoki et al., 2007; Idris et al., 1998; Phillips & Williams, 1993; Sanchez et al., 2002). The obtained AGP aggregates display better emulsifying and rheological properties than the initial gum (Al-Assaf et al., 2007; Castellani et al., 2010; Katayama et al., 2008). Yellowing and browning of GA powders during their incubation in the dry state suggested AGP aggregation might arise from Maillard reactions (Sasaki et al., 2014). These reactions may induce the formation of high molar mass AGPs, aggregates and hydrogels (Al-Assaf et al., 2007; Aoki et al., 2007). In turn, minor changes in A. *senegal* structure after maturation were detected by spectroscopic methods (Cui et al., 2007). Eventually, a shift in ^{H}NMR from 4.5 to 4.8 ppm and two changes in infrared spectra in the regions of 600 cm^{-1} (ring breathing vibration C-C-C-O or C-O-C) and 1600 – 1630 cm^{-1} (COO^{-} asymmetrical stretching COOH from glucuronic acids) occurred. The shift at 4.5 ppm was previously attributed to H-1 of β-DGlcA and β-DGalp (side chains of GA). These observations led to the conclusion that dehydration in the carboxyl group of uronic acids was at the origin of AGP aggregation.

The storage parameters leading to the aggregation of AGPs from demineralized GA were described recently (Antoine-Michard et al., 2022, in publication). Soluble aggregates and insoluble microparticles were formed when demineralized GA powder was submitted to heat from 25 to 70°C. This aggregation reaction was characterized by an activation energy of around 100 $kJ{\cdot}mol^{-1}$ which might be in favor of chemical condensation reactions, considering in particular the storage conditions (*i.e.* the dry state and the acidic pH). This value may be also

related to dehydration of sugars (Maciel et al., 2005; Qi et al., 2010; Zohuriaan & Shokrolahi, 2004). Water desorption energy in GA was estimated by TGA (Thermo Gravimetric Analysis) to 125 kJ·mol^{-1} for A. *senegal* and 155 kJ·mol^{-1} for A. *seyal* (Cozic et al., 2009; Zohuriaan & Shokrolahi, 2004). Qi et al. determined an activation energy of 100 kJ·mol^{-1} for glucose dehydration (Qi et al., 2010). The same value was reported for the total protein-water interaction energy of lysozyme (Camisasca et al., 2016). In this work, the total energy was the sum of two energies, corresponding to the presence of more and less dynamic water than in the bulk. It is interesting to note the found activation energy is also close to the Faraday constant value, *i.e.* 96.5 kJ·mol^{-1}, which corresponds to the energy needed to dissociate a charge; and is not far from the activation energy of electron transfer between Fe^{3+} and Fe^{2+} (80 kJ·mol^{-1}) (Kuharski et al., 1988). In aggregates, energy related to motion of charges and to dehydration, two conditions needed to create a new covalent bonds, seems to be in the same range.

In the present work, we studied with some details the solvent conditions favoring or not the structural stability of these AGP aggregates. It is well known biopolymer self-assembly depends on biopolymer structure and physicochemical properties of the solvent, including pH and ionic strength, and external physical parameters such as temperature, pressure or the presence of a magnetic/electrical field (Efthimiadou et al., 2018; Ganguly et al., 2020; Liang et al., 2017). One objective of the study was to identify the nature of interactions at the origin of the formation of aggregates (electrostatic or hydrogen bond interactions, Van der Waals forces, covalent bond). For this purpose, incubated powders were dispersed in different solvents varying in ionic strength and type of ions (Na^{+}, Ca^{2+}), pH or the presence of urea as a chaotropic agent. The solubility and structure of AGP aggregates and insoluble microparticles in the various used solvents were determined by light scattering, SEC MALLS and optical microscopy. In parallel, the nature of involved chemical bonds were approached using ^{13}C Nuclear Magnetic Resonance (^{13}C NMR) and Fourier Transform Infrared spectroscopy (FTIR).

2. Materials and methods

2.1 Materials

All experiments were carried out with A. *seyal* gum (lot OF183377), provided by Alland & Robert Company—Natural and Organic gums (Port Mort, France). An ionic

exchange resin (Purolite® C160MBH, Purolite Ltd, Llantrisant, Wales) was used to remove all the cations from A. *seyal* gum. All reagents were purchased from Sigma-Aldrich (St. Louis, MO, USA). Ultrapure deionized water (18.2 MΩ·cm) was used in all experiments.

2.2 Preparation of arabic acid powder

A 16 wt% A. *seyal* gum dispersion was prepared in water (pH 4.6) and stirred overnight using a magnetic stirring plate at 250 rpm to allow complete hydration of the gum. Cations were removed from the gum using an ionic exchange resin at a mass ratio gum:resin of 1:1. The pH of the dispersion was verified and the demineralization was complete once it reached the value of 2.1. The demineralized A. *seyal* gum was then named as usual arabic acid. Arabic acid dispersion was centrifuged (12,000 rpm, 30 min, 20 °C) with an Avanti J-26S XP (Beckman Coulter) to remove insoluble material (< 1%) before spray-drying (Büchi B-290, Büchi Labortechnik AGt, Switzerland).

2.3 Incubation of arabic acid powder

About 300 mg of arabic acid powder were incubated in closed glass vessels at 40°C in a HPP 260 climate chamber (Memmert, Schwabach, Germany). Samples were collected after 2, 4 and 7 days of incubation and directly stored at -20°C to stop their aggregation. Incubation times were chosen to cover all the aggregation states previously identified (Antoine-Michard et al., 2022, in publication). In the following, these samples were named t_2, t_4, and t_7.

2.4 Preparation of arabic acid dispersions in various physicochemical conditions

The stability in water of arabic acid aggregates and microparticles at 1wt% concentration was studied by varying the physicochemical properties of dispersion solvent. The effect of chaotropic agent was investigated using 0, 2, 4 and 8 mol.L^{-1} urea solutions at pH 2.4. The influence of pH between 2.4 and 9.5 was studied upon dispersion of arabic acid powder in water (pH 2.4), 50 mmol.L^{-1} acetate buffer (pH 3.7, 4.4, 5.0), 50 mmol.L^{-1} MES buffer (pH 4.5, 5.5, 6.1, 6.5), 50 mmol.L^{-1} Tris buffer (pH 6.7, 7.5, 7.8, 8.1, 8.6) and 50 mmol.L^{-1} Capso buffer (pH 8.7, 9.5). The potential synergy between pH and ionic strength was also studied using water (zero added ionic strength), and 50 mmol.L^{-1} acetate (pH 4.5), MES (pH 6.5), Tris (pH 7.5, 8.5) and CAPSO (pH 9.5) buffers containing 0.1, 0.5 and 1 mol.L^{-1} NaCl to obtain final ionic strength

between about 0 and 1 mol.L^{-1}. We also probed the effect of calcium, the main cation interacting with AGPs, dispersing arabic acid powders in water (pH 2.4) containing 0.8, 10 and 50 mmol.L^{-1} $CaCl_2$. All dispersions were stirred overnight using an orbital plate at 250 rpm before experiments were done.

2.5 Transmittance and solubility measurements

The light transmittance at 657 nm of arabic acid dispersions was measured at 25°C using a UV-VIS-NIR spectrophotometer (UltroSpec 2000, Pharmacia Biotech), to probe the structural stability of dispersions. For solubility measurements, dispersions were centrifuged at 12,000 rpm for 30 min at 20 °C using a Heraeus Fresco 21 microcentrifuge (Thermo Fisher Scientific, Osterode, Germany) to pellet insoluble AGP-based particles. After centrifugation, the supernatants were recovered, their volume was measured and their refractive index was determined using an Abbemat Refractometer (Anton Paar, Graz, Austria). The arabic acid AGPs in the supernatants were quantified using an experimentally determined dn/dc for each dispersion condition (Supplementary data, Table V.2). Insoluble particles were then calculated as:

$$\text{pelleted AGPs (\%)} = 100 \cdot \left(1 - \frac{C'V'}{CV}\right)$$

where C and V are, respectively, the concentration ($g_{GA} \cdot g_{dispersion}^{-1}$) and the volume (mL) of dispersions before centrifugation, and C' and V' are the concentration and the volume of supernatant dispersion after centrifugation.

2.6 Phase contrast microscopy

Arabic acid dispersions were diluted at 0.5wt% in MilliQ water before microscopic observations. Arabic acid-based aggregates and particles were observed by optical microscopy using a phase contrast microscope (Olympus, France) coupled with x10 and x20 objectives. Micrographs were acquired using the CellSens software (Olympus, France) and analyzed with ImageJ software. Picture processing consisted in a conversion from RGB to 8 bits format image, an adjustment of luminosity and contrast and the application of a FFT bandpass filter.

2.7 SEC MALLS characterization

The structural properties of AGPs and soluble aggregates from arabic acid were characterized by multi-detector high performance size exclusion chromatography (HPSEC). These experiments were performed on the supernatants obtained after the centrifugation of the dispersions at 12,000 rpm and 20°C during 30 min using a Heraeus Fresco 21 microcentrifuge (Thermo Fisher Scientific, Osterode, Germany). The supernatants were diluted to obtain final concentration of 1 $mg \cdot mL^{-1}$. 50 µL of diluted supernatants were injected.

The HPSEC line was constituted of a Shimadzu HPLC system (Shimadzu, Kyoto, Japan) connected to a 18 angles Dawn Heleos II (MALLS) detector (Wyatt Technology, Santa Barbara, CA, USA) equipped with a QELS (Wyatt Technology) in position 14, and an OptilabRex differential refractive index detector (Wyatt Technology, Santa Barbara, CA, USA). The HPSEC line was additionally coupled to an online Viscometer (VISCOSTAR II, Wyatt, Santa Barbara, CA, USA), and a UV-VIS detector activated at 280 nm (SPD-20A, Shimadzu). The size exclusion separation of AGPs and soluble aggregates was performed on a OHPAK SB-G guard pre-column followed by four columns in series (OHPAK SB 803, 804, 805 and 806 HQ, Shodex). The mobile phase (0.01M acNa (pH 5.0), 0.3M NaCl, 0.02% NaN_3) was filtered through 0.1 µm filter (Millipore) and pumped at 1 $mL \cdot min^{-1}$.

The data were analyzed using the Zimm's model and an experimentally determined refractive index increment (dn/dC) of 0.145 $mL \cdot g^{-1}$, corresponding to the value of dn/dC measured for A. *seyal* gum and other incubated gums in the eluent. Data processing was operated using the ASTRA software 7.1.2 (Wyatt Technologies, Santa Barbara, CA, USA). The obtained gyration radius (R_g) needs to be considered only for values above 10 nm, which is the sensitivity limit of the MALLS detector.

2.8 Fourier Transform Infrared (FTIR) spectroscopy

Vibrational properties of chemical bonds in GA, arabic acid and incubated arabic acid powders were analyzed using a mid-infrared spectrometer (Vertex 70v, Brüker, Ettlingen, Germany) in Attenuated Total Reflectance (ATR) mode. FTIR-ATR spectra were recorded at room temperature and under vacuum conditions, from 4000 to 800 cm^{-1}, at a spectral resolution of

4 cm^{-1} and averaged over 128 scans. Spectra processing including baseline correction, normalization and smoothing, was carried out using the OPUS software version 8.2.28.

2.9 High-field Nuclear Magnetic Resonance (NMR) spectroscopy

^{13}C NMR spectra were recorded at 25 °C using a Bruker AVANCE III HD spectrometer operating at ^{1}H Larmor frequency of 600 MHz. The spectrometer was equipped with a 3.2 mm magic angle spinning (MAS) probe. ^{13}C NMR spectra were recorded by applying a 90° excitation pulse of 3.82 and 3.9 µs at 120W for t_0 and t_7 samples respectively, and a 2 s recycle delay for accurate integration of the carbon signals. NMR data processing was performed using Topsin 3.5 software.

3. Results and discussion

3.1 Influence of the physicochemical conditions on the stability and structural properties of AGP aggregates

The colloidal dispersion stability of AGP aggregates obtained during the storage at 40°C of arabic acid (t_0) at 2, 4 or 7 days (t_2, t_4 and t_7) was studied in aqueous systems with different urea content, ionic strength or pH. The arabic acid at t_2 was exclusively composed of AGPs and soluble aggregates whereas arabic acid powder stored at t_4 and t_7 also contained insoluble particles, the amount of which was maximum for t_7 (Antoine-Michard et al., 2022, in publication). Incubated powders were first dispersed in water containing urea. Urea is able to disturb water-water and water-biopolymer hydrogen bond interactions, and may induce protein denaturation (Tanford, 1970) and dissociation of protein (Brummitt et al., 2012; Doss-Pepe et al., 1998; Mendoza-Hernández et al., 2000) and proteoglycan (Hardingham, 1979; Schmidt et al., 1982) aggregates. Urea also disrupts the intermolecular hydrogen bond network between polysaccharide chains (Li et al., 2012; McQueen-Mason & Cosgrove, 1994) and can consequently collapse polysaccharide gel networks (Jaishankar et al., 2015; McGrane et al., 2004; Xie et al., 2021). The molar mass of AGPs from GA, arabic acid and arabic acid at t_7 is shown in Figure V.1. Clearly, it did not depend on urea concentration. Since, in addition, AGP aggregates formed faster at higher temperatures, then intermolecular AGP-AGP hydrogen

bond interactions cannot be the main cause of the formation and stability of demineralized arabic acid aggregates.

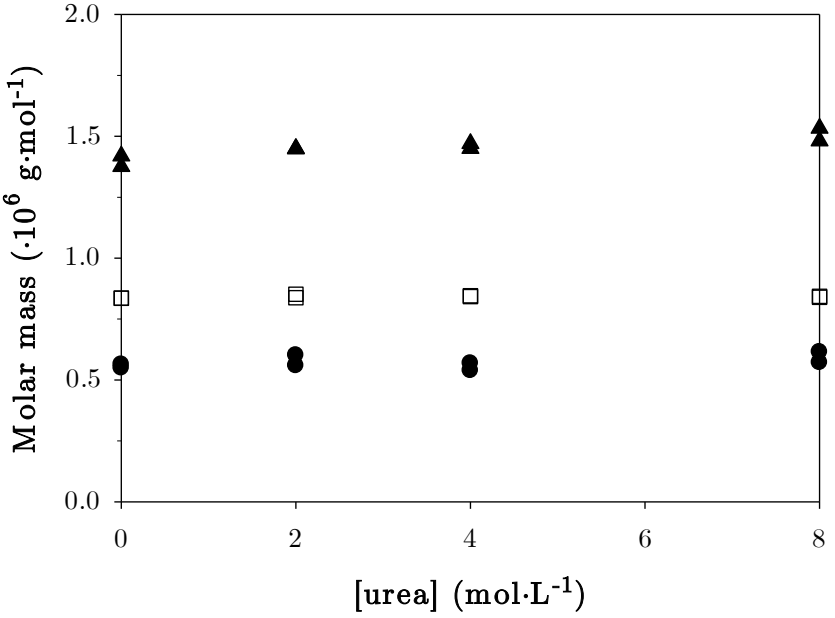

Figure V.1. Influence of the concentration in urea on the molar mass of AGPs from GA (□), arabic acid (▲) and arabic acid incubated for 7 days at 40°C (●).

The stability of AGP aggregates to pH changes was also probed by solubility and transmittance measurements. In the whole pH range studied (2.5 – 9.5), AGPs from GA and arabic acid powder (t_0) were completely soluble and their dispersions showed constant transmittance values around 97 – 100% (Figure V.2). The t_2 aggregates also remain essentially soluble with the pH, however the light transmittance was 91% at pH 3.7 but reach 100% at pH 7.5, which might indicate soluble aggregates are dissociated when increasing the pH above 7.5. For t_4 and t_7 samples, the decrease in transmittance observed between pH 2.4 and 3.5 could arise from changes in optical properties of these AGP aggregates depending on the parameters – notably the amount of cations – of the solvent in which they are dispersed (water or sodium acetate buffer). At higher pH, the evolution of transmittance and solubility for these samples can be divided in 3 zones depending on the pH. For t_4 aggregates, a 10% increase of transmittance is observed between pH 3.5 and pH 7. Further increase in the pH leads to a rise of transmittance up to reach a plateau at a value of 100% for pH above 8.5. In turn, the transmittance of t_7 samples remains constant at 22% between pH 3.5 and pH 7.5 and reaches 100% for pH 8.5. The increase in transmittance of these two samples is due to the dissociation of dispersed AGP aggregates and largest insoluble particles as shown by solubility measurements (Figure V.2B).

Above a critical pH, namely pH 7.8 or 8.7 for t_4 and t_7 respectively, the solubility reaches a plateau at 100% meaning that all the matter is soluble (Figure V.2B). In summary, the structure of AGP aggregates is sensitive to pH and starts to dissociate for pH above 7.5. In addition, the more aggregated the sample, the more alkaline the pH necessary to dissociate all insoluble matter. However, once dissociated at alkaline pH, acidification of the dispersion does not induce the re-aggregation of the AGPs, showing that dissociation at alkaline pH is an irreversible process (data not shown).

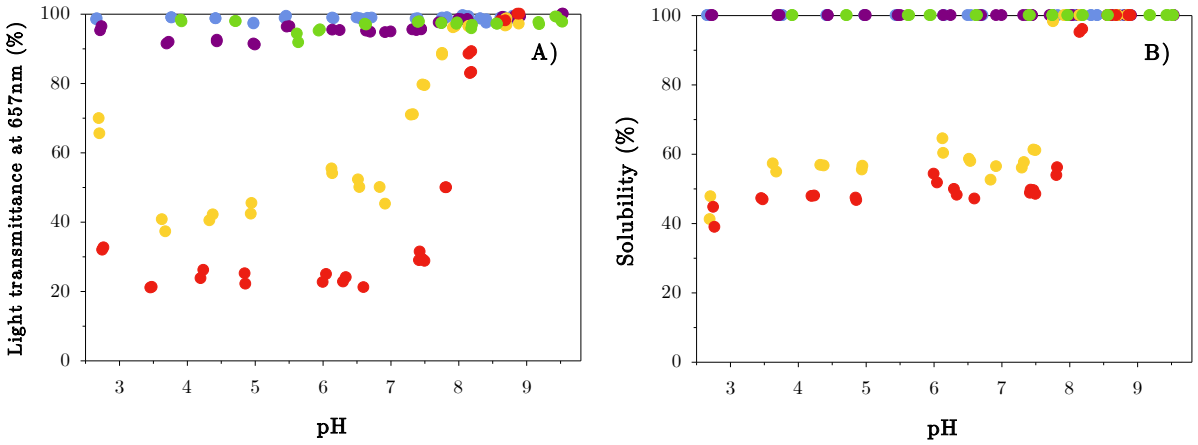

Figure V.2. A) Light transmittance at 657 nm and B) Solubility of aqueous dispersions of AGPs from GA (●), arabic acid (●) and arabic acid powder stored for 2days (●), 4 days (●) or 7 days (●) at 40°C as a function of the pH dispersion.

Since soluble gum and aggregates display a sphere equivalent diameter below 30 nm, changes in light scattering and solubility of t_4 and t_7 aggregates mainly concerned insoluble particles. If we take t_7 as an example, insoluble particles appear as spherical or spheroidal in phase contrast micrographs, with approximate diameters ranging from 10 to around 200 µm (Figure V.3A–D). These particles were similar to those observed in water in our previous work (Antoine-Michard et al., 2022, in publication). The presence of simple or multiple vacuoles in these particles suggest they are powder particles that were resistant to the solvent dispersion process, due certainly to the interfacial AGP crosslinking reaction. The suggestion is further supported by a closer look on micrographs, where more or less fused assemblies of particles suggest insufficient mixing energy. It is important to realize that the work for cavity creation, which is the very first stage in the dispersion process in water of biopolymers, molecules or atoms (Graziano, 2006; Lee, 1985), is definitely prohibitive in the case of very large extended hydrophobic solute. For instance, the free energy for cavity creation ΔG_c, a thermodynamic parameter that may be considered as a liquid's polarity index (Faucon et al., 2022), of a

hydrophobic particle having a diameter of 50 µm is about 0.3 TJ.mol^{-1} at 25°C, a colossal amount of energy, while it is "only" of about 280 MJ.mol^{-1} for an aggregate with 50 nm diameter (C. Sanchez, personal communication). It is then physically impossible to disperse these insoluble microparticles in water without changing the nature of the solvent (or applying high mechanical stresses). As an illustration of the claim, aggregates were still observed at pH 8.2 (Figure V.3E) but not above 8.5 where particle dissociation appears complete at this magnification (Figure V.3F).

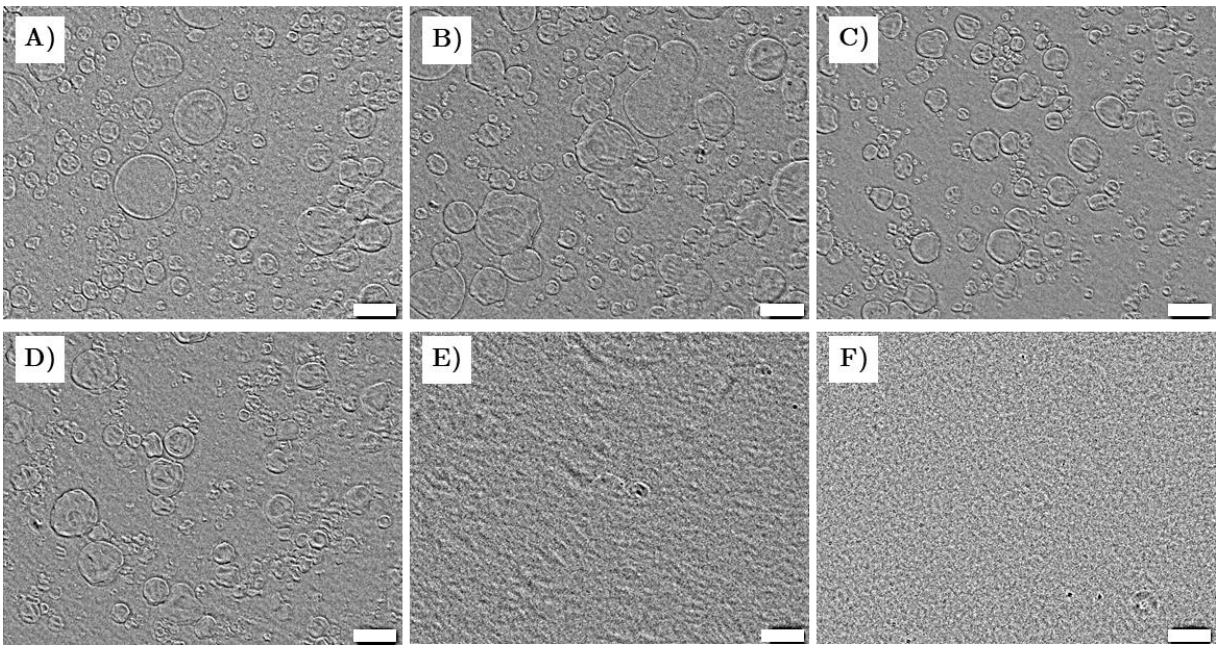

Figure V.3. Influence of pH of dispersion on the structure of arabic acid aggregates developed after dry incubation for 7 days at 40°C. Arabic acid aggregates were dispersed at pH 2.8 (A), 4.2 (B), 6.6 (C), 7.8 (D), 8.2 (E), and 9.5 (F). From optical microscopy. The magnification was x20 with a scale bar indicating 50 µm length.

The molecular structure of GA, arabic acid and soluble arabic acid-based AGP aggregates was characterized using SEC MALLS in the same pH range (2.5 – 9.5) (Figures V.4 and V.5). The mean molar mass and the hydrodynamic radius of A. *seyal* gum remained constant at $M_w = 7.9 \pm 0.3 \cdot 10^5$ g·mol^{-1} and $R_h = 11.2 \pm 0.4$ nm in the whole range of pH studied, which confirms the pH insensitivity of mineral loaded AGPs (data not shown). Molar mass and hydrodynamic radii of arabic acid and AGP aggregates (t_0, t_2, t_4 and t_7) were then normalized by M_w and R_h of GA. These normalized parameters remained constant between pH 2.8 and pH 6.7. However, above pH 7, different trends occurred regarding the initial aggregation state of samples. The M_w and R_h of AGPs from arabic acid (t_0) slightly decreased from $1.4 \cdot 10^6$ g·mol^{-1} (pH 6.7) to $7.7 \cdot 10^5$ g·mol^{-1} (pH 9.5), and from 13.5 nm to 11.0 nm, values close to those of GA.

The M_w and R_h evolution above pH 7 was attributed to the dissociation of soluble AGP aggregates as confirmed by the normalized concentration profile (*i.e.* refractive index) (Figure V.5A). The shoulder observed on arabic acid profiles between 24 and 27 min and corresponding to soluble AGP aggregates dropped above pH 7 until it totally disappeared at pH 9.5. The profile of arabic acid AGPs dispersed at pH 9.5 was closely superimposed to that of AGPs from GA.

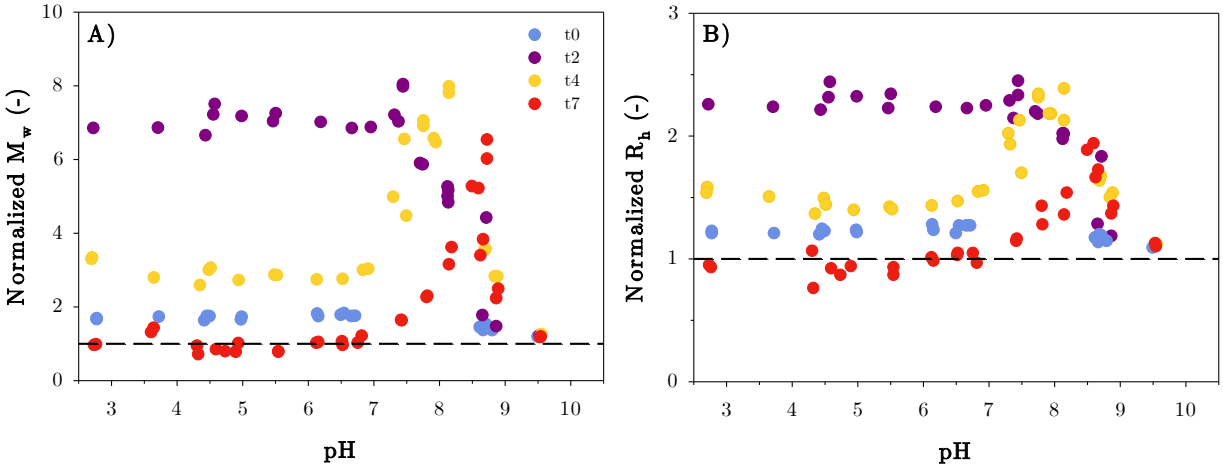

Figure V.4. Normalized molar mass (A) and hydrodynamic radius (B) of AGPs from arabic acid (●) and arabic acid powder stored for 2 days (●), 4 days (●) or 7 days (●) at 40°C as a function of the pH dispersion.

For t_2, initially composed of AGPs and soluble aggregates, M_w and R_h sharply decreased between pH 7.4 and 9.5. The same evolution appeared for t_4 and t_7 aggregates, *i.e.* an increase of molar mass from pH 6.7 to pH 8.2 (t_4) and 8.7 (t_7) up to a maximum, followed by a decrease until pH 9.5. Similarly, their hydrodynamic radii increased between pH 6.7 and ~ 8.5 up to a maximum and then decreased. This evolution of M_w with the pH may suggest that *(i)* for pH in the range 6.7 – 8.5 insoluble microparticles dissociate into smaller soluble aggregates for t_4 and t_7 samples (Figure V.2B), and *(ii)* higher pHs promote the dissociation of soluble aggregates for t_2, t_4 and t_7 samples. At pH 9.5, M_w and R_h of t_0 and initially aggregated samples adopted the same values, *i.e.* $M_w = 9.5 \cdot 10^5$ g·mol^{-1} and $R_h = 12.4$ nm, about 10 – 20% higher than M_w and R_h of GA, highlighting the incomplete reversibility at pH 9.5.

Whatever the initial aggregation state of AGPs from arabic acid (soluble aggregates or insoluble microparticles), aggregates were sensitive to pH above 7, especially to alkaline pH. According to the aggregation state, a partial reversibility of the arabic acid aggregation reaction can be

observed in the studied pH range. At pH 9.5, the profile of arabic acid AGPs was closely superimposed to that of AGPs from A. *seyal* confirming this reversibility (Figure V.5A). For t_2, t_4 and t_7 aggregated samples, the normalized concentration profiles were not superimposed to that of A. *seyal* reflecting the incomplete reversibility of the aggregation reaction (Figure V.5B–D). For the most aggregated samples, it may be necessary to disperse powders in still more alkaline conditions to achieve full reversibility of the aggregation reaction.

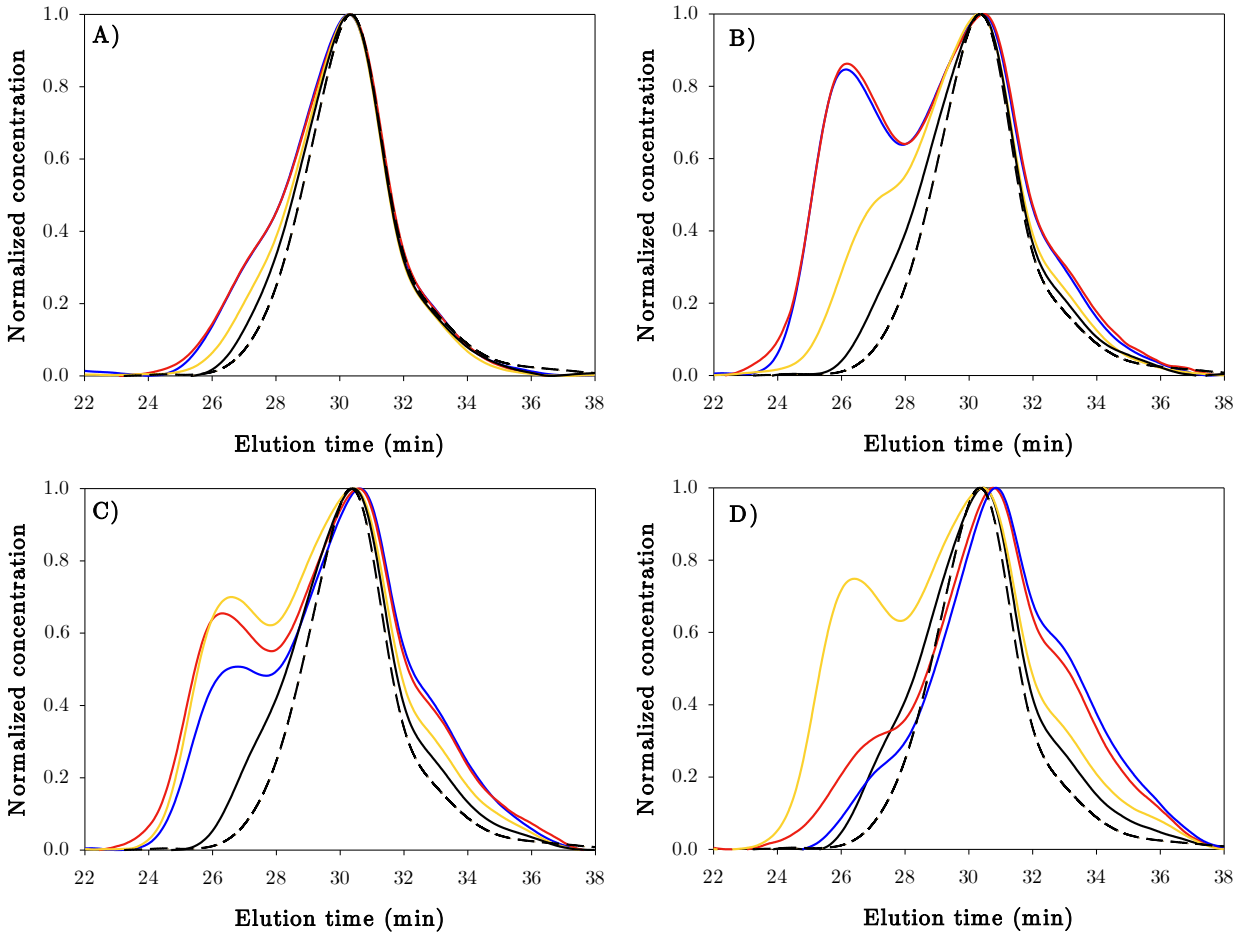

Figure V.5. Normalized concentration profiles as a function of elution time for arabic acid (A), and arabic acid incubated for 2 (B), 4 (C) and 7 days (D) at 40°C, and solubilized at pH 2.4 (●), 7.5 (●), 8.5 (●) or 9.5 (●). The dashed line represents the normalized concentration profile of A. *seyal*, used as a reference. From SEC MALLS data.

The analysis of the R_h vs. M_w conformation plots of arabic acid AGPs and soluble aggregates showed pH did not influence their conformation (Supplementary data, Figure V.11). This would indicate the conformation of soluble aggregates from arabic acid is not disturbed by their dissociation at alkaline pH, pointing to a self-similar fractal structure (Renard et al., 2014). At its natural pH (4.5), A. *seyal* contains negatively charged glucuronic acids and amino acids

either positively (histidine, lysine and arginine) or negatively (aspartic and glutamic acids) charged. Demineralization impacts both the mineral content and the pH of A. *seyal* and so the charge density of its AGPs. Intuitively, the combined presence of negative and positive charges may suggest the development of electrostatic interactions during the storage of acidified AGPs, that would be dissociated at alkaline pH. In addition, the protective effect of minerals against the aggregation propensity of AGPs also points to an important role of charges during aggregation (Antoine-Michard et al., 2022, in publication). The pH-induced dissociation of protein aggregates formed during incubation in the dry state was reported, far from their isoelectric point, due to the repulsions between charged groups as reported, for instance with milk proteins (Ashraf et al., 2013; Schong, 2017). Since electrostatic interactions are notoriously sensitive to ionic strength and salt concentration, the colloidal stability of AGP aggregates and microparticles was probed by dispersing arabic acid powders in water (pH 2.4) and buffers (from pH 3.5 to 9.5) supplemented with various NaCl concentrations, up to 1 mol·L^{-1}. The solubility of AGPs and molar masses of AGPs and soluble aggregates of t_7 sample were then determined and plotted as a function of pH for several ionic strengths (Figure V.6). It can be noticed that in each buffer, the pH was not dramatically modified by the presence of NaCl, even at 1 mol·L^{-1} NaCl.

Below pH 7.5, the solubility of t_7 sample remained constant with values around 45% even if the ionic strength was increased until 1 mol·L^{-1} (Figure V.6A). As observed for the pH effect, the t_7 sample was totally soluble for pH higher than 7.5 showing the dissociation of previously insoluble microparticles (Figure V.6A). The increase of the ionic strength up to 1 mol·L^{-1} does not have a specific effect on the solubility and the structural integrity of arabic acid microparticles. The dissociation observed above pH 7.5 can then be associated to the sole effect of pH. These results were confirmed by phase contrast micrographs of t_7 in 1 mol·L^{-1} NaCl, where spherical microparticles were only found for pH until 8, which is in favor of a dissociation of these microparticles at alkaline pH (Supplementary data Figure V.12).

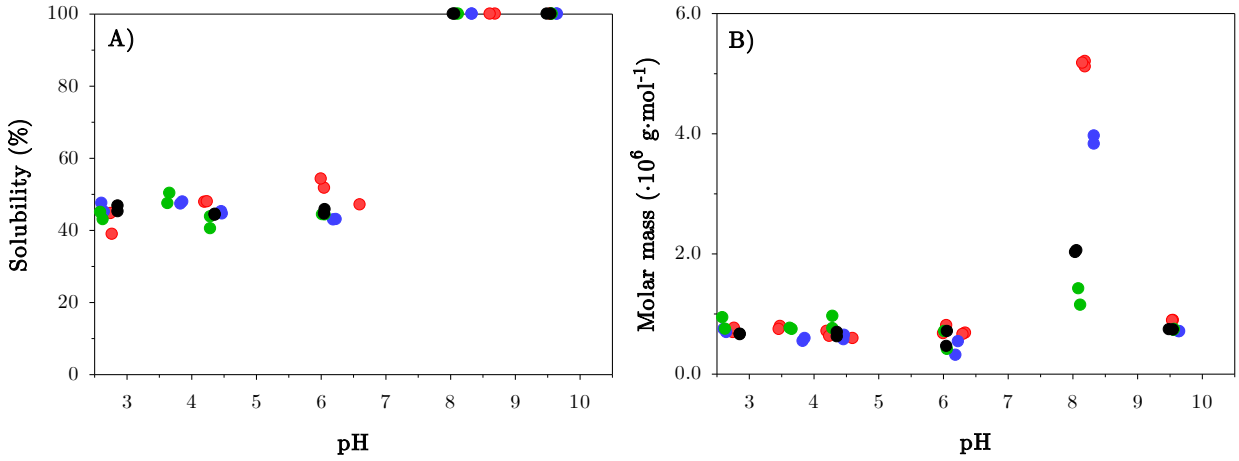

Figure V.6. Solubility (A) and molar mass (B) of AGPs from arabic acid powder stored for 7 days at 40°C and dispersed in NaCl aqueous dispersions at various ionic strength: 0 mol·L^{-1} (●), 0.1 mol·L^{-1} (●), 0.5 mol·L^{-1} (●) and 1 mol·L^{-1} (●), as a function of the dispersion pH.

In terms of AGP molar masses, the M_w was constant around 6.7·10^5 g.mol^{-1} for pH below 6.5 and ionic strength up to 1 mol.L^{-1} (Figure V.6B). This result confirms the integrity of AGPs microparticles to ionic strength as observed for solubility measurement (Figure V.6A). Also, the M_w increased between pH 6.5 to 8 due to the dissociation of microparticles before to further drop at pH 9.5 in relation with the dissociation of soluble aggregates. At pH 9.5, the M_w was constant with value of ~ 8·10^5 g.mol^{-1} whatever the ionic strength. A specific behavior was observed in the transition at pH 8 for which microparticles and soluble aggregates dissociated. At this pH, the M_w decreased from 5.2 to 2.0·10^6 g·mol^{-1} while increasing ionic strength from 0 to 1 mol·L^{-1}. Therefore, even if the ionic strength did not influence the integrity of microparticles below pH 6.5 and at pH 9.5, a synergistic pH/ionic strength effect might be considered in the pH range 6.5 – 9.5. This enhanced sensitivity of aggregates could arise from an increased accessibility of AGPs charges at these specific pHs, either coming from the polysaccharide moiety or the protein part.

From these results, it could be suggested that the sensitivity of aggregates to the pH might originate from the involvement of covalent interactions, in relation to the activation energy described in the introduction. For instance, peptide bonds of lysozyme and α-lactalbumin are cleaved at pH 13 at the C-terminal side of Asn residues (Manabe & Jin, 2005). Polyesteramides degradation through ester bond cleavage can be enhanced in alkaline conditions (Rudnik, 2013). As well, the degradation of ester and ether bonds during alkaline processing of lignocellulose was reported (Giummarella et al., 2019; Košíková et al., 1979). Our reaction conditions

(heating, anhydrous medium and acidic pH) are suitable for chemical condensation reactions such as esterification. For instance, it is possible to formulate pH-sensitive chitosan films (Heras-Mozos et al., 2022) or various hydrogels (Zhang et al., 2018) thanks to the pH-responsiveness of carbonyl-condensation reactions (reactivity of the C=N bond) (Hamid, 1992; Martell & Herbst, 1941; Simat et al., 1994).

Finally, the influence of calcium on the colloidal stability of arabic acid microparticles and aggregates was assessed in aqueous systems with different $CaCl_2$ content ($[CaCl_2]$ = 0 – 50 mmol·L^{-1}). In particular, the concentration of 0.8 mmol·L^{-1} was chosen to mimic the concentration in Ca^{2+} found in GA at 1wt%. AGPs are known to have a particular affinity for calcium, which represents 1% of its global composition (Lamport et al., 2014; Lamport & Várnai, 2013; Lopez-Hernandez et al., 2020; Showalter, 2001). It had also been shown that a concentration of 2 mmol·L^{-1} of $CaCl_2$ was sufficient to prevent plasma proteins from aggregation or induce their dissociation into subunits, because of a high binding affinity between the protein and Ca^{2+} (Cooper et al., 1973; Protopopova et al., 2019; Sussman & Weiss, 1976).

The addition of $CaCl_2$, even at the lowest concentration (*i.e.* 0.8 mmol·L^{-1}), led to a spontaneous decrease by 2 of the aggregate dispersions transmittance, while the AGP aggregates solubility remained constant (Figure V.7). As observed with the acetate buffer and sodium salt (Figure V.2A), Ca^{2+} modifies the optical properties of arabic acid dispersions, and mainly those of microparticles without inducing their dissociation and changing their solubility. The molar mass of AGPs and soluble aggregates neither depends on $CaCl_2$, except at a concentration of 50 mmol·L^{-1} for which M_w of t_7 increased by 43%. This would indicate $CaCl_2$ promotes aggregation of AGPs at this excess calcium concentration, which may be seen as the consequences of high ion concentrations on the water thermodynamic properties and the hydrophobic effect.

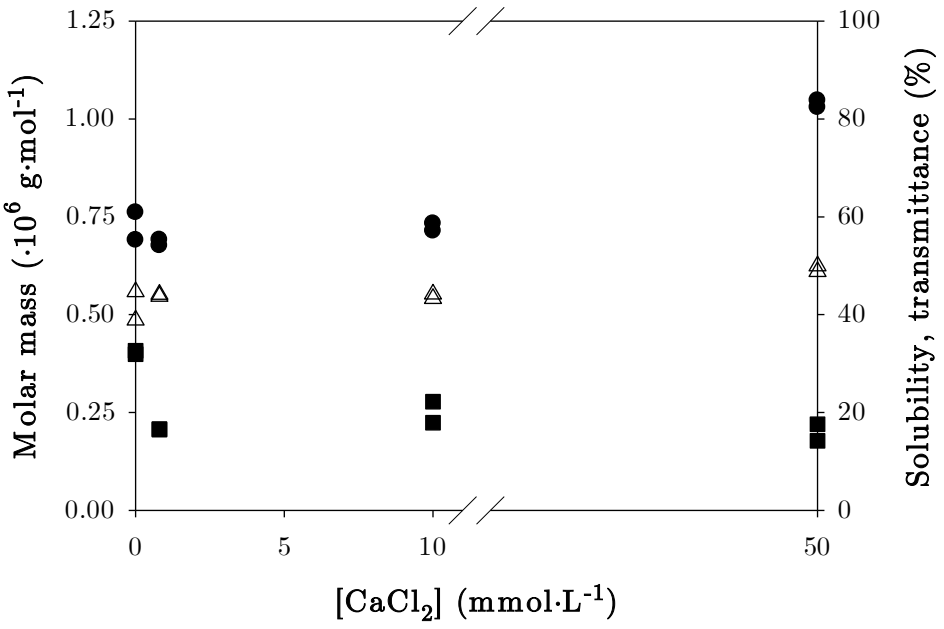

Figure V.7. Influence of the concentration in $CaCl_2$ on the molar mass (●), solubility (Δ) and transmittance (■) of AGPs from arabic acid incubated for 7 days at 40°C.

3.2 Spectroscopic characterization of AGP aggregates

3.2.1. High resolution NMR spectroscopy

Hypothetical covalent interactions involved in the aggregation mechanism of AGPs from arabic acid were looked for using high resolution ^{13}C solid-state NMR experiments. Our reaction conditions and the partial reversibility of aggregation at highly alkaline pH suggested aggregates might form *via* charge condensation reactions such as esterification. NMR spectra revealed no change in the carboxylic acid region from glucuronic acids (~ 180 ppm in ^{13}C NMR spectrum), which might exclude the hypothesis of an ester formation involving carboxylic acid as reagent. Peaks at 93 (α-anomer) or 99 ppm (β-anomer) were previously attributed to the C_1 of glucuronic acids (Amaniampong et al., 2017; Tonković & Bilinski, 1995). The emergence of a peak at 95 ppm for sample t_7 could arise from the formation of an acetal bond (Albert et al., 1986; Chen et al., 2014; Tsukino & Kunitake, 1979). However these bonds are dissociated at acidic pH which is not consistent with our aggregation conditions. It is not excluded that the amount of new formed chemical bonds is too small to be observed by NMR. The sensitivity of the method and the structure complexity of our macromolecular aggregates makes the

attribution difficult. However, the reaction might involve the contribution of glucuronic acids which could be esterified during the AGP storage in dry state.

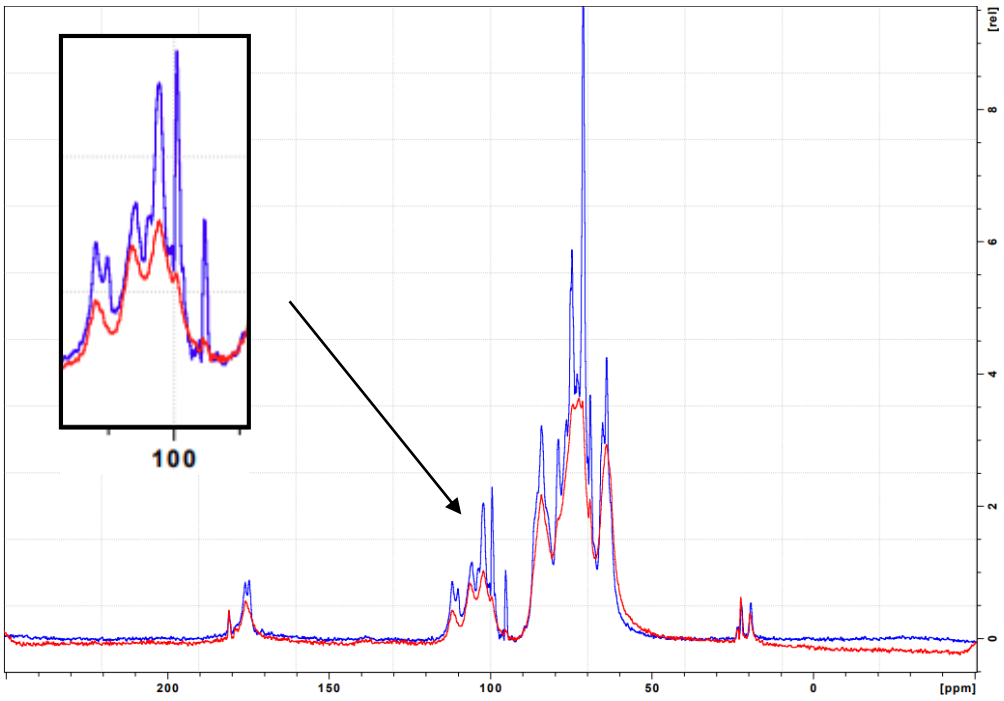

Figure V.8. The ^{13}C NMR spectra of arabic acid powder (red) and aggregated arabic acid (t_7) formed by the storage in the dry state of arabic acid for 7 days at 40°C (blue). Inset highlights the emergence of a peak at 95 ppm in the t_7 spectrum.

3.2.2. Fourier Transform Infrared (FTIR) spectroscopy

Complementary information about the potential interactions involved during incubation of arabic acid powder were obtained via FTIR spectroscopy. IR spectra of A. *seyal*, arabic acid and arabic acid aggregates were recorded between 850 and 3800 cm^{-1}. In the previous chapter, a particular attention was paid in the OH stretching vibration region, that is not further examined in this section. Here, we would like to confirm the involvement of ester bonds and we will focus on two spectral regions of interest: 850 – 1200 and 1500 – 1800 cm^{-1}.

Demineralization of A. *seyal* gum induced major changes between 1500 and 1800 cm^{-1} (Figure V.9). Stretching (C=O) vibration bands of carboxylic acids also appear at around 1420, 1620 and 1720 cm^{-1} (Boulet et al., 2007; Manrique & Lajolo, 2002; Vinod & Sashidhar, 2010). The contribution of the protein part also appears in this region with amide I and amide II

bands at 1650 and 1550 cm^{-1} respectively. Since A. *seyal* contains less than 1% protein but ~ 20% glucuronic acids, these bands were mainly attributed to stretching (C=O) vibrations from the latter.

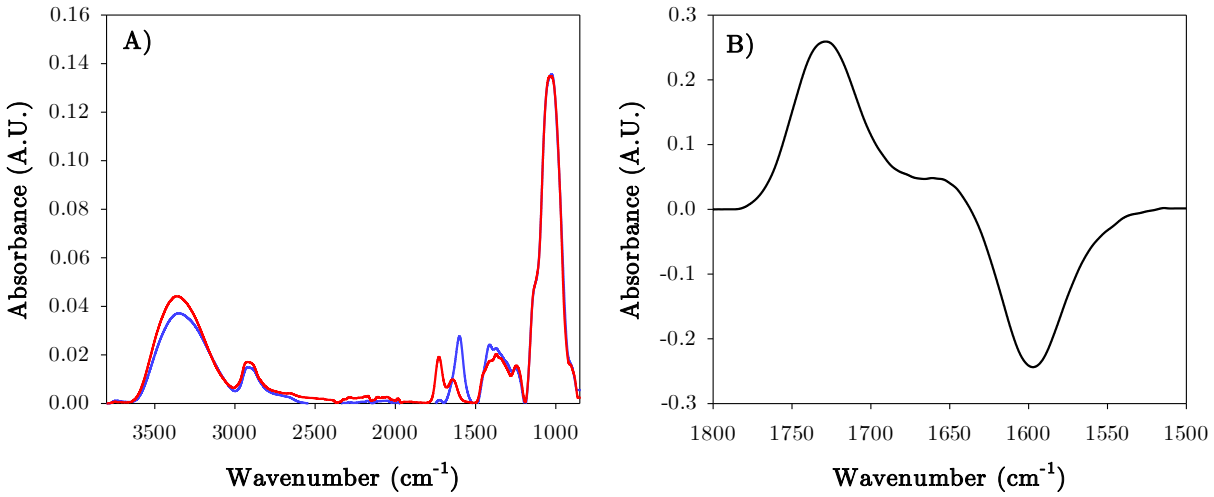

Figure V.9. A) Fourier transform infrared (FTIR) spectra of A. *seyal* (blue) and arabic acid from A. *seyal* (red) gums from 850 to 3800 cm^{-1}. The light blue areas highlight the wavenumber domain of interest that will be examined in this section. B) Spectral subtraction of A. *seyal* from arabic acid in the region 1500 – 1800 cm^{-1}.

The spectral subtraction of A. *seyal* from arabic acid (t_0) in this spectral region revealed major changes at 1597 cm^{-1} and 1730 cm^{-1} (Figure IV.9B). Moreover, the peak at 1597 cm^{-1} blueshifted to 1630 cm^{-1} after demineralization. This shift to higher wavelengths is due primarily to the strentghtening of OH covalent bonds in A. *seyal* (Huang et al., 2015; Sun, 2018; Sun et al., 2013). This was previously observed when studying the effect of a decrease in the pH from 4.1 to 2.4 on the FTIR spectra of xylan-chitosan complexes (Gabrielii & Gatenholm, 1998). The bands at 1597 cm^{-1} and 1730 cm^{-1} are associated to the carboxylic acid groups (in their protonated or deprotonated form) of glucuronic acids composing A. *seyal* (Bhushette & Annapure, 2017; Lopez-Torrez et al., 2015). Yet, in addition to the removal of minerals, demineralization of A. *seyal* induced an acidification of the gum in solution, with the substitution of minerals (cations Na^+, K^+ and Ca^{2+}) by protons H^+. Thus, the differences observed between the two spectra result from a switch of the carboxylic acid groups from their deprotonated form $RCOO^-$ (associated with cations) in A. *seyal* to their protonated form RCOOH in arabic acid.

For arabic acid aggregates, minor changes were also observed at 1630 cm^{-1} which could be ascribed to stretching of $(C{=}O)_{\text{carboxylic acid}}$, or alternatively to a bending vibration mode of

hydration water (Artemov et al., 2020; Seki et al., 2020) (Supplementary data, Figure V.13). The incubation of arabic acid in dry state did not involve the appearance of any new band or the complete disappearance of any band initially present in the FTIR spectrum of arabic acid. However, some differences between samples were observed in the region 850 – 1200 cm^{-1} (Figure V.10). The most important changes appeared during the first day of incubation as shown by the important blueshift between t_0 and t_1, from 1050 to 1073 cm^{-1} (Figure V.10A). The FTIR spectra of aggregated samples also revealed an isobectic point at 1040 cm^{-1} – showing an equilibrium between two species during incubation – and an increase in the intensity of the band at 1065 cm^{-1} concomitant with a decrease in the intensity of the band at 1015 cm^{-1}.

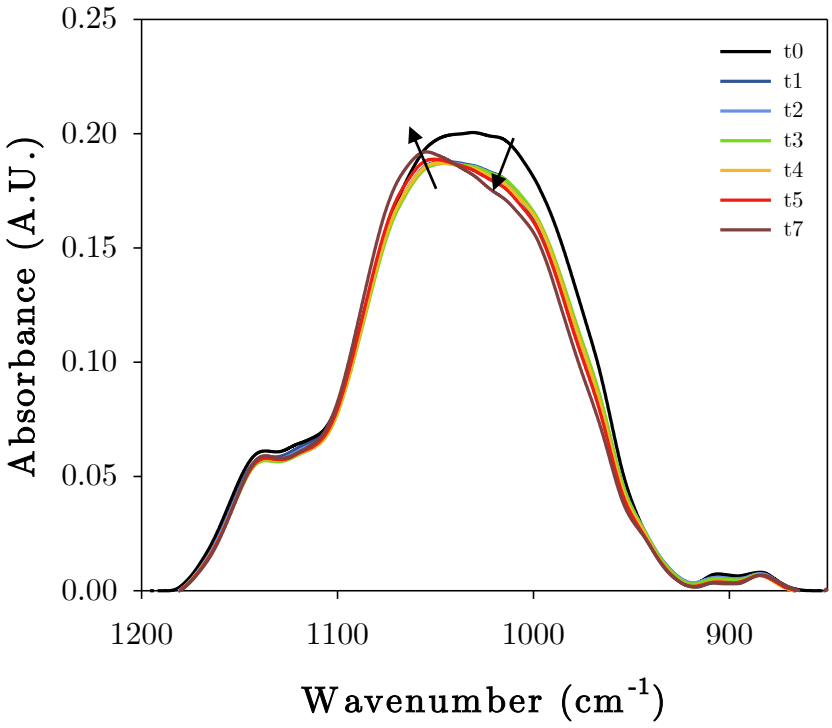

Figure V.10. Fourier transform infrared (FTIR) spectra of arabic acid and aggregated arabic acid samples in the spectral IR region from 850 to 1200 cm^{-1}.

These bands are characteristic of C–O (from C–O–C or C–O–H) stretching vibrations from ethers, esters or acetals (Table V.1) (Kacuráková et al., 2000; Leonor et al., 2013; Vanloot et al., 2012) but due to the complexity of GA structure, attributing accurately these signals to specific chemical groups is far from being trivial. Risica et al. also showed a decrease in the intensity of the band at 1030 cm^{-1} (relative to ν(C-OH) of alcohol) during the formation of guar gum ethers, correlated with the appearance of two bands at 1058 and 1125 cm^{-1} (Risica et al., 2005). However, no change at around 1125 cm^{-1} was observed with our samples.

Table V.1. Characteristics of principal absorbance bands in FTIR spectra (region 1000 – 1100 cm^{-1}) of GA and arabinogalactan with their corresponding vibrations and assignments. From (Kacuráková et al., 2000; Leonor et al., 2013; Vanloot et al., 2012)

	Band position (cm^{-1})	Vibration type	Associated vibrations		References
A. *seyal* gum	1018	Stretching	endocyclic and exocyclic C–O from carbohydrates		(Vanloot et al., 2012)
	1024	Deformation	HCH CCH HCO COH		
A. *senegal* gum	1030	Stretching	C–O (alcohol group)		(Leonor et al., 2013)
	1075		C–O (out-of-ring ether group)		
Arabinogalactan	1043	Stretching	ring vibration overlapped with C–O and C–O–C	Araf in the side chains	(Kacuráková et al., 2000)
	1078			Galp in the backone	

These IR results are consistent with the NMR characterization and could be in accordance with the formation of ester groups during incubation.

4. Conclusions

This work provides new insights about the stability in solvents of arabic acid AGP aggregates regarding the physicochemical properties of the solvent. The factors affecting the structure and controlling the size of these aggregates are essentially the pH and the ionic strength (NaCl and, to a lower extent, $CaCl_2$). Results suggest partial dissociation of AGP aggregates when increasing the pH with first the dissociation of insoluble highly cross-linked microparticles into smaller soluble aggregates (pH = 6.7 – 8.5), which are further dissociated at more alkaline pHs. Ionic strength seems to modify aggregate size in a narrow pH range around pH 8 showing enhanced sensitivity of aggregates that might arise from an increased accessibility of the AGPs charges around this specific pH. These results highlight the importance of the surface charge in the dehydration-induced AGP aggregation mechanism. This reaction might involve the formation of C-O chemical bonds, maybe *via* ester formation.

5. Acknowledgments

The authors gratefully acknowledge ALLAND & ROBERT Company (Port Mort, France) and the French Ministry of Research and Education (2017/1727) for the financial support (Ph.D. Amandine Antoine-Michard). We also would thank A. Vallet and P. Schanda (NMR group, Institut de Biologie Structurale, Grenoble, France) for the NMR experiments.

6. Supplementary data

Table V.2. dn/dC values determined according to pH buffer and ionic strength. The ionic strength was adjusted with NaCl in most of the cases, or with $CaCl_2$ (*).

Buffer	pH buffer	Salt concentration ($mmol \cdot L^{-1}$)	dn/dC ($mL \cdot g^{-1}$)
Acetate	3.5	0	0.1472
	4.5	0	0.1477
		100	0.144
		500	0.1499
		1000	0.1406
	5.5	0	0.1508
MES	5.5	0	0.1464
	6.5	0	0.1469
		100	0.1501
		500	0.147
		1000	0.1428
	7.5	0	0.1514
TRIS	7.5	0	0.149
		100	0.1435
		500	0.1473
		1000	0.1413
	8.5	0	0.1514
		100	0.146
		500	0.1488
		1000	0.1432
	9.5	0	0.1532
CAPSO	10	0	0.148
		100	0.1435
		500	0.154
		1000	0.1425
Water	-	0	0.1492
		0.8*	0.149
		10*	0.1489
		50*	0.1477
		100	0.1446
		500	0.1461
		1000	0.1409

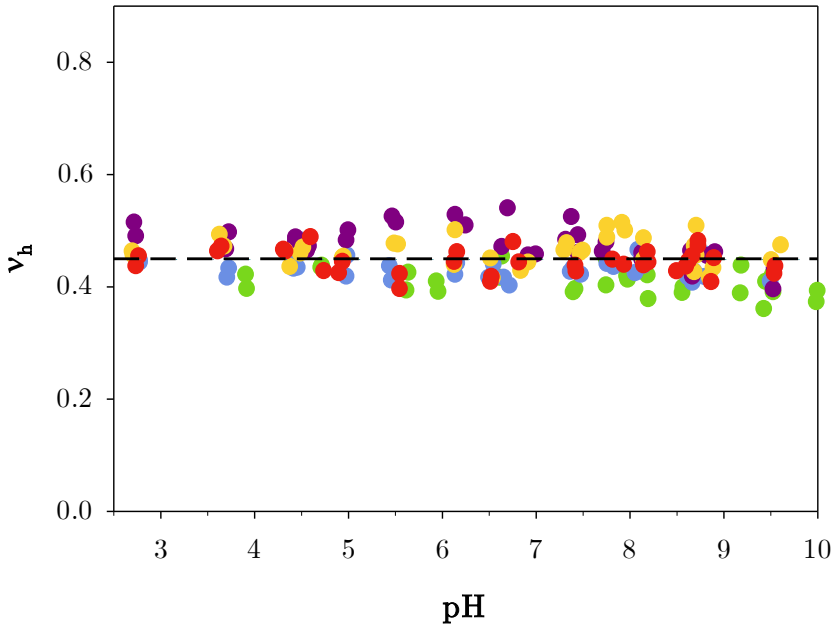

Figure V.11. ν_h exponents from the relation $R_h = K_h M_w^{\nu_h}$ determined from SEC MALLS data for AGPs from GA (●), arabic acid (●) and arabic acid powder stored for 2days (●), 4 days (●) or 7 days (●) at 40°C as a function of the pH dispersion.

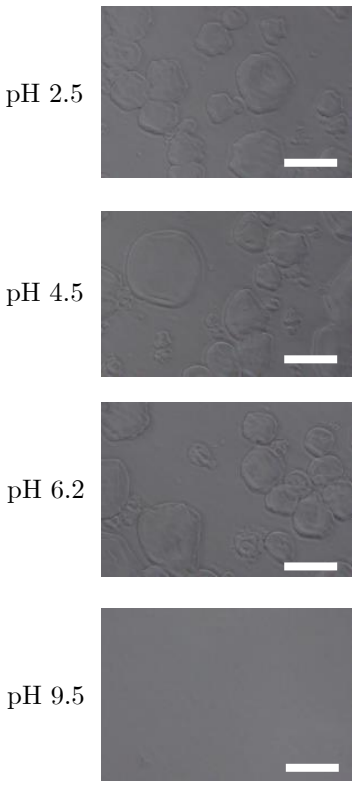

Figure V.12. Influence of the pH of NaCl aqueous solutions ([NaCl] = 1 mol·L^{-1}) on the morphology of AGP aggregates observed by phase-contrast microscopy. The magnification was x20 and the scale bar indicates 50 µm length.

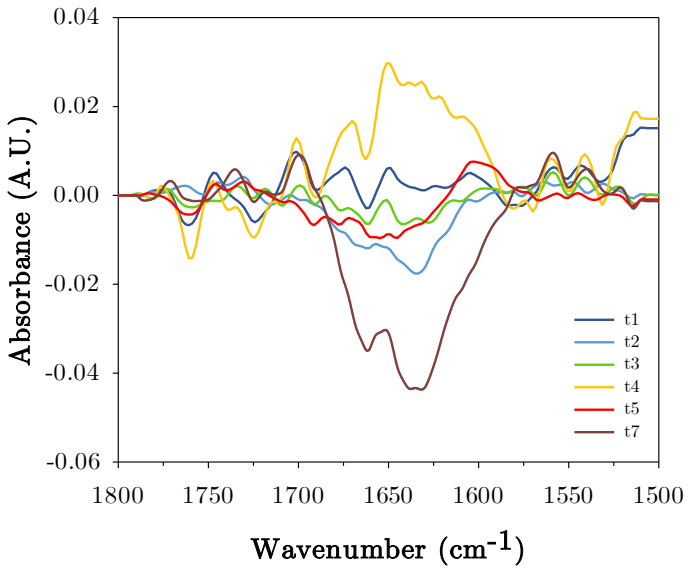

Figure V.13. FTIR spectral subtraction of arabic acid from aggregated arabic acid samples in the region from 1500 to 1800 cm^{-1}.

7. Highlights

In this chapter, we investigated the stability and reversibility of arabic acid AGP aggregates in dilute solvent conditions. The influence of the physicochemical properties (urea content, pH and ionic strength) of the solvent was assessed. A special focus was set on the incubation of demineralized Acacia *seyal* gum (arabic acid) at 40°C. The main results obtained are described below:

- In dispersion, AGP aggregates are stable to acidic pHs up to 6.7, and to urea at concentration from 0 to 8 mol·L^{-1} suggesting that AGP–AGP hydrogen bond interactions are not the main cause of the formation of AGP aggregates.
- At more alkaline pH, AGP solubility increases up to reach 100% at pH ~ 8.5 suggesting that in this pH range cross-linked insoluble microparticles dissociate into smaller soluble aggregates which are further partially dissociated at more alkaline pHs as shown by a decrease in the M_w of soluble aggregates.
- AGP aggregates are sensitive to ionic strength at pH 8, which might indicate that AGP charges are more accessible for condensation reactions around this specific pH. To a lower extent, AGP aggregates are sensitive to divalent calcium ions. $CaCl_2$ seems to promote AGP aggregation at 50 mmol·L^{-1}, maybe due to perturbation of the water thermodynamic properties.
- Spectroscopic characterization of AGP aggregates showed the emergence of a peak at 95 ppm by ^{13}C NMR and an increase in the intensity of the band at 1065 cm^{-1} correlated with a decrease in the intensity of the band at 1015 cm^{-1} by FTIR. This aggregation reaction might involve the formation of covalent C-O bonds, maybe *via* ester formation.

8. References

Al-Assaf, S., Andres-Brull, M., Cirre, J., & Phillips, G. O. (2012). Structural changes following industrial processing of Acacia gums. In J. F. Kennedy, G. O. Phillips, & P. A. Williams (Eds.), *Gum Arabic* (RCS Publishing, pp. 153–168). Kennedy J.F., Phillips G.O., Williams P.A. https://doi.org/10.1039/9781849733106-00153

Al-Assaf, S., Phillips, G. O., Aoki, H., & Sasaki, Y. (2007). Characterization and properties of Acacia senegal (L.) Willd. var. senegal with enhanced properties (Acacia (sen) SUPER GUM™): Part 1—Controlled maturation of Acacia senegal var. senegal to increase viscoelasticity, produce a hydrogel form and convert a poor into a good emulsifier. *Food Hydrocolloids*, *21*(3), 319–328. https://doi.org/10.1016/j.foodhyd.2006.04.011

Albert, K., Peters, B., Bayer, E., Treiber, U., & Zwilling, M. (1986). Crosslinking of Gelatin with Formaldehyde; a 13C NMR Study. *Zeitschrift Für Naturforschung B*, *41*(3), 351–358. https://doi.org/10.1515/znb-1986-0310

Amaniampong, P. N., Karam, A., Trinh, Q. T., Xu, K., Hirao, H., Jérôme, F., & Chatel, G. (2017). Selective and Catalyst-free Oxidation of D-Glucose to D-Glucuronic acid induced by High-Frequency Ultrasound. *Scientific Reports*, *7*(1), 40650. https://doi.org/10.1038/srep40650

Antoine-Michard, A., Charbonnel, C., Jaouen, I., Sanchez, C., & Nigen, M. (2022). Maturation of demineralized arabinogalactan-proteins from Acacia seyal gum in dry state: Aggregation kinetics and structural properties of aggregates. *International Journal of Biological Macromolecules*.

Aoki, H., Al-Assaf, S., Katayama, T., & Phillips, G. O. (2007). Characterization and properties of Acacia senegal (L.) Willd. var. senegal with enhanced properties (Acacia (sen) SUPER GUM™): Part 2—Mechanism of the maturation process. *Food Hydrocolloids*, *21*(3), 329–337. https://doi.org/10.1016/j.foodhyd.2006.04.002

Artemov, V. G., Uykur, E., Roh, S., Pronin, A. V., Ouerdane, H., & Dressel, M. (2020). Revealing excess protons in the infrared spectrum of liquid water. *Scientific Reports*, *10*(1), 11320. https://doi.org/10.1038/s41598-020-68116-w

Ashraf, S., Abbasi, A. Z., Pfeiffer, C., Hussain, S. Z., Khalid, Z. M., Gil, P. R., Parak, W. J., & Hussain, I. (2013). Protein-mediated synthesis, pH-induced reversible agglomeration, toxicity and cellular interaction of silver nanoparticles. *Colloids and Surfaces B: Biointerfaces*, *102*, 511–518. https://doi.org/10.1016/j.colsurfb.2012.09.032

Bhushette, P., & Annapure, U. (2017). Comparative study of Acacia nilotica exudate gum and acacia gum. *International Journal of Biological Macromolecules*, *102*, 266–271. https://doi.org/10.1016/j.ijbiomac.2017.03.178

Boulet, J. C., Williams, P., & Doco, T. (2007). A Fourier transform infrared spectroscopy study of wine polysaccharides. *Carbohydrate Polymers*, *69*(1), 79–85. https://doi.org/10.1016/j.carbpol.2006.09.003

Brummitt, R. K., Andrews, J. M., Jordan, J. L., Fernandez, E. J., & Roberts, C. J. (2012). Thermodynamics of amyloid dissociation provide insights into aggregate stability regimes. *Biophysical Chemistry*, *168–169*, 10–18. https://doi.org/10.1016/j.bpc.2012.06.001

Camisasca, G., De Marzio, M., Corradini, D., & Gallo, P. (2016). Two structural relaxations in protein hydration water and their dynamic crossovers. *Journal of*

Chemical Physics, *145*, 044503. https://doi.org/10.1063/1.4959286

Capataz-Tafur, J., Trejo-Trapia, G., Rodríguez-Monroy, M., & Sepulveda-Jiménez, G. (2011). Arabinogalactan proteins are involved in cell aggregation of cell suspension cultures of Beta vulgaris L. *Plant Cell Tiss Organ Cult*, *106*, 169–177. https://doi.org/10.1007/s11240-010-9905-3

Castellani, O., Guibert, D., Al-Assaf, S., Axelos, M., Phillips, G. O., & Anton, M. (2010). Hydrocolloids with emulsifying capacity. Part 1 – Emulsifying properties and interfacial characteristics of conventional (Acacia senegal (L.) Willd. Var. Senegal) and matured (Acacia (sen) SUPER GUM™) Acacia senegal. *Food Hydrocolloids*, *24*(2–3), 193–199. https://doi.org/10.1016/j.foodhyd.2009.09.005

Chen, T., Yu, H., Yang, N., Wang, M., Ding, C., & Fu, J. (2014). Graphene quantum dot-capped mesoporous silica nanoparticles through an acid-cleavable acetal bond for intracellular drug delivery and imaging. *Journal of Materials Chemistry B*, *2*(31), 4979–4982. https://doi.org/10.1039/C4TB00849A

Cooper, H. A., Griggs, T. R., & Wagner, R. H. (1973). Factor VIII Recombination After Dissociation by CaCl2. *Proceedings of the National Academy of Sciences of the United States of America*, *70*(8), 2326–2329.

Cozic, C., Picton, L., Garda, M.-R., Marlhoux, F., & Le Cerf, D. (2009). Analysis of arabic gum: Study of degradation and water desorption processes. *Food Hydrocolloids*, *23*(7), 1930–1934. https://doi.org/10.1016/j.foodhyd.2009.02.009

Cui, S. W., Phillips, G. O., Blackwell, B., & Nikiforuk, J. (2007). Characterisation and properties of Acacia senegal (L.) Willd. var. senegal with enhanced properties (Acacia (sen) SUPERGUM™): Part 4. Spectroscopic characterisation of Acacia senegal var. senegal and Acacia (sen) SUPERGUM™ arabic. *Food Hydrocolloids*, *21*(3), 347–352. https://doi.org/10.1016/j.foodhyd.2006.05.009

Doss-Pepe, E. W., Carew, E. L., & Koretz, J. F. (1998). Studies of the Denaturation Patterns of Bovine Alpha-Crystallin Using an Ionic Denaturant, Guanidine Hydrochloride and a Non-Ionic Denaturant, Urea. *Experimental Eye Research*, *67*(6), 657–679. https://doi.org/10.1006/exer.1998.0561

Efthimiadou, E. K., Theodosiou, M., Toniolo, G., & Abu-Thabit, N. Y. (2018). 15—Stimuli-responsive biopolymer nanocarriers for drug delivery applications. In A. S. H. Makhlouf & N. Y. Abu-Thabit (Eds.), *Stimuli Responsive Polymeric Nanocarriers for Drug Delivery Applications, Volume 1* (pp. 405–432). Woodhead Publishing. https://doi.org/10.1016/B978-0-08-101997-9.00019-9

Faucon, C., Chalier, P., & Sanchez, C. (2022). On the relationship between volume fluctuations in liquids and the Gibbs free energy of cavity formation. *Journal of Molecular Liquids*, 119845. https://doi.org/10.1016/j.molliq.2022.119845

Gabrielii, I., & Gatenholm, P. (1998). Preparation and properties of hydrogels based on hemicellulose. *Journal of Applied Polymer Science*, *69*(8), 1661–1667. https://doi.org/10.1002/(SICI)1097-4628(19980822)69:8<1661::AID-APP19>3.0.CO;2-X

Ganguly, K., Patel, D. K., Dutta, S. D., Shin, W.-C., & Lim, K.-T. (2020). Stimuli-responsive self-assembly of cellulose nanocrystals (CNCs): Structures, functions, and biomedical applications. *International Journal of Biological Macromolecules*, *155*, 456–469. https://doi.org/10.1016/j.ijbiomac.2020.03.171

Giummarella, N., Pu, Y., Ragauskas, A. J., & Lawoko, M. (2019). A critical review on the analysis of lignin carbohydrate bonds. *Green Chemistry*, *21*(7), 1573–1595. https://doi.org/10.1039/C8GC03606C

Graziano, G. (2006). Scaled particle theory study of the length scale dependence of cavity thermodynamics in different liquids. *The Journal of Physical Chemistry. B*, *110*(23), 11421–11426. https://doi.org/10.1021/jp0571269

Grein-Iankovski, A., Ferreira, J. G. L., Orth, E. S., Sierakowski, M.-R., Cardoso, M. B., Simas, F. F., & Riegel-Vidotti, I. C. (2018). A comprehensive study of the relation between structural and physical chemical properties of acacia gums. *Food Hydrocolloids*, *85*, 167–175. https://doi.org/10.1016/j.foodhyd.2018.07.011

Hamid, J. (1992). *Mechanistic studies of the synthesis and decomposition of some amine-carbonyl condensation products* [Doctoral, Durham University]. http://etheses.dur.ac.uk/6083/

Hardingham, T. E. (1979). The role of link-protein in the structure of cartilage proteoglycan aggregates. *The Biochemical Journal*, *177*(1), 237–247. https://doi.org/10.1042/bj1770237

Heras-Mozos, R., Hernández, R., Gavara, R., & Hernández-Muñoz, P. (2022). Dynamic covalent chemistry of imines for the development of stimuli-responsive chitosan films as carriers of sustainable antifungal volatiles. *Food Hydrocolloids*, *125*, 107326. https://doi.org/10.1016/j.foodhyd.2021.107326

Huang, Y., Zhang, X., Ma, Z., Zhou, Y., Zheng, W., Zhou, J., & Sun, C. Q. (2015). Hydrogen-bond relaxation dynamics: Resolving mysteries of water ice. *Coordination Chemistry Reviews*, *285*, 109–165. https://doi.org/10.1016/j.ccr.2014.10.003

Idris, O. H. M., Williams, P. A., & Phillips, G. O. (1998). Characterisation of gum from Acacia senegal trees of different age and location using multidetection gel permeation chromatography. *Food Hydrocolloids*, *12*(4), 379–388. https://doi.org/10.1016/S0268-005X(98)00058-7

Jaishankar, A., Wee, M., Matia-Merino, L., Goh, K. K. T., & McKinley, G. H. (2015). Probing hydrogen bond interactions in a shear thickening polysaccharide using nonlinear shear and extensional rheology. *Carbohydrate Polymers*, *123*, 136–145. https://doi.org/10.1016/j.carbpol.2015.01.006

Kacuráková, M., Capek, P., Sasinková, V., Wellner, N., & Ebringerová, A. (2000). FT-IR study of plant cell wall model compounds: Pectic polysaccharides and hemicelluloses. *Carbohydrate Polymers*, *43*(2), 195–203. https://doi.org/10.1016/S0144-8617(00)00151-X

Katayama, T., Ogasawara, T., Sasaki, Y., Al-Assaf, S., & Phillips, G. (2008). *Composition Containing Hydrogel Component Derived from Gum Arabic* (United States Patent No. US20080038436A1). https://patents.google.com/patent/US20080038436A1/en

Košíková, B., Joniak, D., & Kosáková, L. (1979). *On the Properties of Benzyl Ether Bonds in the Lignin-Saccharidic Complex Isolated from Spruce*. *33*(1), 11–14. https://doi.org/10.1515/hfsg.1979.33.1.11

Kuharski, R. A., Bader, J. S., Chandler, D., Sprik, M., Klein, M. L., & Impey, R. W. (1988). Molecular model for aqueous ferrous–ferric electron transfer. *The Journal of Chemical Physics*, *89*(5), 3248–3257. https://doi.org/10.1063/1.454929

Lamport, D., & Várnai, P. (2013). Periplasmic arabinogalactan glycoproteins act as a calcium capacitor that regulates plant growth and development. *New*

Phytologist, *197*(1), 58–64. https://doi.org/10.1111/nph.12005

Lamport, D., Varnai, P., & Seal, C. (2014). Back to the future with the AGP-Ca2+ flux capacitor. *Annals of Botany*, *114*. https://doi.org/10.1093/aob/mcu161

Lee, B. (1985). The physical origin of the low solubility of nonpolar solutes in water. *Biopolymers*, *24*(5), 813–823. https://doi.org/10.1002/bip.360240507

Leonor, S. J., Gómez, J. A., Kinoshita, A., Calandreli, I., Tfouni, E., & Baffa, O. (2013). ESR spectroscopic properties of irradiated gum Arabic. *Food Chemistry*, *141*(3), 1860–1864. https://doi.org/10.1016/j.foodchem.2013.04.095

Li, J., Vasanthan, T., & Bressler, D. C. (2012). Improved cold starch hydrolysis with urea addition and heat treatment at subgelatinization temperature. *Carbohydrate Polymers*, *87*(2), 1649–1656. https://doi.org/10.1016/j.carbpol.2011.09.061

Liang, Y., Li, L., Scott, R., & Kiick, K. (2017). 50th Anniversary Perspective: Polymeric Biomaterials: Diverse Functions Enabled by Advances in Macromolecular Chemistry. *Macromolecules*, *50*. https://doi.org/10.1021/acs.macromol.6b02389

Lopez-Hernandez, F., Tryfona, T., Rizza, A., Yu, X., Harris, M. O. B., Webb, A., Kotake, T., & Dupree, P. (2020). Calcium Binding by Arabinogalactan Polysaccharides Is Important for Normal Plant Development. *The Plant Cell*, *32*(10), 3346–3369. https://doi.org/10.1105/tpc.20.00027

Lopez-Torrez, L., Nigen, M., Williams, P., Doco, T., & Sanchez, C. (2015). Acacia senegal vs. Acacia seyal gums – Part 1: Composition and structure of hyperbranched plant exudates. *Food Hydrocolloids*, *51*, 41–53. https://doi.org/10.1016/j.foodhyd.2015.04.019

Maciel, J. S., Silva, D. A., Paula, H. C. B., & de Paula, R. C. M. (2005). Chitosan/carboxymethyl cashew gum polyelectrolyte complex: Synthesis and thermal stability. *European Polymer Journal*, *41*(11), 2726–2733. https://doi.org/10.1016/j.eurpolymj.2005.05.009

Manabe, T., & Jin, Y. (2005). Alkaline cleavage of covalent bonds in chicken insulin and bovine alpha-lactalbumin analyzed by matrix-assisted laser desorption/ionization-mass spectrometry. *Electrophoresis*, *26*(1), 257–267. https://doi.org/10.1002/elps.200406153

Manrique, G. D., & Lajolo, F. M. (2002). FT-IR spectroscopy as a tool for measuring degree of methyl esterification in pectins isolated from ripening papaya fruit. *Postharvest Biology and Technology*, *25*(1), 99–107. https://doi.org/10.1016/S0925-5214(01)00160-0

Martell, A. E., & Herbst, R. M. (1941). Condensation of amides with carbonyl compounds: Benzyl carbamate with aldehydes and alpha keto acids. *The Journal of Organic Chemistry*, *06*(6), 878–887. https://doi.org/10.1021/jo01206a013

McGrane, S. J., Mainwaring, D. E., Cornell, H. J., & Rix, C. J. (2004). The Role of Hydrogen Bonding in Amylose Gelation. *Starch - Stärke*, *56*(3–4), 122–131. https://doi.org/10.1002/star.200300242

McQueen-Mason, S., & Cosgrove, D. J. (1994). Disruption of hydrogen bonding between plant cell wall polymers by proteins that induce wall extension. *Proceedings of the National Academy of Sciences of the United States of America*, *91*(14), 6574–6578.

Mejia Tamayo, V. (2018). *Volumetric properties of Arabinogalactan-proteins from Acacia Gum*. Montpellier SupAgro.

Mendoza-Hernández, G., Minauro, F., & Rendón, J. L. (2000). Aggregation, dissociation and unfolding of glucose dehydrogenase during

urea denaturation. *Biochimica et Biophysica Acta (BBA) - Protein Structure and Molecular Enzymology*, *1478*(2), 221–231. https://doi.org/10.1016/S0167-4838(00)00025-X

Phillips, G. O. (2009). Molecular association and function of arabinogalactan protein complexes from tree exudates. *Structural Chemistry*, *20*(2), 309–315. https://doi.org/10.1007/s11224-009-9422-3

Phillips, G. O., & Williams, P. A. (1993). The specification of the gum Arabic of commerce. In *Food hydrocolloids: Structures, Properties, and Functions* (pp. 45–63). Springer Science + Business Media. 10.1007/978-1-4615-2486-1_4

Protopopova, A. D., Ramirez, A., Klinov, D. V., Litvinov, R. I., & Weisel, J. W. (2019). Factor XIII topology: Organization of B subunits and changes with activation studied with single-molecule atomic force microscopy. *Journal of Thrombosis and Haemostasis: JTH*, *17*(5), 737–748. https://doi.org/10.1111/jth.14412

Qi, X., Watanabe, M., Aida, T. M., & Smith Jr, R. L. (2010). Fast Transformation of Glucose and Di-/Polysaccharides into 5-Hydroxymethylfurfural by Microwave Heating in an Ionic Liquid/Catalyst System. *ChemSusChem*, *3*(9), 1071–1077. https://doi.org/10.1002/cssc.201000124

Renard, D., Lavenant-Gourgeon, L., Lapp, A., Nigen, M., & Sanchez, C. (2014). Enzymatic hydrolysis studies of arabinogalactan-protein structure from Acacia gum: The self-similarity hypothesis of assembly from a common building block. *Carbohydrate Polymers*, *112*, 648–661. https://doi.org/10.1016/j.carbpol.2014.06.041

Risica, D., Dentini, M., & Crescenzi, V. (2005). Guar gum methyl ethers. Part I. Synthesis and macromolecular characterization. *Polymer*, *46*(26), 12247–12255. https://doi.org/10.1016/j.polymer.2005.10.083

Rudnik, E. (2013). 11—Biodegradability Testing of Compostable Polymer Materials. In S. Ebnesajjad (Ed.), *Handbook of Biopolymers and Biodegradable Plastics* (pp. 213–263). William Andrew Publishing. https://doi.org/10.1016/B978-1-4557-2834-3.00011-2

Sanchez, C., Nigen, M., Mejia Tamayo, V., Doco, T., Williams, P., Amine, C., & Renard, D. (2018). Acacia gum: History of the future. *Food Hydrocolloids*, *78*, 140–160. https://doi.org/10.1016/j.foodhyd.2017.04.008

Sanchez, C., Renard, D., Robert, P., Schmitt, C., & Lefebvre, J. (2002). Structure and rheological properties of acacia gum dispersions. *Food Hydrocolloids*, *16*(3), 257–267. https://doi.org/10.1016/S0268-005X(01)00096-0

Sasaki, Y., Ogasawara, T., Katayama, T., & Sakata, M. (2014). *Process for producing modified gum arabic* (United States Patent No. US8722129B2). https://patents.google.com/patent/US8722129B2/en

Schmidt, A., Prager, M., Selmke, P., & Buddecke, E. (1982). Isolation and Properties of Proteoglycans from Bovine Aorta. *European Journal of Biochemistry*, *125*(1), 95–101. https://doi.org/10.1111/j.1432-1033.1982.tb06655.x

Schong, E. (2017). *Assemblages microniques de protéines sériques produits par étuvage à pH 9,5: Mécanisme de formation et propriétés physico-chimiques et fonctionnelles* [Agrocampus Ouest]. http://theses.fr/2017NSARB302

Seki, T., Chiang, K.-Y., Yu, C.-C., Yu, X., Okuno, M., Hunger, J., Nagata, Y., & Bonn, M. (2020). The Bending Mode of Water: A Powerful Probe for Hydrogen Bond Structure of Aqueous Systems. *The Journal of Physical Chemistry Letters*, *11*(19), 8459–8469.

https://doi.org/10.1021/acs.jpclett.0c01259

Showalter, A. M. (2001). Arabinogalactan-proteins: Structure, expression and function. *Cellular and Molecular Life Sciences*, *58*(10), 1399–1417. https://doi.org/10.1007/PL00000784

Simat, T., Meyer, K., & Steinhart, H. (1994). Synthesis and analysis of oxidation and carbonyl condensation compounds of tryptophan. *Journal of Chromatography A*, *661*(1), 93–99. https://doi.org/10.1016/0021-9673(94)85180-8

Sun, C. Q. (2018). Supersolidity of undercoordinated and hydrating water. *Physical Chemistry Chemical Physics*, *20*(48), 30104–30119. https://doi.org/10.1039/C8CP06115G

Sun, C. Q., Zhang, X., Zhou, J., Huang, Y., Zhou, Y., & Zheng, W. (2013). Density, Elasticity, and Stability Anomalies of Water Molecules with Fewer than Four Neighbors. *The Journal of Physical Chemistry Letters*, *4*(15), 2565. https://doi.org/10.1021/jz401029z

Sussman, I. I., & Weiss, H. J. (1976). Spontaneous aggregation of low molecular weight factor VIII and its prevention by 2mM CaCl2. *Thrombosis Research*, *9*(3), 267–276. https://doi.org/10.1016/0049-3848(76)90216-4

Tanford, C. (1970). Protein Denaturation: Part C. In C. B. Anfinsen, J. T. Edsall, & F. M. Richards (Eds.), *Advances in Protein Chemistry* (Vol. 24, pp. 1–95). Academic Press. https://doi.org/10.1016/S0065-3233(08)60241-7

Tonković, M., & Bilinski, H. (1995). Glucose and glucuronic acid interactions with hydrolysed aluminium(III). *Polyhedron*, *14*(8), 1025–1030. https://doi.org/10.1016/0277-5387(94)00341-B

Tsukino, M., & Kunitake, T. (1979). The Microstructure of Poly(divinyl acetal)s as Determined by 13C NMR Spectroscopy. Ring Stereochemistry and Isomerization Propagation. *Polymer Journal*, *11*(6), 437–447. https://doi.org/10.1295/polymj.11.437

Vanloot, P., Dupuy, N., Guiliano, M., & Artaud, J. (2012). Characterisation and authentication of A. senegal and A. seyal exudates by infrared spectroscopy and chemometrics. *Food Chemistry*, *135*(4), 2554–2560. https://doi.org/10.1016/j.foodchem.2012.06.125

Vinod, V., & Sashidhar, R. B. (2010). Surface morphology, chemical and structural assignment of gum Kondagogu (Cochlospermum gossypium DC.): An exudate tree gum of India. *Undefined*. https://www.semanticscholar.org/paper/Surface-morphology%2C-chemical-and-structural-of-gum-Vinod-Sashidhar/d280c01183eceb9853a76de47f5aea150d16b471

Xie, J., Ren, Y., Xiao, Y., Luo, Y., & Shen, M. (2021). Interactions between tapioca starch and Mesona chinensis polysaccharide: Effects of urea and NaCl. *Food Hydrocolloids*, *111*, 106268. https://doi.org/10.1016/j.foodhyd.2020.106268

Zhang, Z., He, C., & Chen, X. (2018). Hydrogels based on pH-responsive reversible carbon–nitrogen double-bond linkages for biomedical applications. *Materials Chemistry Frontiers*, *2*(10), 1765–1778. https://doi.org/10.1039/C8QM00317C

Zohuriaan, M. J., & Shokrolahi, F. (2004). Thermal studies on natural and modified gums. *Polymer Testing*, *23*(5), 575–579. https://doi.org/10.1016/j.polymertesting.2003.11.001

CHAPTER VI.

FUNCTIONAL PROPERTIES OF AGP AGGREGATES OBTAINED FROM DEMINERALIZED ACACIA *SEYAL* GUM

Effect of aggregation on the physicochemical properties of arabinogalactan-proteins from A. *seyal* gum

Amandine Antoine-Michard[a,b], Céline Charbonnel[a], Isabelle Jaouen[b], Christian Sanchez[a] and Michaël Nigen[a,*]

[a] UMR IATE, Univ Montpellier, INRAE, Institut Agro, 34060 Montpellier, France

[b] ALLAND & ROBERT, 75003, Paris, France

* Corresponding author.

E-mail address : michael.nigen@umontpellier.fr

Abbreviations

GA: Acacia gum; AGPs: arabinogalactan-proteins; EGEO: ester gum/sweet orange essential oil

Abstract

Acacia gum (GA) from A. *senegal* and A. *seyal* species is an edible additive used in food industry for its good emulsifying properties. Among the two species authorized by the FAO, A. *senegal* has much better properties. GA does not have interesting rheological properties as it provides low viscosity dispersions even at high concentrations. The storage of demineralized A. *seyal* gum in dry state produces aggregates of controlled solubility and sizes, depending on the incubation time. In spite of similar interfacial properties, the emulsifying properties of A. *seyal* were enhanced by our process with a reduction of the oil droplet size in emulsions by 20, and a stability close to that of A. *senegal* emulsions. At 15%, the viscosity of aggregated demineralized A. *seyal* was increased up to 250 times. In particular, the presence of insoluble microparticles drastically modified the flow behavior of the starting material, with a switch from Newtonian to shear-thinning behavior with aggregation. The formation of a hydrogel at long incubation times indicated that the aggregates formed are highly cross-linked.

Keywords: Acacia gums, Arabinogalactan-proteins, Aggregation, Hydrogel, Emulsion stability.

1. Introduction

Acacia gum (GA) is a hyperbranched polysaccharide found in nature as a mixed salt of a polysaccharide acid, arabic acid (Anderson & Stoddart, 1966; Islam et al., 1997; Verbeken et al., 2003). GA is made of a continuum of arabinogalactan-proteins (AGPs) differing in biochemical composition, charge density, molar mass, size, shape and anisotropy (Islam et al., 1997; Lopez-Torrez et al., 2015; Randall et al., 1989; Renard et al., 2006, 2012, 2014). These biopolymers are composed of more than 90% of sugars, with a small protein fraction (1-3%) and some minor components, which are mainly cationic minerals (Debon & Tester, 2001; Idris et al., 1998; Kunkel et al., 1997) and small amounts of polyphenols (Sanchez et al., 2018).

GA is used as food additive (coded E414 in Europe) and in non-food applications as emulsifier, stabilizer, humectant, bulking agent, coating agent, or antioxidant (Touré, 2008; Verbeken et al., 2003; Wickens et al., 1995). For instance, GA is responsible for the stabilization of aroma compounds, by reducing the surface tension between the two emulsion phases and improving the rigidity of the interfacial film (Castellani, Guibert, et al., 2010; Erni et al., 2007; Glicksman & Sand, 1973; Verbeken et al., 2003). However, GA provides low-viscosity dispersions even at concentrations up to 30% which explains why GA is not used for its rheological properties (viscosifying or gelling), except at these high concentrations (Touré, 2008; Verbeken et al., 2003).

AGPs from GA have a natural propensity to aggregate both *in vivo* during the gum exudation by the Acacia tree and its maturation (Capataz-Tafur et al., 2011; Idris et al., 1998; Phillips, 2009), and *in vitro* after harvest during its processing or storage (Al-Assaf, Phillips, Aoki, et al., 2007; Al-Assaf et al., 2012; Aoki, Al-Assaf, et al., 2007; Idris et al., 1998; Phillips & Williams, 1993; Sanchez et al., 2002). Incubation of GA powder under controlled physicochemical conditions is a promising way to reproduce experimentally the natural maturation process taking place in GA nodules (Al-Assaf, Phillips, Aoki, et al., 2007) and it had been the subject of a series of patents released in the last decades (Al-Assaf et al., 2004; Hayashi, 2002; Katayama et al., 2008; Sasaki et al., 2014). AGP aggregation caused by the dry incubation of GA was reported over a wide range of temperatures and relative humidity (RH), from 20°C to 200°C and from 30 to 100%RH. Al-Assaf et al. showed that M_w of a spray-dried A. *seyal* heated for 24h at 110°C increased from 1.15 to $1.45 \cdot 10^6$ g·mol^{-1}. Under the same conditions, a spray-dried A. *senegal* aggregated to a higher extent as shown by an increase in M_w from $0.60 \cdot 10^6$ to $1.43 \cdot 10^6$ g·mol^{-1} (Al-Assaf et al., 2004).

These molecular associations also affect the size and shape of AGPs, and can consequently deeply modify their physicochemical properties. It had been shown very early that dehydration induced by the storage of GA in the dry state was responsible for an increase in viscosity (Gabel, 1930) and a loss of solubility of the samples (Moorjani & Narwani, 1948). The formation of insoluble compounds during the dehydration of demineralized GA (arabic acid) was also observed (Mantell, 1954). These insoluble biopolymers form a hydrogel upon dry heating that represents 28% of the whole sample after 96h of dry heating at 110°C (Al-Assaf, Phillips, Aoki, et al., 2007) and even reach 92% after 10 days at 120°C (Katayama et al., 2008). Incubation

in dry state also greatly improves the water-binding ability of A. *senegal* as illustrated by an increase by 5 of water-retention ability of GA incubated at 120°C during 24h (Al-Assaf, Phillips, Aoki, et al., 2007; Katayama et al., 2008).

A great interest was shown on the enhancement of the interfacial (Castellani, Al-Assaf, et al., 2010) and emulsifying properties of GA – especially A. *senegal* – by this maturation process (Al-Assaf et al., 2004; Al-Assaf, Phillips, Aoki, et al., 2007; Aoki, Katayama, et al., 2007; Castellani, Guibert, et al., 2010; Hayashi, 2002; Sasaki et al., 2014; Tipvarakarnkoon et al., 2010). Aggregated gums improved the colloidal stability of emulsions, with a reduction of oil droplet size compared to the control gum, higher homogeneity of the oil droplet size distribution and less destabilization over time (Al-Assaf et al., 2004; Hayashi, 2002; Sasaki et al., 2014). The volumetric droplet size ($D_{4,3}$) decreased by 31% in emulsions freshly prepared using raw GA stored for 12h at 60°C and 70%RH compared to control GA (Hayashi, 2002). After storage of cracked GA for 36h at 110°C, this decrease was 20% (Castellani, Guibert, et al., 2010). The differences observed arise from the relative humidity conditions and the gum particle size which both influence the aggregation kinetics. After the ageing of emulsions for 7 days at 60°C, the presence of aggregates had even a stronger effect with 82% decrease in $D_{4,3}$ for the emulsion formulated with raw GA stored for 12h at 60°C (Hayashi, 2002). Castellani et al. showed that these properties are directly correlated with the good interfacial properties of matured gums at the air/water and oil/water interfaces (Castellani, Al-Assaf, et al., 2010; Castellani, Guibert, et al., 2010). At the air/water interface, the adsorption kinetics were 3 times faster with matured gum compared to control gum and after 3h of experiment the interfacial tension dropped from 70 to 57.4 and 52 $mN \cdot m^{-1}$ for matured and control gum, respectively (Castellani, Guibert, et al., 2010). Good interfacial properties of GA are usually related to the content of high molar mass protein-rich AGPs, the accessibility of the protein moiety to the interface, the net surface charge (mainly due to uronic acid content), surface hydrophobicity and flexibility (Aphibanthammakit et al., 2020; Beverung et al., 1999; Dickinson et al., 1988). Matured gums contain a higher amount of high molar mass AGPs combined with a greater number of intermolecular interaction and a more accessible protein part compared to control gum (Al-Assaf, Phillips, Aoki, et al., 2007; Castellani, Al-Assaf, et al., 2010; Castellani, Guibert, et al., 2010). All these features can explain the improved interfacial properties of aggregated gums and in turn their emulsifying properties.

Recently, we evidenced the aggregation of AGPs from demineralized A. *seyal* gum incubated in dry state at T = 25 – 70 °C. According to the incubation time, soluble aggregates and insoluble microparticles with controlled size (from 20 nm to 200 µm) were obtained (Antoine-Michard et al., 2022, in publication). This study aimed to examine the influence of these AGP aggregates and microparticles on the physico-chemical properties of A. *seyal* gum. A characterization of the flow and viscoelastic properties of soluble aggregates and microparticles was first carried out. The interfacial (interfacial tension kinetics and interfacial dilatational rheology) and emulsifying properties of soluble AGP aggregates were studied and compared to those of unmodified A. *seyal* gum and A. *senegal* gum.

2. Materials and methods

2.1 Materials

A. *seyal* gum (lot OF183377), A. *senegal* gum (lot OF152413) and a mix of sweet orange essential oil and ester gum at a ratio 1:1 (used as oil phase to formulate emulsions) were provided by ALLAND & ROBERT Company—Natural and Organic gums (Port Mort, France). An ionic exchange resin (Purolite® C160MBH, Purolite Ltd, Llantrisant, Wales) was used to remove all the minerals (cations) from A. *seyal* gum. All reagents were purchased from Sigma-Aldrich (St. Louis, MO, USA). Ultrapure deionized water (18.2 MΩ·cm) was used in all experiments.

2.2 Preparation of arabic acid powder

A 16wt% A. *seyal* gum dispersion was prepared in water (pH 4.6) and stirred overnight using a magnetic stirring plate at 250 rpm to allow complete hydration of the gum. Cations from A. *seyal* gum were removed using an ionic exchange resin at a mass ratio gum:resin of 1:1. The pH of the dispersion was verified and the demineralization was complete once it reached the value of 2.1. The demineralized A. *seyal* gum was then named as usual arabic acid. Arabic acid dispersion was centrifuged (12,000 rpm, 30 min, 20 °C) with an Avanti J-26S XP (Beckman Coulter) to remove insoluble material (<1%) before spray-drying (Büchi B-290, Büchi Labortechnik AGt, Switzerland).

2.3 Incubation of arabic acid powder and preparation of arabic acid dispersions

About 300 mg of arabic acid powder were incubated in closed glass vessels at 40°C in a HPP 260 climate chamber (Memmert, Schwabach, Germany). Samples were regularly collected during incubation kinetics and directly stored at -20°C to stop their aggregation. The GA dispersions at concentrations from 0.5 to 30wt% (db) were prepared in milliQ water using A. *seyal*, A. *senegal*, and incubated arabic acid powder. Dispersions were stirred overnight using an orbital plate at 250 rpm. At 5wt%, the pH of arabic acid dispersions was around 2.4 whereas pH of GA (A. *seyal* and A. *senegal* gums) was around 4.5.

For studying interfacial and emulsifying properties, the pH of arabic acid dispersions was adjusted to the pH of A. *seyal* at the same concentration, using a mixture of $Ca(OH)_2$, $Mg(OH)_2$ and KOH. Salt hydroxide ratio was adapted to mimic the mineral composition of A. *seyal* gum and dispersions were further centrifuged (12,000 rpm, 30 min, 25°C) to remove insoluble material.

2.4 Rheological measurements

Steady-shear and dynamic viscoelastic properties of GA and arabic acid dispersions at 1 – 30wt% were determined at 25 °C using a stress-controlled MCR 702 TwinDrive rheometer (Anton Paar, les Ulis, France) coupled with a sanded coaxial cylindrical geometry (CC20) with 1 mm gap and an outer radius/inner radius ratio of 1.1. Before experiments, all samples were pre-sheared at 5 – 10 s^{-1} for 3min. All experiments were done in duplicate.

2.4.1 Steady-shear measurements

For A. *seyal* and arabic acid dispersions, flow curves were recorded for shear rates decreasing from 1000 to 0.1 s^{-1}, whereas for arabic acid AGP aggregates dispersions, the lower shear rate bound was decreased to 10^{-6} s^{-1}.

2.4.2 Dynamic measurements

Dynamic oscillatory rheological properties of GA dispersions (15wt %) at 25 °C were determined by frequency sweep measurements at 1% strain for a frequency range from 1 to 100 rad·s^{-1}. The mechanical behavior of samples was analyzed by measuring the frequency-dependent storage (G') and loss (G'') moduli.

2.5 Interfacial properties of AGPs from A. seyal and arabic acid

The interfacial tension and dilatational rheological properties at 25°C of arabic acid samples were determined through the rising droplet shape method using a drop tensiometer (Tracker, IT concept, Longessaigne, France). Limonene and octanol were selected as organic compounds representative of hydrophobic and more polar liquids, respectively. A 500 µL syringe was filled with limonene or octanol, and connected to a curved needle. A drop of liquid was formed at the end of the needle immersed in a 5 mL glass cuvette containing a 5 wt% gum dispersion. The droplet volume of limonene and octanol was 10 µL and 2.5 µL, respectively, due to differences in stability of the formed droplets. The shape of the drop was monitored by a CCD camera and data were recorded for 24h.

The interfacial tension γ was calculated using the Young-Laplace equation:

$$\Delta P = \gamma \cdot \left(\frac{1}{R} + \frac{1}{R'}\right) \quad \text{(VI.1)}$$

where R and R' are the main radii of curvature of droplets and ΔP is the Laplace pressure corresponding to the pressure difference across the interface.

Interfacial viscoelastic parameters were obtained by applying a sinusoidal variation to the droplet volume (and thus compression/expansion cycles) at 10% of amplitude (ΔV/V), and 0.1 Hz of oscillation frequency ω. Measurements consisted of a repetition of 5 oscillation cycles, of 10s each, followed by a 50s blank period. The surface dilatational viscoelasticity (Eq. VI.4) and the phase angle were obtained from the sinusoidal change in interfacial tension γ (Eq. VI.2) resulting from a small change in the surface area (Eq. VI.3):

$$\gamma = \gamma_0 \sin(\omega t + \delta) \quad \text{(VI.2)}$$

$$A = A_0 \sin(\omega t) \quad \text{(VI.3)}$$

$$E = A(\Delta\gamma)/\Delta A \quad \text{(VI.4)}$$

The obtained modulus (E*) is a complex quantity that can be expressed as

$$E^* = E' + iE''$$

where the real part E' is dilatational elasticity and the imaginary part E" corresponds to the surface dilatational viscosity. All measurements were performed in duplicate.

2.6 Emulsifying properties of AGPs from A. seyal and arabic acid

2.6.1 Preparation of oil-in-water emulsions

Two different liquids were used to formulate oil-in-water emulsions, namely limonene and a mix ester gum/sweet orange essential oil (EGEO) formulated at a ratio 1:1. Oil was added to GA dispersion and the system was premixed using rotor/stator homogenizer (Silverson L4RT, Evry, France) equipped with a square hole high shear screen stator at 7,500 rpm for 5min at room temperature (25°C). Then, the coarse emulsions were homogenized using a microfluidizer with a F12Y diamond interaction chamber (LM20, Microfluidics Corporation, MA, USA) operating at a pressure of 440 bars. The emulsion was passed through the homogenizer 2 times. In order to control the temperature during the emulsification step, the emulsion was recovered in a container immersed in an ice bath. All emulsions were prepared in triplicate.

2.6.2 Volumetric size distribution of emulsion droplets

The volumetric droplet size distribution of emulsions was determined by laser light scattering using a LS 13 320 XR laser diffraction particle size analyzer equipped with the Universal Liquid Module ULM (Beckman Coulter). The obscuration was set up at ~ 10%. Refractive index of 1.33 for water, 1.47 for limonene and 1.50 for EGEO were used. For all emulsions, three cycles of measurements were performed 10 minutes after the emulsification step. The mean volume diameter ($D_{4,3}$) was calculated as follows:

$$D_{4,3} = \sum n_i d_i^4 \Big/ \sum n_i d_i^3 \qquad \text{(VI.5)}$$

where n_i is the number of droplets of diameter d_i.

2.6.3 Estimation of emulsion stability

The colloidal stability of emulsions was monitored using a Turbiscan Tower (Formulaction, Toulouse, France) that allowed characterizing destabilization phenomena such as creaming, sedimentation, flocculation and coalescence. 15 mL emulsion sample were loaded into cylindrical glass cells about 5 minutes after emulsification and scanned over the whole height.

The light backscattering (BS in %) and transmittance (T in %) signals from a pulsed near infrared light source (λ = 880 nm) were recorded at least every 5 minutes during the first 24 hours before recording one measurement at days 2, 3, 7, and then once a week during the storage of emulsions at 25°C. Signals were then analyzed using the TowerSoft software version 1.3.1.85.

Based on the evolution of backscattered or transmitted light during storage, the Creaming Index (CI) and the Turbiscan Stability Index (TSI) were calculated. The CI is usually calculated as the serum layer height relative to the total emulsion height (Keowmaneechai & McClements, 2002). In our emulsions, the serum layer was hard to measure in the bottom of emulsions tubes and an alternative formula was preferred (Fligner et al., 1991) in order to better discriminate among our emulsions:

$$\mathrm{CI}\ (\%) = 100 \times \frac{H_c}{H_t}$$

where H_c is the height of the cream layer and H_t is the total height of emulsion.

While CI is a specific stability index, the TSI parameter is an indicator of the global stability of emulsions over time. It is arbitrarily calculated using the equation:

$$\mathrm{TSI(t)} = \frac{1}{N_h}\sum_{t_i=1}^{t_{max}}\sum_{z_i=z_{min}}^{z_{max}}|\mathrm{BST}(t_i, z_i) - \mathrm{BST}(t_{i-1}, z_i)| \qquad \text{(VI.6)}$$

with t_{max} the time t at which the TSI is calculated, z_{min} and z_{max} the lower and upper selected height limits respectively, $N_h = (z_{max} - z_{min}) \,/\, \Delta h$ the number of height positions in the selected zone of the scan and BST the light intensity. BST takes values of the BS signal when $T < 0.2\%$ and values of the T signal otherwise.

3. Results and discussion

AGP aggregates were obtained by the storage at 40°C of arabic acid powder (t_0). In the following, these aggregates will be named as t_i with i the incubation time. Aggregates of different sizes and solubility were formed during storage, from soluble aggregates between 0 and 2 days to insoluble microparticles for longer incubation times (3 – 7 days).

3.1 Rheological properties

The rheological properties of Acacia gum and arabic acid throughout incubation time were investigated at 25 °C. Figure VI.1 shows the apparent viscosity (Pa·s) of A. *seyal* gum dispersions at concentrations between 15 and 30wt% as a function of the shear-rate (s^{-1}). At all concentrations studied, the flow behavior of A. *seyal* gum dispersions displayed a Newtonian behavior, characterized by a viscosity plateau in the shear rate range 0.5 – 1000 s^{-1}. An increase of apparent viscosity by 13 between 15wt% (η = 16 mPa·s) and 30wt% (η = 204 mPa·s) was observed. The apparent viscosity value at 20wt% (η = 38 mPa·s) is close than the value of 29 mPa.s reported in the prior Aphibanthammakit Ph.D. project (Aphibanthammakit, 2018) for A. *seyal* gum dispersion at the same concentration.

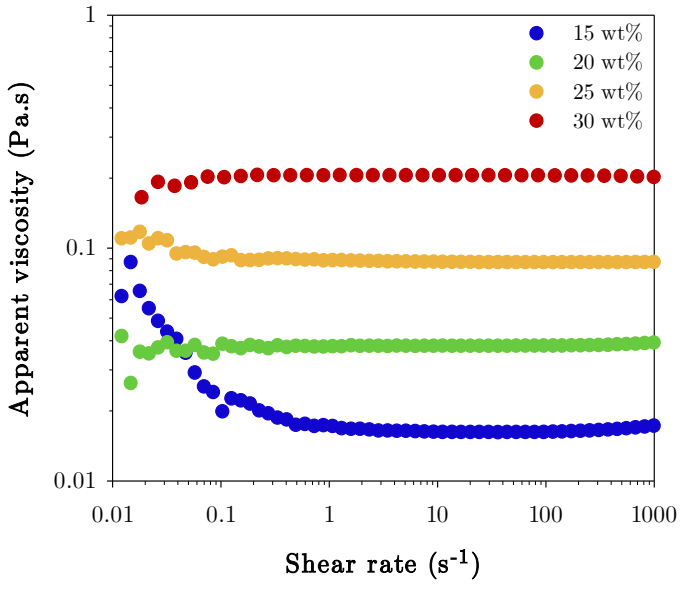

Figure VI.1. Flow curves of A. *seyal* gum dispersions prepared at concentrations ranging from 15 to 30wt%. Measurements were done at decreasing shear rates, from 1000 s^{-1} to 10^{-2} s^{-1}, using a low shear Couette-type rheometer.

Under low shear rates ($< 1s^{-1}$), 15wt% A. *seyal* gum presented a decrease in apparent viscosity while increasing the shear rate, *i.e.* a shear-thinning flow behavior. This had been also observed by Lopez-Torrez for low shear rate conditions ($< 5\ s^{-1}$) and at low A. *seyal* gum concentrations (< 5wt%) (Lopez-Torrez, 2016). This observation was attributed to the presence of micro aggregates, that could be dissociated when applying high shear (Mothé & Rao, 1999); but could also be caused by the surface properties of Acacia gum AGPs – as it was observed with BSA (Sharma et al., 2011) – which can form an interfacial viscoelastic film at the sample interface (Sanchez et al., 2002). As this shear-thinning behavior at low shear rate is not observed at concentrations higher than 15wt% it could be suggested that the viscosity is controlled either by the bulk properties at high concentrations or by the interfacial film at lower concentration under low shear rates.

The flow behavior of 15wt% arabic acid dispersions throughout incubation time of arabic acid powder was also studied. Figure VI.2A shows that the flow behavior of arabic acid dispersion displayed a Newtonian behavior above 0.1 s^{-1}. Apparent viscosity of arabic acid ($\eta = 14$ mPa·s) was very close to viscosity of A. *seyal* gum at the same concentration ($\eta = 16$ mPa·s). The pH of 15wt% arabic acid dispersion (pH 2.1) differs from those of A. *seyal* dispersion at the same concentration (pH 4.6). Thus, one could expect a higher viscosity gap between the two gums due to different electrostatic potential. However, the overlap concentration of A. *seyal*, *i.e.* the concentration which delineates dilute from semi-dilute polymer solutions, had been found to be 14% (Lopez-Torrez, 2016). Above this concentration, neighboring chains overlap and interact and charges are partially screened (Dou & Colby, 2006), which could explain the similar values of apparent viscosity obtained.

Likewise, soluble AGP aggregates dispersions (from 0 to 2 days) were characterized by a Newtonian behavior up to 16 hours of incubation, with a viscosity plateau in the shear rate range 5 – 1000 s^{-1}. During the first day of incubation at 40°C, an increase in apparent viscosity from 14 mPa.s to 39 mPa.s was observed, caused by the presence of soluble aggregates (Antoine-Michard et al., 2022, in publication). At two days of incubation and above, the apparent viscosity of arabic acid dispersions became shear rate-dependent on the whole range of shear rate. Indeed, as the shear rate decreases from 1000 to $10^{-6}\ s^{-1}$, apparent viscosity keeps increasing, showing a shear-thinning behavior of the dispersions. For these samples, no Newtonian plateau was observed in the whole range of shear rate considered. This change in

viscosity profile is concomitant with the beginning of microparticles formation, having a size bigger than 10 µm and may be the sign of changes in AGP aggregates organization in dispersion, from an ordered and compact system to a more entangled one. This type of pattern was also reported for dispersions of dry heated whey protein isolates (T = 100°C), forming microspheres with a size ranging from 60 to 80 µm (Schong & Famelart, 2018) and for other whey protein concentrates, either conjugated with dextran or not (Lillard et al., 2009). A drastic modification of the flow behavior of 30wt% A. *seyal* gum dispersions from Newtonian to shear-thinning after submitting the gum in solid state to radiation treatment (26 kGy) had been also reported, with an increase of apparent viscosity at 100 s^{-1} by 5 from η = 0.2 Pa·s to η = 1 Pa·s (Al-Assaf, Phillips, Williams, et al., 2007; Al-Assaf & Phillips, 2006).

For a given shear rate, apparent viscosity increases with incubation time and the lower the shear rate, the higher the viscosity gap between the samples. The flow curves of arabic acid dispersions incubated for 4 days or more nearly overlapped. This is consistent with the increase in the amount of insoluble microparticles from 0 (2 days) until reaching the maximum plateau at 80% (at 4 – 5 days) as shown in Figure VI.2B. The proximity of these large microparticles (D(4,3) ~ 70 µm) formed during extended heating promotes interactions between aggregates, and create a strong network responsible for the increase in viscosity. Also, the apparent viscosities reached at low shear rates (< 0.001 s^{-1}) were particularly high, suggesting that arabic acid aggregates dispersions did not flow at rest.

Flow curves of arabic acid incubated for 2 days at 40°C were also studied at different concentrations of t_2 – which contains soluble AGP aggregates – to investigate if the flow behavior of these AGP aggregates was concentration-dependent (Figure VI.2C). When measured in the shear rate range 1000 – 0.01 s^{-1}, t_2 exhibited shear-thinning behavior at all concentrations studied (C = 1 – 15wt%) and this shear-thinning behavior was more pronounced at low concentrations, as observed with A. *seyal* gum. As a comparison, at 100 s^{-1}, 10wt% t_2 dispersion displays the same apparent viscosity than 20wt% A. *seyal* dispersion (~ 40 mPa.s). The formation of microgels obtained with matured A. *senegal* gum and whey protein isolates had been also reported in literature (Katayama et al., 2008; Schong & Famelart, 2018).

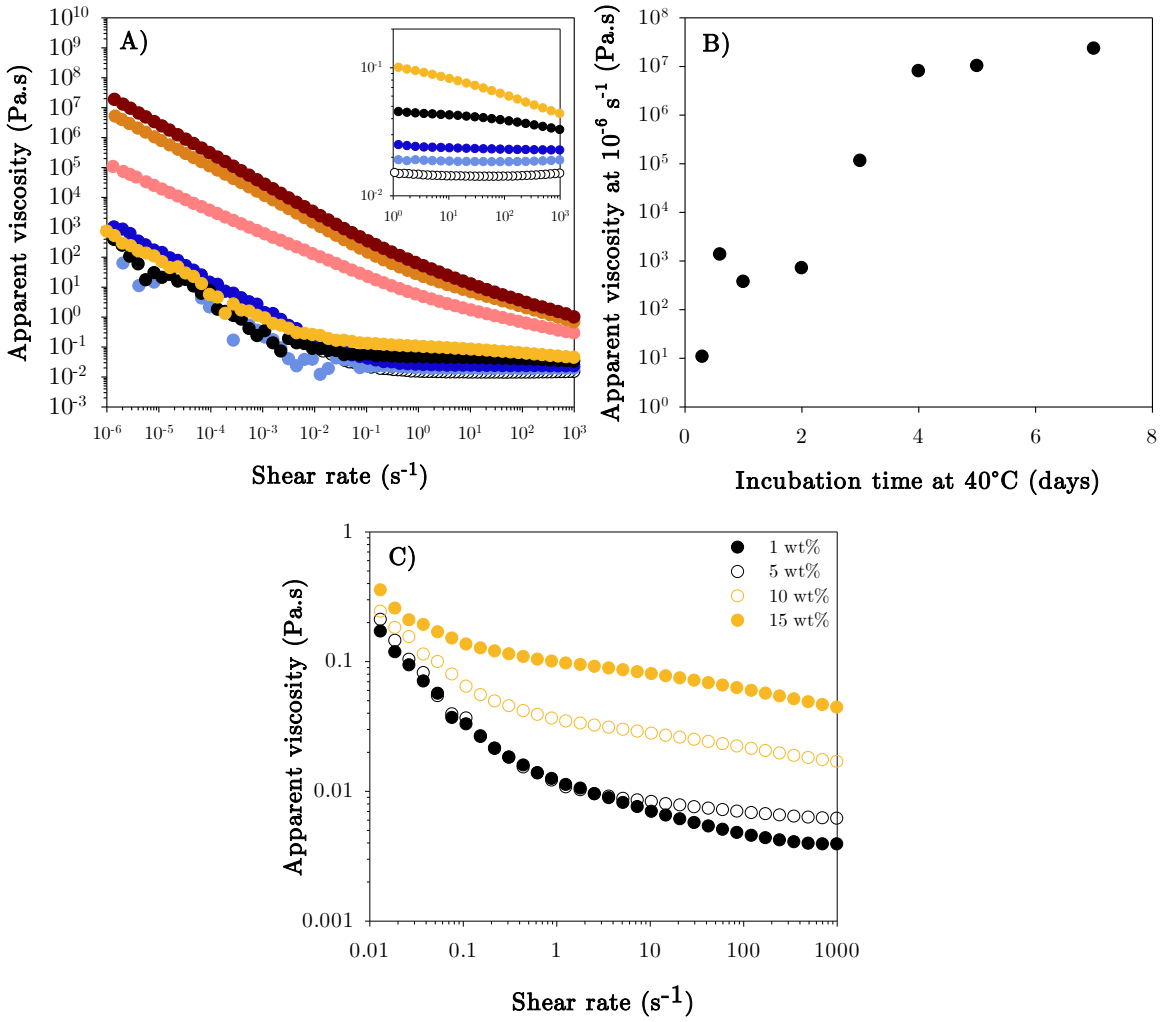

Figure VI.2. A) Flow curves of 15wt% arabic acid powder dispersions before (○) and after incubation of the powder for 8h (●), 16h (●), 1 day (●), 2 days (●), 3 days (●), 4 days (●), and 7 days (●) at 40°C. Inset highlights the differences in apparent viscosity of soluble aggregates. B) Apparent viscosity at 10^{-6} s^{-1} determined from Figure VI.2A, and C) Flow curves of 1wt% (●), 5wt% (○), 10wt% (○) and 15wt% (●) arabic acid powder dispersions after incubation of the powder for 2 days at 40°C. Measurements were done at decreasing shear rates, from 1000 s^{-1} to 10^{-6} s^{-1}, using a low shear Couette-type rheometer.

Viscoelastic properties of arabic acid dispersions at 15wt% were then studied using dynamic oscillatory measurements, at 1% strain and 25°C. The storage (G') and the loss (G'') moduli of arabic acid before (t_0) and after 2 (t_2) and 7 days of incubation (t_7) at 40°C are presented in Figure VI.3A. These samples are characterized by different stages of aggregation: a few soluble aggregates were present in t_0 after spray-drying, t_2 is composed of 100% of soluble aggregates and AGPs whereas t_7 contains 80% of insoluble microparticles (Antoine-Michard et al., 2022, in publication).

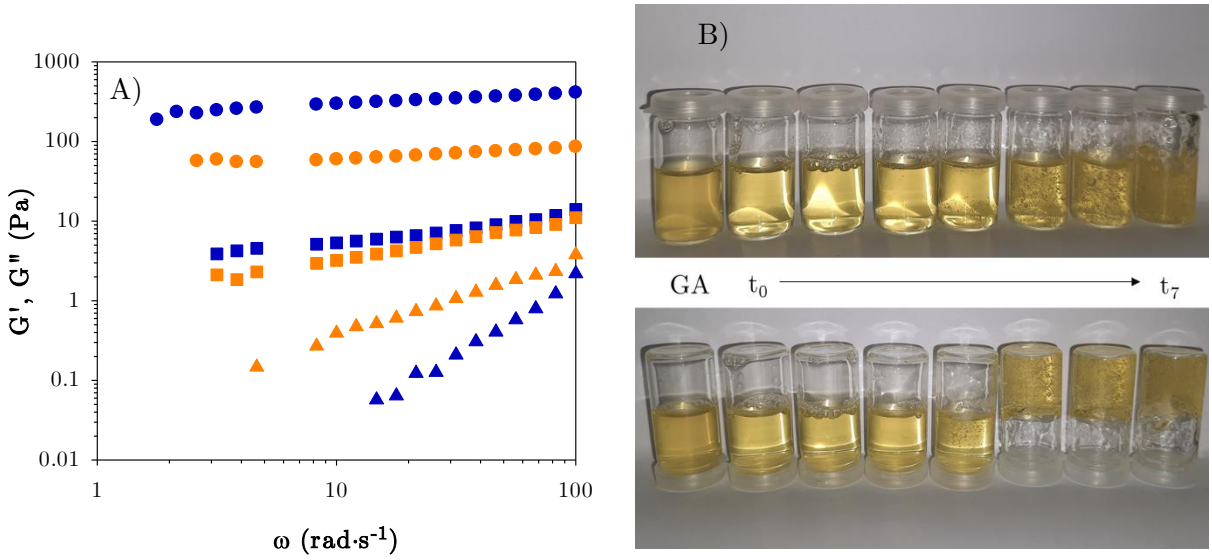

Figure VI.3. A) Storage G' (blue) and loss G'' (orange) moduli of 15wt% arabic acid powder dispersions at different incubations stages: before (▲), and after incubation of powders for 2 days (■), and 7 days (●) at 40°C. All experiments were performed at 1% strain. B) Visual observation of 15wt% aqueous dispersions of GA, arabic acid (t_0) and arabic acid AGP aggregates (from left to right: t_1, t_2, t_3, t_4, t_5, t_7).

For arabic acid (t_0), the loss modulus G" was above the storage modulus G' throughout all range of frequency studied indicating a liquid-like behavior, with a gap between G' and G'' higher at low frequencies. The moduli followed a power-law pattern with exponents equal to 1.9 and 0.9 for G' and G", respectively, which are classical values found for viscoelastic fluids. These values were higher than the 1.4 and 0.8 exponents for 6wt% dispersions of A. *senegal* gum, suggesting a less structured organization in arabic acid dispersions (Sanchez et al., 2002).

After 2 days of incubation at 40°C, G'' and G' curves were almost superimposed (with exponents of 0.4 and 0.5, respectively), with G' becoming slightly larger than G", indicating a transition to a solid-like behavior. At 7 days of incubation at 40°C, the gap between G'' and G' widened with G' even higher than G" and the moduli were found to be almost frequency independent (exponents of 0.15 and 0.14, respectively). This behavior is characteristic of the building up of a gel, with a predominantly elastic structure ($\tan \delta < 1$). These results illustrate well the flow behavior of the samples observed visually (Figure VI.3B): t_4, t_5 and t_7 do not flow out when turning the sample vials upside down.

In the past years, several methods (*e.g.* physical or radiation cross-linking) had been developed to produce hydrogels from Acacia gum, in order to improve its functional properties (Gulrez et al., 2011). Al-Assaf & Phillips showed that it was possible to tune the amount of gum hydrogel

produced after irradiation by controlling the radiation dose (Al-Assaf & Phillips, 2006). Maturation of A. *senegal* gum at 110°C is also a good way to produce highly cross-linked AGPs (Aoki, Al-Assaf, et al., 2007; Aoki, Katayama, et al., 2007), prone to form a hydrogel network, after aggregation induced by heating at high temperatures. We showed that our maturation process is also able to improve rheological properties of AGPs, even in mild conditions (T = 40°C). Depending on the incubation time, these properties can be tuned to form gels with various viscosity and viscoelastic behavior.

Viscoelastic properties of arabic acid dispersions of t_7 were also assessed at lower concentrations (5 and 10wt%) in order to determine if the formation of the hydrogel was concentration-dependent (Figure VI.4). At 10wt%, t_7 still exhibited solid-like behavior, but the gap between G' and G" shrunk. Further decrease in concentration was marked by a critical transition between solid-like (at C = 10wt%) and liquid-like behavior (at C = 5wt%). Same results were obtained with other hyperbranched polymers such as dextran derivatives (Szafulera et al., 2018) (C = 20 g·L^{-1}). Therefore, the flow behavior of AGPs insoluble microparticles switched from elastic to more fluid at a concentration C ~ 10wt%. Increasing concentration brings microparticles closer to each other. When concentration becomes high enough, contacts are favored up to the building up of a gel, with G' being higher than G".

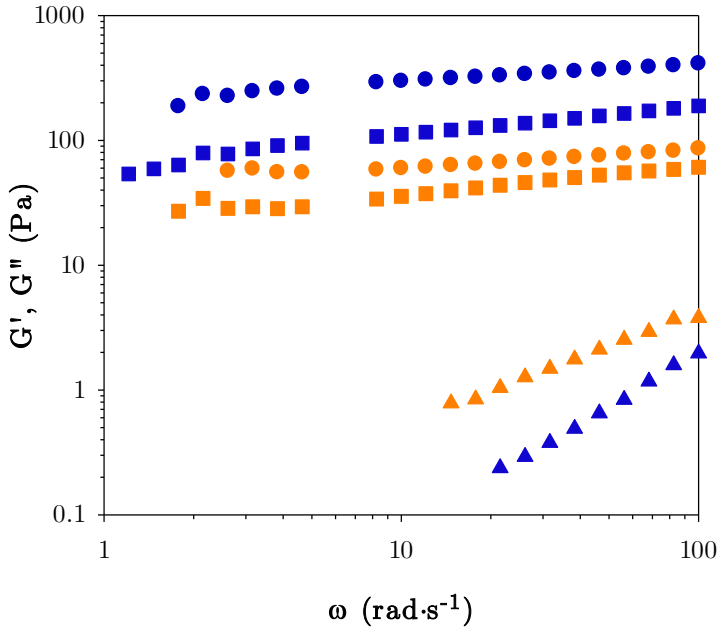

Figure VI.4. A) Storage G' (blue) and loss G'' (orange) moduli of t_7 dispersions at different concentrations: 5wt% (▲), 10wt% (■) and 15wt% (●). All experiments were performed at 1% strain.

3.2 Interfacial properties

The interfacial tension of two organic compounds of different polarity, namely limonene and octanol was measured in presence of 5wt% A. *seyal* gum samples. To further study the viscoelastic properties of the interfacial films, dilatational rheology was used and viscous and elastic moduli were recorded for 24h. Most of the studies reported in literature studying interfacial properties with a drop tensiometer deal with lower concentrations ($< 1\%$), but the choice of $C_{gum} = 5wt\%$ was made to approach conditions found in emulsion formulation with Acacia gums. The pH of arabic acid and incubated arabic acid was adjusted from 2.5 to the pH of 5wt% GA (*i.e.* pH 4.5) with a mixture of $Ca(OH)_2$, $Mg(OH)_2$ and KOH in order to mimic the mineral composition of A. *seyal* gum. In the following, such samples will be referred as "remeniralized".

3.2.1 Effect of the presence of minerals on interfacial properties of A. *seyal* gum

The interfacial properties of A. *seyal* gum and remineralized arabic acid at the limonene/water interface were assessed. Figure VI.5A displayed a continuous increase in surface pressure with time showing that AGPs from both gums are prone to decrease the interfacial tension at the limonene/water interface. This increase was more pronounced during the first 20 minutes, which can be explained by a diffusion-controlled adsorption of AGPs at the interface (Ward & Tordai, 1946), as already observed in literature for A. *seyal* gum (Aphibanthammakit, 2018; Castellani, Al-Assaf, et al., 2010). However, at 5wt%, GA diffuses from the bulk phase to the interface very fast. For longer times, this increase in surface pressure was slower, corresponding to a restructuration of the interfacial film; and no equilibrium was reached after 24h of experiment. Isobe et al. suggested that this further increase in surface pressure might be the result of *(i)* deformation or *(ii)* reorientation of A. *seyal* gum molecules at the interface, or *(iii)* dispersion of aggregated molecules; all three resulting in an increase in oil droplet coverage (Isobe et al., 2020).

Changes in surface pressure can also be explained in terms of interfacial water thermodynamics (Pérez-Díaz et al., 2012; Rao & Damodaran, 2000). When the limonene droplet is formed in GA dispersion and because limonene has a hydrophobic character, a layer depleted in water molecules is formed at the interface (Chandler, 1941). In this zone, important volume fluctuations allow the accumulation of AGPs inducing the dehydration of the interface (Coe et

al., 2022; Jamadagni et al., 2011; Lum et al., 1999). This causes the creation of an interfacial film associated with an increase in surface pressure.

The comparison of interfacial adsorption kinetics of A. *seyal* gum and remineralized arabic acid showed a lower increase in surface pressure after 24h with A. *seyal* (π_{24h} = 12.5 mN·m^{-1}) compared to remineralized arabic acid (π_{24h} = 15.0 mN·m^{-1}). This highlights a strong adsorption of the two gums at the interface, with an enhanced efficiency for remineralized arabic acid.

Dilatational rheology experiments revealed that the elastic modulus E' was always above the viscous one for the first 24h. This demonstrates the elastic nature of the interfacial film, as commonly found in literature (Castellani, Al-Assaf, et al., 2010; Erni et al., 2007, 2012; Sanchez et al., 2018; Vasile et al., 2016). Both moduli were found to increase continuously with time, up to reach a maximum, the maximum of E" being reached before those of E' and then decreased. The times when the E" and E' maximal values were reached were 125 s and 425 s for A. *seyal* gum, and 130 s and 570 s for remineralized arabic acid.

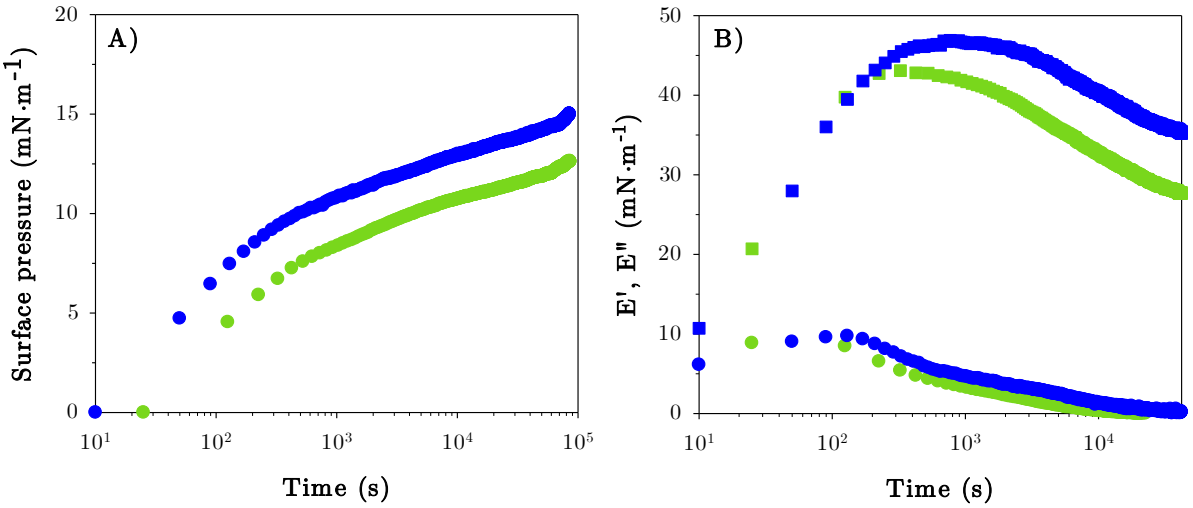

Figure VI.5. Evolution of interfacial properties of AGPs from A. *seyal* gum powder (●) and remineralized arabic acid (●) at the limonene/water interface: surface pressure (A) and viscous (●) and elastic (■) moduli (B). The experiments were performed for 24h, at C = 5wt% and pH = 5.

This decrease in E' was also observed with numerical simulations (Yeung & Zhang, 2006) and might arise from surface fluctuations at the surface of the limonene droplet. The dilational modulus can be considered in terms of interfacial thermodynamics. Indeed, interfacial fluctuations can be defined in two dimensions, in a similar way than volumetric parameters describe volume fluctuations in three dimensions (see part IV.3.1) (Rosenholm et al., 2003; Tschoegl, 1958). In this way, the maximum in E would correspond to a maximum in film

rigidity, and the following decrease would be characteristic of an increase in compressibility induced by a rearrangement of the interface (Beverung et al., 1999; Bouyer et al., 2011). However, one has to keep in mind that the determination of the elastic and viscous moduli is based on the drop shape of a rising drop submitted to an oscillatory deformation. Because of the elongated shape of the drop associated with a heterogeneous distribution of AGPs at the interface, the deformation will generate a heterogeneous distribution of stresses, with stronger stress to the drop neck (Nagel et al., 2017; Stanimirova et al., 2011). The apparition of wrinkles on the surface of the limonene droplet during measurement tends to confirm that the interfacial film presents zones of different rigidity (Stanimirova et al., 2011). Yet, the equation which relates the interfacial tension to the droplet shape requires a homogeneous distribution of constraints (isotropic tension field) to determine properly the interfacial tension and the viscoelastic viscous moduli and fails to describe the behavior of highly elastic fluids (Stanimirova et al., 2011). Thus, the decrease in E' observed might be an artefact created by the method limitations.

Keeping this in mind, it is still interesting to compare the values of the E' maxima reached for each gum. These values were somewhat different between the two gums (Figure VI.5B), with E'_{max} = 42.8 mN·m^{-1} and E'_{max} = 46.8 mN·m^{-1} for A. *seyal* gum and remineralized arabic acid, respectively. The surface pressure and elastic modulus measurements evidenced the highest interfacial properties of AGPs from remineralized arabic acid, reflecting differences in polarity between both gums. It has been shown that good interfacial properties of Acacia gum arise from its high M_w protein-rich AGPs (Elmanan et al., 2008) and that the gum would adsorb to the interface *via* its proteinaceous part (Dickinson, 2003; Fauconnier et al., 2000; Fincher et al., 1983). However, the protein content in the two gums is very similar, and even slightly higher for A. *seyal* gum (0.96wt% for A. *seyal* gum and 0.83wt% for remineralized arabic acid) so this could not explain the variation in interfacial behavior observed. It was shown by volumetric measurements (partial specific volume and partial specific adiabatic compressibility, section IV.3.1) that AGPs from arabic acid are more hydrophobic than those of A. *seyal* gum. Therefore, even if arabic acid was remineralized for these interfacial properties measurements, it is not certain that the remineralization took place in the same way as in A. *seyal* gum which could explain these differences in polarity and therefore in interfacial properties.

3.2.2 Effect of the presence of aggregates on interfacial properties of remineralized arabic acid

The surface pressure and interfacial rheological properties at the limonene/water and octanol/water interfaces of arabic acid AGPs and soluble aggregates (t_2) were investigated (Figure VI.6). Limonene and octanol were selected because they have different polarity, the former being more hydrophobic. Surprisingly, in the conditions of the measurement, neither the surface pressure nor the viscous and elastic moduli were affected by the presence of aggregates (Figure VI.6 and Figure VI.7), showing the same interfacial behavior for the two samples. A similar value of $\pi \sim 15.3$ mN·m^{-1} and $\pi = 2.9$ mN·m^{-1} was reached after 24h, at the limonene/water interface and at the octanol/water interface, respectively. These values show that gums are not strongly adsorbed at the octanol/water interface, because of the high polarity of octanol.

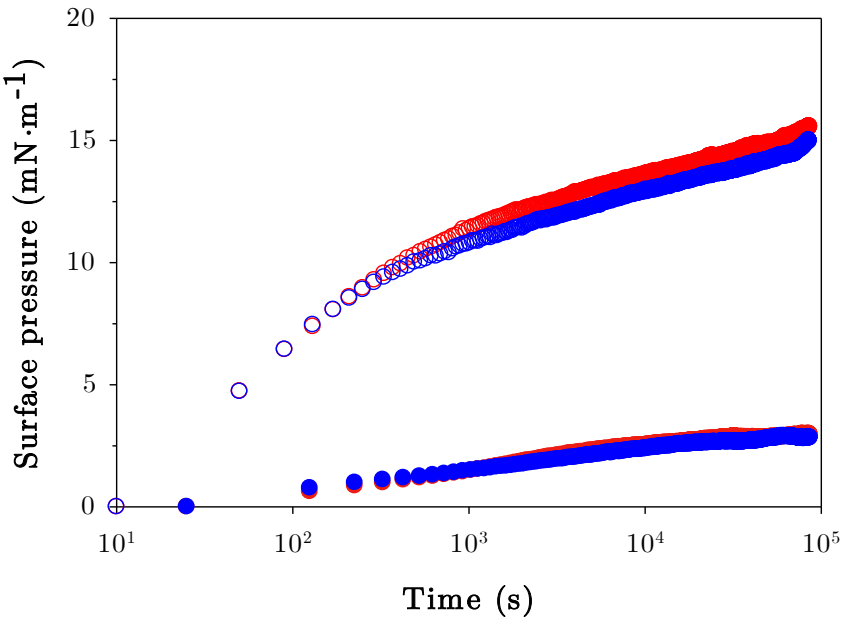

Figure VI.6. Evolution of surface pressure at the limonene/water interface (open symbols) and octanol/water interface (filled symbols) of AGPs from remineralized arabic acid (●) and t_2 (●). The experiments were performed during 24h, at C = 5wt% and pH = 5.

Arabic acid and incubated arabic acid interfacial films both exhibited a highly elastic nature, whatever the organic compound polarity. With limonene, E' and E" reached maxima values of $E'_{max} = 46.8$ mN·m^{-1} and $E"_{max} = 9.7$ mN·m^{-1} after 570 and 130 s, respectively. With octanol, these values were $E'_{max} = 9.2$ mN·m^{-1} and $E"_{max} = 1.5$ mN·m^{-1} after 13225 and 725 s, respectively. The maximum values of E' and E" obtained and the delay in the film formation

observed with octanol compared to limonene illustrate once again the effect of the oil polarity on the interfacial adsorption kinetics. However, similar results were obtained with the two gums.

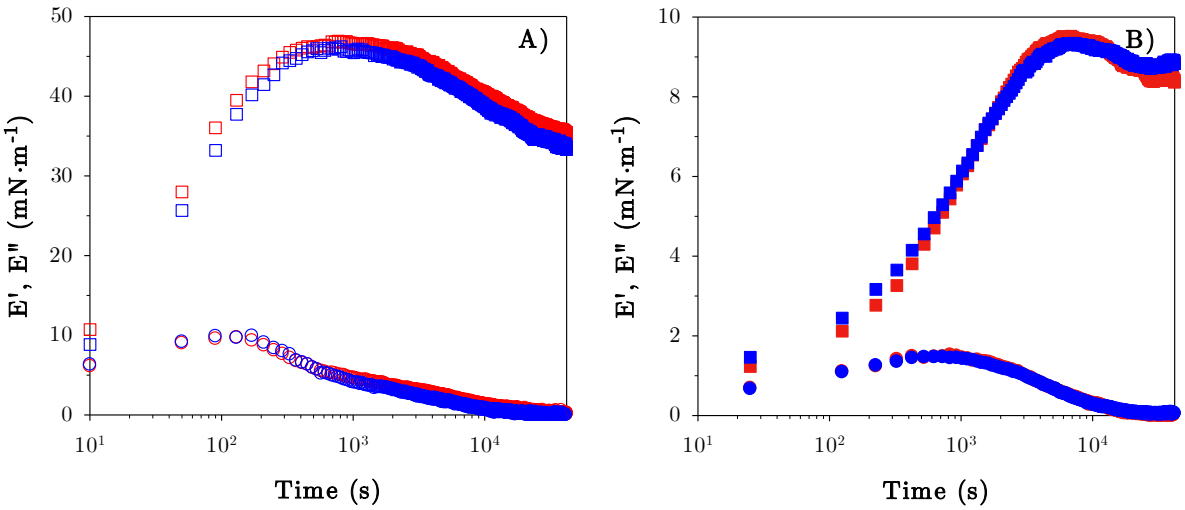

Figure VI.7. Evolution of viscous (●) and elastic (■) moduli surface pressure at the limonene/water interface (A) and octanol/water interface (B) of AGPs from remineralized arabic acid (●) and t_2 (●). The experiments were performed during 24h, at C = 5wt% and pH = 5.

Interfacial properties were shown to be dependent on the concentration. For instance, Zhou et al. reported whey protein isolates had better capacity to decrease the interfacial tension at the milk fat/water interface when used at 0.1wt% whereas at higher concentration (C = 4wt%), whey protein aggregates and isolates had the same interfacial properties (Zhou et al., 2020). In our study, at a lower concentration, C = 0.5wt% (Supplementary data Figure VI.12), for which the adsorption kinetics would be lower, no difference in terms of interfacial properties was observed neither.

Our results are not in agreement with studies on the interfacial properties of matured A. *senegal* gum which showed that aggregated gums were more prone to decrease the interfacial tension and adsorbed faster at the air/water interface compared to native gum (Castellani, Guibert, et al., 2010). However, Mahmoudi et al. showed that the air/water interfacial properties of whey proteins were almost not affected by the presence of aggregates and that the adsorption behavior of whey protein aggregates could be described by the residual non-aggregated fraction (Mahmoudi et al., 2010). Similarly, Chen et al. demonstrated that insoluble casein micelles aggregates were probably not taking part of the air/water interface, as the surface rheology was not modified by the presence of this insoluble fraction. They suggested they could be

randomly attached to a primary layer of peptides, caseins and small micelles (Chen et al., 2017). Thus, one could imagine that the presence of high molar mass AGP aggregates does not play a role in stabilizing the limonene/water or octanol/water interface and that the molecules responsible for the decrease in interfacial tension are the same for incubated and non-incubated samples. A previous characterization of the structural and volumetric properties of AGP soluble aggregates showed that t_2 and arabic acid had a similar conformation (section III.4.3.2.2) and polarity (section IV.3.1). Since these two parameters mainly determine the formation and structure of interfaces, this could explain why aggregation does not modify the surface properties of AGPs in our experimental conditions.

3.3 Emulsifying properties

Emulsions were formulated using limonene as *oil* phase and GA as emulsifier at [GA] = 10wt% or 20wt%. The 20wt% concentration was chosen in order to formulate emulsions with a continuous phase of the same apparent viscosity at 100 s^{-1}: η (A. *seyal* 20wt%) $\simeq$ η (A. *senegal* 20wt%) $\simeq$ η (t_2 10wt%) $\simeq$ 40 mPa.s.

Figure VI.8 presents the volumetric distributions of limonene droplet size in emulsions and the mean D(4,3). All emulsions were characterized by multimodal distributions (Figure VI.8A). A. *senegal* distributions were centered on 0.7 and 0.4 µm, with a shoulder at 0.4 and 1.2 µm for [GA] = 10wt% and 20wt%, respectively. The other distributions were characterized by 3 peaks, and shifted to higher size values in the following order: A. *senegal* 10% < A. *senegal* 20% < t_2 10% < A. *seyal* 20% < A. *seyal* 10%. In average, the smallest D(4,3) was obtained when using A. *senegal* as emulsifier (Figure VI.8B). t_2 allowed a reduction of the D(4,3) by a factor of at least 2 compared to A. *seyal*, highlighting an improvement of emulsifying properties of A. *seyal* by our process. The reasons why A. *senegal* is a better emulsifier than A. *seyal* were extensively described elsewhere (Aphibanthammakit, 2018; Chanamai & Mcclements, 2001; Dickinson et al., 1988; Islam et al., 1997) and include a higher surface hydrophobicity of A. *senegal* associated with a higher protein content, a lower content in arabinose and a higher content in negatively charged glucuronic acids (Aphibanthammakit et al., 2018; Lopez-Torrez et al., 2015; Mejia Tamayo et al., 2018).

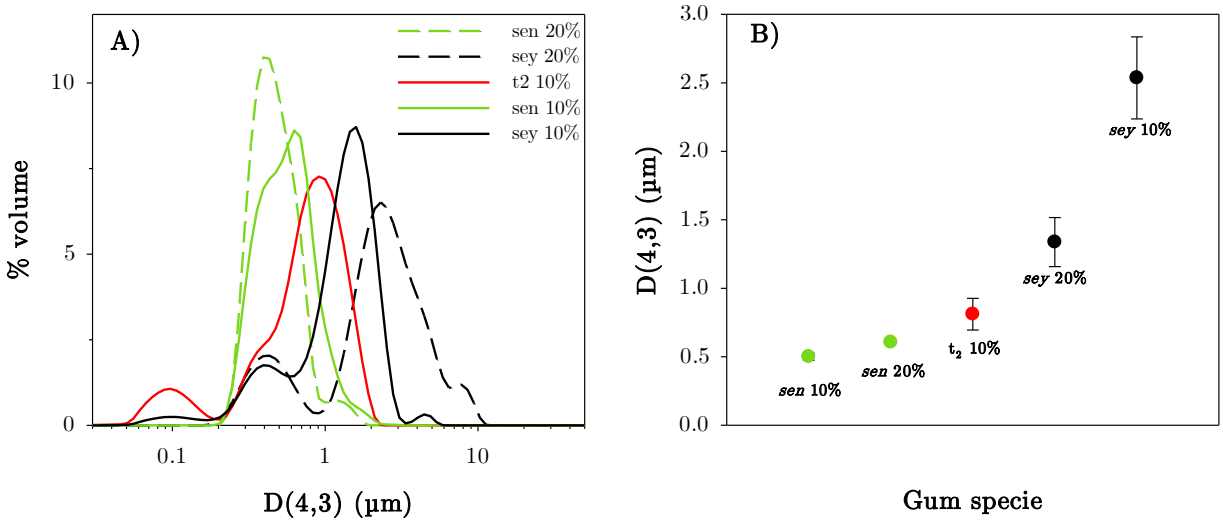

Figure VI.8. Droplet size distribution (A) and volume mean diameter D(4,3) (B) of limonene emulsions stabilized by A. *senegal*, A. *seyal* and t_2.

The colloidal stability of emulsions was also investigated by measuring the changes in backscattering and transmittance intensity with time. From these signals, the Turbiscan Stability Index parameter (TSI) was calculated. This parameter is an indicator of the destabilization processes involved during the ageing of emulsions: the higher the TSI value, the less stable the emulsion. TSI followed the same trend for all emulsions characterized by an exponential rise shape (Figure VI.9). The slope of the TSI was the highest during the first times of ageing (48h), indicating that destabilization was faster at this time. None of the gums used is suitable to efficiently stabilize limonene emulsions over a long period. However, after one day of ageing, the emulsion stabilized by A. *senegal* was 40% less unstable than the others (inset of Figure VI.9).

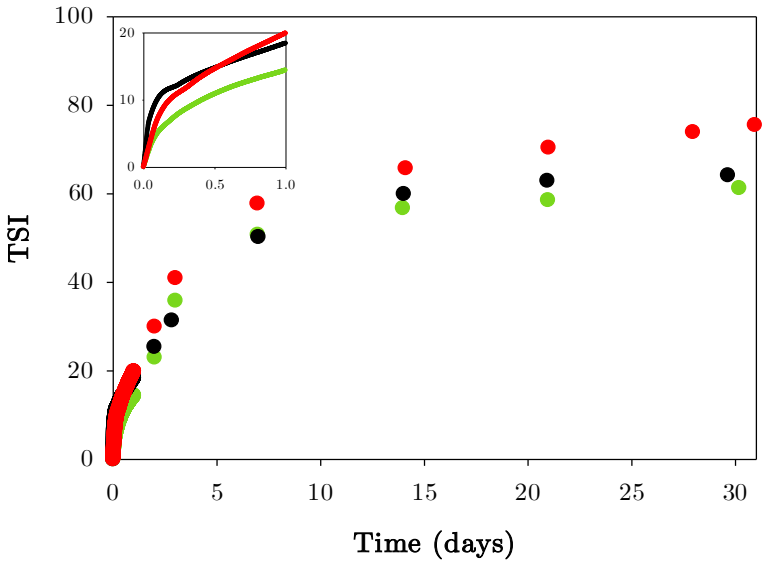

Figure VI.9. Stability of limonene emulsions stabilized by 20% A. *senegal* (●) and A. *seyal* (●) or 10% t_2 (●). These concentrations were chosen to obtain continuous phases with the same viscosity for all emulsions. The inset focuses on the first 24h of emulsion ageing.

The kinetics of instability (creaming or sedimentation) v ($m \cdot s^{-1}$) are determined by the Stokes' law:

$$v = -\frac{2gr^2(\rho_d - \rho_c)}{9\eta_c}$$

With r the emulsion droplet radius, g the gravity acceleration, ρ_c and ρ_d the density of the continuous and dispersed phase, respectively, and η_c the viscosity of the continuous phase. Thus, emulsion stability can be improved either by reducing the density gap between the continuous and the dispersed phase, or by increasing the viscosity of the continuous phase (Chanamai & McClements, 2000; Jafari et al., 2012; Zhang et al., 2015). The viscosity of the dispersed phase also has to be well-chosen in order to avoid coalescence issues (Qian & McClements, 2011; Schultz et al., 2004; Walstra, 1993). In this regard, the use of weighting agents such as ester gum or sucrose acetate isobutyrate (SAIB) had appeared as a good way to improve emulsion stability (Chanamai & McClements, 2000; Taherian et al., 2008; Zhang et al., 2015). For the rest of this study, ester gum was added in a ratio 1:1 to sweet orange essential oil, a commercial essential oil typically used in the formulation of flavor emulsions and whose main constituent (> 90%) is limonene.

Figure VI.10 displays the volumetric distributions of oil droplet size and the mean D(4,3) in emulsions formulated with a mix ester gum/sweet orange essential oil formulated at a ratio 1:1 (EGEO) as oil phase. 10% A. *senegal* emulsion was characterized by a monomodal distribution centered on 0.4 µm. Other distributions presented at least two peaks and emulsifiers were classified in the same order than in limonene emulsions with A. *senegal* 20% > A. *senegal* 10% > t_2 10% > A. *seyal* 20%. With this oil phase, A. *seyal* appeared as a particularly poor emulsifier with a mean D(4,3) = 22 µm (Figure VI.10B). It could be suggested that during the emulsification process, at the first contact between the two phases, the interface is already partially stabilized by the ester gum present in oil phase. While the emulsification progresses, there is a competition for the interface between the ester gum molecules and the AGPs from A. *seyal*.

t_2 showed intermediate emulsifying behavior between A. *senegal* and A. *seyal* but aggregation greatly improved emulsifying properties of A. *seyal* as depicted by the decrease of D(4,3) by 20. The continuous phase of emulsions stabilized with t_2 contained a high amount of aggregates as attested by $M_w(t_2)$; and 100% of high molar mass AGPs (having a $M_w > 10^6$ g·mol^{-1}) (Table VI.1), yet it had been shown that the higher content in high molar mass protein-rich AGPs and aggregates confers to A. *senegal* better emulsifying properties compared to A. *seyal* (Aphibanthammakit, 2018). Moreover, maturation of GA enhances its emulsifying and stabilizing properties, as it had been extensively studied in literature (Table I.6), with a reduction of oil droplet size compared to the native gum, and less destabilization over time (Al-Assaf et al., 2004; Castellani, Guibert, et al., 2010; Hayashi, 2002; Sasaki et al., 2014). For instance, $D_{4,3}$ was decreased by 31% in emulsions freshly prepared using A. *senegal* matured for 12h at 60°C and 70%RH (Hayashi, 2002).

Table VI.1. Structural and viscosity characteristics of the continuous phase

	η_{app} (mPa.s)	M_w (g·mol^{-1})	% high M_w AGPs
A. *seyal* 20wt%	38	$8.2 \cdot 10^5$	28
A. *senegal* 20wt%	41	$7.3 \cdot 10^5$	17
t_2 10wt%	42	$5.9 \cdot 10^6$	100

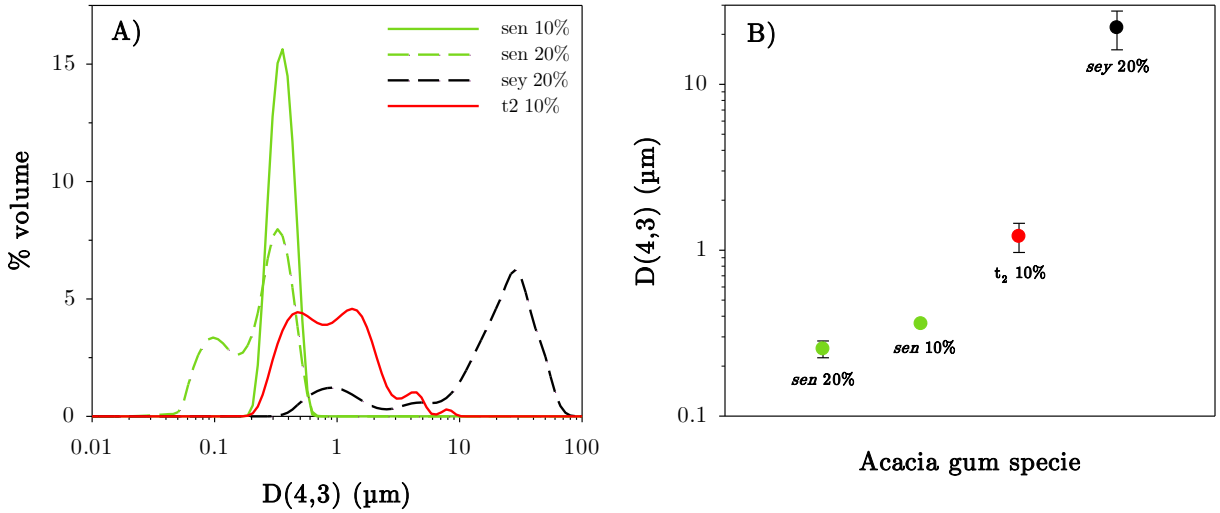

Figure VI.10. Droplet size distribution (A) and volume mean diameter D(4,3) (B) of EGEO emulsions stabilized by A. *senegal*, A. *seyal* and t_2.

In comparison with limonene, the change in oil phase rendered emulsions more stable whatever the emulsifier used (Figure VI.11). The colloidal stability of emulsions was first observed visually (Figure VI.11A). Even in their initial stage, the emulsions stabilized by A. *senegal* and t_2 appeared whiter whereas the emulsion stabilized by A. *seyal* had a yellowish color. Besides, creaming was observed in A. *seyal* emulsion after 1 month of ageing. This creaming phenomenon came with clarification at the bottom of the tubes for t_2 and A. *seyal* emulsions.

Emulsion colloidal stability was further characterized by the creaming index (CI) determined at different ageing times (Figure VI.11B). With A. *senegal*, no creaming was observed. However, both A. *seyal* and t_2 emulsions exhibited creaming, as shown by the increase in CI between 1h and 7 days of ageing from 3 to 14% and 0 to 8% for A. *seyal* and t_2 respectively.

The evolution of the TSI in EGEO emulsions highlighted the differences previously observed between the three gums (Figure VI.11C), emulsions formulated with A. *senegal* being very stable during 30 days, A. *seyal* acting as a poor emulsifier and t_2 exhibiting intermediate behavior between the two gums. However, after 1 and 7 days of ageing, compared to A. *seyal* emulsions, TSI of emulsions stabilized with t_2 was reduced by 8 and 5, respectively. It is important to precise that this improvement in t_2 emulsion stability was obtained with half the amount of gum compared to A. *seyal*. It would be interesting to study if emulsion stability is still improved with an even smaller amount of t_2.

The evolution of the TSI vs. time was then divided in 4 zones and the slope of the curves was determined, showing that the destabilization kinetics were faster in the first zone (0 – 2h) for all emulsions studied, A. *seyal* emulsion being the fastest to destabilize (Supplementary data Table VI.2).

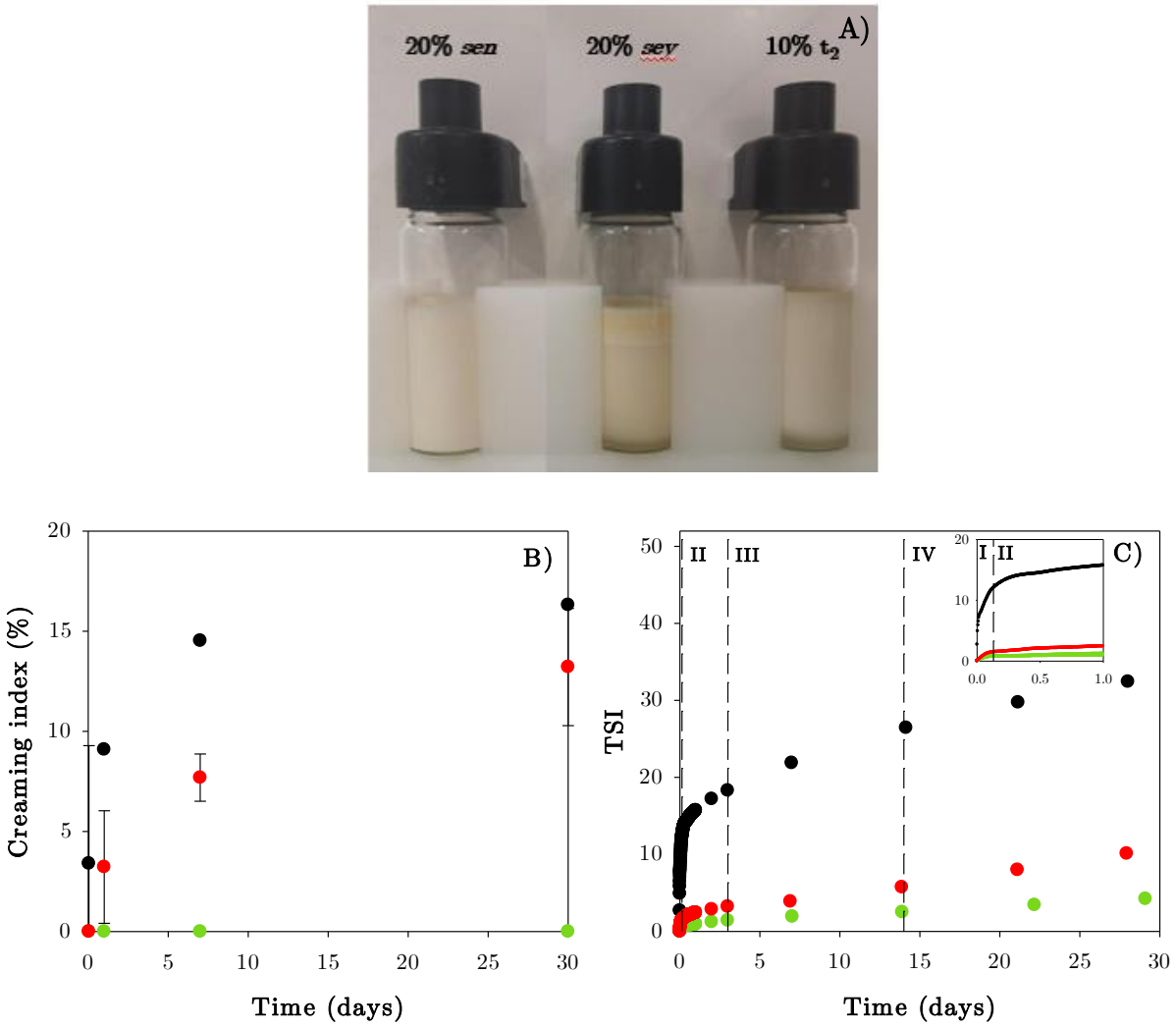

Figure VI.11. Stability of EGEO emulsions stabilized by 20% A. *senegal* (●) and A. *seyal* (●) or 10% t_2 (●) evaluated from visual observations after 1 month of ageing (A), creaming index (B) and TSI (C) determination.

Unlike CI, the TSI parameter gives a global characterization of all the destabilization phenomena which take place in the emulsion (creaming, clarification, coalescence/flocculation). This is why in spite of similar creaming behavior, A. *seyal* and t_2 exhibit very different TSI values. Measuring changes in backscattering intensity (ΔBS) allows a more accurate description of the destabilization phenomena (Supplementary data FigureVI.13). Initially, ΔBS in the

middle of the A. *seyal* emulsion decreased over a large range of height (0 – 25 mm) due to a global increase in droplet sizes related to flocculation/coalescence phenomena. From 8h of ageing, a decrease of ΔBS in the bottom of emulsions related to a decrease of the concentration of the droplets in this part was observed. This decrease was concomitant with an increase of ΔBS in the top of emulsions from 1 week of ageing, characteristic of an increase of the concentration of the dispersed phase. This illustrates clarification and creaming phenomena, respectively. As a comparison, ΔBS intensity of t_2 remained rather constant in the middle of the tube. However, clarification and creaming phenomena were observed, as shown by the decrease of ΔBS in the bottom and the increase of ΔBS in the top of emulsions.

4. Conclusions

The aggregation of AGPs from arabic acid *via* its incubation in the dry state at 40°C confers to GA good rheological properties and enhances its emulsifying properties. The apparent viscosity of arabic acid dispersions increased with the aggregation time. According to the initial aggregation stage, different flow behaviors were adopted: soluble aggregates displayed a Newtonian behavior whereas the most aggregated samples had a shear-thinning flow behavior. At long incubation times and concentrations high enough (C ≥ 10wt%), the formation of a hydrogel was observed. Interfacial properties were not modified by the presence of soluble aggregates in the bulk phase, suggesting that these aggregates might not influence the adsorption kinetics of AGPs at the interface nor the properties of the viscoelastic interfacial film. However, even at 10wt%, aggregated arabic acid was more prone to stabilize oil/water emulsions than 20% A. *seyal* gum: the initial oil droplet size in emulsion and the global instability after a week of emulsion ageing decreased by 20 and 5 respectively for aggregated arabic acid compared to A. *seyal* gum.

5. Acknowledgments

The authors gratefully acknowledge ALLAND & ROBERT Company (Port Mort, France) and the French Ministry of Research and Education (2017/1727) for the financial support (Ph.D. Amandine Antoine-Michard).

6. Supplementary data

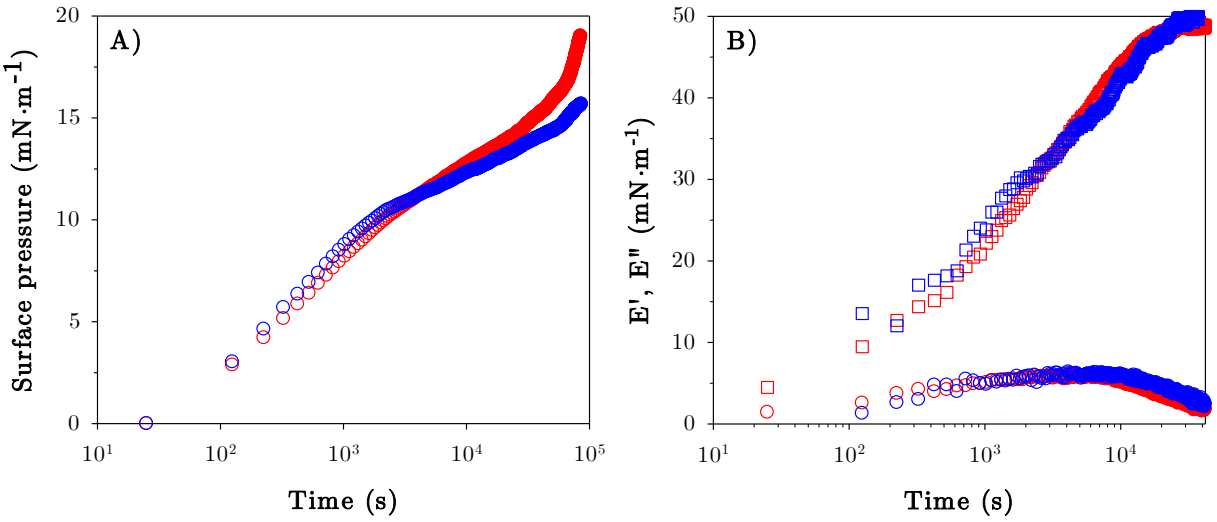

Figure VI.12. Evolution of interfacial properties of AGPs from remineralized arabic acid powder (●) and t_2 (●) at the limonene/water interface: surface pressure (A) and viscous (■) and elastic (●) moduli (B). The experiments were performed for 24h, at C = 0.5wt% and pH = 5.

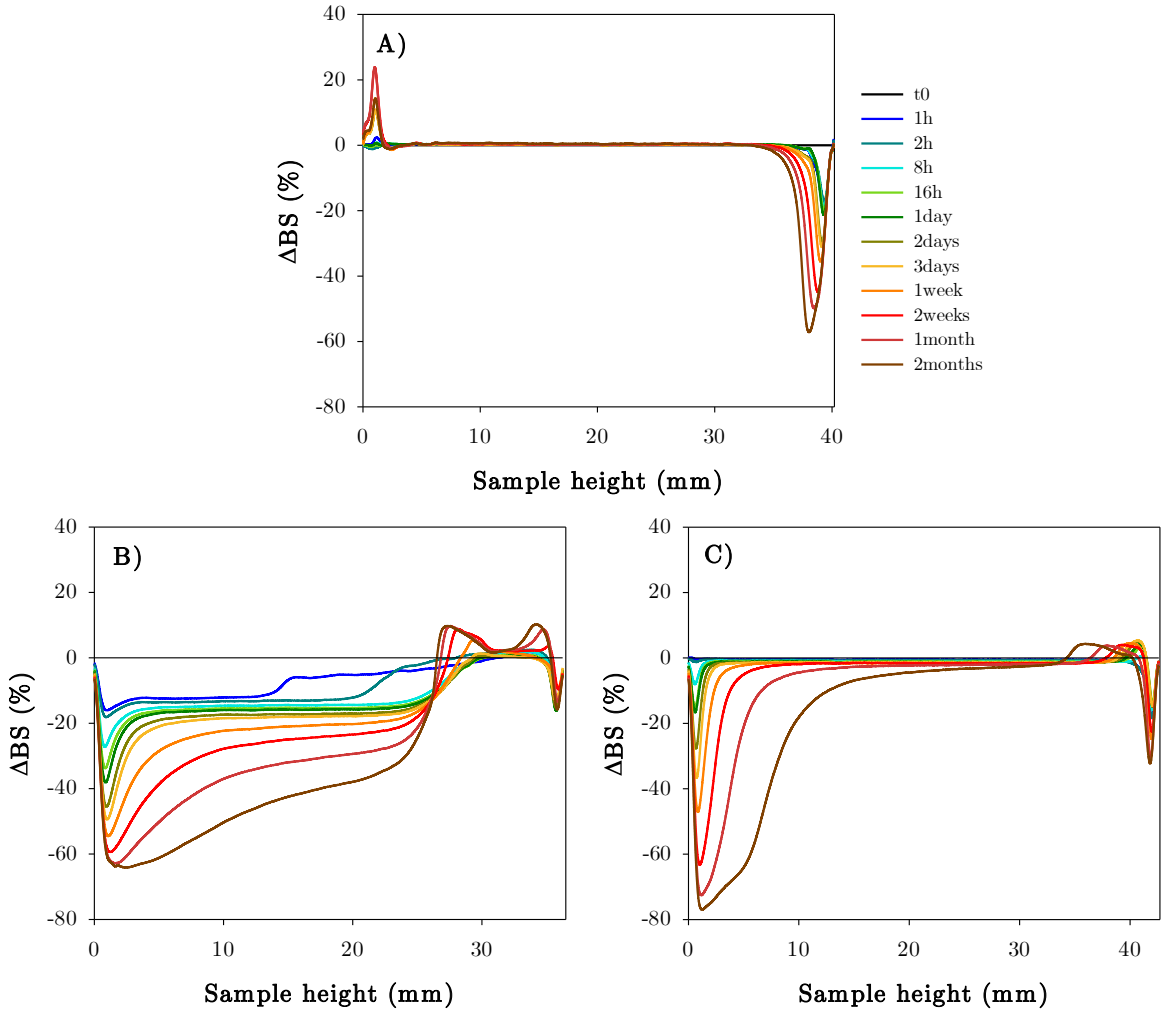

Figure VI.13. Differential change in the backscattering signal (ΔBS) profile of emulsions formulated with EGEO as oil phase and A) A. *senegal* (C = 20wt%), B) A. *seyal* (C = 20wt%) and C) t_2 (C = 10wt%) as emulsifier.

Table VI.2. Determination of the destabilization kinetics of emulsions formulated with EGEO as oil phase and A. *senegal*, A. *seyal* and t_2 as emulsifier. From the calculation of the TSI slopes.

	A. *senegal* 20%	A. *seyal* 20%	t_2 10%
Zone I: 0 – 3h	12.0 ± 4.9	73.0 ± 18.9	4.7 ± 0.7
Zone II: 3h – 3days	0.3 ± 0.1	9.6 ± 1.9	0.9 ± 0.2
Zone III: 3 – 14days	0.3 ± 0.1	1.8 ± 0.2	0.9 ± 0.2
Zone IV: 14 – 30days	0.1 ± 0.0	0.5 ± 0.1	0.4 ± 0.2

7. Complementary studies

For the shortest storage times, when diffusion predominates and controls the adsorption process, the Ward and Tordai equation (Ward & Tordai, 1946) can be used to correlate the change in interfacial tension γ ($N \cdot m^{-1}$) with time:

$$\gamma = \gamma_0 - 2RTC_0\sqrt{\alpha t} \qquad \text{(VI.7)}$$

With $\alpha = \frac{D}{\pi}$, where C_0 is the concentration in the bulk phase ($mol \cdot m^{-3}$), R is the universal gas constant (8.314 $J \cdot mol^{-1} \cdot K^{-1}$), T is the absolute temperature (K), D is the diffusion coefficient ($m^2 \cdot s^{-1}$), and t is the adsorption time (s). Thus, plotting γ against $t^{1/2}$ gives access to the diffusion coefficient D, given by the slope of this plot. Diffusion coefficients obtained by this method for A. *seyal* gum, demineralized A. *seyal* gum and soluble aggregates are given in Table VI.3.

The molar mass of aggregates being much higher than that of A. *seyal* gum, one could expect faster diffusion rates (and higher diffusion coefficients) for GA than for aggregated samples. However, the values obtained for all samples were essentially similar, $D \sim 10^{-10}\ m^2 \cdot s^{-1}$, whatever the aggregation state. This would mean that when interface stabilization is diffusion-limited, the fastest molecules to go to the interface are the same.

Table VI.3. Diffusion coefficient values obtained from the Ward-Tordai equation (eq. VI.7) and interfacial tension measurements during 25s.

Sample	D ($*10^{-10}\ m^2 \cdot s^{-1}$)
GA	1.2
t_0	1.3
t_2	1.14

8. Highlights

In this chapter, we characterized the physicochemical properties of AGP aggregates from demineralized A. *seyal* gum obtained during their storage in the dry state at 40°C. The interfacial and emulsifying properties of soluble aggregates formed at moderate incubation times (< 2days) were investigated. The rheological properties (flow curves and viscoelastic behavior) of the soluble aggregates and insoluble microparticles were evaluated. We also compared the physicochemical properties of A. *seyal* before and after demineralization. The main results obtained are described below:

Interfacial properties of AGP aggregates:

- A. *seyal*, arabic acid and soluble AGP aggregates were all prone to stabilize limonene/water and octanol/water interfaces.
- Highly elastic films were formed by all gums at the interface.
- After remineralization, arabic acid displayed better interfacial properties (lower interfacial tension and higher viscoelastic moduli) compared to A. *seyal* gum, in line with the more hydrophobic character (less polar) of arabic acid.
- The presence of soluble AGP aggregates did not modify the interfacial properties of arabic acid whatever the organic phase polarity and the gum concentration used. This suggested either that AGP groups responsible for the stabilization of the interface are not affected by the storage or alternatively that the flexibility and polarity of native and aggregated AGPs is similar.

Emulsifying properties of AGP aggregates:

- None of the gums used in this study (A. *senegal*, A. *seyal*, soluble AGP aggregates from A. *seyal*) was prone to stabilize limonene/water emulsions. However, at C = 10%, emulsions formulated with aggregates had an intermediate droplet size D(4,3) (0.7 µm) between the one in A. *senegal* (0.5 µm) and A. *seyal* emulsions (2.5 µm).
- Gums display different emulsifying behavior for emulsions formulated with a mix sweet orange essential oil/ester gum (weighting agent). At equivalent continuous phase apparent viscosity, the colloidal stability of emulsions

formulated with aggregates was improved compared to A. *seyal*. AGP aggregates also greatly decreased the oil droplet D(4,3) in emulsions, from 22 µm (A. *seyal*) to 1.1 µm (t_2). However, A. *senegal* was the most efficient to stabilize these emulsions and exhibited lower D(4,3) compared to the two other gums.

Rheological properties of AGP aggregates:

- AGP aggregates provide A. *seyal* good rheological properties, both in terms of apparent viscosity and viscoelasticity.
- Arabic acid and soluble aggregates exhibited Newtonian behavior over a wide range of shear rate (5 – 1000 s^{-1}) and shear-thinning behavior at lower shear rates. On contrary, the most aggregated samples displayed shear-thinning like flow curves at all shear rates (10^{-6} – 1000 s^{-1}).
- Apparent viscosity of arabic acid (14 mPa.s) dramatically increased with aggregation up to reach $\eta \sim 3.5$ Pa.s (at 100 s^{-1}) after 7 days of storage at 40°C.
- The presence of insoluble microparticles in samples led to changes in viscoelastic behavior, from liquid-like ($t < 2$ days) to solid-like. The hydrogel formed with samples stored for 7 days at 40°C was sensitive to AGPs concentration and formed only at concentrations > 10%.

9. References

Al-Assaf, S., Andres-Brull, M., Cirre, J., & Phillips, G. O. (2012). Structural changes following industrial processing of Acacia gums. In J. F. Kennedy, G. O. Phillips, & P. A. Williams (Éds.), *Gum Arabic* (RCS Publishing, p. 153-168). Kennedy J.F., Phillips G.O., Williams P.A. https://doi.org/10.1039/9781849733106-00153

Al-Assaf, S., & Phillips, G. (2006). Controlling the molecular structure of food hydrocolloids. *Food Hydrocolloids*, *20*, 369-377. https://doi.org/10.1016/j.foodhyd.2005.03.017

Al-Assaf, S., Phillips, G. O., Aoki, H., & Sasaki, Y. (2007). Characterization and properties of Acacia senegal (L.) Willd. var. senegal with enhanced properties (Acacia (sen) SUPER GUM^{TM}) : Part 1—Controlled maturation of Acacia senegal var. senegal to increase viscoelasticity, produce a hydrogel form and convert a poor into a good emulsifier. *Food Hydrocolloids*, *21*(3), 319-328. https://doi.org/10.1016/j.foodhyd.2006.04.011

Al-Assaf, S., Phillips, G. O., Sasaki, Y., & Katayama, T. (2004). *Modified gum arabic* (Patent N° WO 2004/089991 A1).

Al-Assaf, S., Phillips, G. O., Williams, P. A., & du Plessis, T. A. (2007). Application of ionizing radiations to produce new polysaccharides and proteins with enhanced functionality. *Nuclear Instruments and Methods in Physics Research Section B: Beam Interactions with Materials and Atoms*, *265*(1), 37-43. https://doi.org/10.1016/j.nimb.2007.08.015

Anderson, D. M. W., & Stoddart, J. F. (1966). Studies on uronic acid materials : Part XV. The use of molecular-sieve chromatography in studies on acacia senegal gum (gum arabic). *Carbohydrate Research*, *2*(2), 104-114. https://doi.org/10.1016/S0008-6215(00)81474-3

Antoine-Michard, A., Charbonnel, C., Jaouen, I., Sanchez, C., & Nigen, M. (2022). Maturation of demineralized arabinogalactan-proteins from Acacia seyal gum in dry state : Aggregation kinetics and structural properties of aggregates. *International Journal of Biological Macromolecules*.

Aoki, H., Al-Assaf, S., Katayama, T., & Phillips, G. O. (2007). Characterization and properties of Acacia senegal (L.) Willd. var. senegal with enhanced properties (Acacia (sen) SUPER GUM^{TM}) : Part 2—Mechanism of the maturation process. *Food Hydrocolloids*, *21*(3), 329-337. https://doi.org/10.1016/j.foodhyd.2006.04.002

Aoki, H., Katayama, T., Ogasawara, T., Sasaki, Y., Al-Assaf, S., & Phillips, G. O. (2007). Characterization and properties of Acacia senegal (L.) Willd. var. Senegal with enhanced properties (Acacia (sen) SUPER GUM^{TM}) : Part 5. Factors affecting the emulsification of Acacia senegal and Acacia (sen) SUPER GUM^{TM}. *Food Hydrocolloids*, *21*(3), 353-358. https://doi.org/10.1016/j.foodhyd.2006.04.014

Aphibanthammakit, C. (2018). *Interfacial and emulsifying properties of Acacia gums and their fractions* [Montpellier SupAgro]. http://www.theses.fr/2018NSAM0029

Aphibanthammakit, C., Barbar, R., Nigen, M., Sanchez, C., & Chalier, P. (2020). Emulsifying properties of Acacia

senegal gum : Impact of high molar mass protein-rich AGPs. *Food Chemistry: X*, *6*, 100090. https://doi.org/10.1016/j.fochx.2020.100090

Aphibanthammakit, C., Nigen, M., Gaucel, S., Sanchez, C., & Chalier, P. (2018). Surface properties of Acacia senegal vs Acacia seyal films and impact on specific functionalities. *Food Hydrocolloids*, *82*, 519-533. https://doi.org/10.1016/j.foodhyd.2018.04.032

Beverung, C., Radke, C., & Blanch, H. (1999). Protein adsorption at the oil/water interface : Characterization of adsorption kinetics by dynamic interfacial tension measurements. *Biophysical Chemistry*, *81*(1), 59-80. https://doi.org/10.1016/S0301-4622(99)00082-4

Bouyer, E., Mekhloufi, G., Le Potier, I., de Kerdaniel, T., Grossiord, J., Rosilio, V., & Agnely, F. (2011). Stabilization mechanism of oil-in-water emulsions by β-lactoglobulin and gum arabic. *Journal of Colloid and Interface Science*, *354*(2), 467-477. https://doi.org/10.1016/j.jcis.2010.11.019

Capataz-Tafur, J., Trejo-Trapia, G., Rodríguez-Monroy, M., & Sepulveda-Jiménez, G. (2011). Arabinogalactan proteins are involved in cell aggregation of cell suspension cultures of Beta vulgaris L. *Plant Cell Tiss Organ Cult*, *106*, 169-177. https://doi.org/10.1007/s11240-010-9905-3

Castellani, O., Al-Assaf, S., Axelos, M., Phillips, G., & Anton, M. (2010). Hydrocolloids with emulsifying capacity. Part 2 – Adsorption properties at the n-hexadecane–Water interface. *Food Hydrocolloids*, *24*(2), 121-130. https://doi.org/10.1016/j.foodhyd.2009.07.006

Castellani, O., Guibert, D., Al-Assaf, S., Axelos, M., Phillips, G. O., & Anton, M. (2010). Hydrocolloids with emulsifying capacity. Part 1 – Emulsifying properties and interfacial characteristics of conventional (Acacia senegal (L.) Willd. Var. Senegal) and matured (Acacia (sen) SUPER GUM^{TM}) Acacia senegal. *Food Hydrocolloids*, *24*(2-3), 193-199. https://doi.org/10.1016/j.foodhyd.2009.09.005

Chanamai, R., & Mcclements, D. (2001). Depletion Flocculation of Beverage Emulsions by Gum Arabic and Modified Starch. *Journal of Food Science*, *66*, 457-463. https://doi.org/10.1111/j.1365-2621.2001.tb16129.x

Chanamai, R., & McClements, D. J. (2000). Impact of weighting agents and sucrose on gravitational separation of beverage emulsions. *Journal of Agricultural and Food Chemistry*, *48*(11), 5561-5565. https://doi.org/10.1021/jf0002903

Chandler, R. C. (1941). Nature of bound water in colloidal systems. *Plant physiology*, *16*, 273-291. https://doi.org/10.1104/PP.16.2.273

Chen, M., Sala, G., Meinders, M., van Valenberg, H., van der Linden, E., & Sagis, L. (2017). Interfacial properties, thin film stability and foam stability of casein micelle dispersions. *Colloids and Surfaces B: Biointerfaces*, *149*, 56-63. https://doi.org/10.1016/j.colsurfb.2016.10.010

Coe, M. K., Evans, R., & Wilding, N. B. (2022). Density depletion and enhanced fluctuations in water near hydrophobic solutes : Identifying the underlying physics. *Physical Review Letters*, *128*(4), 045501. https://doi.org/10.1103/PhysRevLett.128.045501

Debon, S. J. J., & Tester, R. F. (2001). In vitro binding of calcium, iron and zinc by

non-starch polysaccharides. *Food Chemistry*, *73*(4), 401-410. https://doi.org/10.1016/S0308-8146(00)00312-5

Dickinson, E. (2003). Hydrocolloids at interfaces and the influence on the properties of dispersed systems. *Food Hydrocolloids*, *17*(1), 25-39. https://doi.org/10.1016/S0268-005X(01)00120-5

Dickinson, E., Murray, B. S., Stainsby, G., & Anderson, D. M. W. (1988). Surface activity and emulsifying behaviour of some Acacia gums. *Food Hydrocolloids*, *2*(6), 477-490. https://doi.org/10.1016/S0268-005X(88)80047-X

Dou, S., & Colby, R. H. (2006). Charge density effects in salt-free polyelectrolyte solution rheology. *Journal of Polymer Science Part B: Polymer Physics*, *44*(14), 2001-2013. https://doi.org/10.1002/polb.20853

Elmanan, M., Al-Assaf, S., Phillips, Glyn. O., & Williams, Peter. A. (2008). Studies on Acacia exudate gums : Part VI. Interfacial rheology of Acacia senegal and Acacia seyal. *Food Hydrocolloids*, *22*(4), 682-689. https://doi.org/10.1016/j.foodhyd.2007.02.008

Erni, P., Jerri, H., Wong, K., & Parker, A. (2012). Interfacial viscoelasticity controls buckling, wrinkling and arrest in emulsion drops undergoing mass transfer. *Soft Matter*, *8*, 6958-6967. https://doi.org/10.1039/C2SM25438G

Erni, P., Windhab, E. J., Gunde, R., Graber, M., Pfister, B., Parker, A., & Fischer, P. (2007). Interfacial rheology of surface-active biopolymers : Acacia senegal gum versus hydrophobically modifed starch. *Biomacromolecules*, *8*(11), 3458-3466. https://doi.org/10.1021/bm700578z

Fauconnier, M., Blecker, C., Groyne, J., Razafindralambo, H., Vanzeveren, E., Marlier, M., & Paquot, M. (2000). Characterization of Two Acacia Gums and Their Fractions Using a Langmuir Film Balance. *Journal of Agricultural and Food Chemistry*, *48*(7), 2709-2712. https://doi.org/10.1021/jf990749x

Fincher, G. B., Stone, B. A., & Clarke, A. E. (1983). Arabinogalactan-Proteins : Structure, Biosynthesis, and Function. *Annual Review of Plant Physiology*, *34*(1), 47-70. https://doi.org/10.1146/annurev.pp.34.060183.000403

Fligner, K. L., Fligner, M. A., & Mangino, M. E. (1991). Accelerated tests for predicting long-term creaming stability of infant formula emulsion systems. *Food Hydrocolloids*, *5*(3), 269-280. https://doi.org/10.1016/S0268-005X(09)80113-6

Gabel, L. F. (1930). The effect of heat on acacia. *Journal of the american pharmaceutical association*, *19*(8), 828-830. https://doi.org/10.1002/jps.3080190807

Glicksman, M., & Sand, R. E. (1973). Gum arabic. In *Industrial Gums : Polysaccharides and Their Derivatives* (Academic press, p. 223-226). Whistler. https://doi.org/10.1016/B978-0-12-746252-3.X5001-1

Gulrez, S., Al-Assaf, S., & Phillips, G. (2011). Hydrogels : Methods of Preparation, Characterisation and Applications. In *Progress in Molecular and Environmental Bioengineering—From Analysis and Modeling to Technology Applications* (Vol. 51, p. 117-150). 10.5772/24553

Hayashi, H. (2002). *Method of modifying gum arabic* (European Union Patent N° EP1505078B1). https://patents.google.com/patent/EP1505078B1/ja

Idris, O. H. M., Williams, P. A., & Phillips, G. O. (1998). Characterisation of gum from Acacia senegal trees of different age and

location using multidetection gel permeation chromatography. *Food Hydrocolloids*, *12*(4), 379-388. https://doi.org/10.1016/S0268-005X(98)00058-7

Islam, A. M., Phillips, G. O., Sljivo, A., Snowden, M. J., & Williams, P. A. (1997). A review of recent developments on the regulatory, structural and functional aspects of gum arabic. *Food Hydrocolloids*, *11*(4), 493-505. https://doi.org/10.1016/S0268-005X(97)80048-3

Isobe, N., Sagawa, N., Ono, Y., Fujisawa, S., Kimura, S., Kinoshita, K., Miuchi, T., Iwata, T., Isogai, A., Nishino, M., & Deguchi, S. (2020). Primary structure of gum arabic and its dynamics at oil/water interface. *Carbohydrate Polymers*, *249*, 116843. https://doi.org/10.1016/j.carbpol.2020.116843

Jafari, S., Beheshti, P., & Assadpoor, E. (2012). Rheological behavior and stability of D-limonene emulsions made by a novel hydrocolloid (Angum gum) compared with Arabic gum. *Journal of Food Engineering*, *109*, 1-8. https://doi.org/10.1016/j.jfoodeng.2011.10.016

Jamadagni, S. N., Godawat, R., & Garde, S. (2011). Hydrophobicity of proteins and interfaces : Insights from density fluctuations. *Annual Review of Chemical and Biomolecular Engineering*, *2*, 147-171. https://doi.org/10.1146/annurev-chembioeng-061010-114156

Katayama, T., Ogasawara, T., Sasaki, Y., Al-Assaf, S., & Phillips, G. (2008). *Composition Containing Hydrogel Component Derived from Gum Arabic* (United States Patent N° US20080038436A1). https://patents.google.com/patent/US20080038436A1/en

Keowmaneechai, E., & McClements, D. J. (2002). Influence of EDTA and citrate on physicochemical properties of whey protein-stabilized oil-in-water emulsions containing CaCl2. *Journal of Agricultural and Food Chemistry*, *50*(24), 7145-7153. https://doi.org/10.1021/jf020489a

Kunkel, M. E., Seo, A., & Minten, T. A. (1997). Magnesium binding by gum arabic, locust bean gum, and arabinogalactan. *Food Chemistry*, *59*(1), 87-93. https://doi.org/10.1016/S0308-8146(96)00173-2

Lillard, J. S., Clare, D. A., & Daubert, C. R. (2009). Glycosylation and expanded utility of a modified whey protein ingredient via carbohydrate conjugation at low pH. *Journal of Dairy Science*, *92*(1), 35-48. https://doi.org/10.3168/jds.2008-1263

Lopez-Torrez, L. (2016). *Characterisation of Acacia gums and development of heat-induced Acacia gum/potato proteins microparticles*. Montpellier SupAgro.

Lopez-Torrez, L., Nigen, M., Williams, P., Doco, T., & Sanchez, C. (2015). Acacia senegal vs. Acacia seyal gums—Part 1 : Composition and structure of hyperbranched plant exudates. *Food Hydrocolloids*, *51*, 41-53. https://doi.org/10.1016/j.foodhyd.2015.04.019

Lum, K., Chandler, D., & Weeks, J. D. (1999). Hydrophobicity at Small and Large Length Scales. *The Journal of Physical Chemistry B*, *103*(22), 4570-4577. https://doi.org/10.1021/jp984327m

Mahmoudi, N., Gaillard, C., Boué, F., Axelos, M. A. V., & Riaublanc, A. (2010). Self-similar assemblies of globular whey proteins at the air–water interface : Effect of the structure. *Journal of Colloid and Interface Science*, *345*(1), 54-63. https://doi.org/10.1016/j.jcis.2010.01.036

Mantell, C. (1954). Technology of Gum Arabic. *Natural plant hydrocolloids*, *11*, 20-32.

https://doi.org/10.1021/ba-1954-0011.ch005

Mejia Tamayo, V., Nigen, M., Apolinar-Valiente, R., Williams, P., Doco, T., Renard, D., & Sanchez, C. (2018). *Flexibility and hydration of amphiphilic hyperbranched Arabinogalactan-protein from plant exudate : A volumetric perspective*. https://doi.org/10.3390/colloids2010011

Moorjani, M. N., & Narwani, C. S. (1948). Influence of heat on the physico-chemical properties of gum-arabic. *Current science*, *17*(4), 123-124.

Mothé, C. G., & Rao, M. A. (1999). Rheological behavior of aqueous dispersions of cashew gum and gum arabic : Effect of concentration and blending. *Food Hydrocolloids*, *13*(6), 501-506. https://doi.org/10.1016/S0268-005X(99)00035-1

Nagel, M., Tervoort, T., & Vermant, J. (2017). From Drop-Shape Analysis to Stress-Fitting Elastometry. *Advances in Colloid and Interface Science*, *247*. https://doi.org/10.1016/j.cis.2017.07.008

Pérez-Díaz, J. L., Álvarez-Valenzuela, M. A., & García-Prada, J. C. (2012). The effect of the partial pressure of water vapor on the surface tension of the liquid water–air interface. *Journal of Colloid and Interface Science*, *381*(1), 180-182. https://doi.org/10.1016/j.jcis.2012.05.034

Phillips, G. O. (2009). Molecular association and function of arabinogalactan protein complexes from tree exudates. *Structural Chemistry*, *20*(2), 309-315. https://doi.org/10.1007/s11224-009-9422-3

Phillips, G. O., & Williams, P. A. (1993). The specification of the gum Arabic of commerce. In *Food hydrocolloids : Structures, Properties, and Functions* (p. 45-63). Springer Science + Business Media. 10.1007/978-1-4615-2486-1_4

Qian, C., & McClements, D. J. (2011). Formation of nanoemulsions stabilized by model food-grade emulsifiers using high-pressure homogenization : Factors affecting particle size. *Food Hydrocolloids*, *25*(5), 1000-1008. https://doi.org/10.1016/j.foodhyd.2010.09.017

Randall, R. C., Phillips, G. O., & Williams, P. A. (1989). Fractionation and characterization of gum from Acacia senegal. *Food Hydrocolloids*, *3*(1), 65-75. https://doi.org/10.1016/S0268-005X(89)80034-7

Rao, C. S., & Damodaran, S. (2000). Is Surface Pressure a Measure of Interfacial Water Activity? Evidence from Protein Adsorption Behavior at Interfaces. *Langmuir*, *16*(24), 9468-9477. https://doi.org/10.1021/la0007168

Renard, D., Garnier, C., Lapp, A., Schmitt, C., & Sanchez, C. (2012). Structure of arabinogalactan-protein from Acacia gum : From porous ellipsoids to supramolecular architectures. *Carbohydrate Polymers*, *90*(1), 322-332. https://doi.org/10.1016/j.carbpol.2012.05.046

Renard, D., Lavenant-Gourgeon, L., Ralet, M.-C., & Sanchez, C. (2006). Acacia senegal Gum : Continuum of Molecular Species Differing by Their Protein to Sugar Ratio, Molecular Weight, and Charges. *Biomacromolecules*, *7*(9), 2637-2649. https://doi.org/10.1021/bm060145j

Renard, D., Lepvrier, E., Garnier, C., Roblin, P., Nigen, M., & Sanchez, C. (2014). Structure of glycoproteins from Acacia gum : An assembly of ring-like glycoproteins modules. *Carbohydrate Polymers*, *99*, 736-747. https://doi.org/10.1016/j.carbpol.2013.08.090

Rosenholm, J., Ihalainen, P., & Peltonen, J. (2003). Thermodynamic characterization of Langmuir monolayers of thiolipids : A conceptual analysis. *Colloids and Surfaces A: Physicochemical and Engineering Aspects*, *228*(1), 119-130. https://doi.org/10.1016/S0927-7757(03)00301-7

Sanchez, C., Nigen, M., Mejia Tamayo, V., Doco, T., Williams, P., Amine, C., & Renard, D. (2018). Acacia gum : History of the future. *Food Hydrocolloids*, *78*, 140-160. https://doi.org/10.1016/j.foodhyd.2017.04.008

Sanchez, C., Renard, D., Robert, P., Schmitt, C., & Lefebvre, J. (2002). Structure and rheological properties of acacia gum dispersions. *Food Hydrocolloids*, *16*(3), 257-267. https://doi.org/10.1016/S0268-005X(01)00096-0

Sasaki, Y., Ogasawara, T., Katayama, T., & Sakata, M. (2014). *Process for producing modified gum arabic* (United States Patent N° US8722129B2). https://patents.google.com/patent/US8722129B2/en

Schong, E., & Famelart, M. (2018). Dry heating of whey proteins leads to formation of microspheres with useful functional properties. *Food Research International*, *113*, 210-220. https://doi.org/10.1016/j.foodres.2018.07.004

Schultz, S., Wagner, G., Urban, K., & Ulrich, J. (2004). High-Pressure Homogenization as a Process for Emulsion Formation. *Chemical Engineering & Technology*, *27*(4), 361-368. https://doi.org/10.1002/ceat.200406111

Sharma, V., Jaishankar, A., Wang, Y., & McKinley, G. (2011). Rheology of globular proteins : Apparent yield stress, high shear rate viscosity and interfacial viscoelasticity of bovine serum albumin solutions. *Soft Matter*, *7*(11), 5150-5160. https://doi.org/10.1039/C0SM01312A

Stanimirova, R., Marinova, K., Tcholakova, S., Denkov, N. D., Stoyanov, S., & Pelan, E. (2011). Surface Rheology of Saponin Adsorption Layers. *Langmuir*, *27*(20), 12486-12498. https://doi.org/10.1021/la202860u

Szafulera, K., Wach, R. A., Olejnik, A. K., Rosiak, J. M., & Ulański, P. (2018). Radiation synthesis of biocompatible hydrogels of dextran methacrylate. *Radiation Physics and Chemistry*, *142*, 115-120. https://doi.org/10.1016/j.radphyschem.2017.01.004

Taherian, A., Fustier, P., Britten, M., & Ramaswamy, H. (2008). Rheology and Stability of Beverage Emulsions in the Presence and Absence of Weighting Agents : A Review. *Food Biophysics*, *3*, 279-286. https://doi.org/10.1007/s11483-008-9093-4

Tipvarakarnkoon, T., Einhorn-Stoll, U., & Senge, B. (2010). Effect of modified Acacia gum (SUPER GUM^{TM}) on the stabilization of coconut o/w emulsions. *Food Hydrocolloids*, *24*(6), 595-601. https://doi.org/10.1016/j.foodhyd.2010.03.002

Touré, S. (2008). *Gum Arabic*. Market News Service (MNS) (Quaterly edition). International Trading Center. https://ngara.org/pdf/GumArabic_MarketNewsService%20Issue1_08.pdf

Tschoegl, N. (1958). Elastic moduli in monolayers. *Journal of Colloid Science*, *13*(5), 500-507. https://doi.org/10.1016/0095-8522(58)90058-8

Vasile, F., Martinez, M., V., V., Judis, M., & Mazzobre, M. (2016). Physicochemical, interfacial and emulsifying properties of a non-conventional exudate gum (Prosopis alba) in comparison with gum

arabic. *Food Hydrocolloids*, *56*, 245-253. https://doi.org/10.1016/j.foodhyd.2015.12.016

Verbeken, D., Dierckx, S., & Dewettinck, K. (2003). Exudate gums : Occurrence, production, and applications. *Applied Microbiology and Biotechnology*, *63*(1), 10-21. https://doi.org/10.1007/s00253-003-1354-z

Walstra, P. (1993). Principles of emulsion formation. *Chemical Engineering Science*, *48*(2), 333-349. https://doi.org/10.1016/0009-2509(93)80021-H

Ward, A., & Tordai, L. (1946). Time-dependence of boundary tensions of solutions I. The role of diffusion in time-effects. *The Journal of Chemical Physics*, *14*(7), 453-461. https://doi.org/10.1063/1.1724167

Wickens, G. E., Seif ElDin, A. G., Sita, G., & Nahal, I. (1995). *Role of Acacia Species in the Rural Economy of Dry Africa and the Near East*. Food & Agriculture Org.

Yeung, A., & Zhang, L. (2006). Shear Effects in Interfacial Rheology and Their Implications on Oscillating Pendant Drop Experiments. *Langmuir*, *22*(2), 693-701. https://doi.org/10.1021/la051795w

Zhang, J., Peppard, T., & Reineccius, G. (2015). Preparation and characterization of nanoemulsions stabilized by food biopolymers using microfluidization. *Flavour and Fragrance Journal*, *30*, 288-294. https://doi.org/10.1002/ffj.3244

Zhou, X., Sala, G., & Sagis, L. (2020). Bulk and interfacial properties of milk fat emulsions stabilized by whey protein isolate and whey protein aggregates. *Food Hydrocolloids*, *109*, 106100. https://doi.org/10.1016/j.foodhyd.2020.106100

CHAPTER VII.

GENERAL CONCLUSIONS AND PERSPECTIVES

1. Summary

This work was carried out in the context of an industrial project between the Alland & Robert Society and the Joint Research Unit IATE (Ingénierie des Agropolymères et Technologies Émergentes) in Montpellier. The main objective of this Ph.D. thesis was to study the influence of storage conditions on the structural and physicochemical properties of arabinogalactan-proteins (AGPs) from demineralized spray-dried Acacia *seyal* gum. For this purpose, a commercial A. *seyal* gum was first demineralized, spray-dried and the resulting powder was stored under controlled environment in closed vessels at T = 25 – 70°C. The specific objectives of this work were to characterize: *(i)* the AGP aggregation kinetics during their incubation in dry state, and the structural properties of AGP aggregates (Chapter III), *(ii)* the interrelated effect of hydration dynamics on the aggregation kinetics of AGPs and their structural properties, *(iii)* the stability of AGP aggregates according to the solvent properties (Chapter V) and *(iv)* the changes in the physicochemical properties of AGPs (rheological, interfacial and emulsifying) induced by their aggregation (Chapter VI).

1.1. AGPs from demineralized A. seyal gum aggregate following a self-similar assembly mechanism during their incubation in dry state

Solubility and molar mass measurements showed that the reactivity and ability of AGPs from GA to aggregate was enhanced in the order: arabic acid (pH 2.4, absence of minerals) >> acidified GA (pH 2.4, presence of minerals) > GA (pH 4.5, presence of minerals). This suggests that the removal of minerals (Ca, Na, K) from GA influences the chemical and colloidal stability of AGPs by promoting their reactivity for their aggregation in dry state and mild temperature conditions (25°C to 70°C). From the aggregation kinetics studied at 25, 40, 55 and 70°C, an activation energy of 90 – 100 $kJ \cdot mol^{-1}$ was calculated. AGPs from arabic acid follow a self-similar assembly mechanism during their incubation in dry state. The two first days of heating at 40°C were characterized by the formation of soluble aggregates whose molar mass increased by 6 to reach $M_w = 6.7 \cdot 10^6$ $g \cdot mol^{-1}$ as determined by SEC MALLS measurements. These soluble aggregates adopted a similar conformation to that of not aggregated AGPs. Longer incubation times promote the formation of highly cross-linked insoluble microparticles

with a mean size D(4,3) around 70 µm, and whose shape depends on the drying method used (spray-drying or freeze-drying).

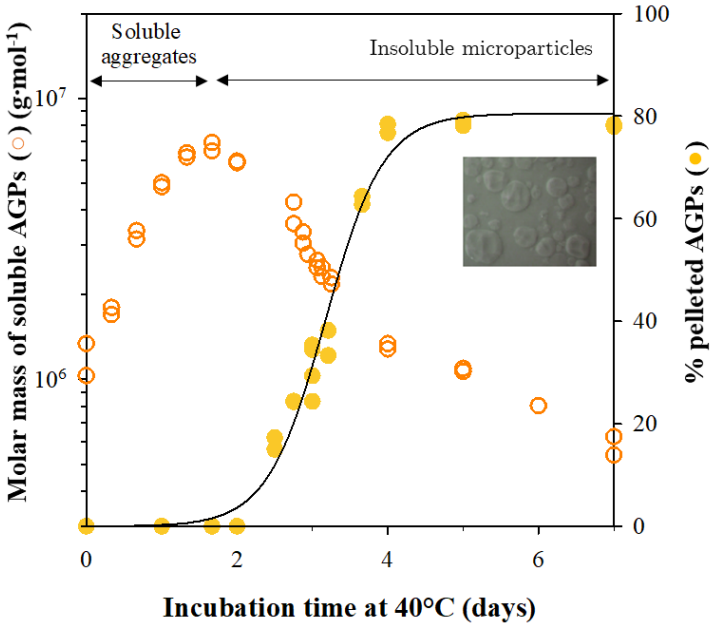

Figure VII.1. Incubation of arabic acid powder leads to the formation of AGP aggregates of different size and solubility: calculated mean molar mass determined by SEC MALLS experiments (○) from AGPs and soluble aggregates and pelleted fraction (●) of arabic acid incubated between 0 and 7 days at 40°C. The continuous line represents the fit of the data obtained at 40°C with SigmaPlot software.

1.2. AGPs hydration dynamics are closely related to the structure of aggregates

The hydration properties of aggregates were characterized all along the aggregation kinetics at 40°C using a combination of volumetric and spectroscopic techniques. We aimed to point out a correlation between the AGP hydration water thermodynamic properties and their aggregation state. For the first time, we characterized the intrinsic volumetric properties of AGP aggregates, namely the intrinsic density and the intrinsic ultrasound velocity, *i.e.* the propagation of an AGP matter wave. From the AGP intrinsic density value ρ_{AGP} it is possible to calculate an AGP sphere-equivalent radius $R_{h\,eq}$:

$$R_{h\,eq} = \left(\frac{3M_w}{4\pi\rho_{AGP}N_A}\right)^{1/3}$$

with M_w the AGP molar mass and N_A the Avogadro number.

For arabic acid we found a $R_{h\ eq}$ value of 7.2 nm in the order of magnitude of R_h = 15 nm determined by SEC MALLS. In spite of their high sugar content, AGPs hydration properties of AGP aggregates are closer to those of globular proteins.

Demineralization of GA dramatically modified the dynamics of interfacial hydration water. The contribution of hydrophilic water dynamics dominates at low incubation times when soluble aggregates are formed. However, for longer incubation times the contribution of the hydrophobic water increases and controls the formation of insoluble microparticles.

Using FTIR, we suggested an interesting correlation between interfacial water and C–H bonds from sugars and/or amino acids and O–H bonds from free water. AGP-water hydrogen bond interactions weaken after demineralization.

1.3. AGP aggregates are particularly sensitive to the pH and dissociate at highly basic pH

The sensitivity of aggregates to the physicochemical properties of the solvent was assessed to better understand how AGP aggregate during storage and, in combination with spectroscopic characterization, to eventually point out hypothetical chemical bonds/groups involved in this reaction mechanism. Aggregates were dispersed in water and buffer solutions supplemented by various amounts of urea, NaCl and $CaCl_2$. Aggregates are not dissociated in presence of urea suggesting that intermolecular AGP-AGP hydrogen bond interactions are not the main driving force in the aggregation of demineralized arabic acid. The addition of $CaCl_2$ does not modify AGP aggregates solubility and molar mass of soluble aggregates except at a concentration of 50 mmol·L^{-1} for which $CaCl_2$ promotes aggregation of AGPs in solution. However, aggregates dissociate at basic pHs (Figure VII.2). We suggested that when increasing the pH, insoluble microparticles first dissociate into soluble aggregates at pH ~ 6.7, resulting in an increase in molar mass measured by SEC MALLS. These soluble aggregates further dissociate into smaller AGPs having a smaller molar mass (pH ~ 8 – 8.5) down to reach a molar mass of ~ 10^6 g·mol^{-1} at pH 9.5. This dissociation in alkaline conditions combined with the activation energy calculated of 90 – 100 kJ·mol^{-1} and the aggregation conditions (acidic pH of arabic acid in dispersion, dry state, heating) might suggest that AGP aggregates formed *via* chemical condensation reactions such as esterification. A synergestic effect pH/ionic strength was

reported in a narrow pH range around pH 8 showing enhanced sensitivity of aggregates which could arise from an increased accessibility of the AGPs charges at this specific pH.

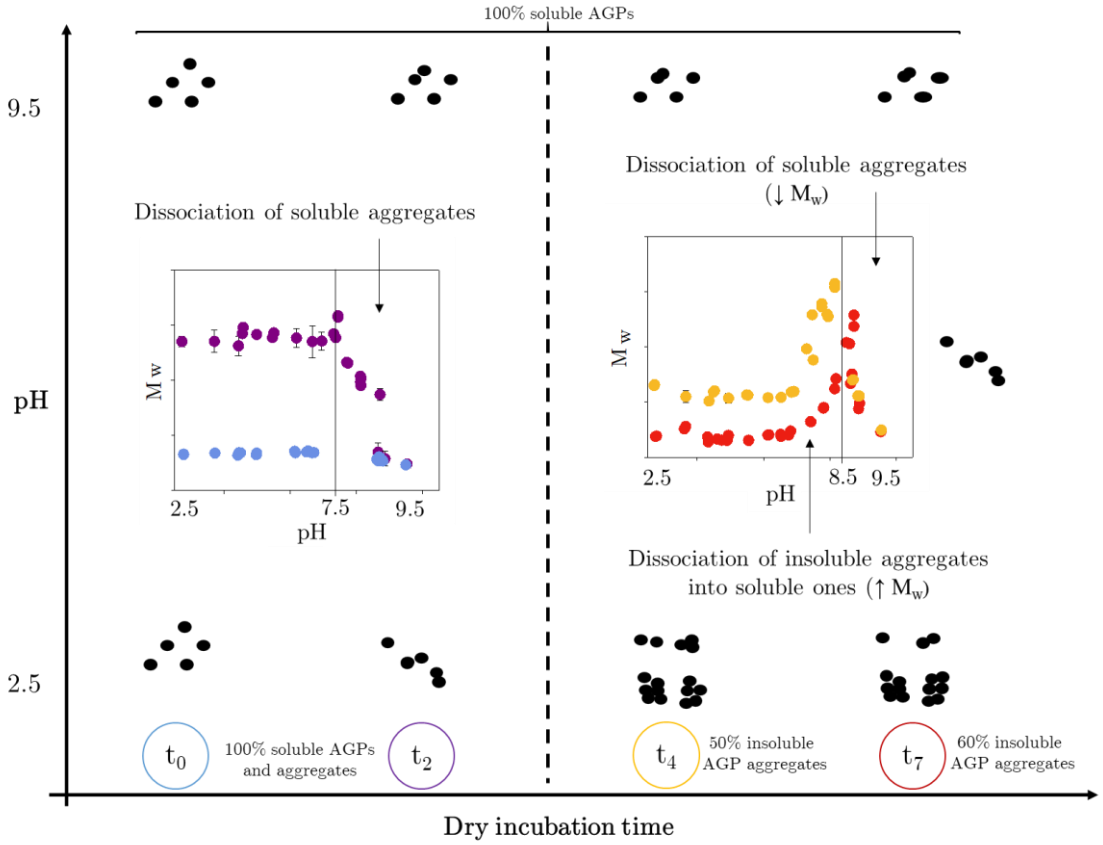

Figure VII.2. Stability to the solvent pH of arabic acid AGP aggregates.

Since AGP are complex hyperbranched biopolymers made of a continuum of macromolecules, their spectroscopic characterization is far from being evident. Attempts to decipher chemical modifications between A. *seyal*, arabic acid and aggregates was carried out using NMR and FTIR spectroscopy. Demineralization induced an acidification of A. *seyal* from pH 4.5 to pH 2.4. FTIR confirmed that this demineralization induced a switch of carboxylic acid moieties from their deprotonated form $RCOO^-$ to their protonated form RCOOH (pKa = 3 – 4 (Grein-Iankovski et al., 2018)). With aggregation, only minor changes were observed in this spectral region. However, between 850 and 1200 cm^{-1}, an increase in the intensity of the band at 1065 cm^{-1} concomitant with a decrease in the intensity of the band at 1015 cm^{-1} was observed, suggesting the involvement of C–O bonds, which could arise from the formation of ester species. The formation of a peak at 95 ppm observed by NMR would confirm this assumption.

1.4. Incubation in dry state enhances A. seyal gum AGPs physicochemical properties

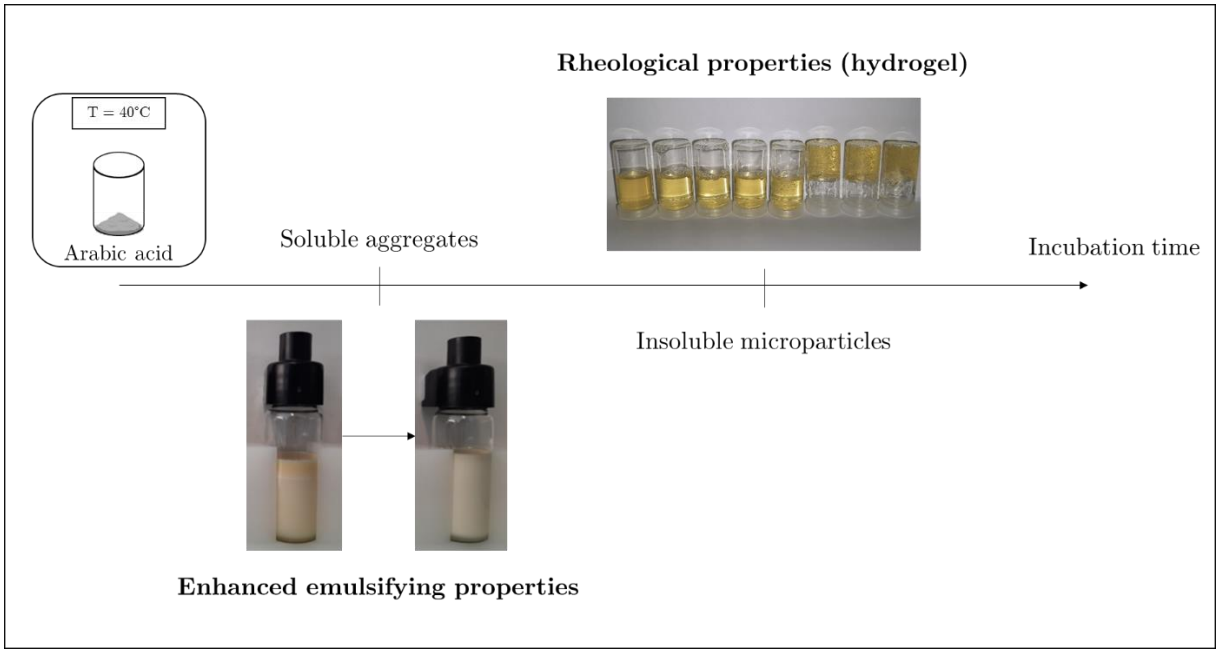

Figure VII.3. Major changes in arabic acid physicochemical properties caused by AGP aggregation during their storage in dry state.

Interfacial and emulsifying properties of soluble AGP aggregates were studied. Rheological properties were characterized over the whole range of aggregate sizes, from soluble aggregates to insoluble microparticles. Results showed a significant increase in apparent viscosity η at C = 15wt% with storage, from η = 14 mPa.s at t_0 to η = 3.5 Pa.s at t_7. Up to 2 days of storage, the flow behaviour of AGPs is Newtonian-like, and then becomes shear-thinning, which might reflect changes in AGP aggregates organization in dispersion, from an ordered and compact system to a more entangled one. With aggregation, AGPs viscoelastic behavior in dispersion switches from a liquid-like behavior to a solid-like behavior. At long incubation time, micrometric insoluble microparticles (D(4,3) = 80 µm) cause the formation of a hydrogel with a predominantly elastic structure, as observed in Figure VII.3. The formation of this hydrogel at concentrations C ≥ 10% is due to molecular crowding.

Since arabic acid is more hydrophobic than A. *seyal*, its better affinity for the organic phase makes it more prone to stabilize limonene/water interface. On the contrary, interfacial properties of arabic acid are not improved further after aggregation, probably due to similar polarity and conformation between arabic acid and soluble aggregates.

In spite of these similar interfacial properties, since *(i)* the molar mass M_w of AGPs greatly increased with storage and *(ii)* 100% of AGPs have a $M_w > 10^6$ g·mol^{-1}, soluble aggregates display enhanced emulsifying behavior compared to A. *seyal*. In emulsions formulated with EGEO, the oil droplet size D(4,3) is decreased by 20 in emulsions stabilized by 10% aggregates compared to 20% A. *seyal* and the global stability increases by 5 after a month of emulsion ageing, even if clarification and creaming is observed in the bottom and at the top of the emulsion tube, respectively. However, in these conditions, the emulsifying properties of A. *senegal* remain better than those of AGP aggregates.

2. Perspectives

2.1 Tracking relative humidity of powders during storage

The storage of arabic acid powders under controlled temperature and relative humidity was done in glass vessels closed with a plastic cap. However, *(i)* release of water molecules from the powder into the headspace and eventually *(ii)* modification of the headspace environment *via* transfers through the plastic cap change the hydration of arabic acid powders during their storage, and consequently, the way they aggregate. It would be interesting to have access to water activity of arabic acid powders in real time for a better control and understanding of mechanisms that occur during the storage. For that purpose, we thought about measuring the water vapor pressure P_{vap} which is related to the relative humidity in air %RH *via*:

$$\%RH = \frac{P_{vap}}{P_{sat}(T)} * 100$$

where $P_{sat}(T)$ is the vapor pressure at the temperature T.

Preliminary curves were determined to link relative humidity and water activity in powders. Once done, it would be interesting to store arabic acid powders with different water contents. We already know that AGPs from arabic acid, after being dispersed in water, do not aggregate during the storage. This study would bring knowledge about how powder hydration influences AGP aggregation.

2.2 Better understanding AGP aggregation mechanism

AGPs from demineralized A. *senegal* did not aggregate during their storage in dry state. A. *seyal* is known to have a higher content of phenolic acids than A. *senegal* which provides to the former a more brown color (Mhinzi, 2003). In food industry where GA is used as a food additive, the color is of particular importance. For this reason, prior to its use in industry, A. *seyal* is bleached with hydrogen peroxide H_2O_2. This chemical treatment oxidizes C=C from the phenyl ring thus modifying the reactivity of phenolic acids, and liberates free radicals in solution. By considering this treatment, it should be interesting to investigate the involvement of polyphenols in the AGP aggregation mechanism. Kjellbom et al. showed that the cross-linking of acidic AGPs could be promoted in oxidative environment (Kjellbom et al., 1997). They assumed the possible involvement of amino acids such as Tyrosine – maybe via its phenolic group – in the intermolecular linkages between acidic AGPs. To test our assumption, we think about working with a raw untreated A. *seyal* gum. We plan to carry out in parallel two sets of experiments. Both gums will be demineralized and stored at 40°C, but one will be peroxidized prior to demineralization to assess the influence of bleaching on the reactivity of AGPs. Characterizing the phenolic compound composition of gums before and after aggregation is also envisioned. These upcoming experiments are also supported by the fact that phenolic acids such as gallic acid (pKphenol = 8.90), sinapic acid (pKphenol = 8.94), p-coumaric acid (pKphenol = 9.21) and ferulic acid (pKphenol = 9.21) are dissociated at basic pHs (Amorati et al., 2006; Friedman & Jürgens, 2000).

TD-NMR gave us access to the spin-spin relaxation times of interfacial water protons. T_2 relaxation is an entropic process. It would be interesting to measure T_1 relaxation, which is an enthalpic process. It would give complementary information to better characterize the hydration properties of aggregates. AGP aggregates showed partial reversibility when dispersed in Capso buffer at pH 9.5. We plan to disperse these aggregates in more extreme pH conditions (pH > 9.5) to see if complete reversibility of aggregation can be reached.

2.3 Importance of the mineral composition with respect to AGP aggregation

Mineral content plays a major role in AGP reactivity during storage in dry state. We showed that the presence of minerals inhibited aggregation as no aggregates were formed with A. *seyal* loaded in minerals compared to arabic acid. It would be interesting to probe the effect of the mineral composition on the reactivity of AGPs. For instance, we think about varying the amount and composition in minerals of GA by remineralizing arabic acid exclusively with calcium, sodium or potassium. AGPs particularly interact with calcium *via* their glucuronic acid moieties (Lamport & Várnai, 2013). We showed the importance of charges in the AGP aggregation mechanism and suggested that condensation of charges might be at the origin of aggregation. We have seen also that the main hydration changes occurred during the demineralization step, which highly reduced the polarity of GA. We would like to characterize volumetric properties of arabic acid remineralized at the same mineral composition than A. *seyal* to probe to which extent its polarity is modified and to better understand why cations limit dehydration/aggregation of AGPs during storage.

2.4 Exploring the emulsifying potential of AGP aggregates

AGP aggregates improved the emulsifying properties of A. *seyal*, both in terms of oil droplet size and emulsion stability. Interfacial tension measurements showed that arabic acid had better interfacial properties than A. *seyal*, in line with its more hydrophobic character. However, AGP aggregation did not improved further arabic acid interfacial properties. Demineralization of GA (Buffo et al., 2001), sweet whey (Acem et al., 2018) or animal blood plasma (Del Hoyo et al., 2008) induces an improvement of their emulsifying properties. In particular, demineralization was shown to be a good way to enhance emulsion stability of A. *senegal*, especially at pH 4.5 (Buffo et al., 2001). Emulsifying properties are governed by the polarity of the emulsifier and so its ability to go and stabilize the oil/water interface, but also by the viscosity of the continuous phase. Even if arabic acid viscosity is by 10 times lower than that of t_2 at the same concentration, we are curious to characterize emulsifying properties of arabic acid. It would be relevant also to formulate emulsions with t_2 at the same GA concentration, *i.e.* 20% to see if GA emulsifying properties can be further improved. We also think about characterizing the emulsifying potential of reconstituted gum composed of a mix

GA/AGP aggregates. These aggregates could be either soluble aggregates, or even insoluble microparticles, which would greatly affect the emulsion continuous phase viscosity.

3. References

Acem, K., Choukri, A., Saoudet, N., Tergou, S., & Trari, H. (2018). Demineralization Effect on the Physicochemical and Interfacial Properties of Sweet Whey. *Proceedings of the Third International Symposium on Materials and Sustainable Development*, 516–526. https://doi.org/10.1007/978-3-319-89707-3_56

Amorati, R., Pedulli, G. F., Cabrini, L., Zambonin, L., & Landi, L. (2006). Solvent and pH Effects on the Antioxidant Activity of Caffeic and Other Phenolic Acids. *Journal of Agricultural and Food Chemistry*, *54*(8), 2932–2937. https://doi.org/10.1021/jf053159+

Buffo, R. A., Reineccius, G. A., & Oehlert, G. W. (2001). Factors affecting the emulsifying and rheological properties of gum acacia in beverage emulsions. *Food Hydrocolloids*, *15*(1), 53–66. https://doi.org/10.1016/S0268-005X(00)00050-3

Del Hoyo, P., Rendueles, M., & Díaz, M. (2008). Effect of processing on functional properties of animal blood plasma. *Meat Science*, *78*(4), 522–528. https://doi.org/10.1016/j.meatsci.2007.07.024

Friedman, M., & Jürgens, H. S. (2000). Effect of pH on the Stability of Plant Phenolic Compounds. *Journal of Agricultural and Food Chemistry*, *48*(6), 2101–2110. https://doi.org/10.1021/jf990489j

Grein-Iankovski, A., Ferreira, J. G. L., Orth, E. S., Sierakowski, M.-R., Cardoso, M. B., Simas, F. F., & Riegel-Vidotti, I. C. (2018). A comprehensive study of the relation between structural and physical chemical properties of acacia gums. *Food Hydrocolloids*, *85*, 167–175. https://doi.org/10.1016/j.foodhyd.2018.07.011

Lamport, D., & Várnai, P. (2013). Periplasmic arabinogalactan glycoproteins act as a calcium capacitor that regulates plant growth and development. *New Phytologist*, *197*(1), 58–64. https://doi.org/10.1111/nph.12005

Mhinzi, G. S. (2003). Intra-species variation of the properties of gum exudates from Acacia Senegal var. Senegal and Acacia seyal var. Fistula from Tanzania. *Bulletin of the Chemical Society of Ethiopia*, *17*(1). https://doi.org/10.4314/bcse.v17i1.61734

Valorization

Scientific article

Antoine-Michard, A., Charbonnel, C., Jaouen, I., Sanchez, C., & Nigen, M. (2022). Maturation of demineralized arabinogalactan-proteins from Acacia *seyal* gum in dry state : Aggregation kinetics and structural properties of aggregates. *International Journal of Biological Macromolecules*, in publication.

National and international communications

10th international colloids conference, December 2020, poster session (online), "Impact of processing conditions on the aggregation behavior of arabinogalactan proteins from Acacia *seyal* gum."

NMR group meeting, January 2021, oral presentation, Institut de biologie structurale (IBS), Grenoble, France, oral presentation, "Aggregation of arabinogalactan-proteins from Acacia *seyal* gum in low-moisture environment: structure, interactions and functionality."

Scientific animation, JRU IATE, April 2021, oral presentation, "Agrégation des arabinogalactane-protéines de la gomme d'Acacia *seyal* en milieu peu hydraté: structure, interactions et fonctionnalité."

Seminar protein interactions and assembly, GdR SLAMM, May 2021, oral presentation (online), "Agrégation des arabinogalactane-protéines de la gomme d'Acacia *seyal* en milieu peu hydraté: structure, interactions et fonctionnalité."

35th conference of the European colloids and interface society (ECIS), Athens, Greece, September 2021, poster session, "Impact of processing conditions on the aggregation behavior of demineralized arabinogalactan-proteins from Acacia *seyal* gum."

7th international polysaccharide conference (EPNOE), Nantes, France, October 2021, oral presentation, "Aggregation of arabinogalactan-proteins from Acacia *seyal* gum in low-hydration state."

Aggregation of arabinogalactan-proteins from demineralized Acacia *seyal* gum in low hydration state

Acacia *seyal* gum (GA, E414), is an edible dried gummy exudate obtained from the trunk and branches of Acacia *Seyal* trees. GA biopolymers belong to the arabinogalactan-protein (AGP) family. GA properties are partly related to the AGPs molecular distribution and especially to their protein rich-high molar mass AGPs content. AGPs are known to self-assemble and aggregate during the maturation step of GA and its post harvesting treatments as their demineralization. The objectives of this Ph.D. thesis were to investigate the *(i)* aggregation mechanism of demineralized AGPs from Acacia *seyal* powder (*i.e.* arabic acid) according to their storage temperature (25 – 70°C), and to characterize the *(ii)* hydration and *(iii)* physicochemical properties of the elaborated aggregates. In contrary to GA, AGPs from arabic acid aggregate following a self-similar assembly mechanism at all temperatures studied, with the formation of soluble aggregates which grow further into cross-linked insoluble microparticles. These AGP aggregates are sensitive to pH as they start to dissociate at pH 6.7 up to pH 9.5 for which the initial molar mass and conformation of arabic acid AGPs are recovered. These results suppose the aggregation occurs by chemical condensation reactions induced by the AGPs surface dehydration with a calculated activation energy around 100 kJ·mol^{-1}. Water dynamics associated to the formation of these aggregates clearly depend on the aggregation stage. As AGP aggregation progresses, aggregates appear more porous and less hydrated. By this physical processing, the physicochemical properties of AGPs from arabic acid are enhanced with the improvement of the emulsifying properties by the uses of soluble aggregates, and the formation of insoluble microparticle hydrogel for concentration upper than 10%.

Keywords: Acacia gum, demineralization, aggregation, arabinogalactan-proteins, hydration, physicochemical properties

Agrégation des arabinogalactane-protéines de gomme d'Acacia *seyal* déminéralisée en milieu peu hydraté

La gomme d'Acacia *seyal* (GA, E414) est un exsudat gommeux séché comestible obtenu à partir du tronc et des branches de l'Acacia *Seyal*. Les biopolymères qui constituent GA appartiennent à la famille des arabinogalactane-protéines (AGPs). Les propriétés de GA sont en partie liées à la distribution moléculaire de ses AGPs et surtout à sa teneur en AGPs de hausse masse molaire riches en protéines. Les AGPs sont connus pour s'auto-assembler et s'agréger pendant la maturation de GA et son traitement après récolte, et notamment pendant la déminéralisation. Les objectifs de cette thèse étaient d'étudier *(i)* le mécanisme d'agrégation des AGPs déminéralisés de la poudre de gomme d'Acacia *seyal* (*i.e.* acide arabique) en fonction de leur température de stockage (25 – 70°C), et de caractériser *(ii)* l'hydratation et *(iii)* les propriétés physico-chimiques des agrégats formés. Contrairement à GA, les AGPs d'acide arabique s'agrègent selon un mécanisme d'assemblage auto-similaire à toutes les températures étudiées, avec la formation d'agrégats solubles qui, sur des temps de stockage prolongés vont former des microparticules insolubles réticulées. Ces agrégats sont sensibles au pH et commencent à se dissocier à pH 6,7 jusqu'à pH 9,5 où ils retrouvent la masse molaire et la conformation initiale des AGPs d'acide arabique. Ces résultats suggèrent que l'agrégation se produit *via* des réactions de condensation chimique induites par la déshydratation à la surface des AGPs avec une énergie d'activation calculée autour de 100 kJ·mol^{-1}. La dynamique de l'eau associée à la formation de ces agrégats dépend clairement de l'état d'agrégation. Au fur et à mesure de l'agrégation, les agrégats apparaissent plus poreux et moins hydratés. A l'issue de ce traitement physique, les propriétés physico-chimiques des AGPs d'acide arabique sont améliorées, avec d'une part de meilleures propriétés émulsifiantes (avec les agrégats solubles), et la formation d'hydrogels de microparticules insolubles à une concentration en gomme supérieure à 10%.

Mots-clés: Gomme d'acacia, déminéralisation, agrégation, arabinogalactane-protéines, hydratation, propriétés physicochimiques